AN ABSTRACT OF A THESIS

MODELING, ANALYSIS AND PERFORMANCE OF VARIABLE SPEED NINE-PHASE ELECTRIC DRIVES

Amrit Gautam

Master of Science in Electrical and Computer Engineering

Multiphase machines are of increased interest due to their potential advantages of increased reliability, greater fault tolerance, harmonic current reduction and extended speed torque capability. A better understanding of the utilization of higher order harmonics, modes of operation and torque capability in different modes are necessary to realize these possible advantages of higher phase order machines. Due to the high number of coupled variables, the proper modeling and analysis of the higher phase order machine turns out to be a challenging task.

In this thesis, a new approach is proposed for the better torque improvement of 9-phase Interior Permanent Magnet (IPM) machine by the utilization of higher order harmonics which contribute positively to the resultant torque. An approximate Fourier series model and full order q-d model based on winding function theory is proposed for the generalization of the dynamic model of the 9-phase IPM machine with and without the inclusion of damper rotor bars. Analytical Finite Element Simulation is also performed for the accurate prediction of the air gap flux characteristics of the 9-phase IPM machine under the rated operating conditions. Similarly, for the verification of the model, the full order model is simulated and induced EMFs on phase windings is compared with the Experimental observations. This approach of Fourier series approximation and q-d full order modeling is also extended to three machine configuration of 9-phase IPM machine and 9-phase induction machine to observe the significance of torque contribution from each machine sets which aids for the realization of better fault tolerance and increased reliability of the system.

For the extended speed/torque operation of 9-phase induction machine, the concept of Pole Phase Modulation is introduced to operate 9-phase induction machine as 9-phase, 4-pole or 3-phase, 12-pole configurations. With the new design method based on basic principle of turn and winding functions, both operation of the machine is examined at rated condition with the realization in Finite Elements. For the precise estimation of the parameters, different estimation methods are applied in both configurations and a comparative analysis is presented. The full order simulation is performed using MATLAB/Simulink and with the help of Finite Elements, the vector control is realized to verify the extended speed/torque operation for pole phase modulated induction machine.

MODELING, ANALYSIS AND PERFORMANCE OF VARIABLE SPEED NINE-PHASE ELECTRIC DRIVES

A Thesis

Presented to

The Faculty of the Graduate School

Tennessee Technological University

by

Amrit Gautam

In Partial Fulfillment

Of the Requirements of the Degree

MASTER OF SCIENCE

Electrical Engineering

December 2012

CERTIFICATE OF APPROVAL OF THESIS

MODELING, ANALYSIS AND PERFORMANCE OF VARIABLE SPEED NINE-PHASE ELECTRIC DRIVES

by

Amrit Gautam

Graduate Advisory Committee:

Joseph Ojo, Chairperson	Date
Ghadir Radman	Date
Ahmed Kamal	Date

Approved for the Faculty:

Francis Otuonye
Associate Vice President
for Research and Graduate Studies

Date

DEDICATION

This work is dedicated to my parents

ACKNOWLEDGEMENTS

I would like to express my deepest gratitude to the chairperson of my advisory committee, Dr. Joseph Ojo for his generous support, guidance and encouragement during the course of the research. I would also like to express my sincere thanks to Dr. Ghadir Radman and Dr. Ahmed Kamal for their effort in evaluating my work.

I am indebted to the office of the Center for Energy Systems Research (CESR) for the financial support during my Masters study in Tennessee Tech. I would also like to thank my supervisor for creating nice lab environment and special thanks goes to Mr. Robert Peterson, Mr Conard Murray and Mr. Tony Greenway for their invaluable support.

I would like to express my gratitude to my relatives and family in US for their care and support during my stay. I would also like to thank my lab members, Sosthenes Karugaba, Hossein Karimi, Kennedy Aganah, Jianfu fu, Meharagzi Abraham, Will Mefford, Mehdy Khayamy, Adeniyi Babalola, Mehari Bule, Waheed Oyeknami and Manideep Angirekula. My greatest appreciation goes to Mehdi Ramezani who helped me for the DSP and FPGA implementation for PWM generation in operation of 9-phase induction machine. I am also grateful to my roommates Bijaya Pokharel, Puran Adhikari and Melaku Mihret for their technical support and making my stay so pleasant.

Lastly, I offer my regards and blessings to all of those who supported me in any respect during the completion of the work.

TABLE OF CONTENTS

Page

Page

Page

Page

LIST OF TABLES

Page

LIST OF FIGURES

Page

Page

Page

Page

Page

Page

Page

Page

Page

Page

Page

Page

Page

Page

CHAPTER 1

INTRODUCTION

1.1 Introduction

This chapter presents brief introductory concepts of multiphase systems and their applications for varying speed and torque requirements. The primary focus of this thesis is on the design, modeling, analysis and performance of 9-phase electric drives. Firstly, a brief overview of multiphase systems is given followed by different transformations utilized in multiphase systems. Similarly, different stator connection strategies of 9-phase machine are discussed with introduction on pole phase modulation. Finally, the motivations and objectives behind the research are discussed with the outline of the thesis.

1.2 Overview of Multiphase Systems

The invention of power electronic converters has led to the increased interest in multiphase systems during the last two decades [1]. This increasing trend of research in multiphase drives has shown that those drives with phase numbers greater than three has various advantages over the 3-phase counterparts, such as harmonic current reduction, increase in per phase current without increase of per phase voltage, reduction of torque pulsations, increase of fault tolerance and greater number of degrees of freedom.

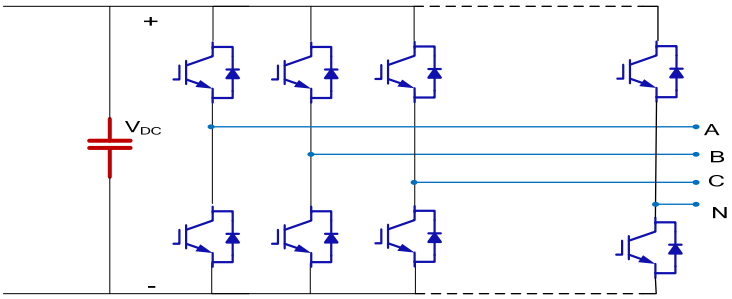

Figure 1.1 An N-phase two level multiphase inverter

In addition to these advantages, in machine with the concentrated windings, the control of fundamental as well as spatial low order harmonic components of magnetic field in air gap can be performed. The reduction of torque pulsations are performed by the analysis of the harmonic components greater than the fundamental component.

Additionally, the multiphase machine also has the advantages of noise reduction and higher efficiency. Similarly, utilization of more than 3-phases gives the freedom of splitting the power into various converter legs; hence, semiconductor switching can also be controlled. Figure 1.1 gives the typical example of *N*-phase two-level multiphase converter. Similarly, in case of multiphase converter, the control of switching allows the multiphase drive to operate in different configurations. From recent years, the concept of pole changing is also being utilized for multiphase drives to account for varying speed torque requirements.

The pole changing capability with the changing of number of phases can be visualized in 9-phase induction machine where, switching of the converters gives the change of poles and phases instead of reconfiguration of the windings to achieve the pole change [54, 55].

1.2.1 Transformations

The m-phase systems are transformed into equivalent orthogonal system for utilizing the energy conversion characteristics. The study of Electric machinery involves the study of different circuits in the relative motion. Unfortunately, it became difficult to analyze the ac machines at an early stage due to high number of coupling circuits. It was overcome in 1929 by R.H. Park, who formulated the transformation equations (Park's transformation) from actual 3-phase stator currents and voltages to different equivalent currents and voltages. This 3-phase transformation was extended by Stanley, Kron, Krause and Thomas to apply in different conditions.

The transformation of the variables in other equivalent circuits is adopted from the concept of the rotating reference frames. The rotating reference frames are of the central importance in the analysis of the electric machines. As described in [2], the variables of the 3-phase system can be transformed into an equivalent orthogonal system by transforming the real axes into the arbitrary plane which is referred as q-d-0 plane. Figure 1.2 shows the transformation of the 3-phases into equivalent q-d-0 plane where θ is the transformation angle and ω is the frequency of the transformation.

The 3-phase system now can be transformed into the q-d equivalent plane simply by using the transformation matrix:

$$T(\theta)=\frac{2}{3}\begin{bmatrix}\cos\theta & \cos(\theta-\alpha) & \cos(\theta-2\alpha)\\ \sin\theta & \sin(\theta-\alpha) & \sin(\theta-2\alpha)\\ 1/2 & 1/2 & 1/2\end{bmatrix} \tag{1.1}$$

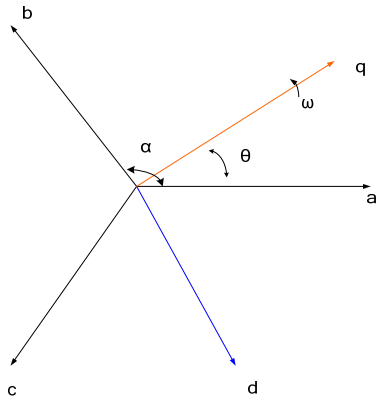

Figure 1.2 3-phase transformation into two dimensional q-d-0 plane

The 3-phase transformation was then extended to higher order phase systems. In [75], the transformation was extended to 5-phase systems, where the q-d reference frame transformation was utilized without any inclusion of harmonic components. In [16], the 5-phase transformation is adopted to analyze the effect of different harmonics. This basic concept can be generalized to a (2n+1)-phase motor, where it can be easily seen that there exist *n* orthogonal q-d spaces, where each odd harmonic with the order of less than (2*n*+1) of phase variables has its own q-d space. In other words, all the time harmonics, which can contribute to the torque positively, can be equivalently and orthogonally represented as dc components. Figure 1.3 shows the two orthogonal two dimensional spaces of 5-phase motor as described in [16], where, u,v…z defines the phase sequences of the motor.

As the number of phase increases, the harmonics that contribute to the total torque positively can be represented in greater number of q-d spaces. Taking into account of the 9-phase systems, there exists 4 orthogonal q-d space due to the effect of fundamental, 3rd harmonics, 5th harmonics and the 7th harmonics.

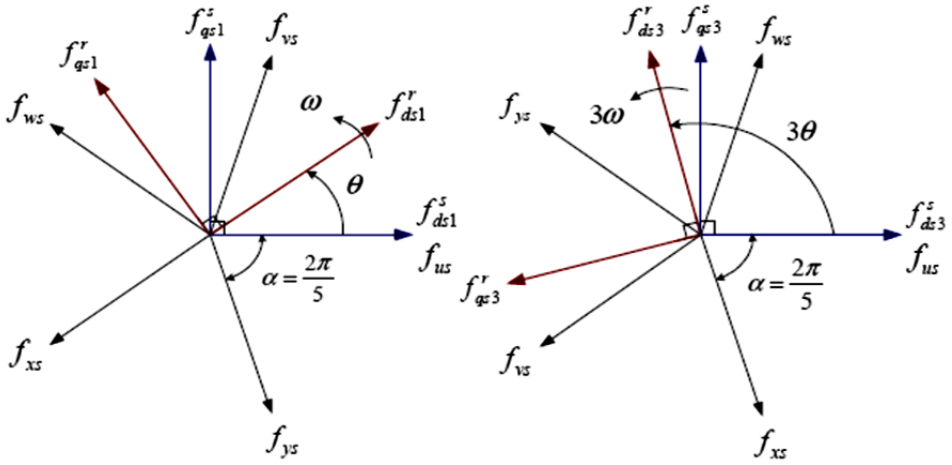

(a) (b)

Figure 1.3 Two orthogonal two dimensional spaces of 5-phase system (a) Fundamental (b) 3rd harmonics

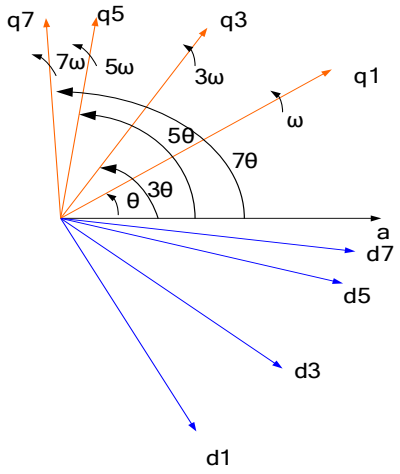

Figure 1.4 Four orthogonal spaces of 9-phase system

Figure 1.4 shows the orthogonal spaces in q-d frame obtained from the inclusion of higher order harmonics for 9-phase machines. With reference to Figure 1.4, the

transformation matrix with the inclusion of higher order harmonic terms can be defined as Equation (1.2) where, 'c' represents cosine, 's' denotes sine and α denotes the phase shift between the two adjacent phase of the 9-phase system.

$$T(\theta)=\frac{2}{9}\begin{bmatrix} c(\theta) & c(\theta-\alpha) & c(\theta-2\alpha) & c(\theta-3\alpha) & c(\theta-4\alpha) & c(\theta-5\alpha) & c(\theta-6\alpha) & c(\theta-7\alpha) & c(\theta-8\alpha) \\ s(\theta) & s(\theta-\alpha) & s(\theta-2\alpha) & s(\theta-3\alpha) & s(\theta-4\alpha) & s(\theta-5\alpha) & s(\theta-6\alpha) & s(\theta-7\alpha) & s(\theta-8\alpha) \\ c(3\theta) & c3(\theta-\alpha) & c3(\theta-2\alpha) & c3(\theta-3\alpha) & c3(\theta-4\alpha) & c3(\theta-5\alpha) & c3(\theta-6\alpha) & c3(\theta-7\alpha) & c3(\theta-8\alpha) \\ s(3\theta) & s3(\theta-\alpha) & s3(\theta-2\alpha) & s3(\theta-3\alpha) & s3(\theta-4\alpha) & s3(\theta-5\alpha) & s3(\theta-6\alpha) & s3(\theta-7\alpha) & s3(\theta\theta-8\alpha) \\ c(5\theta) & c5(\theta-\alpha) & c5(\theta-2\alpha) & c5(\theta-3\alpha) & c5(\theta-4\alpha) & c5(\theta-5\alpha) & c5(\theta-6\alpha) & c5(\theta-7\alpha) & c5(\theta-8\alpha) \\ s(5\theta) & s5(\theta-\alpha) & s5(\theta-2\alpha) & s5(\theta-3\alpha) & s5(\theta-4\alpha) & s5(\theta-5\alpha) & s5(\theta-6\alpha) & s5(\theta-7\alpha) & s5(\theta-8\alpha) \\ c(7\theta) & c7(\theta-\alpha) & c7(\theta-2\alpha) & c7(\theta-3\alpha) & c7(\theta-4\alpha) & c7(\theta-5\alpha) & c7(\theta-6\alpha) & c7(\theta-7\alpha) & c7(\theta-8\alpha) \\ s(7\theta) & s7(\theta-\alpha) & s7(\theta-2\alpha) & s7(\theta-3\alpha) & s7(\theta-4\alpha) & s7(\theta-5\alpha) & s7(\theta-6\alpha) & s7(\theta-7\alpha) & s7(\theta-8\alpha) \\ 1/2 & 1/2 & 1/2 & 1/2 & 1/2 & 1/2 & 1/2 & 1/2 & 1/2 \end{bmatrix} \quad (1.2)$$

1.2.2 Connections of 9-Phase Machine

Conventionally, in the operation of the 3-phase machines, it is observed that the machine can be operated as star or delta connection schemes. It has also been observed that for any machine with odd number of phases, there exists (m+1)/2 ways with which the stator windings can be connected.

Thus for the 9-phase machines there exist five different configurations with which the stator winding can be connected and thus producing different magnitudes and phase angles of the voltages across the stator phase windings. These connections are described in this section with the possible phase voltage across each winding.

a. One star connection: This connection is similar to the star connection in 3-phase machines as shown in Figure 1.5. The phase voltages in this case are

$$v_{as}=V_m\cos(\theta+\phi_0) \quad (1.3)$$

$$v_{es}=V_m\cos(\theta+\phi_0-4\beta) \quad (1.4)$$

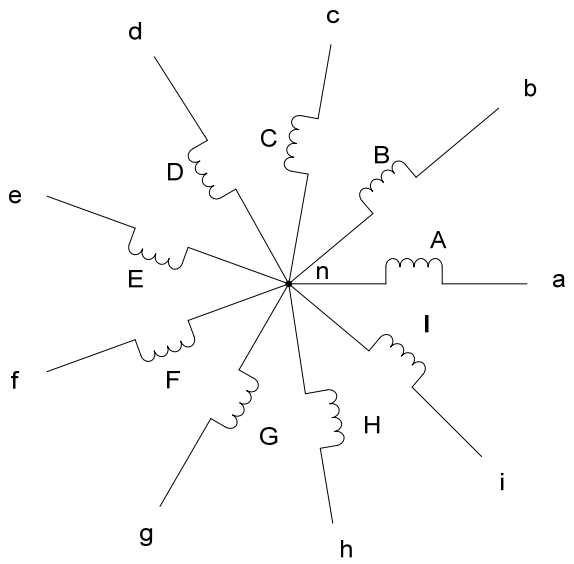

Figure 1.5 One Star Connection

$$v_{bs} = V_m \cos(\theta + \phi_0 - \beta) \tag{1.5}$$

$$v_{fs} = V_m \cos(\theta + \phi_0 - 5\beta) \tag{1.6}$$

$$v_{cs} = V_m \cos(\theta + \phi_0 - 2\beta) \tag{1.7}$$

$$v_{gs} = V_m \cos(\theta + \phi_0 - 6\beta) \tag{1.8}$$

$$v_{ds} = V_m \cos(\theta + \phi_0 - 3\beta) \tag{1.9}$$

$$v_{hs} = V_m \cos(\theta + \phi_0 - 7\beta) \tag{1.10}$$

$$v_{is} = V_m \cos(\theta + \phi_0 - 8\beta) \tag{1.11}$$

$$\beta = 2\pi/9 \tag{1.12}$$

where, V_m and ϕ_0 gives the peak voltage magnitude and initial angle, respectively.

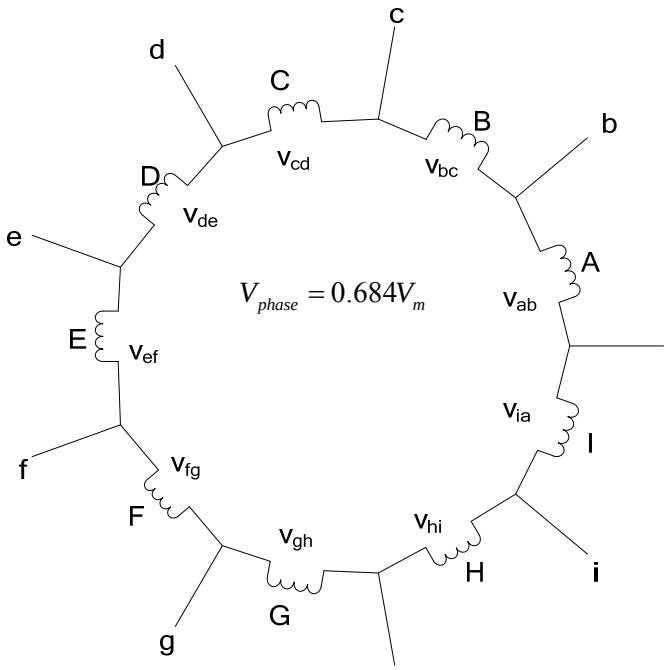

Figure 1.6 Connection A-B-C-D-E-F-G-H-I of 9-phase machine

b. Connection A-B-C-D-E-F-G-H-I: This connection is illustrated in Figure 1.6. If the individual windings of the machine are visualized, the phase voltage of any winding is equal to the line to line voltages connected across the particular winding. Hence, the phase voltage in this connection is not the same as the star connection. Considering the connection as in Figure 1.6,

$$v_{ab} = v_{as} - v_{bs} = V_m\left(\cos(\theta + \phi_0) - \cos(\theta + \phi_0 - \beta)\right) \tag{1.13}$$

Hence,

$$v_{ab} = v_{as} - v_{bs} = V_{mab}\cos(\theta + \phi_0 + \phi_{ab}) \tag{1.14}$$

where, $V_{mab} = V_m\sqrt{2(1-\cos\beta)} = 0.684V_m$

$$\phi_{ab} = \tan^{-}\left(\frac{\sin\beta}{1-\cos\beta}\right) = 70^0 = \frac{7\pi}{18}rad \tag{1.15}$$

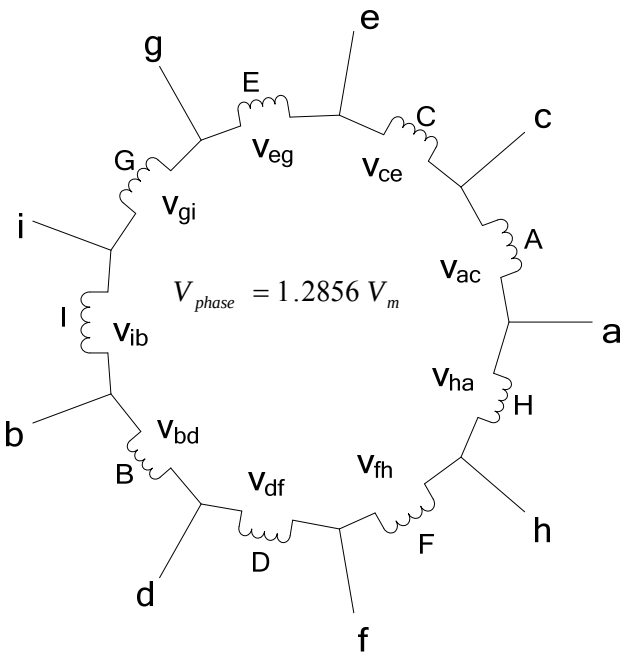

Figure 1.7 Connection A-C-E-G-I-B-D-F-H of 9-phase machine

Hence, the phase voltage v_{ab} is given as

$$v_{ab} = 0.684 V_m \cos\left(\theta - \phi_0 + \frac{7\pi}{18}\right) \tag{1.16}$$

Similarly, the other phase angles are 30^0, -10^0, -50^0, -90^0, -130^0, -170^0, 150^0 and 110^0, for the line-to-line voltages v_{bc}, v_{cd}, v_{de}, v_{ef}, v_{fg}, v_{gh}, v_{hi} and $v_{ia,}$, respectively.

c. Connection A-C-E-G-I-B-D-F-H: This connection is also similar to the previous connection with the winding displaced as given in Figure 1.7. From the figure,

$$v_{ac} = v_{as} - v_{cs} = V_m\left[\cos(\theta + \phi_0) - \cos(\theta + \phi_0 - 2\beta)\right] = V_{mac}\cos(\theta + \phi_0 + \phi_{AC}) \tag{1.17}$$

$$V_{mac} = \sqrt{2(1 - \cos 2\beta)}V_m = 1.2856 V_m$$

$$\phi_{AC} = \tan^{-1}\left(\frac{\sin 2\beta}{1 - \cos 2\beta}\right) = 50^0 = \frac{5\pi}{18} \tag{1.18}$$

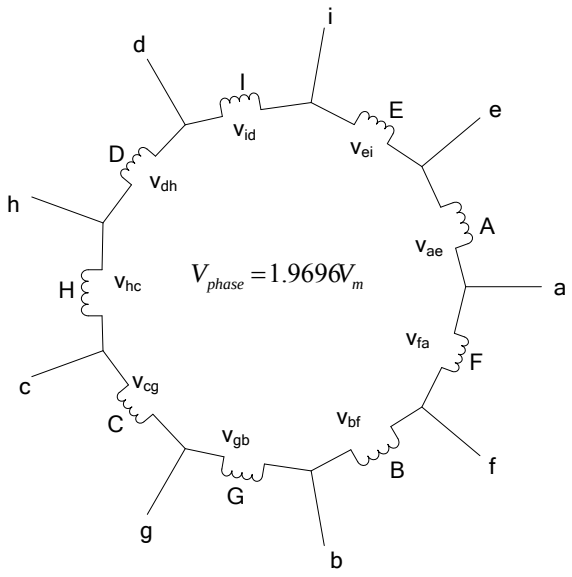

Figure 1.8 Connection A-E-I-D-H-C-G-B-F of 9-phase machine

Hence, the phase voltage v_{ac} is given as

$$v_{ac} = 1.2856V_m \cos\left(\theta + \phi_0 + \frac{5\pi}{18}\right) \tag{1.19}$$

Similarly the phase angles for other line voltages will be -30^0, -110^0, 170^0, 90^0, 10^0, -70^0, -150^0 and 130^0, for the line-to-line voltages v_{ce}, v_{eg}, v_{gi}, v_{ib}, v_{bd}, v_{df} , v_{fh} and v_{ha}, respectively.

d. Connection A-E-I-D-H-C-G-B-F: This type of connection is drawn and the layout is given in Figure 1.8. From the figure,

$$v_{ae} = v_{as} - v_{es} = V_m\left[\cos(\theta + \phi_0) - \cos(\theta + \phi_0 - 4\beta)\right] = V_{mae}\cos(\theta + \phi_0 + \phi_{AE}) \tag{1.20}$$

$$V_{mae} = \sqrt{2(1-\cos 4\beta)}V_m = 1.9696V_m$$

$$\phi_{AE} = \tan^{-1}\left(\frac{\sin 4\beta}{1-\cos 4\beta}\right) = 10^0 = \frac{\pi}{18} \tag{1.21}$$

Hence, the phase voltage v_{ae} is given as

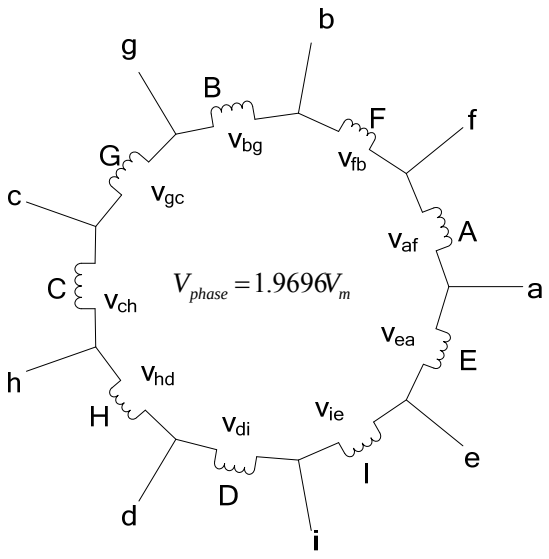

Figure 1.9 Connection A-F-B-G-C-H-D-I-E of 9-phase machine

$$v_{ae} = 1.9696V_m \cos\left(\theta + \phi_0 + \frac{\pi}{18}\right) \tag{1.22}$$

Similarly, the other phase angles will be -150^0, 50^0, -110^0, 90^0, -70^0, 130^0, -30^0, and 170^0, for the line-to-line voltages v_{ei}, v_{id}, v_{dh}, v_{hc}, v_{cg}, v_{gb} , v_{bf} and v_{fa},, respectively.

e. Connection A-F-B-G-C-H-D-I-E: The connection diagram of this configuration is given in Figure 1.9. From the figure,

$$\begin{aligned} v_{af} = v_{as} - v_{fs} &= V_m\left[\cos(\theta + \phi_0) - \cos(\theta + \phi_0 - 5\beta)\right] \\ &= V_{maf}\cos(\theta + \phi_0 + \phi_{AF}) \end{aligned} \tag{1.23}$$

$$V_{maf} = \sqrt{2(1-\cos 4\beta)}V_m = 1.9696V_m$$

$$\phi_{AF} = \tan^{-1}\left(\frac{\sin 5\beta}{1-\cos 5\beta}\right) = -10^0 = -\frac{\pi}{18} \tag{1.24}$$

Hence, the phase voltage v_{af} is given as

$$v_{af} = 1.9696V_m \cos\left(\theta + \phi_0 - \frac{\pi}{18}\right) \quad (1.25)$$

The other phase angles will be will be 30^0, -130^0, 70^0, -90^0, 110^0, -50^0, 150^0 and -10^0, for the line-to-line voltages v_{fb}, v_{bg}, v_{gc}, v_{ch}, v_{hd}, v_{di} , v_{ie} and $v_{ea,,}$ respectively.

The following configurations have the same line-to-line magnitudes with opposite phase shifts:

A-B-C-D-E-F-G-H-I and A-I-G-F-E-D-C-B have the same magnitude of 0.684 p.u. and phase angles 70^0 and -70^0, respectively.

A-C-E-G-I-B-D-F-H and A-H-F-D-B-I-G-E-C have the same magnitude of 1.2856 p.u. and phase angles 50^0 and -50^0, respectively.

A-E-I-D-H-C-G-B-F and A-F-B-G-C-H-D-I-E have the same magnitude of 1.9696 p.u. and phase angles 10^0 and -10^0, respectively.

f. Three Phase Connections:

The following configurations will results into three 3-phase delta connections: A-D-G, B-E-H and C-F-I. These will give the line-to-line voltages with the same magnitude 1.7321 p.u. and phase angles of 30^0, 10^0 and 50^0, respectively.

1.2.3 Pole Phase Modulation

The 9-phase squirrel-cage induction motor designed for 4-pole operation can also be utilized to operate in 3-phase, 12-pole configuration by rearranging the stator winding connections using the pole phase modulation technique (PPM). The 9-phase, 4-pole

configuration can be used for extended high speed and low torque requirement, whereas the 3-phase, 12-pole arrangement can be utilized for low speed and high torque applications. By switching from one stator winding configuration to another, the 9-phase induction machine can be used for high torque, low speed and extended high speed range and low torque requirements in applications such as the electric vehicle and high speed elevators. Figure 1.10 shows the 3-phase, 12-pole, stator winding connections reconfigured from the 9-phase, 4-pole stator winding connections. The pole phase modulation scheme can be explained from the torque capability graph given in Figure 1.11. As shown in figure, for low speed, higher developed torque is produced utilizing the 3-phase connection, and as speed increases, the 9-phase stator winding arrangement produces a higher torque.

1.2.4 DSP-FPGA Interfacing for 9-phase Machine Control

A control system is proposed using the TMS320C6713 floating point DSP and Xilinx Spartan 3E FPGA with Nexys 2 board to operate and control the 9-phase machine. Figure 1.12 shows the proposed control algorithm where the control program is written in DSP in C programming language using Code Composer Studio. There exists duplex communications between DSP and FPGA with the modulation index obtained from DSP to output the PWM signals from FPGA by comparison with triangular carrier. The PWM signals thus obtained is sent to PWM generation board, where the switching signals are generated to drive the 9 leg inverter.

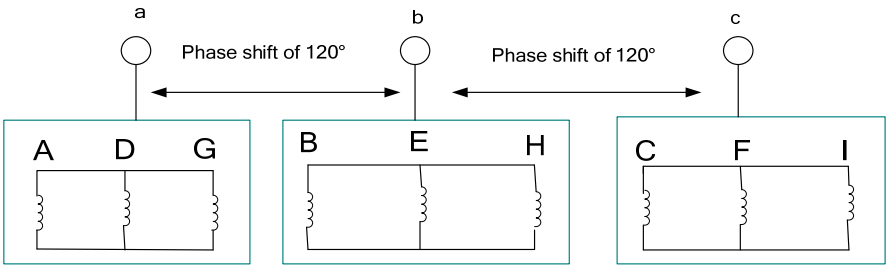

Figure 1.10 3-phase, 12-pole, stator winding connections reconfigured from the 9-phase, 4-pole stator winding connections.

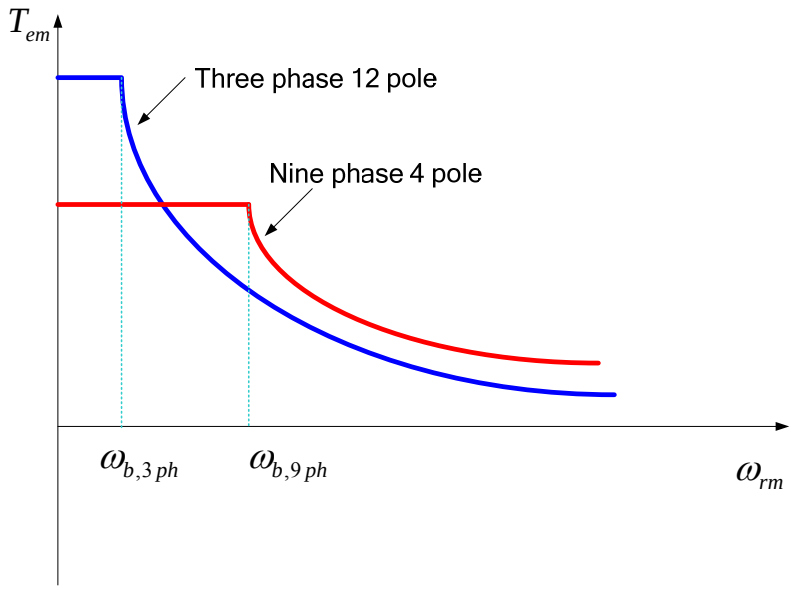

Figure 1.11 Torque capability of the pole phase modulated induction machine

The speed and current sensors are used to sense the speed and current and fed into FPGA through Analog to Digital converters. Finally, the communication between FPGA and DSP ensures the real time digital processing of the system for varying operating conditions.

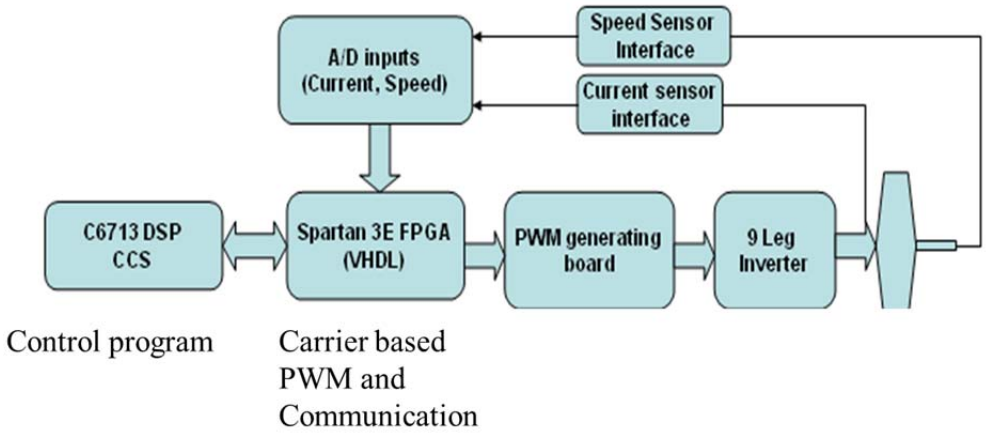

Figure 1.12 Control algorithms for DSP-FPGA interfacing for 9-phase machines

1.3 Motivation and Objectives of the Thesis

The operation of multiphase machine for its potential advantages of greater reliability, extended speed/torque capability and improvement of torque requires the better understandings of utilization of higher order harmonics, mode of operation and torque capability in these modes. There exists significant research in the literatures but due to the large number of coupled variables, proper modeling and analysis of high phase order machines is a challenging task. The existing works are full of assumptions and proper utilization of higher order harmonics is neglected, particularly when dealing with the generalization in modeling and performance analysis of high phase order machines. This thesis serves to fill the gap that exists on the modeling and performance analysis of the machine by generalizing the model of the machine by use of Fourier series approximations of the winding functions. The advantages of multiphase machines in

torque improvement, increased reliability and extended torque capability are also analyzed analytically.

The major objectives of the thesis are as follows:

- To model and analyze the contribution of higher order harmonics in overall system dynamics of the 9-phase Interior Permanent Magnet (IPM) machine using Fourier series approximations of winding functions.
- To perform the full order q-d model including harmonics for 9-phase IPM machine with the inclusion of damper rotor bars using winding functions of stator and rotor and the analysis of induced EMF due to permanent magnet.
- To perform the analysis of 3 machine configuration of 9-phase IPM machine with Fourier series approximations of winding functions, full order q-d model and the analysis of induced EMF on each machine sets due to permanent magnet.
- To perform the air gap flux analysis of 9-phase IPM machine considering the effects of permanent magnet flux and armature currents using analytical finite element simulations.
- To perform the full order modeling, design and simulation of 9-phase induction machine operated as pole phase modulation for extended speed/torque capability.
- To perform the finite element realization of pole phase modulation of 9-phase induction machine with torque capability, performance and vector control.
- To perform the modeling and simulation of 9-phase induction machine connected as three sets of 3-phase machines to observe the individual torque contribution.

- To develop a hardware system implementing Digital Signal Processor (DSP) and Field Programmable Gate Array (FPGA) in order to produce the switching signals to drive the 9-phase inverter.

1.4 Thesis Outline

This thesis is categorized into 10 chapters. Chapter 1 presents the overview of multiphase systems and recent trends in multiphase drives. The transformations for resolving the system into two variables in different phase systems are presented. Similarly, this chapter also presents the research motivations and objectives of the thesis which is followed by the outline of the thesis. In Chapter 2, brief Literature Review is presented to outline the previous works performed in the field of multiphase systems.

In Chapter 3, Fourier series approximation of winding function and magnet flux density is utilized to model the 9-phase interior permanent magnet machine with inclusion of higher order harmonics to observe their effect in overall system performance. With the approximation of winding function and air gap function with Fourier series, the derivation of inductance matrix in real variables is presented using step by step integrations. The contribution of the harmonic components in the performance parameters and overall torque is investigated with number of calculation steps. Similarly, the air gap field analysis is also presented in this chapter with finite element simulations.

Chapter 4 presents the full order q-d modeling and simulation of 9-phase IPM machine using actual turn and winding functions with the inclusion of high order harmonics. Initially, the turn and winding functions of stator and rotor bars are

transformed into stationary reference frame graphically. With the help of model equations, the inductances are derived in the rotor reference frame by using the integration of the transformed winding functions. The full order simulation is performed with the help of stator and rotor winding functions to study the transient and steady state results. Similarly this chapter also deals with the air gap flux analysis of the 9-phase IPM machine using magnetic circuit concepts, where the fields caused by the armature currents and permanent magnet flux in the air gap are analyzed using finite element simulations.

In order to realize the equivalent three phase analysis of the 9-phase systems, the three machine configuration of IPM machine is derived using the Fourier approximations of winding function and contribution of each machine set to the overall performance is analyzed in Chapter 5. Similarly, the q-d full order model is also implemented in the three machine configuration to observe the performance parameters of each machine with the idea of the induced EMF on each machine windings.

Chapter 6 presents the new method of modeling and simulation of 9-phase induction machine for pole phase modulation scheme. The realization of PPM to operate the machine as 9-phase, 4-pole and 3-phase, 12-pole is presented with the help of winding functions, winding designs and finite element simulations. Different estimation techniques are utilized to derive the parameters of the 9-phase induction machine in pole phase modulated schemes. The coupled model of the machine is performed with the help of parameters derived and the simulation of both operations is carried out. The comparison of the results obtained while operating the machine in pole phase modulation are also carried out.

In Chapter 7, connection of 9-phase induction machine with the help of the three sets of 3-phase power electronics converters is discussed. The 3-phase system is connected to three sets of power electronics converters and these converters supply the three sets of 3-phase voltages of 9-phase induction machine shifted by angle of 60/*n*, where *n* is the number of 3-phase sets. The contribution of each machine torque is observed for the overall torque production of the machine. Similarly steady state analysis of 9-phase induction generator is also performed operating as three machine configuration connected to converters and different loads.

The extended torque/speed operation of 9-phase induction machine is realized in Chapter 8 with the finite element realization for torque capability in different connection schemes. With the development of the rotor field orientation scheme, the stator and rotor model is performed in finite element Software. Similarly, with the help of LUA rotor field orientation is realized and torque capability is studied under pole phase modulation and other connection schemes.

A brief overview of the progress made on experiments using DSP and FPGA interfacing in producing 9-phase switching signals is presented in Chapter 9. The experimental setup is presented and final results on the experiments are discussed in this chapter.

Finally, Chapter 10 gives the concluding remarks and summary of the work performed. Moreover, future recommendations for the work are also discussed with the contributions made from the research work.

CHAPTER 2

LITERATURE REVIEW

A survey of historical developments related to this thesis is presented in this chapter. The chapter consists of four sections. In Section 2.1, the development of multiphase systems is reviewed with the considerations of multiphase converters, 5-phase, 6-phase, 7-phase, 9-phase and higher order systems. Section 2.2 discusses the progress made on parameter estimation and modeling of multiphase drives. Similarly, Section 2.3 discusses a survey of pole phase modulation technique developed for pole changing operation of drives for varying speed and torque requirements. Finally in Section 2.4, the developments on DSP-FPGA interfacing specially designed to interface electrical drives are discussed.

2.1 Development of Multiphase Systems

The key origin of the research in multiphase machines started in late 1950s, when the development of inverter fed ac-drives were in initial stage. The 3-phase inverter operation has the particular problem of the low frequency torque ripple. An increase in number of phases of the machine appeared to be the best solution, when it was realized that the lowest torque ripple in an *n*-phase system is caused by the time harmonics of the supply of the order of $2n \pm 1$, i.e., its frequency is $2n$ times higher than the supply frequency. Hence, significant efforts had been put forth in the development of 5-phase

and 6-phase variable speed drives supplied from voltage and current source inverters until mid-80s. The other main reason for the development of the multiphase machine is the better fault tolerance and the possibility of splitting the motor power across a higher number of phases, thus reducing the converter switching which is the method of power segmentation [1].

2.1.1 Development of Multiphase Converters

Recent developments in the area of multiphase variable speed drives, for potential applications like electric aircraft, electric ship propulsion, electric and hybrid-electric vehicles, and other high power industries, have led to a corresponding development of pulse width modulation (PWM) schemes for multiphase inverters used in these drives. A generalized form of space vector modulation for *n*-phase system is developed in [3], for operation of the machine in pole phase modulation scheme with the 9-phase machine implementation. Similarly, a novel analysis is proposed in [4], on a multiphase SVPWM in order to realize a non-sinusoidal phase voltage. Based on the concept of an arbitrary reference voltage vector, a five-phase ac motor is synthesized in terms of the applying times of available switching vectors in a five-phase PWM inverter. The problem of the space vector modulation (SVM) of multiphase inverters is solved introducing the concept of reciprocal vector in [5]. The full exploitation of the dc input voltage and the modulation of voltage space vectors in different d–q planes can be achieved simultaneously using this approach. The discontinuous space vector PWM (DPWM) for a five-phase voltage source inverter is presented in [6], with the utilization of large and

medium vectors to synthesize the input reference in discontinuous mode. Similarly, a multi-frequency output voltage generation with arbitrary values of various sinusoidal components is developed in [7]. The scheme is experimentally verified for 5-phase voltage source inverter. A realization of three to 9-phase matrix converters is performed in [8], where PWM technique is developed for the ac–ac converter named as a non-square three-to-9-phase matrix converter. In [9], an FPGA implementation of space vector pulse width modulation (SVPWM) algorithm for multilevel multiphase voltage source converters is presented, with the implementation for 5-phase motor. A comprehensive relation between the multiphase carrier based PWM and SVPWM is established in [10] in terms of modulation signals and space vector sectors. Similarly, in this paper, distribution of zero vectors is also discussed, leading to different types of modulation schemes.

2.1.2 Development of 5-phase Systems

With the development of multiphase converters, significant research has been accomplished to realise the 5-phase machine scheme in industrial applications. The main focus on development of these machines is to utilize the higher order harmonics that contribute to the resultant torque positively. The general model for the 5-phase induction machine is performed in [11], allowing harmonics in air gap field. Considering the higher order time and space harmonics, and with the help of the general equations, the behaviour of the machine is determined in any operating condition. The behaviour of 5-phase induction machine is studied in [12], with a vector control method developed based on

the $q_1d_1q_3d_{3n}$ reference frame using the independent control of both flux and torque. The DSP implementation is also performed in TMS320C32 DSP which shows that the control by using the combined fundamental and 3rd harmonic current achieves the desired current and flux waveforms. The same concept of vector control is extended to 5-phase permanent magnet motor in [13], where the effect of the 3rd harmonic currents in the overall torque production is analyzed with experimental results. It is also shown that the performance of the 5-phase PMSM is better than the BLDC counterpart due to the controllability and compatibility with the vector control technique in the field weakening regions. Similarly, the 5-phase PMSM analyzed for the 3rd harmonic injection in [14], where the equivalent circuit is developed using the model and experimental results are compared with the simulation results with the combined effect of fundamental and 3rd harmonic currents. Similarly, due to the potential advantage of higher order harmonics, analysis and simulation of 5-phase synchronous reluctance motor is presented in [15], with the inclusion of 3rd harmonic of air gap. With the help of d-q model of the motor, computer simulation is carried out and results are compared with experiments. A synchronous frame current control of 5-phase PMSM is introduced in [16, 17], where the harmonics of current and voltage which can contribute to the torque positively are equivalently expressed as dc components under asymmetric fault conditions. With the help of simulation and experiments, each contribution of individual harmonics is analyzed. Furthermore, for the analysis of fault tolerant 5-phase drive, fault-tolerant control techniques for 5-phase permanent magnet motors with trapezoidal back electromotive forces under various open-circuit conditions is analyzed in [18].

The 5-phase machines thus developed are extended to multi-motor drives connected in series. A 5-phase synchronous reluctance machine is connected in series in [19], with 5-phase induction machine and the verification of decoupling dynamics is presented. Similarly, in [20], two 5-phase induction motors are connected in series and a complete decoupling of flux/torque producing currents is realized between the two machines.

2.1.3 Development of 6-phase and Dual Stator Systems

With the development of n-leg inverter system as specified in [3], the development of the multiphase system advances into the 6-phase and dual stator systems. Many of the 6-phase systems are analyzed with the concept of the split phase systems with the splitting of 30 degrees between the two sets of 3-phase systems. This approach is utilized in [21], where a d-q model of 6-phase induction machine is derived with the analysis of the slot leakage coupling between the two 3-phase groups. Similarly the simple indirect FOC scheme for operation and control of a 6-phase induction machine is analyzed in [22] with an arbitrary displacement between the two 3-phase winding sets. It is also shown that the independent control of the two stator winding currents allows for the elimination of the problem of the unbalanced current sharing between the two 3-phase winding sets. Similarly, the DTC solution for dual 3-phase induction motor drives is implemented in [23], to simplify the control scheme and improve the dynamic performance by elimination of the current control loops. It was experimentally shown that the good response of stator flux and torque in both constant torque region and field

weakening region can be achieved by using the DTC scheme. In [24], 3rd harmonic injection for 6-phase permanent magnet synchronous machine and its effects are analyzed. Here, it is shown that the creation of an additional rotating field with angular speed equal to the fundamental angular speed has the effect on the output power capability (OPC) of the interior PMSM. Similarly, in [25], the establishment of direct torque control of split phase induction machine is presented. The two new methods of DTC technique for an SPIM is developed and it was shown that the torque ripple of the motor can be reduced significantly compared to 3-phase DTC. In [26], the concept of vector decomposition used for the dual 3-phase machine is developed where the voltages and currents of original six dimensional vector space are mapped into three two dimensional orthogonal subspaces. This gives the machine model as three sets of decoupled equations. Similarly, a new space vector PWM technique is also developed based on the vector space decomposition. It is shown that the existence of zero sequence component provides the optimum current regulation of the multiphase machine. In [27], the 2-motor configuration is extended to 6-phase two motor configuration for decoupled control. Here, 6-phase induction machine is used in series with 3-phase induction machine driven from a 6-phase inverter. Full decoupling of the two machines is realized by using the vector control. In [28], the torque density improvement of a 6-phase induction motor with 3rd harmonic current injection is discussed. Here it is shown that the injection of 3rd harmonic zero sequence components in phase current greatly improves the machine torque density. Analytical, finite-element, and experimental results are presented to show the system operation and to demonstrate the improvement on the torque density.

2.1.4 Development of 7-phase Systems

The increasing trend of research in multiphase systems was also extended to 7-phase systems in some literatures. In [29], control of multiphase machine with odd number of phases under open-circuit phase fault is analyzed for 7-phase induction motor. The mathematical analysis is based on the space vector representation of the multiphase system and is valid either in transient or steady-state operating conditions. In [30], easy-to-implement control strategies are developed when a seven-phase axial flux permanent magnet machine is supplied by a seven-leg voltage source inverter in fault operation mode. In this case, using a vectorial multi-machine description, a seven-phase machine presenting a heightened ability to be controlled with one or two open-circuited phases has been designed and new current references are calculated to avoid high-torque ripples using vectorial approaches.

2.1.5 Development of 9-phase Systems

With the evolution of the multiphase machines and the concept to utilize the higher harmonics of air gap, 9-phase systems were developed in recent years. In [31], design, test and harmonic analysis of 9-phase armature windings is performed. A harmonic analysis of the designed winding in induction machine is also performed in this paper. In [32], a 9-phase permanent magnet synchronous motor drive system is developed based on multiple 3-phase voltage source inverters. The mathematical model is simplified and drive system is controlled by using the d-q control theory. Similarly, [33] presents the

study of different configurations of an axial-flux 9-phase concentrated-winding permanent-magnet synchronous generator for direct-drive wind turbine. Here, an optimization process is utilized to minimize the total active mass, maximize the power factor and also validation and measurements are performed in a small scale prototype. In [34], a fully generalized lumped parameter d-q model of an n phase synchronous machine is developed along with a multiple harmonic synchronous reference frame control technique implemented using a carrier based pulse width modulator. The analytical machine model is verified analytically through the characterization of a 9-phase synchronous machine prototype.

2.1.6 Development of Higher Phase Order Systems

To get the advantage of the higher phase order, research and analysis is still on-going for higher phase order systems. In [35], an n-phase PMSM is analyzed for the generation of optimal current references in normal or fault mode (open-circuited phases). It also proposes a novel way of generating optimal current references in real time in order to obtain a constant torque regardless of the number of open-circuited phases of an *n*-phase PMSM. An indirect vector control scheme with an improved flux pattern using 3rd harmonic injection is developed in [36], for the case of 11-phase induction machine. An improved machine power density was realized by independently controlling both flux and torque and to generate a nearly rectangular air-gap flux.

2.2 Parameter Estimation of Multiphase Machines and Modeling

The electromagnetic design of an induction motor follows the determination of the inductor motor parameters to be used to analyze the motor performances (torque, current, efficiency and so on). Several patent applications are also filed for the accurate determination of the induction machine parameters [37]. The fastest and viable approach is the use of experimental method to determine the inductance parameters; however, this method is based on measurements and approximation. New methods are developed in [38, 39] which give the precise estimation of the parameters from the experimental observation and the magnetic analysis of the structure. Magnetic field analysis is performed in [40] to determine all the parameters of the machine including the coupled parameters. Similarly in [41, 42], a finite element approach is developed for the model which utilizes the analysis of the model using finite element simulations.

The modeling of the 3-phase machine in arbitrary reference frame is performed in [2] by using reference frame transformation. In [43], modeling and control of 5-phase induction machine with the inclusion of 3rd harmonics is performed. Similarly, in [44], modeling and analysis of dual stator induction machine is performed and contribution of 3rd harmonic current injection is analyzed. The modeling of 5-phase permanent magnet synchronous machine is performed in [14] with the inclusion of effects of 3rd harmonic injection. In [45], both stator and rotor circuits are modeled by the set of only four coupled differential equations which are the d-q model of the machine. The model equations are utilized to model any number of rotor bars with skewing. Modeling of 3-

phase induction machine under rotor field orientation is realized in [46] using finite element analysis.

2.3 Development of Pole Changing Operation of Induction Machine

A significant research is on-going to realize the advantage of multiphase machine to operate in varying speed torque characteristics. With the invention of electronic pole changing efforts has been made to utilize the machine with the varying number of poles and phases. The speed variation using the pole changing concept without changing the number of phases is utilized in the conventional methods like Dahlander or pole amplitude modulation (PAM) scheme, where number of phases of the stator windings at both speed ranges is the same [47]. The pole changing capability of a four pole machine is investigated in [48]. The windings are reconfigured such that the machine operates as 4-pole until the constant power region, thereafter it acts as 2 pole machine. As a result the operating speed of the motor doubles from the switch of the pole number. Similarly, in [49] comparison of the power and torque capability of pole changing induction drive is performed. It also compares the power and torque capability of this drive with conventional four-pole and two-pole induction machine drives. Similarly, in [50], a new six-phase pole-changing induction motor drive is proposed to extend the constant-power operating range for electric vehicle application. Both phase shifts between two references and between two carriers of the six-phase PWM inverter are proposed to achieve electronic pole changing and harmonic suppression. In [51], a new double layer 3-phase 4 to 6 pole-changing winding, with 48 slots and 6 terminals is realized. A 2D FEM field-

circuit models is developed to simulate the operation of the experimental model equipped with the newly proposed winding. In [52], the extension of the speed-control range up to nine times the base speed through online reconfiguration of the motor windings is realized. It also deals with the switchover of the windings, either from one pole to another pole which causes small transients with the application in electrical vehicle drives. However, for the additional degree of freedom, the number of phases is also changed in modern designs using the principles of stator winding pole phase modulation (PPM) [53], In earlier works the stator winding design considerations using the pole phase modulation schemes have been proposed [53, 54]. Several patent applications also have been granted which cover the (PPM) techniques. [55, 56]. In order to realize the varying torque and speed operation, the pole phase modulation is realized in [53], where a general winding design rule for the PPM of induction machines is proposed. With the example of three types of windings viz. conventional winding machine, toroidal winding machine and dual-rotor toroidal winding machine operated in the same mode the comparison is made by using the finite element software JMAG-studio. The results show that both conventional winding machine and dual-rotor toroidal winding machine present good performances if pole phase modulation is performed. In the same way, in [57], pole phase modulation is realized in 9-phase, 4-pole induction machine where a method is presented for the accomplishment of a 12/4-pole change by modeling as two independent machines on same load producing independent torque. The pole changing is accomplished in this paper by increase of the torque of one machine and decreasing the torque of another one.

2.4 FPGA-DSP Interfacing and Control

In order to realize the control of electrical machines with the higher phase orders, different DSP and FPGA based control systems are implemented in literatures. In [58], the investigation of new space-vector PWM (SVPWM) techniques suitable for 6-phase machine is developed. The proposed system is carried out on a 15-kW prototype machine and using a low-cost fixed-point TMS320F240 digital signal processor. Similarly, in [59], the design, implementation, and test of an industrial multiprocessor controller based on a floating-point digital signal processor (DSP) and a FPGA, to operate on a 150-kVA back-to-back three-level neutral-point-clamped voltage source converter is developed to be utilized for wind turbine applications. In [60], implementation of digital controllers using field-programmable gate array (FPGA) components is presented. To this purpose, a variety of current control techniques, which is applied to alternating current machine drives, is designed and implemented with the realization of ON-OFF controllers and PI controllers. In [61], a new approach using field-programmable gate array (FPGA) to implement a fully digital control algorithm of active power filter (APF) is proposed including synchronous-reference-frame transform, low-pass filter, 3-phase phase-locked loop, inverter-current controller, etc. [62] reviews the state of the art of field programmable gate array (FPGA) design methodologies with a focus on industrial control system applications. The direct torque control for induction motor drives and the control of a diesel-driven synchronous stand-alone generator is with the help of fuzzy logic by interfacing with FPGA. In [63], the back to back neutral point clamped (NPC) converter is realized with the use of DSP and FPGA interfacing. The control electronic

platform assembly, the distribution of the tasks between the two selected processors, a floating-point DSP and an FPGA, and the programming of these devices is performed to utilize the control of electronic systems as applicable to wind turbines. Similarly in [64], a fully digital controller based on multiple DSP and FPGA is proposed for parallel operated cascaded multilevel inverters for use in Flexible AC Transmission Systems.

CHAPTER 3

MODELING AND ANALYSIS OF 9-PHASE INTERIOR PERMANENT MAGNET (IPM) MACHINE USING FOURIER SERIES APPROXIMATION

3.1 Introduction

In this chapter, the Fourier series approximated modeling of 9-phase interior permanent magnet machine is performed keeping into account the different harmonic components of the winding function and air gap field flux due to magnet. For better torque improvement, the study of the individual harmonic contribution needs to be analyzed in the case of multiphase machines. By generalizing the concept given in [16] to a (2*n*+1) phase system, it is observed that there exists *n* orthogonal d-q spaces where each odd harmonic with order of less than (2*n*+1) can be expressed equivalently as dc components. This concept gives the analysis of fundamental, 3rd harmonics, fifth and 7th harmonics in 9-phase motor to contribute to the resultant torque. As described in Chapter 1, four rotating frames are also utilized for this analysis, one rotating at fundamental frequency and other three rotating at three times, five times and seven times the fundamental frequency, respectively. The self-harmonic and inter-harmonic inductances are derived using this concept with their contribution to the resulting torque of the machine. Similarly, the air gap analysis of the machine due to armature current and permanent magnet flux is analyzed taking into consideration the contribution of the magnet and armature current to the overall performance of the machine.

3.2 Modeling of IPM Machine using Fourier Series of Winding Function with Harmonics

In the modeling of the 3-phase motor, the winding functions are expressed as Fourier series and then all higher order harmonics are truncated except the fundamental harmonic [2]. It signifies that only the fundamental harmonic producing ripple free dc torque is taken into account and other pulsating torque related harmonics are neglected. In the same way, for the higher phase order machines, the inclusion of fundamental, 3rd harmonic, 5th harmonic and 7th harmonic produces the ripple free torque and the combination of each harmonic components also aid in the production of total torque. Hence in the derivation of the IPM machine that follows, odd order harmonics until 7^{th} are taken into account. The modeling of the IPM machine in this chapter assumes that the phase has full pitched concentrated windings in stator and there is no existence of even order harmonics. Similarly there is no influence of flux saturation, hysteresis loss, eddy current losses, cogging torque and slot effects. The effect of damper rotor bars is also not taken into account in this modeling.

3.2.1 Voltage and Flux Equations in Natural Variables

Keeping the assumptions presented in Section 3.2, the phase voltages for phases a, b, c….i in 9-phase IPM machine are given as

$$v_{abcdefghis} = r_s i_{abcdefghis} + p\lambda_{abcdefghis} \tag{3.1}$$

where, r_s is the stator resistance matrix. The voltage, current and flux linkage matrixes are, respectively given as

$$v_{abcdefghis} = [v_{as} \quad v_{bs} \quad v_{cs} \quad v_{ds} \quad v_{es} \quad v_{fs} \quad v_{gs} \quad v_{hs} \quad v_{is}]^T \tag{3.2}$$

$$\begin{aligned} i_{abcdefghis} &= [I_{as} \quad I_{bs} \quad I_{cs} \quad I_{ds} \quad I_{es} \quad I_{fs} \quad I_{gs} \quad I_{hs} \quad I_{is}]^T \\ \lambda_{abcdefghis} &= [\lambda_{as} \quad \lambda_{bs} \quad \lambda_{cs} \quad \lambda_{ds} \quad \lambda_{es} \quad \lambda_{fs} \quad \lambda_{gs} \quad \lambda_{hs} \quad \lambda_{is}]^T \end{aligned} \tag{3.3}$$

As the effect of damper bars is not included in the analysis, the total flux linkage in the stator is due to the resultant flux linkage from stator and permanent magnet.

$$\lambda_{abcdefghis} = \lambda_{abcdefghis\_s} + \lambda_{abcdefghis\_m} = L_{ss} i_{abcdefghis} + \lambda_{abcdefghis\_m} \tag{3.4}$$

Equation (3.4) defines the total flux linkage in the stator windings due to stator inductance, L_{ss} and the magnet flux, $\lambda_{abcdefghis\_m}$. L_{ss} defines the inductance matrix with diagonal part as self-inductances of each phases and off-diagonals as mutual inductance between them and it is shown in Equation (3.5)

$$L_{ss} = \begin{bmatrix} L_{ls}+L_{aa} & L_{ab} & L_{ac} & L_{ad} & L_{ae} & L_{af} & L_{ag} & L_{ah} & L_{ai} \\ L_{ba} & L_{ls}+L_{bb} & L_{bc} & L_{bd} & L_{be} & L_{bf} & L_{bg} & L_{bh} & L_{bi} \\ L_{ca} & L_{cb} & L_{ls}+L_{cc} & L_{cd} & L_{ce} & L_{cf} & L_{cg} & L_{ch} & L_{ci} \\ L_{da} & L_{db} & L_{dc} & L_{ls}+L_{dd} & L_{de} & L_{df} & L_{dg} & L_{dh} & L_{di} \\ L_{ea} & L_{eb} & L_{ec} & L_{ed} & L_{ls}+L_{ee} & L_{ef} & L_{eg} & L_{eh} & L_{ei} \\ L_{fa} & L_{fb} & L_{fc} & L_{fd} & L_{fe} & L_{ls}+L_{ff} & L_{fg} & L_{fh} & L_{fi} \\ L_{ga} & L_{gb} & L_{gc} & L_{gd} & L_{ge} & L_{gf} & L_{ls}+L_{gg} & L_{gh} & L_{gi} \\ L_{ha} & L_{hb} & L_{hc} & L_{hd} & L_{he} & L_{hf} & L_{hg} & L_{ls}+L_{hh} & L_{hi} \\ L_{ia} & L_{ib} & L_{ic} & L_{id} & L_{ie} & L_{if} & L_{ig} & L_{ih} & L_{ls}+L_{ii} \end{bmatrix} \tag{3.5}$$

Similarly, the second part of Equation (3.4) defines the flux due to permanent magnet induced on each phases of the stator windings.

$$\lambda_{abcdefghis\_m} = [\lambda_{am} \quad \lambda_{bm} \quad \lambda_{cm} \quad \lambda_{dm} \quad \lambda_{em} \quad \lambda_{fm} \quad \lambda_{gm} \quad \lambda_{hm} \quad \lambda_{im}]^T \tag{3.6}$$

In the following sections, each term of Equation (3.5) and (3.6) is derived.

3.2.2 Stator Inductance Matrix

As described in Section 3.2, the winding functions are expressed as Fourier series with the inclusion of higher harmonics in the modeling of the multiphase motor. The Fourier series approximation of the winding function is used for the derivation of stator inductance matrix. Figure 3.1 shows the winding function of phase '*a*' of the 9-phase IPM machine. In general, the winding function is expressed as

$$n_x = N_1 \sin(\varphi - k\alpha) + N_3 \sin 3(\varphi - k\alpha) + N_5 \sin 5(\varphi - k\alpha) + N_7 \sin 7(\varphi - k\alpha) \tag{3.7}$$

$$x = a, b, c.....i, \qquad k = 0,1,2,3...8, \quad \alpha = \frac{2\pi}{9}$$

Due to the saliency of the IPM machine, the air-gap is not constant, but it is the function of spatial and the rotor angles. If the flux plot of the machine is used, the air gap length can be easily calculated as a function of spatial angle. However, in this analysis, the air gap function of the machine is approximated as Figure 3.2. Practically, it is observed that the design of the rotor includes an even number of symmetrically placed poles and an equal number of south and north poles. This gives an idea that the inverse air gap function consists of an average term plus even order harmonics. If τ_p is the rotor pole arc, the inverse gap function is given by Equation (3.8) [15].

$$g^{-1}(\phi - \theta) = a - \frac{2b}{k} \sin \frac{k\tau_p}{2} \cos k(\phi - \theta) \tag{3.8}$$

where,

$$a = \frac{1}{2}\left(\frac{1}{g_{\min}} + \frac{1}{g_{\max}} \right), \; b = \frac{1}{2}\left(\frac{1}{g_{\min}} - \frac{1}{g_{\max}} \right) \tag{3.9}$$

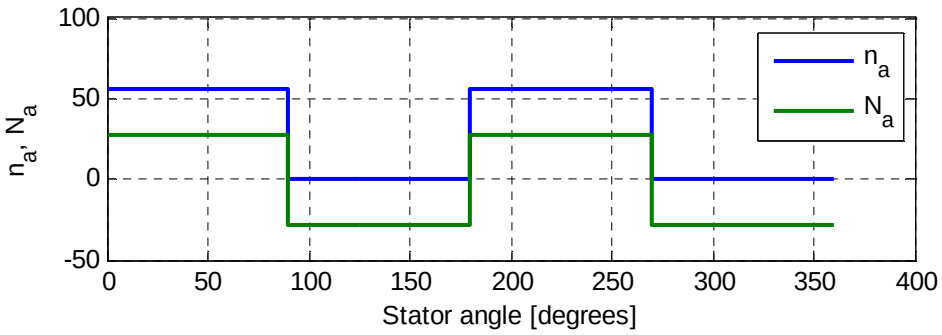

Figure 3.1 Winding function for phase a

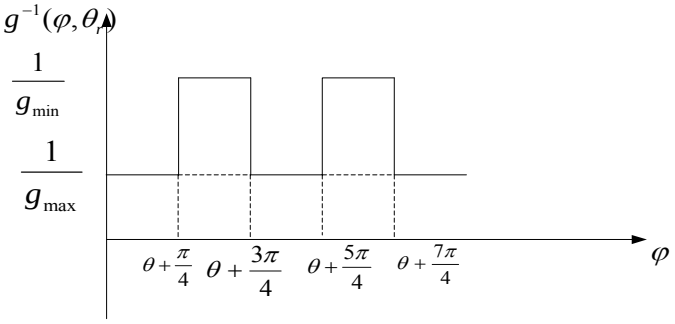

Figure 3.2 Inverse air gap density function

where $g_{\min}$ and $g_{\max}$ represent the minimum and maximum values of effective air gap lengths, respectively. In this analysis, pole arc, τ_p is taken to be $90°$ and Fourier series components up to the 5th term are considered.

As a result, the generalized inverse air gap function is obtained as

$$g^{-1}(\varphi,\theta_r) = a_0 + a_1\cos 2(\varphi-\theta_r) + a_2\cos 6(\varphi-\theta_r) + a_3\cos 10(\varphi-\theta_r) + a_4\cos 14(\varphi-\theta_r) \quad (3.10)$$

where, a_0, a_1, a_3, a_4 are the Fourier series amplitude for the inverse air gap function obtained from Equation 3.10. They are given as

$$a_0 = a,\ a_1 = -b,\ a_2 = -\frac{b}{3},\ a_3 = -\frac{b}{5},\ a_4 = -\frac{b}{7} \tag{3.11}$$

If current i_{as} is flowing through a-phase winding, the spatial MMF in 'a' phase winding is expressed as

$$f_a = \int_{\varphi}^{\varphi+\pi} n_a i_{as} d\varphi = 2\left(N_1 \cos(\varphi) + \frac{N_3}{3}\cos 3(\varphi) + \frac{N_5}{5}\cos 5(\varphi) + \frac{N_7}{7}\cos 7(\varphi) \right) i_{as} \tag{3.12}$$

The air gap flux density due to current flowing in phase 'a' is given as

$$b_a = \frac{\mu_0}{2} g^{-1} f_a = \mu_0 \left(2\left(N_1 \cos(\varphi) + \frac{N_3}{3}\cos 3(\varphi) + \frac{N_5}{5}\cos 5(\varphi) + \frac{N_7}{7}\cos 7(\varphi) \right) \right) \tag{3.13}$$
$$*\left(a_0 + a_1 \cos 2(\varphi - \theta_r) + a_2 \cos 6(\varphi - \theta_r) + a_3 \cos 10(\varphi - \theta_r) + a_4 \cos 14(\varphi - \theta_r)\right)$$

From Equations (3.7) and (3.13), the 'a'-phase flux linkage due to 'a'-phase current is derived as

$$\lambda_{aa} = rl \int_{-\frac{\pi}{2}}^{\frac{\pi}{2}} \left(\int_{\varphi}^{\varphi+\pi} n_a d\zeta \right) b_a d\varphi \tag{3.14}$$

where r and l denote the effective radius and stack lengths, respectively.

The self-inductance of phase 'a' is now given as

$$L_{aa} = \frac{\lambda_{aa}}{i_{aa}} \tag{3.15}$$

Substituting b_a from Equation (3.13) and n_a from Equation (3.7) into Equation (3.14), the self-inductance of phase 'a' is obtained as

$$L_{aa} = L_{ls} + k \begin{bmatrix} \pi N_1^{\,2} a_0 + \frac{\pi N_3^{\,2} a_0}{9} + \frac{\pi N_5^{\,2} a_0}{25} + \frac{\pi N_7^{\,2} a_0}{49} + \frac{\pi N_1^{\,2} a_2}{2}\cos\theta_r + \frac{\pi N_3^{\,2} a_2}{18}\cos 6\theta_r \\ + \frac{\pi N_1 N_3 a_1}{3}\cos 2\theta_r + \frac{\pi N_1 N_5 a_2}{5}\cos 6\theta_r + \frac{\pi N_3 N_5 a_1}{15}\cos 2\theta_r + \frac{\pi N_1 N_7 a_2}{7}\cos 6\theta_r \\ + \frac{\pi N_5^{\,2} a_3}{50}\cos 10\theta_r + \frac{\pi N_7^{\,2} a_4}{98}\cos 10\theta_r + \frac{\pi N_5 N_7 a_1}{35}\cos 2\theta_r + \frac{\pi N_3 N_7 a_3}{21}\cos 10\theta_r \end{bmatrix} \tag{3.16}$$

where, $k = \dfrac{\mu_0 rl}{4}$

In the similar way, the mutual inductance between phase 'a' and phase 'b' is given as

$$L_{ab} = L_{ba} = \frac{\lambda_{ab}}{i_{aa}} \tag{3.17}$$

where,

$$\lambda_{ab} = rl\int_{-\frac{\pi}{2}+\alpha}^{\frac{\pi}{2}+\alpha}\left(\int_{\varphi}^{\varphi+\pi} n_b d\zeta\right) b_a d\varphi \tag{3.18}$$

With the substitution of the Equations (3.7), (3.13) and (3.17), the mutual inductance between phase 'a' and phase 'b' is evaluated as

$$L_{ab} = k\left[\begin{array}{l}
\pi N_1^{\,2} a_0 \cos\alpha + \dfrac{\pi N_3^{\,2} a_0}{9}\cos 3\alpha + \dfrac{\pi N_5^{\,2} a_0}{25}\cos 5\alpha + \dfrac{\pi N_7^{\,2} a_0}{49}\cos 7\alpha + \\
\dfrac{\pi N_1^{\,2} a_2}{2}\cos(2\theta_r - \alpha) + \dfrac{\pi N_3^{\,2} a_2}{18}\cos 6(\theta_r - 3\alpha) + \dfrac{\pi N_1 N_3 a_1}{6}[\cos(2\theta_r + \alpha) + \\
\cos(2\theta_r - 3\alpha)] + \dfrac{\pi N_1 N_5 a_2}{10}[\cos(6\theta_r - \alpha) + \cos(6\theta_r - 5\alpha)] + \dfrac{\pi N_3 N_5 a_1}{30}[\cos(2\theta_r + 3\alpha) + \\
\cos(2\theta_r - 5\alpha)] + \dfrac{\pi N_1 N_7 a_2}{14}[\cos(6\theta_r + \alpha) + \cos(6\theta_r - 7\alpha)] + \dfrac{\pi N_5^{\,2} a_3}{50}\cos(10\theta_r - 5\alpha) + \\
\dfrac{\pi N_7^{\,2} a_4}{98}\cos(14\theta_r - 7\alpha) + \dfrac{\pi N_5 N_7 a_1}{35}[\cos(2\theta_r + 5\alpha) + \cos(2\theta_r - 7\alpha)] + \\
\dfrac{\pi N_3 N_7 a_3}{21}[\cos(10\theta_r - 3\alpha) + \cos(10\theta_r - 7\alpha)]
\end{array}\right] \tag{3.19}$$

Equations (3.15) and (3.19) illustrate the derivation of self and mutual inductances in real variables with the inclusion of amplitude of each harmonics of winding functions and air gap constants. Taking a close view at these two equations, it is observed that there exists a pattern of the cosine of rotor angles and cosine of phase shifts as each phase inductances are taken into account. A definite pattern exists in the derivation of other inductance terms of Equation (3.5). This pattern is given in Table 3.1,

however, these patterns are needed to be multiplied by the constant $k = \frac{\mu_0 rl}{4}$ and then each row should be added, before deriving the actual inductances. Similarly, leakage inductance terms exist in every self- inductance terms.

3.2.3 Flux Due to Permanent Magnet

In the analysis of the induced flux in the air gap due to the permanent magnet, the flux density waveform also should be represented in terms of the Fourier series. If the flux density is plotted, it is also observed to contain the odd order harmonics with the variation of the spatial angle as shown in Figure 3.3.

Approximating Figure 3.3 in terms of the Fourier series, and taking the terms of the series until the 7th harmonics the air gap flux density due to permanent magnet can be approximated as

$$b_m = B_1 \sin(\varphi - \theta_r) + B_3 \sin 3(\varphi - \theta_r) + B_5 \sin 5(\varphi - \theta_r) + B_7 \sin 7(\varphi - \theta_r) \tag{3.20}$$

where, B_1, B_3, B_5 and B_7 denote the amplitude of fundamental, 3rd, fifth and 7th harmonics, respectively. Utilizing Equation (3.20) and Equation (3.7), the flux linkage induced in the 'a' phase winding of the stator due to the permanent magnet is given as

$$\lambda_{am} = rl \int_{-\frac{\pi}{2}}^{\frac{\pi}{2}} \left(\int_{\varphi}^{\varphi+\pi} n_a d\xi \right) b_m d\varphi \tag{3.21}$$

Table 3.2 Inductance patterns of 9-phase IPM machine

	$\pi N_1^2 a_0$	$\frac{\pi N_3^2 a_0}{9}$	$\frac{\pi N_5^2 a_0}{25}$	$\frac{\pi N_7^2 a_0}{49}$	$\frac{\pi N_1^2 a_1}{2}$	$\frac{\pi N_3^2 a_2}{18}$	$\frac{\pi N_5^2 a_3}{50}$	$\frac{\pi N_7^2 a_4}{98}$
L_{aa}	1	1	1	1	$\cos 2\theta_r$	$\cos 6\theta_r$	$\cos(10\theta_r)$	$\cos(14\theta_r)$
L_{ab}	$\cos\alpha$	$\cos 3\alpha$	$\cos 5\alpha$	$\cos 7\alpha$	$\cos(2\theta_r - \alpha)$	$\cos(6\theta_r - 3\alpha)$	$\cos(10\theta_r - 5\alpha)$	$\cos(14\theta_r - 7\alpha)$
L_{ac}	$\cos 2\alpha$	$\cos 6\alpha$	$\cos 10\alpha$	$\cos 14\alpha$	$\cos(2\theta_r - 2\alpha)$	$\cos(6\theta_r - 6\alpha)$	$\cos(10\theta_r - 10\alpha)$	$\cos(14\theta_r - 14\alpha)$
L_{ad}	$\cos 3\alpha$	$\cos 9\alpha$	$\cos 15\alpha$	$\cos 21\alpha$	$\cos(2\theta_r - 3\alpha)$	$\cos(6\theta_r - 9\alpha)$	$\cos(10\theta_r - 15\alpha)$	$\cos(14\theta_r - 21\alpha)$
L_{ae}	$\cos 4\alpha$	$\cos 12\alpha$	$\cos 20\alpha$	$\cos 28\alpha$	$\cos(2\theta_r - 4\alpha)$	$\cos(6\theta_r - 12\alpha)$	$\cos(10\theta_r - 20\alpha)$	$\cos(14\theta_r - 28\alpha)$
L_{af}	$\cos 5\alpha$	$\cos 15\alpha$	$\cos 25\alpha$	$\cos 35\alpha$	$\cos(2\theta_r - 5\alpha)$	$\cos(6\theta_r - 15\alpha)$	$\cos(10\theta_r - 25\alpha)$	$\cos(14\theta_r - 35\alpha)$
L_{ag}	$\cos 6\alpha$	$\cos 18\alpha$	$\cos 30\alpha$	$\cos 42\alpha$	$\cos(2\theta_r - 6\alpha)$	$\cos(6\theta_r - 18\alpha)$	$\cos(10\theta_r - 30\alpha)$	$\cos(14\theta_r - 42\alpha)$
L_{ah}	$\cos 7\alpha$	$\cos 21\alpha$	$\cos 35\alpha$	$\cos 49\alpha$	$\cos(2\theta_r - 7\alpha)$	$\cos(6\theta_r - 21\alpha)$	$\cos(10\theta_r - 35\alpha)$	$\cos(14\theta_r - 49\alpha)$
L_{ai}	$\cos 8\alpha$	$\cos 24\alpha$	$\cos 40\alpha$	$\cos 56\alpha$	$\cos(2\theta_r - 8\alpha)$	$\cos(6\theta_r - 24\alpha)$	$\cos(10\theta_r - 40\alpha)$	$\cos(14\theta_r - 56\alpha)$
L_{bb}	1	1	1	1	$\cos(2\theta_r - 2\alpha)$	$\cos(6\theta_r - 6\alpha)$	$\cos(10\theta_r - 10\alpha)$	$\cos(14\theta_r - 14\alpha)$
L_{bc}	$\cos\alpha$	$\cos 3\alpha$	$\cos 5\alpha$	$\cos 7\alpha$	$\cos(2\theta_r - 3\alpha)$	$\cos(6\theta_r - 9\alpha)$	$\cos(10\theta_r - 15\alpha)$	$\cos(14\theta_r - 21\alpha)$
L_{bd}	$\cos 2\alpha$	$\cos 6\alpha$	$\cos 10\alpha$	$\cos 14\alpha$	$\cos(2\theta_r - 4\alpha)$	$\cos(6\theta_r - 12\alpha)$	$\cos(10\theta_r - 20\alpha)$	$\cos(14\theta_r - 28\alpha)$
L_{be}	$\cos 3\alpha$	$\cos 9\alpha$	$\cos 15\alpha$	$\cos 21\alpha$	$\cos(2\theta_r - 5\alpha)$	$\cos(6\theta_r - 15\alpha)$	$\cos(10\theta_r - 25\alpha)$	$\cos(14\theta_r - 35\alpha)$
L_{bf}	$\cos 4\alpha$	$\cos 12\alpha$	$\cos 20\alpha$	$\cos 28\alpha$	$\cos(2\theta_r - 6\alpha)$	$\cos(6\theta_r - 18\alpha)$	$\cos(10\theta_r - 30\alpha)$	$\cos(14\theta_r - 42\alpha)$
L_{bg}	$\cos 5\alpha$	$\cos 15\alpha$	$\cos 25\alpha$	$\cos 35\alpha$	$\cos(2\theta_r - 7\alpha)$	$\cos(6\theta_r - 21\alpha)$	$\cos(10\theta_r - 35\alpha)$	$\cos(14\theta_r - 49\alpha)$
L_{bh}	$\cos 6\alpha$	$\cos 18\alpha$	$\cos 30\alpha$	$\cos 42\alpha$	$\cos(2\theta_r - 8\alpha)$	$\cos(6\theta_r - 24\alpha)$	$\cos(10\theta_r - 40\alpha)$	$\cos(14\theta_r - 56\alpha)$
L_{bi}	$\cos 7\alpha$	$\cos 21\alpha$	$\cos 35\alpha$	$\cos 49\alpha$	$\cos(2\theta_r - 9\alpha)$	$\cos(6\theta_r - 27\alpha)$	$\cos(10\theta_r - 45\alpha)$	$\cos(14\theta_r - 63\alpha)$

Table 3.2 cont'd Inductance patterns of 9-phase IPM machine

	$\pi N_1^2 a_0$	$\frac{\pi N_3^2 a_0}{9}$	$\frac{\pi N_5^2 a_0}{25}$	$\frac{\pi N_7^2 a_0}{49}$	$\frac{\pi N_1^2 a_1}{2}$	$\frac{\pi N_3^2 a_2}{18}$	$\frac{\pi N_5^2 a_3}{50}$	$\frac{\pi N_7^2 a_4}{98}$
L_{cc}	1	1	1	1	$\cos(2\theta_r - 4\alpha)$	$\cos(6\theta_r - 12\alpha)$	$\cos(10\theta_r - 20\alpha)$	$\cos(14\theta_r - 28\alpha)$
L_{cd}	$\cos\alpha$	$\cos 3\alpha$	$\cos 5\alpha$	$\cos 7\alpha$	$\cos(2\theta_r - 5\alpha)$	$\cos(6\theta_r - 15\alpha)$	$\cos(10\theta_r - 25\alpha)$	$\cos(14\theta_r - 35\alpha)$
L_{ce}	$\cos 2\alpha$	$\cos 6\alpha$	$\cos 10\alpha$	$\cos 14\alpha$	$\cos(2\theta_r - 6\alpha)$	$\cos(6\theta_r - 18\alpha)$	$\cos(10\theta_r - 30\alpha)$	$\cos(14\theta_r - 42\alpha)$
L_{cf}	$\cos 3\alpha$	$\cos 9\alpha$	$\cos 15\alpha$	$\cos 21\alpha$	$\cos(2\theta_r - 7\alpha)$	$\cos(6\theta_r - 21\alpha)$	$\cos(10\theta_r - 35\alpha)$	$\cos(14\theta_r - 49\alpha)$
L_{cg}	$\cos 4\alpha$	$\cos 12\alpha$	$\cos 20\alpha$	$\cos 28\alpha$	$\cos(2\theta_r - 8\alpha)$	$\cos(6\theta_r - 24\alpha)$	$\cos(10\theta_r - 40\alpha)$	$\cos(14\theta_r - 56\alpha)$
L_{ch}	$\cos 5\alpha$	$\cos 15\alpha$	$\cos 25\alpha$	$\cos 35\alpha$	$\cos(2\theta_r - 9\alpha)$	$\cos(6\theta_r - 27\alpha)$	$\cos(10\theta_r - 45\alpha)$	$\cos(14\theta_r - 63\alpha)$
L_{ci}	$\cos 6\alpha$	$\cos 18\alpha$	$\cos 30\alpha$	$\cos 42\alpha$	$\cos(2\theta_r - 10\alpha)$	$\cos(6\theta_r - 30\alpha)$	$\cos(10\theta_r - 50\alpha)$	$\cos(14\theta_r - 70\alpha)$
L_{dd}	1	1	1	1	$\cos(2\theta_r - 6\alpha)$	$\cos(6\theta_r - 18\alpha)$	$\cos(10\theta_r - 30\alpha)$	$\cos(14\theta_r - 42\alpha)$
L_{de}	$\cos\alpha$	$\cos 3\alpha$	$\cos 5\alpha$	$\cos 7\alpha$	$\cos(2\theta_r - 7\alpha)$	$\cos(6\theta_r - 21\alpha)$	$\cos(10\theta_r - 35\alpha)$	$\cos(14\theta_r - 49\alpha)$
L_{df}	$\cos 2\alpha$	$\cos 6\alpha$	$\cos 10\alpha$	$\cos 14\alpha$	$\cos(2\theta_r - 8\alpha)$	$\cos(6\theta_r - 24\alpha)$	$\cos(10\theta_r - 40\alpha)$	$\cos(14\theta_r - 56\alpha)$
L_{dg}	$\cos 3\alpha$	$\cos 9\alpha$	$\cos 15\alpha$	$\cos 21\alpha$	$\cos(2\theta_r - 9\alpha)$	$\cos(6\theta_r - 27\alpha)$	$\cos(10\theta_r - 45\alpha)$	$\cos(14\theta_r - 63\alpha)$
L_{dh}	$\cos 4\alpha$	$\cos 12\alpha$	$\cos 20\alpha$	$\cos 28\alpha$	$\cos(2\theta_r - 10\alpha)$	$\cos(6\theta_r - 30\alpha)$	$\cos(10\theta_r - 50\alpha)$	$\cos(14\theta_r - 70\alpha)$
L_{di}	$\cos 5\alpha$	$\cos 15\alpha$	$\cos 25\alpha$	$\cos 35\alpha$	$\cos(2\theta_r - 11\alpha)$	$\cos(6\theta_r - 33\alpha)$	$\cos(10\theta_r - 55\alpha)$	$\cos(14\theta_r - 77\alpha)$
L_{ee}	1	1	1	1	$\cos(2\theta_r - 8\alpha)$	$\cos(6\theta_r - 24\alpha)$	$\cos(10\theta_r - 40\alpha)$	$\cos(14\theta_r - 56\alpha)$
L_{ef}	$\cos\alpha$	$\cos 3\alpha$	$\cos 5\alpha$	$\cos 7\alpha$	$\cos(2\theta_r - 9\alpha)$	$\cos(6\theta_r - 27\alpha)$	$\cos(10\theta_r - 45\alpha)$	$\cos(14\theta_r - 63\alpha)$
L_{eg}	$\cos 2\alpha$	$\cos 6\alpha$	$\cos 10\alpha$	$\cos 14\alpha$	$\cos(2\theta_r - 10\alpha)$	$\cos(6\theta_r - 30\alpha)$	$\cos(10\theta_r - 50\alpha)$	$\cos(14\theta_r - 70\alpha)$
L_{eh}	$\cos 3\alpha$	$\cos 9\alpha$	$\cos 15\alpha$	$\cos 21\alpha$	$\cos(2\theta_r - 11\alpha)$	$\cos(6\theta_r - 33\alpha)$	$\cos(10\theta_r - 55\alpha)$	$\cos(14\theta_r - 77\alpha)$
L_{ei}	$\cos 4\alpha$	$\cos 12\alpha$	$\cos 20\alpha$	$\cos 28\alpha$	$\cos(2\theta_r - 12\alpha)$	$\cos(6\theta_r - 36\alpha)$	$\cos(10\theta_r - 60\alpha)$	$\cos(14\theta_r - 84\alpha)$

Table 3.2 cont'd Inductance patterns of 9-phase IPM machine

	$\pi N_1^2 a_0$	$\frac{\pi N_3^2 a_0}{9}$	$\frac{\pi N_5^2 a_0}{25}$	$\frac{\pi N_7^2 a_0}{49}$	$\frac{\pi N_1^2 a_1}{2}$	$\frac{\pi N_3^2 a_2}{18}$	$\frac{\pi N_5^2 a_3}{50}$	$\frac{\pi N_7^2 a_4}{98}$
L_{ff}	1	1	1	1	$\cos(2\theta_r - 10\alpha)$	$\cos(6\theta_r - 30\alpha)$	$\cos(10\theta_r - 50\alpha)$	$\cos(14\theta_r - 70\alpha)$
L_{fg}	$\cos\alpha$	$\cos 3\alpha$	$\cos 5\alpha$	$\cos 7\alpha$	$\cos(2\theta_r - 11\alpha)$	$\cos(6\theta_r - 33\alpha)$	$\cos(10\theta_r - 55\alpha)$	$\cos(14\theta_r - 77\alpha)$
L_{fh}	$\cos 2\alpha$	$\cos 6\alpha$	$\cos 10\alpha$	$\cos 14\alpha$	$\cos(2\theta_r - 12\alpha)$	$\cos(6\theta_r - 36\alpha)$	$\cos(10\theta_r - 60\alpha)$	$\cos(14\theta_r - 84\alpha)$
L_{fi}	$\cos 3\alpha$	$\cos 9\alpha$	$\cos 15\alpha$	$\cos 21\alpha$	$\cos(2\theta_r - 13\alpha)$	$\cos(6\theta_r - 39\alpha)$	$\cos(10\theta_r - 70\alpha)$	$\cos(14\theta_r - 91\alpha)$
L_{gg}	1	1	1	1	$\cos(2\theta_r - 12\alpha)$	$\cos(6\theta_r - 36\alpha)$	$\cos(10\theta_r - 60\alpha)$	$\cos(14\theta_r - 84\alpha)$
L_{gh}	$\cos\alpha$	$\cos 3\alpha$	$\cos 5\alpha$	$\cos 7\alpha$	$\cos(2\theta_r - 13\alpha)$	$\cos(6\theta_r - 39\alpha)$	$\cos(10\theta_r - 65\alpha)$	$\cos(14\theta_r - 91\alpha)$
L_{gi}	$\cos 2\alpha$	$\cos 6\alpha$	$\cos 10\alpha$	$\cos 14\alpha$	$\cos(2\theta_r - 14\alpha)$	$\cos(6\theta_r - 42\alpha)$	$\cos(10\theta_r - 70\alpha)$	$\cos(14\theta_r - 98\alpha)$
L_{hh}	1	1	1	1	$\cos(2\theta_r - 14\alpha)$	$\cos(6\theta_r - 42\alpha)$	$\cos(10\theta_r - 80\alpha)$	$\cos(14\theta_r - 98\alpha)$
L_{hi}	$\cos\alpha$	$\cos 3\alpha$	$\cos 5\alpha$	$\cos 7\alpha$	$\cos(2\theta_r - 15\alpha)$	$\cos(6\theta_r - 45\alpha)$	$\cos(10\theta_r - 85\alpha)$	$\cos(14\theta_r - 105\alpha)$
L_{ii}	1	1	1	1	$\cos(2\theta_r - 16\alpha)$	$\cos(6\theta_r - 48\alpha)$	$\cos(10\theta_r - 90\alpha)$	$\cos(14\theta_r - 112\alpha)$

Table 3.2 cont'd Inductance patterns of 9-phase IPM machine

	$\frac{\pi N_1 N_3 a_1}{6}$	$\frac{\pi N_3 N_1 a_1}{6}$	$\frac{\pi N_1 N_5 a_2}{10}$	$\frac{\pi N_5 N_1 a_2}{10}$	$\frac{\pi N_3 N_5 a_1}{30}$	$\frac{\pi N_5 N_3 a_1}{30}$
L_{aa}	$\cos 2\theta_r$	$\cos 2\theta_r$	$\cos 6\theta_r$	$\cos 6\theta_r$	$\cos 2\theta_r$	$\cos 2\theta_r$
L_{ab}	$\cos(2\theta_r + \alpha)$	$\cos(2\theta_r - 3\alpha)$	$\cos(6\theta_r - \alpha)$	$\cos(6\theta_r - 5\alpha)$	$\cos(2\theta_r + 3\alpha)$	$\cos(2\theta_r - 5\alpha)$
L_{ac}	$\cos(2\theta_r + 2\alpha)$	$\cos(2\theta_r - 6\alpha)$	$\cos(6\theta_r - 2\alpha)$	$\cos(6\theta_r - 10\alpha)$	$\cos(2\theta_r + 6\alpha)$	$\cos(2\theta_r - 10\alpha)$
L_{ad}	$\cos(2\theta_r + 3\alpha)$	$\cos(2\theta_r - 9\alpha)$	$\cos(6\theta_r - 3\alpha)$	$\cos(6\theta_r - 15\alpha)$	$\cos(2\theta_r + 9\alpha)$	$\cos(2\theta_r - 15\alpha)$
L_{ae}	$\cos(2\theta_r + 4\alpha)$	$\cos(2\theta_r - 12\alpha)$	$\cos(6\theta_r - 4\alpha)$	$\cos(6\theta_r - 20\alpha)$	$\cos(2\theta_r + 12\alpha)$	$\cos(2\theta_r - 20\alpha)$
L_{af}	$\cos(2\theta_r + 5\alpha)$	$\cos(2\theta_r - 15\alpha)$	$\cos(6\theta_r - 5\alpha)$	$\cos(6\theta_r - 25\alpha)$	$\cos(2\theta_r + 15\alpha)$	$\cos(2\theta_r - 25\alpha)$
L_{ag}	$\cos(2\theta_r + 6\alpha)$	$\cos(2\theta_r - 18\alpha)$	$\cos(6\theta_r - 6\alpha)$	$\cos(6\theta_r - 30\alpha)$	$\cos(2\theta_r + 18\alpha)$	$\cos(2\theta_r - 30\alpha)$
L_{ah}	$\cos(2\theta_r + 7\alpha)$	$\cos(2\theta_r - 21\alpha)$	$\cos(6\theta_r - 7\alpha)$	$\cos(6\theta_r - 35\alpha)$	$\cos(2\theta_r + 21\alpha)$	$\cos(2\theta_r - 35\alpha)$
L_{ai}	$\cos(2\theta_r + 8\alpha)$	$\cos(2\theta_r - 24\alpha)$	$\cos(6\theta_r - 8\alpha)$	$\cos(6\theta_r - 40\alpha)$	$\cos(2\theta_r + 24\alpha)$	$\cos(2\theta_r - 40\alpha)$
L_{bb}	$\cos(2\theta_r - 2\alpha)$	$\cos(2\theta_r - 2\alpha)$	$\cos(6\theta_r - 6\alpha)$	$\cos(6\theta_r - 6\alpha)$	$\cos(2\theta_r - 2\alpha)$	$\cos(2\theta_r - 2\alpha)$
L_{bc}	$\cos(2\theta_r - \alpha)$	$\cos(2\theta_r - 5\alpha)$	$\cos(6\theta_r - 7\alpha)$	$\cos(6\theta_r - 11\alpha)$	$\cos(2\theta_r + \alpha)$	$\cos(2\theta_r - 7\alpha)$
L_{bd}	$\cos(2\theta_r)$	$\cos(2\theta_r - 8\alpha)$	$\cos(6\theta_r - 8\alpha)$	$\cos(6\theta_r - 16\alpha)$	$\cos(2\theta_r + 4\alpha)$	$\cos(2\theta_r - 12\alpha)$
L_{be}	$\cos(2\theta_r + \alpha)$	$\cos(2\theta_r - 11\alpha)$	$\cos(6\theta_r - 9\alpha)$	$\cos(6\theta_r - 21\alpha)$	$\cos(2\theta_r + 7\alpha)$	$\cos(2\theta_r - 17\alpha)$
L_{bf}	$\cos(2\theta_r + 2\alpha)$	$\cos(2\theta_r - 14\alpha)$	$\cos(6\theta_r - 10\alpha)$	$\cos(6\theta_r - 26\alpha)$	$\cos(2\theta_r + 10\alpha)$	$\cos(2\theta_r - 22\alpha)$
L_{bg}	$\cos(2\theta_r + 3\alpha)$	$\cos(2\theta_r - 17\alpha)$	$\cos(6\theta_r - 11\alpha)$	$\cos(6\theta_r - 31\alpha)$	$\cos(2\theta_r + 13\alpha)$	$\cos(2\theta_r - 27\alpha)$
L_{bh}	$\cos(2\theta_r + 4\alpha)$	$\cos(2\theta_r - 20\alpha)$	$\cos(6\theta_r - 12\alpha)$	$\cos(6\theta_r - 36\alpha)$	$\cos(2\theta_r + 16\alpha)$	$\cos(2\theta_r - 32\alpha)$
L_{bi}	$\cos(2\theta_r + 5\alpha)$	$\cos(2\theta_r - 23\alpha)$	$\cos(6\theta_r - 13\alpha)$	$\cos(6\theta_r - 41\alpha)$	$\cos(2\theta_r + 19\alpha)$	$\cos(2\theta_r - 37\alpha)$

Table 3.2 cont'd Inductance patterns of 9-phase IPM machine

	$\frac{\pi N_1 N_3 a_1}{6}$	$\frac{\pi N_3 N_1 a_1}{6}$	$\frac{\pi N_1 N_5 a_2}{10}$	$\frac{\pi N_5 N_1 a_2}{10}$	$\frac{\pi N_3 N_5 a_1}{30}$	$\frac{\pi N_5 N_3 a_1}{30}$
L_{cc}	$\cos(2\theta_r - 4\alpha)$	$\cos(2\theta_r - 4\alpha)$	$\cos(6\theta_r - 12\alpha)$	$\cos(6\theta_r - 12\alpha)$	$\cos(2\theta_r - 4\alpha)$	$\cos(2\theta_r - 4\alpha)$
L_{cd}	$\cos(2\theta_r - 3\alpha)$	$\cos(2\theta_r - 7\alpha)$	$\cos(6\theta_r - 13\alpha)$	$\cos(6\theta_r - 17\alpha)$	$\cos(2\theta_r - \alpha)$	$\cos(2\theta_r - 9\alpha)$
L_{ce}	$\cos(2\theta_r - 2\alpha)$	$\cos(2\theta_r - 10\alpha)$	$\cos(6\theta_r - 14\alpha)$	$\cos(6\theta_r - 22\alpha)$	$\cos(2\theta_r + 2\alpha)$	$\cos(2\theta_r - 14\alpha)$
L_{cf}	$\cos(2\theta_r - \alpha)$	$\cos(2\theta_r - 13\alpha)$	$\cos(6\theta_r - 15\alpha)$	$\cos(6\theta_r - 27\alpha)$	$\cos(2\theta_r + 5\alpha)$	$\cos(2\theta_r - 19\alpha)$
L_{cg}	$\cos(2\theta_r)$	$\cos(2\theta_r - 16\alpha)$	$\cos(6\theta_r - 16\alpha)$	$\cos(6\theta_r - 32\alpha)$	$\cos(2\theta_r + 8\alpha)$	$\cos(2\theta_r - 24\alpha)$
L_{ch}	$\cos(2\theta_r + \alpha)$	$\cos(2\theta_r - 19\alpha)$	$\cos(6\theta_r - 17\alpha)$	$\cos(6\theta_r - 37\alpha)$	$\cos(2\theta_r + 11\alpha)$	$\cos(2\theta_r - 29\alpha)$
L_{ci}	$\cos(2\theta_r + 2\alpha)$	$\cos(2\theta_r - 22\alpha)$	$\cos(6\theta_r - 18\alpha)$	$\cos(6\theta_r - 42\alpha)$	$\cos(2\theta_r + 14\alpha)$	$\cos(2\theta_r - 34\alpha)$
L_{dd}	$\cos(2\theta_r - 6\alpha)$	$\cos(2\theta_r - 6\alpha)$	$\cos(6\theta_r - 18\alpha)$	$\cos(6\theta_r - 18\alpha)$	$\cos(2\theta_r - 6\alpha)$	$\cos(2\theta_r - 6\alpha)$
L_{de}	$\cos(2\theta_r - 5\alpha)$	$\cos(2\theta_r - 9\alpha)$	$\cos(6\theta_r - 19\alpha)$	$\cos(6\theta_r - 23\alpha)$	$\cos(2\theta_r - 3\alpha)$	$\cos(2\theta_r - 11\alpha)$
L_{df}	$\cos(2\theta_r - 4\alpha)$	$\cos(2\theta_r - 12\alpha)$	$\cos(6\theta_r - 20\alpha)$	$\cos(6\theta_r - 28\alpha)$	$\cos(2\theta_r)$	$\cos(2\theta_r - 16\alpha)$
L_{dg}	$\cos(2\theta_r - 3\alpha)$	$\cos(2\theta_r - 15\alpha)$	$\cos(6\theta_r - 21\alpha)$	$\cos(6\theta_r - 33\alpha)$	$\cos(2\theta_r + 3\alpha)$	$\cos(2\theta_r - 21\alpha)$
L_{dh}	$\cos(2\theta_r - 2\alpha)$	$\cos(2\theta_r - 18\alpha)$	$\cos(6\theta_r - 22\alpha)$	$\cos(6\theta_r - 38\alpha)$	$\cos(2\theta_r + 6\alpha)$	$\cos(2\theta_r - 26\alpha)$
L_{di}	$\cos(2\theta_r - \alpha)$	$\cos(2\theta_r - 21\alpha)$	$\cos(6\theta_r - 23\alpha)$	$\cos(6\theta_r - 43\alpha)$	$\cos(2\theta_r + 9\alpha)$	$\cos(2\theta_r - 31\alpha)$
L_{ee}	$\cos(2\theta_r - 8\alpha)$	$\cos(2\theta_r - 8\alpha)$	$\cos(6\theta_r - 24\alpha)$	$\cos(6\theta_r - 24\alpha)$	$\cos(2\theta_r - 8\alpha)$	$\cos(2\theta_r - 8\alpha)$
L_{ef}	$\cos(2\theta_r - 7\alpha)$	$\cos(2\theta_r - 11\alpha)$	$\cos(6\theta_r - 25\alpha)$	$\cos(6\theta_r - 29\alpha)$	$\cos(2\theta_r - 5\alpha)$	$\cos(2\theta_r - 13\alpha)$
L_{eg}	$\cos(2\theta_r - 6\alpha)$	$\cos(2\theta_r - 14\alpha)$	$\cos(6\theta_r - 26\alpha)$	$\cos(6\theta_r - 34\alpha)$	$\cos(2\theta_r - 2\alpha)$	$\cos(2\theta_r - 18\alpha)$
L_{eh}	$\cos(2\theta_r - 5\alpha)$	$\cos(2\theta_r - 17\alpha)$	$\cos(6\theta_r - 27\alpha)$	$\cos(6\theta_r - 39\alpha)$	$\cos(2\theta_r + \alpha)$	$\cos(2\theta_r - 23\alpha)$
L_{ei}	$\cos(2\theta_r - 4\alpha)$	$\cos(2\theta_r - 20\alpha)$	$\cos(6\theta_r - 28\alpha)$	$\cos(6\theta_r - 44\alpha)$	$\cos(2\theta_r + 4\alpha)$	$\cos(2\theta_r - 28\alpha)$

Table 3.2 cont'd Inductance patterns of 9-phase IPM machine

	$\frac{\pi N_1 N_3 a_1}{6}$	$\frac{\pi N_3 N_1 a_1}{6}$	$\frac{\pi N_1 N_5 a_2}{10}$	$\frac{\pi N_5 N_1 a_2}{10}$	$\frac{\pi N_3 N_5 a_1}{30}$	$\frac{\pi N_5 N_3 a_1}{30}$
L_{ff}	$\cos(2\theta_r - 10\alpha)$	$\cos(2\theta_r - 10\alpha)$	$\cos(6\theta_r - 30\alpha)$	$\cos(6\theta_r - 30\alpha)$	$\cos(2\theta_r - 10\alpha)$	$\cos(2\theta_r - 10\alpha)$
L_{fg}	$\cos(2\theta_r - 9\alpha)$	$\cos(2\theta_r - 13\alpha)$	$\cos(6\theta_r - 31\alpha)$	$\cos(6\theta_r - 35\alpha)$	$\cos(2\theta_r - 7\alpha)$	$\cos(2\theta_r - 15\alpha)$
L_{fh}	$\cos(2\theta_r - 8\alpha)$	$\cos(2\theta_r - 16\alpha)$	$\cos(6\theta_r - 32\alpha)$	$\cos(6\theta_r - 40\alpha)$	$\cos(2\theta_r - 4\alpha)$	$\cos(2\theta_r - 20\alpha)$
L_{fi}	$\cos(2\theta_r - 7\alpha)$	$\cos(2\theta_r - 19\alpha)$	$\cos(6\theta_r - 33\alpha)$	$\cos(6\theta_r - 45\alpha)$	$\cos(2\theta_r - \alpha)$	$\cos(2\theta_r - 25\alpha)$
L_{gg}	$\cos(2\theta_r - 12\alpha)$	$\cos(2\theta_r - 12\alpha)$	$\cos(6\theta_r - 36\alpha)$	$\cos(6\theta_r - 36\alpha)$	$\cos(2\theta_r - 12\alpha)$	$\cos(2\theta_r - 12\alpha)$
L_{gh}	$\cos(2\theta_r - 11\alpha)$	$\cos(2\theta_r - 15\alpha)$	$\cos(6\theta_r - 37\alpha)$	$\cos(6\theta_r - 41\alpha)$	$\cos(2\theta_r - 9\alpha)$	$\cos(2\theta_r - 17\alpha)$
L_{gi}	$\cos(2\theta_r - 10\alpha)$	$\cos(2\theta_r - 18\alpha)$	$\cos(6\theta_r - 38\alpha)$	$\cos(6\theta_r - 46\alpha)$	$\cos(2\theta_r - 6\alpha)$	$\cos(2\theta_r - 28\alpha)$
L_{hh}	$\cos(2\theta_r - 14\alpha)$	$\cos(2\theta_r - 14\alpha)$	$\cos(6\theta_r - 42\alpha)$	$\cos(6\theta_r - 42\alpha)$	$\cos(2\theta_r - 14\alpha)$	$\cos(2\theta_r - 14\alpha)$
L_{hi}	$\cos(2\theta_r - 13\alpha)$	$\cos(2\theta_r - 17\alpha)$	$\cos(6\theta_r - 43\alpha)$	$\cos(6\theta_r - 47\alpha)$	$\cos(2\theta_r - 11\alpha)$	$\cos(2\theta_r - 19\alpha)$
L_{ii}	$\cos(2\theta_r - 16\alpha)$	$\cos(2\theta_r - 16\alpha)$	$\cos(6\theta_r - 48\alpha)$	$\cos(6\theta_r - 48\alpha)$	$\cos(2\theta_r - 16\alpha)$	$\cos(2\theta_r - 16\alpha)$

Table 3.2 cont'd Inductance patterns of 9-phase IPM machine

	$\frac{\pi N_1 N_7 a_2}{14}$	$\frac{\pi N_7 N_1 a_2}{14}$	$\frac{\pi N_5 N_7 a_1}{70}$	$\frac{\pi N_7 N_5 a_1}{70}$	$\frac{\pi N_3 N_7 a_3}{42}$	$\frac{\pi N_7 N_3 a_3}{42}$
L_{aa}	$\cos(6\theta_r)$	$\cos(6\theta_r)$	$\cos(2\theta_r)$	$\cos(2\theta_r)$	$\cos(10\theta_r)$	$\cos(10\theta_r)$
L_{ab}	$\cos(6\theta_r+\alpha)$	$\cos(6\theta_r-7\alpha)$	$\cos(2\theta_r+5\alpha)$	$\cos(2\theta_r-7\alpha)$	$\cos(10\theta_r+3\alpha)$	$\cos(10\theta_r-7\alpha)$
L_{ac}	$\cos(6\theta_r+2\alpha)$	$\cos(6\theta_r-14\alpha)$	$\cos(2\theta_r+10\alpha)$	$\cos(2\theta_r-14\alpha)$	$\cos(10\theta_r+6\alpha)$	$\cos(10\theta_r-14\alpha)$
L_{ad}	$\cos(6\theta_r+3\alpha)$	$\cos(6\theta_r-21\alpha)$	$\cos(2\theta_r+15\alpha)$	$\cos(2\theta_r-21\alpha)$	$\cos(10\theta_r+9\alpha)$	$\cos(10\theta_r-21\alpha)$
L_{ae}	$\cos(6\theta_r+4\alpha)$	$\cos(6\theta_r-28\alpha)$	$\cos(2\theta_r+20\alpha)$	$\cos(2\theta_r-28\alpha)$	$\cos(10\theta_r+12\alpha)$	$\cos(10\theta_r-28\alpha)$
L_{af}	$\cos(6\theta_r+5\alpha)$	$\cos(6\theta_r-35\alpha)$	$\cos(2\theta_r+25\alpha)$	$\cos(2\theta_r-35\alpha)$	$\cos(10\theta_r+15\alpha)$	$\cos(10\theta_r-35\alpha)$
L_{ag}	$\cos(6\theta_r+6\alpha)$	$\cos(6\theta_r-42\alpha)$	$\cos(2\theta_r+30\alpha)$	$\cos(2\theta_r-42\alpha)$	$\cos(10\theta_r+18\alpha)$	$\cos(10\theta_r-42\alpha)$
L_{ah}	$\cos(6\theta_r+7\alpha)$	$\cos(6\theta_r-49\alpha)$	$\cos(2\theta_r+35\alpha)$	$\cos(2\theta_r-49\alpha)$	$\cos(10\theta_r+21\alpha)$	$\cos(10\theta_r-49\alpha)$
L_{ai}	$\cos(6\theta_r+8\alpha)$	$\cos(6\theta_r-56\alpha)$	$\cos(2\theta_r+40\alpha)$	$\cos(2\theta_r-56\alpha)$	$\cos(10\theta_r+24\alpha)$	$\cos(10\theta_r-56\alpha)$
L_{bb}	$\cos(6\theta_r-6\alpha)$	$\cos(6\theta_r-6\alpha)$	$\cos(2\theta_r-2\alpha)$	$\cos(2\theta_r-2\alpha)$	$\cos(10\theta_r-10\alpha)$	$\cos(10\theta_r-10\alpha)$
L_{bc}	$\cos(6\theta_r-5\alpha)$	$\cos(6\theta_r-13\alpha)$	$\cos(2\theta_r+3\alpha)$	$\cos(2\theta_r-9\alpha)$	$\cos(10\theta_r-7\alpha)$	$\cos(10\theta_r-17\alpha)$
L_{bd}	$\cos(6\theta_r-4\alpha)$	$\cos(6\theta_r-20\alpha)$	$\cos(2\theta_r+8\alpha)$	$\cos(2\theta_r-16\alpha)$	$\cos(10\theta_r-4\alpha)$	$\cos(10\theta_r-24\alpha)$
L_{be}	$\cos(6\theta_r-3\alpha)$	$\cos(6\theta_r-27\alpha)$	$\cos(2\theta_r+13\alpha)$	$\cos(2\theta_r-23\alpha)$	$\cos(10\theta_r-\alpha)$	$\cos(10\theta_r-31\alpha)$
L_{bf}	$\cos(6\theta_r-2\alpha)$	$\cos(6\theta_r-34\alpha)$	$\cos(2\theta_r+18\alpha)$	$\cos(2\theta_r-30\alpha)$	$\cos(10\theta_r+2\alpha)$	$\cos(10\theta_r-38\alpha)$
L_{bg}	$\cos(6\theta_r-\alpha)$	$\cos(6\theta_r-41\alpha)$	$\cos(2\theta_r+23\alpha)$	$\cos(2\theta_r-37\alpha)$	$\cos(10\theta_r+5\alpha)$	$\cos(10\theta_r-45\alpha)$
L_{bh}	$\cos(6\theta_r)$	$\cos(6\theta_r-48\alpha)$	$\cos(2\theta_r+28\alpha)$	$\cos(2\theta_r-44\alpha)$	$\cos(10\theta_r+8\alpha)$	$\cos(10\theta_r-52\alpha)$
L_{bi}	$\cos(6\theta_r+\alpha)$	$\cos(6\theta_r-55\alpha)$	$\cos(2\theta_r+33\alpha)$	$\cos(2\theta_r-51\alpha)$	$\cos(10\theta_r+11\alpha)$	$\cos(10\theta_r-59\alpha)$

Table 3.2 cont'd Inductance patterns of 9-phase IPM machine

	$\frac{\pi N_1 N_7 a_2}{14}$	$\frac{\pi N_7 N_1 a_2}{14}$	$\frac{\pi N_5 N_7 a_1}{70}$	$\frac{\pi N_7 N_5 a_1}{70}$	$\frac{\pi N_3 N_7 a_3}{42}$	$\frac{\pi N_7 N_3 a_1}{42}$
L_{cc}	$\cos(6\theta_r - 12\alpha)$	$\cos(6\theta_r - 12\alpha)$	$\cos(2\theta_r - 4\alpha)$	$\cos(2\theta_r - 4\alpha)$	$\cos(10\theta_r - 20\alpha)$	$\cos(10\theta_r - 20\alpha)$
L_{cd}	$\cos(6\theta_r - 11\alpha)$	$\cos(6\theta_r - 19\alpha)$	$\cos(2\theta_r + \alpha)$	$\cos(2\theta_r - 4\alpha)$	$\cos(10\theta_r - 17\alpha)$	$\cos(10\theta_r - 27\alpha)$
L_{ce}	$\cos(6\theta_r - 10\alpha)$	$\cos(6\theta_r - 26\alpha)$	$\cos(2\theta_r + 6\alpha)$	$\cos(2\theta_r - 4\alpha)$	$\cos(10\theta_r - 14\alpha)$	$\cos(10\theta_r - 34\alpha)$
L_{cf}	$\cos(6\theta_r - 9\alpha)$	$\cos(6\theta_r - 33\alpha)$	$\cos(2\theta_r + 11\alpha)$	$\cos(2\theta_r - 4\alpha)$	$\cos(10\theta_r - 11\alpha)$	$\cos(10\theta_r - 41\alpha)$
L_{cg}	$\cos(6\theta_r - 8\alpha)$	$\cos(6\theta_r - 40\alpha)$	$\cos(2\theta_r + 16\alpha)$	$\cos(2\theta_r - 4\alpha)$	$\cos(10\theta_r - 8\alpha)$	$\cos(10\theta_r - 48\alpha)$
L_{ch}	$\cos(6\theta_r - 7\alpha)$	$\cos(6\theta_r - 47\alpha)$	$\cos(2\theta_r + 21\alpha)$	$\cos(2\theta_r - 4\alpha)$	$\cos(10\theta_r - 5\alpha)$	$\cos(10\theta_r - 55\alpha)$
L_{ci}	$\cos(6\theta_r - 6\alpha)$	$\cos(6\theta_r - 54\alpha)$	$\cos(2\theta_r + 26\alpha)$	$\cos(2\theta_r - 4\alpha)$	$\cos(10\theta_r - 2\alpha)$	$\cos(10\theta_r - 62\alpha)$
L_{dd}	$\cos(6\theta_r - 18\alpha)$	$\cos(6\theta_r - 18\alpha)$	$\cos(2\theta_r - 6\alpha)$	$\cos(2\theta_r - 6\alpha)$	$\cos(10\theta_r - 30\alpha)$	$\cos(10\theta_r - 30\alpha)$
L_{de}	$\cos(6\theta_r - 17\alpha)$	$\cos(6\theta_r - 25\alpha)$	$\cos(2\theta_r - \alpha)$	$\cos(2\theta_r - 13\alpha)$	$\cos(10\theta_r - 27\alpha)$	$\cos(10\theta_r - 37\alpha)$
L_{df}	$\cos(6\theta_r - 16\alpha)$	$\cos(6\theta_r - 32\alpha)$	$\cos(2\theta_r + 4\alpha)$	$\cos(2\theta_r - 20\alpha)$	$\cos(10\theta_r - 24\alpha)$	$\cos(10\theta_r - 44\alpha)$
L_{dg}	$\cos(6\theta_r - 15\alpha)$	$\cos(6\theta_r - 39\alpha)$	$\cos(2\theta_r + 9\alpha)$	$\cos(2\theta_r - 27\alpha)$	$\cos(10\theta_r - 21\alpha)$	$\cos(10\theta_r - 51\alpha)$
L_{dh}	$\cos(6\theta_r - 14\alpha)$	$\cos(6\theta_r - 46\alpha)$	$\cos(2\theta_r + 14\alpha)$	$\cos(2\theta_r - 34\alpha)$	$\cos(10\theta_r - 18\alpha)$	$\cos(10\theta_r - 58\alpha)$
L_{di}	$\cos(6\theta_r - 13\alpha)$	$\cos(6\theta_r - 53\alpha)$	$\cos(2\theta_r + 19\alpha)$	$\cos(2\theta_r - 41\alpha)$	$\cos(10\theta_r - 15\alpha)$	$\cos(10\theta_r - 65\alpha)$
L_{ee}	$\cos(6\theta_r - 24\alpha)$	$\cos(6\theta_r - 24\alpha)$	$\cos(2\theta_r - 8\alpha)$	$\cos(2\theta_r - 8\alpha)$	$\cos(10\theta_r - 40\alpha)$	$\cos(10\theta_r - 40\alpha)$
L_{ef}	$\cos(6\theta_r - 23\alpha)$	$\cos(6\theta_r - 31\alpha)$	$\cos(2\theta_r - 3\alpha)$	$\cos(2\theta_r - 15\alpha)$	$\cos(10\theta_r - 37\alpha)$	$\cos(10\theta_r - 47\alpha)$
L_{eg}	$\cos(6\theta_r - 22\alpha)$	$\cos(6\theta_r - 38\alpha)$	$\cos(2\theta_r + 2\alpha)$	$\cos(2\theta_r - 22\alpha)$	$\cos(10\theta_r - 34\alpha)$	$\cos(10\theta_r - 54\alpha)$
L_{eh}	$\cos(6\theta_r - 21\alpha)$	$\cos(6\theta_r - 45\alpha)$	$\cos(2\theta_r + 7\alpha)$	$\cos(2\theta_r - 29\alpha)$	$\cos(10\theta_r - 31\alpha)$	$\cos(10\theta_r - 61\alpha)$
L_{ei}	$\cos(6\theta_r - 20\alpha)$	$\cos(6\theta_r - 52\alpha)$	$\cos(2\theta_r + 12\alpha)$	$\cos(2\theta_r - 36\alpha)$	$\cos(10\theta_r - 28\alpha)$	$\cos(10\theta_r - 68\alpha)$

Table 3.2 cont'd Inductance patterns of 9-phase IPM machine

	$\frac{\pi N_1 N_7 a_2}{14}$	$\frac{\pi N_7 N_1 a_2}{14}$	$\frac{\pi N_5 N_7 a_1}{70}$	$\frac{\pi N_7 N_5 a_1}{70}$	$\frac{\pi N_3 N_7 a_3}{42}$	$\frac{\pi N_7 N_3 a_1}{42}$
L_{ff}	$\cos(6\theta_r - 30\alpha)$	$\cos(6\theta_r - 30\alpha)$	$\cos(2\theta_r - 10\alpha)$	$\cos(2\theta_r - 10\alpha)$	$\cos(10\theta_r - 50\alpha)$	$\cos(10\theta_r - 50\alpha)$
L_{fg}	$\cos(6\theta_r - 29\alpha)$	$\cos(6\theta_r - 37\alpha)$	$\cos(2\theta_r - 5\alpha)$	$\cos(2\theta_r - 17\alpha)$	$\cos(10\theta_r - 47\alpha)$	$\cos(10\theta_r - 57\alpha)$
L_{fh}	$\cos(6\theta_r - 28\alpha)$	$\cos(6\theta_r - 44\alpha)$	$\cos(2\theta_r)$	$\cos(2\theta_r - 24\alpha)$	$\cos(10\theta_r - 44\alpha)$	$\cos(10\theta_r - 64\alpha)$
L_{fi}	$\cos(6\theta_r - 27\alpha)$	$\cos(6\theta_r - 51\alpha)$	$\cos(2\theta_r + 5\alpha)$	$\cos(2\theta_r - 31\alpha)$	$\cos(10\theta_r - 41\alpha)$	$\cos(10\theta_r - 71\alpha)$
L_{gg}	$\cos(6\theta_r - 36\alpha)$	$\cos(6\theta_r - 36\alpha)$	$\cos(2\theta_r - 12\alpha)$	$\cos(2\theta_r - 12\alpha)$	$\cos(10\theta_r - 60\alpha)$	$\cos(10\theta_r - 60\alpha)$
L_{gh}	$\cos(6\theta_r - 35\alpha)$	$\cos(6\theta_r - 43\alpha)$	$\cos(2\theta_r - 7\alpha)$	$\cos(2\theta_r - 19\alpha)$	$\cos(10\theta_r - 57\alpha)$	$\cos(10\theta_r - 57\alpha)$
L_{gi}	$\cos(6\theta_r - 34\alpha)$	$\cos(6\theta_r - 50\alpha)$	$\cos(2\theta_r - 2\alpha)$	$\cos(2\theta_r - 26\alpha)$	$\cos(10\theta_r - 54\alpha)$	$\cos(10\theta_r - 54\alpha)$
L_{hh}	$\cos(6\theta_r - 42\alpha)$	$\cos(6\theta_r - 42\alpha)$	$\cos(2\theta_r - 14\alpha)$	$\cos(2\theta_r - 14\alpha)$	$\cos(10\theta_r - 70\alpha)$	$\cos(10\theta_r - 70\alpha)$
L_{hi}	$\cos(6\theta_r - 41\alpha)$	$\cos(6\theta_r - 49\alpha)$	$\cos(2\theta_r - 9\alpha)$	$\cos(2\theta_r - 21\alpha)$	$\cos(10\theta_r - 67\alpha)$	$\cos(10\theta_r - 77\alpha)$
L_{ii}	$\cos(6\theta_r - 48\alpha)$	$\cos(6\theta_r - 48\alpha)$	$\cos(2\theta_r - 16\alpha)$	$\cos(2\theta_r - 16\alpha)$	$\cos(10\theta_r - 80\alpha)$	$\cos(10\theta_r - 80\alpha)$

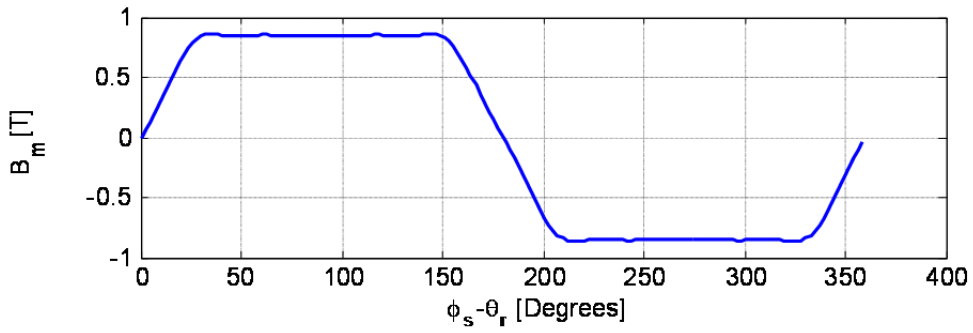

Figure 3.3 Trapezoidal approximation of magnet flux density due to permanent magnet

Solving Equation (3.21) with the substitution of the Equations (3.7) and (3.20), the flux linkage due to magnet and phase 'a' can be determined. Expressing in matrix form, the flux linkage due to magnet and all corresponding phases of the 9-phase machine is given as

$$\lambda_{abcdefghi\_m} = rl[k_1 \cos(\theta_r - k\alpha) + k_3 \cos 3(\theta_r - k\alpha) + k_5 \cos 5(\theta_r - k\alpha) + k_5 \cos 7(\theta_r - k\alpha)] \tag{3.22}$$

where, $k_1 = \pi B_1 N_1, k_3 = \frac{\pi B_3 N_3}{3}, k_5 = \frac{\pi B_5 N_5}{5}, k_7 = \frac{\pi B_7 N_7}{7}, \quad k = 0,1,2..8$ (3.23)

3.2.4 Synchronously Rotating q-d Voltage and Flux Equations

After the derivation of inductances in real variable form, equivalent transformation of 9-phase variables is the next task to be performed to decompose the higher phase orders into synchronously rotating axes with the reference frame angle of θ Recalling the transformation matrix as discussed in Chapter (1),

$$T(\theta)=\frac{2}{9}\begin{bmatrix} c(\theta) & c(\theta-\alpha) & c(\theta-2\alpha) & c(\theta-3\alpha) & c(\theta-4\alpha) & c(\theta-5\alpha) & c(\theta-6\alpha) & c(\theta-7\alpha) & c(\theta-8\alpha) \\ s(\theta) & s(\theta-\alpha) & s(\theta-2\alpha) & s(\theta-3\alpha) & s(\theta-4\alpha) & s(\theta-5\alpha) & s(\theta-6\alpha) & s(\theta-7\alpha) & s(\theta-8\alpha) \\ c3(\theta) & c3(\theta-\alpha) & c3(\theta-2\alpha) & c3(\theta-3\alpha) & c3(\theta-4\alpha) & c3(\theta-5\alpha) & c3(\theta-6\alpha) & c3(\theta-7\alpha) & c3(\theta-8\alpha) \\ s(3\theta) & s3(\theta-\alpha) & s3(\theta-2\alpha) & s3(\theta-3\alpha) & s3(\theta-4\alpha) & s3(\theta-5\alpha) & s3(\theta-6\alpha) & s3(\theta-7\alpha) & s3(\theta-8\alpha) \\ c(5\theta) & c5(\theta-\alpha) & c5(\theta-2\alpha) & c5(\theta-3\alpha) & c5(\theta-4\alpha) & c5(\theta-5\alpha) & c5(\theta-6\alpha) & c5(\theta-7\alpha) & c5(\theta-8\alpha) \\ s(5\theta) & s5(\theta-\alpha) & s5(\theta-2\alpha) & s5(\theta-3\alpha) & s5(\theta-4\alpha) & s5(\theta-5\alpha) & s5(\theta-6\alpha) & s5(\theta-7\alpha) & s5(\theta-8\alpha) \\ c(7\theta) & c7(\theta-\alpha) & c7(\theta-2\alpha) & c7(\theta-3\alpha) & c7(\theta-4\alpha) & c7(\theta-5\alpha) & c7(\theta-6\alpha) & c7(\theta-7\alpha) & c7(\theta-8\alpha) \\ s(7\theta) & s7(\theta-\alpha) & s7(\theta-2\alpha) & s7(\theta-3\alpha) & s7(\theta-4\alpha) & s7(\theta-5\alpha) & s7(\theta-6\alpha) & s7(\theta-7\alpha) & s7(\theta-8\alpha) \\ 1/2 & 1/2 & 1/2 & 1/2 & 1/2 & 1/2 & 1/2 & 1/2 & 1/2 \end{bmatrix} \tag{3.24}$$

where,'s' denotes the sine and 'c' denotes the cosine of the angles. Similarly, θdenotes the transformation angle and α denotes the phase shift angle which is equal to $\frac{2\pi}{9}$ radians.

Hence, multiplying both sides of Equation (3.1) by the transformation matrix $T(\theta)$,

$$T(\theta)V_{xs}=T(\theta)r_{xs}i_{xs}+T(\theta)p\lambda_{xs} \tag{3.25}$$

Denoting the transformed variables in q-d variables,

$$V_{qdxs}=T(\theta)r_{xs}T(\theta)^{-1}i_{qdxs}+T(\theta)p\lambda_{xs} \tag{3.26}$$

where, subscript 'xs' denotes the stator phases a,b,c…i of the 9-phase machine.

As described in Section (3.1), the flux linkage in each phase consists of flux due to the armature currents and the magnet flux, i.e.,

$$\lambda_{xs}=L_{ss}i_{xs}+\lambda_{xm} \tag{3.27}$$

where, λ_{xm} gives the flux due to the permanent magnet on the stator windings.

For evaluation of Equation (3.26), each term is considered separately. The first term of the equation gives the stator resistance matrix with constant stator resistance in the diagonal terms as

$$T(\theta)T(\theta)^{-1}=I \tag{3.28}$$

For the manipulation of second term,

$$T(\theta)p\lambda_{xs} = T(\theta)p\left(T(\theta)^{-1}\lambda_{qdoxs}\right) = T(\theta)pT(\theta)^{-1}\lambda_{qdoxs} + T(\theta)T(\theta)^{-1}p\lambda_{qdoxs} \quad (3.29)$$

The first term in Equation (3.29) gives the flux linkage due to speed component. The term $T(\theta)pT(\theta)^{-1}$ gives the matrix of Equation (3.30).

$$T(\theta)pT(\theta)^{-1} = \omega \begin{bmatrix} 0 & 1 & 0 & 0 & 0 & 0 & 0 & 0 & 0 \\ -1 & 0 & 0 & 0 & 0 & 0 & 0 & 0 & 0 \\ 0 & 0 & 0 & 3 & 0 & 0 & 0 & 0 & 0 \\ 0 & 0 & -3 & 0 & 0 & 0 & 0 & 0 & 0 \\ 0 & 0 & 0 & 0 & 0 & 5 & 0 & 0 & 0 \\ 0 & 0 & 0 & 0 & -5 & 0 & 0 & 0 & 0 \\ 0 & 0 & 0 & 0 & 0 & 0 & 0 & 7 & 0 \\ 0 & 0 & 0 & 0 & 0 & 0 & -7 & 0 & 0 \\ 0 & 0 & 0 & 0 & 0 & 0 & 0 & 0 & 0 \end{bmatrix} \quad (3.30)$$

where, ω is the angular speed of the reference frame of transformation.

For the second term of Equation (3.29), applying the transformation matrix given in Equation (3.24)

$$\lambda_{qd0xs} = T(\theta)\lambda_{xs} = T(\theta)L_{ss}i_{xs} + T(\theta)\lambda_{xm} \quad (3.31)$$

$$\lambda_{qd0xs} = T(\theta)L_{ss}T(\theta)^{-1}i_{qdxs} + T(\theta)\lambda_{xm} = L_{qd0xs}i_{qd0xs} + T(\theta)\lambda_{xm} \quad (3.32)$$

where, $L_{qd0xs} = T(\theta)L_{ss}T(\theta)^{-1}$ (3.33)

The q-d inductance as obtained in Equation (3.33) needs to be formulated with the help of equations of inductances derived in Table (3.1) and transformation matrix given in Equation (3.24). The use of identities given in Appendix A aids for the easy calculation of the q-d inductances in the evaluation of this inductance matrix. A simple example of the utilization of the identities for the derivation of one inductance element of Equation (3.33) is also given in Appendix A. There is the existence of self-inductance

terms for each harmonic and inter-harmonic inductance terms. The matrix given by Equation (3.33) has the following form:

$$L_{qd0xs} = \begin{bmatrix} L_{q1} & 0 & L_{13} & 0 & L_{15} & 0 & L_{17} & 0 & 0 \\ 0 & L_{d1} & 0 & L_{13} & 0 & L_{15} & 0 & L_{17} & 0 \\ L_{31} & 0 & L_{q3} & 0 & L_{35} & 0 & L_{37} & 0 & 0 \\ 0 & L_{31} & 0 & L_{d3} & 0 & L_{35} & 0 & L_{37} & 0 \\ L_{51} & 0 & L_{53} & 0 & L_{q5} & 0 & L_{57} & 0 & 0 \\ 0 & L_{51} & 0 & L_{35} & 0 & L_{d5} & 0 & L_{57} & 0 \\ L_{71} & 0 & L_{73} & 0 & L_{75} & 0 & L_{q7} & 0 & 0 \\ 0 & L_{71} & 0 & L_{73} & 0 & L_{75} & 0 & L_{d7} & 0 \\ 0 & 0 & 0 & 0 & 0 & 0 & 0 & 0 & L_0 \end{bmatrix} \tag{3.34}$$

After using the transformation matrix and applying the concept of balanced trigonometric identities as in Appendix A, the diagonal and off diagonal terms of Equation (3.34) are given as

$$L_{q1} = \frac{18\mu_0 rl}{16}\pi N_1^{\,2}[a_0 + \frac{a_1}{2}] + L_{ls} \tag{3.35}$$

$$L_{d1} = \frac{18\mu_0 rl}{16}\pi N_1^{\,2}[a_0 - \frac{a_1}{2}] + L_{ls} \tag{3.36}$$

$$L_{q3} = \frac{18\mu_0 rl}{9*16}\pi N_3^{\,2}[a_0 + \frac{a_2}{2}] + L_{ls} \tag{3.37}$$

$$L_{d3} = \frac{18\mu_0 rl}{9*16}\pi N_3^{\,2}[a_0 - \frac{a_2}{2}] + L_{ls} \tag{3.38}$$

$$L_{q5} = \frac{18\mu_0 rl}{25*16}\pi N_5^{\,2}[a_0 + \frac{a_3}{2}] + L_{ls} \tag{3.39}$$

$$L_{d5} = \frac{18\mu_0 rl}{25*16}\pi N_5^{\,2}[a_0 - \frac{a_3}{2}] + L_{ls} \tag{3.40}$$

$$L_{q7} = \frac{18\mu_0 rl}{49*16}\pi N_7^{\,2}[a_0 + \frac{a_4}{2}] + L_{ls} \tag{3.41}$$

$$L_{d7} = \frac{18\mu_0 rl}{49*16}\pi N_7^{\,2}[a_0 - \frac{a_4}{2}] + L_{ls} \tag{3.42}$$

$$L_0 = L_{ls} \tag{3.43}$$

$$L_{13} = \frac{8\mu_0 rl\pi N_1 N_3}{16}\frac{a_1}{3} \tag{3.44}$$

$$L_{15} = \frac{8\mu_0 rl\pi N_1 N_5}{16}\frac{a_2}{5} \tag{3.45}$$

$$L_{17} = \frac{8\mu_0 rl\pi N_1 N_7}{16}\frac{a_2}{7} \tag{3.46}$$

$$L_{35} = \frac{8\mu_0 rl\pi N_3 N_5}{16}\frac{a_1}{15} \tag{3.47}$$

$$L_{37} = \frac{8\mu_0 rl\pi N_3 N_7}{16}\frac{a_3}{21} \tag{3.48}$$

$$L_{57} = \frac{8\mu_0 rl\pi N_5 N_7}{16}\frac{a_1}{35} \tag{3.49}$$

The series of derivations from Equations (3.35) to (3.49) gives the clear picture of the effect of harmonics in derivation of the q-d inductances. Looking at Equation (3.35), the expression for L_{q1} shows that it has only the term with N_1. Similarly, Equation (3.36) consists the term only with N_3, i.e., the 3rd harmonics. The same result can be implied from Equations (3.38) to (3.42) for other harmonic numbers. Similarly from Equations (3.44) to (3.49), the inter-harmonic interactions give rise to different mutual inductances. In the expressions of inductances due to the effect of first and 3rd harmonics, as observed in Equation (3.44), it contains the term with N_1 and N_3. Similar results are obtained when Equations (3.45) to (3.49) are considered. Hence, this method gives an easy and generalized approach to determine the q-d inductances for higher phase order systems without the need of rigorous mathematical manipulations.

After the determination of the self and inter-harmonic inductances of stator windings, the mutual inductance between each harmonic component and the permanent magnet flux needs to be determined in order to account for the induced electromagnetic force in the stator windings. Applying the transformation in the flux equation described by Equation (3.22) and solving by the use of trigonometric identities, the induced magnet flux can be determined by Equation (3.50).

$$T(\theta)\lambda_{xm} = \begin{bmatrix} 0 \\ \frac{1}{2}\pi B_1 N_1 rl \\ 0 \\ \frac{1}{6}\pi B_3 N_3 rl \\ 0 \\ \frac{1}{10}\pi B_5 N_5 rl \\ 0 \\ \frac{1}{14}\pi B_7 N_7 rl \\ 0 \end{bmatrix} \tag{3.50}$$

It is also observed that, the flux linkage vector due to each harmonic component only has the terms associated in d- axes and corresponding harmonics of stator only interact with corresponding harmonics in permanent magnet flux. The q-axes components are zero as shown in Equation (3.50). The fundamental, 3rd, fifth and 7th harmonic q-d voltages induced in stator windings can be simply obtained by the multiplication of flux linkage with the corresponding speed of the harmonics. For example, the fundamental q-axis induced EMF is obtained by the product of fundamental speed, ω and second element of matrix given by Equation (3.50). Now using the set of Equations (3.25) to (3.50), the q-d voltage and flux equations are expressed as

$$
\begin{aligned}
V_{q1s} &= r_s i_{q1s} + \omega\lambda_{d1s} + p\lambda_{q1s} \\
V_{d1s} &= r_s i_{d1s} - \omega\lambda_{q1s} + p\lambda_{d1s} \\
V_{q3s} &= r_s i_{q3s} + 3\omega\lambda_{d3s} + p\lambda_{q3s} \\
V_{d3s} &= r_s i_{d3s} - 3\omega\lambda_{q3s} + p\lambda_{d3s} \\
V_{q5s} &= r_s i_{q5s} + 5\omega\lambda_{d5s} + p\lambda_{q5s} \\
V_{d5s} &= r_s i_{d5s} - 5\omega\lambda_{q5s} + p\lambda_{d5s} \\
V_{q7s} &= r_s i_{q7s} + 7\omega\lambda_{d7s} + p\lambda_{q7s} \\
V_{d7s} &= r_s i_{d7s} - 7\omega\lambda_{q7s} + p\lambda_{d7s} \\
V_{0s} &= r_s i_{0s} + p\lambda_{os}
\end{aligned}
\tag{3.51}
$$

$$
\begin{aligned}
\lambda_{q1s} &= L_{q1} i_{q1} + L_{13} i_{q3} + L_{15} i_{q5} + L_{17} i_{q7} \\
\lambda_{d1s} &= L_{d1} i_{d1} + L_{13} i_{d3} + L_{15} i_{d5} + L_{17} i_{d7} + \lambda_{md1} \\
\lambda_{q3s} &= L_{31} i_{q1} + L_{q3} i_{q3} + L_{35} i_{q5} + L_{37} i_{q7} \\
\lambda_{d3s} &= L_{31} i_{d1} + L_{d3} i_{d3} + L_{35} i_{d5} + L_{37} i_{d7} + \lambda_{md3} \\
\lambda_{q5s} &= L_{51} i_{q1} + L_{53} i_{q3} + L_{q5} i_{q5} + L_{57} i_{q7} \\
\lambda_{d5s} &= L_{51} i_{d1} + L_{53} i_{d3} + L_{d5} i_{d5} + L_{57} i_{d7} + \lambda_{md5} \\
\lambda_{q7s} &= L_{71} i_{q1} + L_{73} i_{q3} + L_{75} i_{q5} + L_{q7} i_{q7} \\
\lambda_{d7s} &= L_{71} i_{d1} + L_{73} i_{d3} + L_{75} i_{d5} + L_{d7} i_{d7} + \lambda_{md7} \\
\lambda_{0s} &= L_{0s} i_{0s}
\end{aligned}
\tag{3.52}
$$

With the use of Equations (3.51) and (3.52), it is now convenient to draw the equivalent circuit of the system including the effect of all harmonic components. Figure 3.4 shows the q-axis equivalent circuit and Figure 3.5 shows the d-axis equivalent circuit.

3.2.5 Derivation of the Torque Equation

After the derivation of the inductance equations, voltage and flux equations, the next step is the derivation of the torque equation to show the effect of individual harmonics in the resultant torque of the system. In this section, electromagnetic torque is

derived using the concept of co-energy and energy stored which can be given in terms of stator current and magnet flux linkage as

$$W_{co} = \frac{1}{2} I_s{}^t L_{ss} I_s + I_s{}^t \lambda_m \tag{3.53}$$

where, I_s is the current matrix and L_{ss} is the inductance matrix

From the relation between co-energy and electromagnetic torque,

$$T_e = \frac{\partial W_{co}}{\partial \theta_{rm}} \tag{3.54}$$

The evaluation of (3.54) follows from the the partial derivative of equation of co-energy, given in Equation (3.53).

Taking the partial derivative and differentiating by parts,

$$T_e = \frac{1}{2} I_s{}^t \frac{\partial L_{ss}}{\partial \theta_{rm}} I_s + I_s{}^t \frac{\partial \lambda_m}{\partial \theta_{rm}} \tag{3.55}$$

Using the relation between the mechanical angle θ_{rm} electrical angle θ_r in rotational systems,

$$\theta_r = \frac{P}{2} \theta_{rm} \tag{3.56}$$

Hence, Equation (3.55) becomes

$$T_e = \frac{P}{2} \frac{1}{2} I_s{}^t \frac{\partial L_{ss}}{\partial \theta_r} I_s + \frac{P}{2} I_s{}^t \frac{\partial \lambda_m}{\partial \theta_r} \tag{3.57}$$

Applying the reference frame transformation, and rearranging the terms, Equation (3.57) turns into

$$T_e = \frac{9}{2} \frac{P}{2} \frac{1}{2} \left[I_{qdos} \right]^t T(\theta) \frac{\partial L_{ss}}{\partial \theta_r} T(\theta)^{-1} I_{qdos} + \frac{9}{2} \frac{P}{2} \left[I_{qdos} \right]^t T(\theta) \frac{\partial \lambda_m}{\partial \theta_r} \tag{3.58}$$

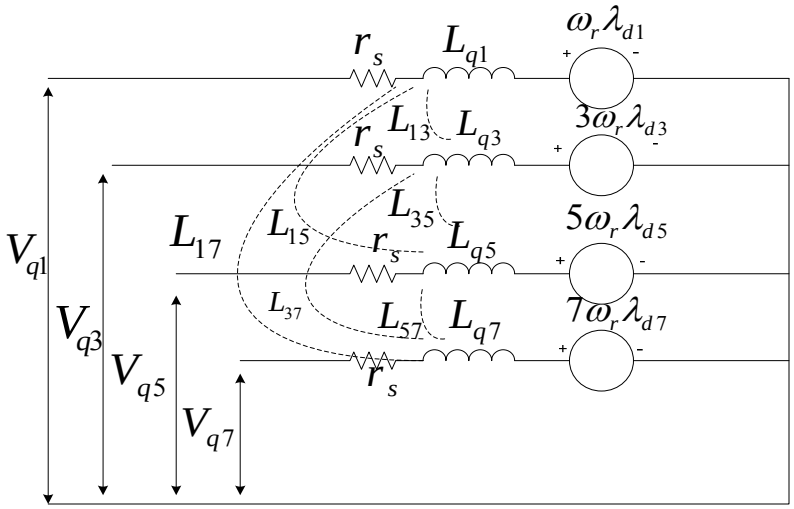

Figure 3.4 q axis equivalent circuit

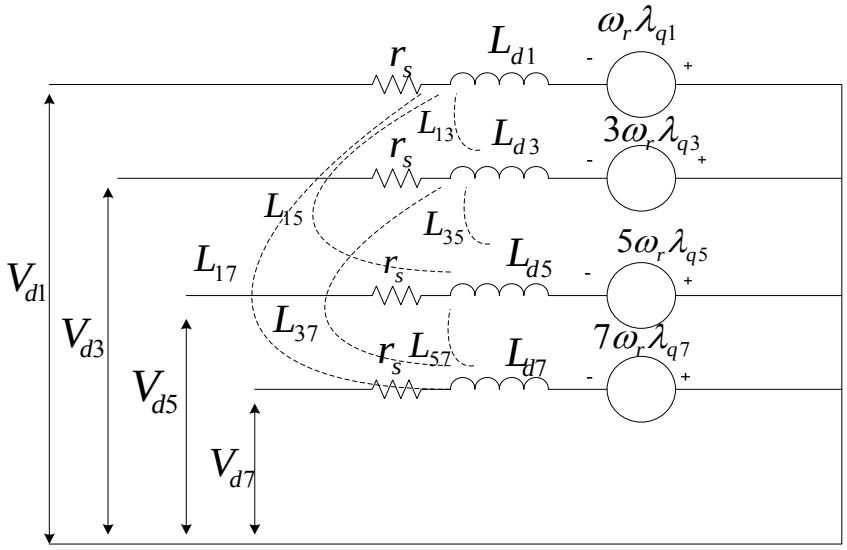

Figure 3.5 d axis equivalent circuit

In Equation (3.58), the expression of the torque involves the partial derivative of inductance matrix with respect to the rotor angle, and similarly the partial derivative of magnet flux with respect to the rotor angle. Applying the derivatives and use of identities

as described in Appendix A gives the torque equation in terms of q and d inductance matrix with the induced flux linkages as

$$\begin{aligned} T_e = {} & \frac{9P}{4}[(L_{q1}-L_{d1})i_{q1}i_{d1}+3(L_{q3}-L_{d3})i_{q3}i_{d3} \\ & +5(L_{q5}-L_{d5})i_{q5}i_{d5}+7(L_{q7}-L_{d7})i_{q7}i_{d7} \\ & +2L_{m13}(i_{q1}i_{d3}-i_{d1}i_{q3})+6L_{m15}(i_{q1}i_{d5}-i_{d1}i_{q5}) \\ & +6L_{m17}(i_{q1}i_{d7}-i_{d1}i_{q7})+2L_{m35}(i_{q3}i_{d5}-i_{d3}i_{q5}) \\ & +2L_{m57}(i_{q5}i_{d7}-i_{q7}i_{d5})+10L_{m37}(i_{q3}i_{d7}-i_{q7}i_{d3})] \\ & +\frac{9P}{4}[i_{q1}\lambda_{dm1}+3i_{q3}\lambda_{dm3}+5i_{q5}\lambda_{dm5}+7i_{q7}\lambda_{dm7}] \end{aligned} \tag{3.59}$$

The expression of Equation 3.59 gives an interesting observation regarding the harmonic components and the total torque contribution. The contribution of each harmonic component can be observed and inter-harmonic inductances are also in torque formulation contributing to the total torque. This observation signifies the importance of including the higher time and space harmonics in the analysis of the system. Hence, improvement of torque is obtained through the injection of higher order harmonic currents in the motor which is verified by Equation (3.59). The individual harmonic current control algorithm can be utilized to perform the feedback control of the machine for the better improvement of the machine torque.

3.3 Air-gap Flux Analysis of 9-Phase IPM Machine

The analysis of air gap flux is performed to observe the performance characteristics of the drive under any operating conditions. The knowledge of air gap flux leads to steady state and dynamic analysis of the machine under different operating

conditions. Similarly, in the case of permanent magnet machines, the determination of induced flux linkage induced EMF and other parameter estimations are performed only after the analysis of the air gap flux. In this section, the 9-phase machine is analyzed extensively using the fundamental concepts of Ampere's law and magnetic circuits. With the help of reference frame transformation, the analysis is performed in d-q reference frame which aids for the easier mathematical evaluations.

3.3.1 Basic Machine Model Used for Analysis

The stator of the machine to be analyzed has m-phase winding with $\frac{NK_w}{P}$ sinusoidally distributed turns per pole.

where,

N = Number of stator turns

K_w = Winding factor

P = Number of poles

Suppose that currents $i_a, i_b \ldots i_m$ flow through each of the phase windings. For the purpose of analysis, the air gap is increased by the Carter's coefficient which is calculated in [40]. In particular, the equivalent air gap is given in terms of actual air gap *g'* as

$$g = g' k_{cs} k_{cr} k_s \tag{3.60}$$

where, k_{cs} and k_{cr} are carter coefficients for stator and rotor slotted surfaces and k_s is a saturation factor for the iron parts of the machine. The transformation of the voltages and

flux linkages to a d-q reference model is made using the Park's transformation. In this analysis only the fundamental component is taken into account, hence, for the 9-phase machine, the Park's transformation with the fundamental component is given as

$$T(\theta)=\frac{2}{9}\begin{bmatrix} c(\theta) & c(\theta-2\alpha) & c(\theta-3\alpha) & c(\theta-4\alpha) & c(\theta-5\alpha) & c(\theta-6\alpha) & c(\theta-7\alpha) & c(\theta-8\alpha) \\ s(\theta) & s(\theta-2\alpha) & s(\theta-3\alpha) & s(\theta-4\alpha) & s(\theta-5\alpha) & s(\theta-6\alpha) & s(\theta-7\alpha) & s(\theta-8\alpha) \end{bmatrix} \quad (3.61)$$

The analysis of the machine has following assumptions:

a. The relative motion between stator and rotor can be represented by identical configurations but having no relative motion.

b. The representation of m-phase stator can be applied as a d and q winding, each being equivalent to the original winding except that their axes lie, respectively along d and q axes.

c. The values of magneto-motive force on the stator surface at any angle θ from the d axis are given as

$$F_d = \frac{4}{\pi}\frac{m/2(\sqrt{2}I_d)Nk_w}{P}\cos\frac{P}{2}\theta \quad (3.62)$$

$$F_q = \frac{4}{\pi}\frac{m/2(\sqrt{2}I_q)Nk_w}{P}\cos\frac{P}{2}\theta \quad (3.63)$$

where

m = No. of phases

I_d = d-axis current

I_q = q-axis current,

P = No. of poles

k_w= Winding factor

The flux lines in the air gap are radial flux lines across the magnets lie in perpendicular direction to the face of the magnet.

3.4 Fields Caused by the Magnets Acting Alone

In the analysis of the permanent magnet machine, the flux in the air gap which is caused by magnet alone will induce a voltage called the open-circuit voltage E_0. The flux which exists due to magnet is a d-axis flux since it is represented symmetrically over a pole. [73].

3.4.1 Representation of Magnet

The normal B-H characteristic of a magnet is assumed to be linear and it lies in the second quadrant. This is true to many of the materials made for the magnet, particularly ferrites and earth materials. The B-H characteristic of the magnet is represented in terms of residual flux density, B_r as

$$B = -\mu' H + B_r \tag{3.64}$$

where, μ' is the permeability of the magnetic material.

This linear characteristic of the magnetic material is shown in Figure 3.6.

In terms of the residual magnetic flux density and coercive force, the slope of Figure 3.6 is given as

$$\mu' = \frac{B_r}{H_c} \tag{3.65}$$

This property is applicable to the permanent magnet material but not to the entire magnet. For the magnet characteristics Ampere's law is applied as following for calculation of total flux in the system

$$\varphi = BA_m \tag{3.66}$$

$$F = HL_m \tag{3.67}$$

where, A_m and L_m are the magnetic area and length. From Figure 3.6 and Equations (3.66) and (3.67) it is observed that the magnet characteristic is linear with the intercepts equal to residual flux, $\phi_r = B_r A_m$ and coercive force, $F_c = H_c L_m$

Hence, from Equations (3.66) and (3.67), the total flux in the system can be given in terms of residual magnetic flux and coercive force as

$$\phi = -\left(\frac{\phi_r}{F_c} F + \phi_r\right) \tag{3.68}$$

In the Equation (3.68), the quantity $\frac{F_c}{\phi_r}$ is represented as reluctance of the magnet

$$\frac{F_c}{\phi_r} = \frac{H_c L_m}{B_r A_m} = \frac{L_m}{\mu' A_m} = R_m \tag{3.69}$$

3.4.2 Equation Form of Magnet Configuration

The magnet configuration for the IPM machine provided is given in Figure 3.7, where 1/4th of the machine configuration with the magnet is presented.

For this configuration, there are two integral paths as observed in Figure 3.7. First path is located entirely on the rotor and links only the rotor magnets while another one links the stator and the magnet part. Now the resultant consists of the line integrals with these two configurations.

Using Ampere's integral law for the two paths,

$$\begin{aligned} H_1 L_1 - H_2 L_2 &= 0 \\ 2gH_f - H_1 L_1 &= 0 \end{aligned} \tag{3.70}$$

where, L_1 and L_2 are the lengths of the corresponding segments and g is the air gap length.

Now a flux balance equation is needed in addition to the integral quantities discussed. The flux ϕ_m for the magnet sections is considered to be sum of magnet air gap flux ϕ_f and the steel bridge leakage flux ϕ_l with stack length, l_s

$$\phi_m = 2l_s\left(h_1 B_1 + h_2 B_2\right) = \phi_f + \phi_l \tag{3.71}$$

where, h_1 and h_2 are the magnet width for Path 1 and 2, respectively.

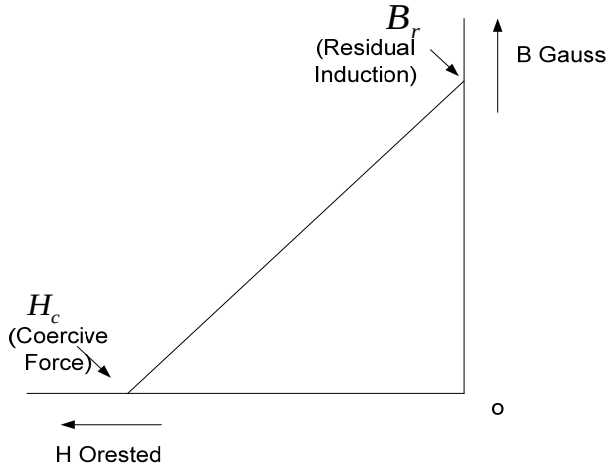

Figure 3.6 B-H characteristics of a magnetic material

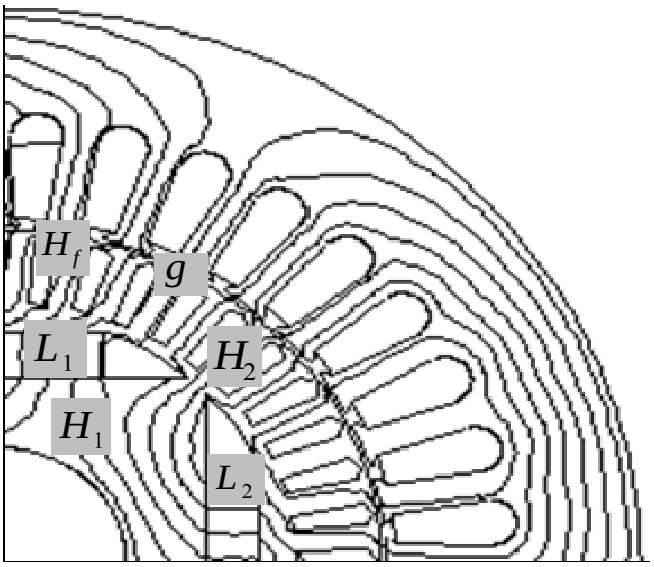

Figure 3.7 Flux pattern for 1/4th of the machine

To define B_1 and B_2 one should go towards the fundamental of Ampere's law and Figure 3.7. In general they are given in terms of residual flux densities B_{r1} and B_{r2} for Sections 1 and 2, respectively:

$$B_1 = -\mu_1 H_1 + B_{r1} \tag{3.72}$$

$$B_2 = -\mu_2 H_2 + B_{r2} \tag{3.73}$$

3.4.3 Leakage Flux in Steel Bridges

The leakage flux in the steel bridge is the resultant of the magnet effect and the armature reaction (i.e., caused by the stator currents on the magnet). This analysis is performed only using the magnet part. For this analysis, suppose that the stator is open circuited, i.e., there is no armature reaction.

Considering the particular case of the steel bridge as in Figure 3.8, the Amperes law for bridge and air gap parts yields,

$$\begin{aligned} H_1 L_1 - H_{t1} L_1 &= 0 \\ 2gH_f - H_1 L_1 &= 0 \end{aligned} \tag{3.74}$$

Also from Figure 3.8, the field strength on the bridge is found to be $H_{t1} = 2gH_f L_1$. Hence for the two bridges, the total flux is

$$\phi_{l1} = B_{t1} 2t_1 l_s = 2gH_f \mu_1 2t_1 \frac{l_s}{L_1} = 2\phi_f \frac{R_g}{R_{l1}} \tag{3.75}$$

where

$$R_g = \frac{g}{A_g}, R_{l1} = \frac{L_1}{\mu_1 2t_1 l_s}, \phi_f = B_f A_g \tag{3.76}$$

The total leakage flux per pole is the leakage in two bridges of dimensions L_1, t_1, μ_1 and L_2, t_2, μ_2. The total leakage flux per pole is

$$\phi_l = \phi_{l1} + \phi_{l2} = 2\phi_f \frac{R_g}{R_l} \tag{3.77}$$

where

$$R_l = \frac{1}{\left(\frac{\mu_1 t_1}{L_1} + \frac{\mu_2 t_2}{L_2} \right) 2l_s} \tag{3.78}$$

3.4.4 Air-gap Flux Due to Magnets

From the combination of the derivations (3.74)-(3.78), the following equations can be achieved for the field of the magnet.

$$
\begin{aligned}
&H_1 L_1 - H_2 L_2 = 0 \\
&2gH_f - H_1 L_1 = 0 \\
&2l_s\left(h_1 B_1 + h_2 B_2\right) = \phi_f + \phi_l \\
&B_1 = -\mu_1 H_1 + B_{r1} \\
&B_2 = -\mu_2 H_2 + B_{r2} \\
&\phi_l = 2\phi_f R_g / R_l
\end{aligned}
\tag{3.79}
$$

Solving these equations simultaneously,

$$
\phi_f = \frac{\phi_r}{1 + \beta k_l} \tag{3.80}
$$

where

ϕ_r = Remnant flux = $2l_s\left(h_1 B_{r1} + h_2 B_{r2}\right)$

$$
k_l = \text{Leakage factor} = 1 + \frac{R_m}{R_l} \tag{3.81}
$$

$$
\begin{aligned}
&\beta = 2R_g / R_m \\
&R_g = g / A_g
\end{aligned}
\tag{3.82}
$$

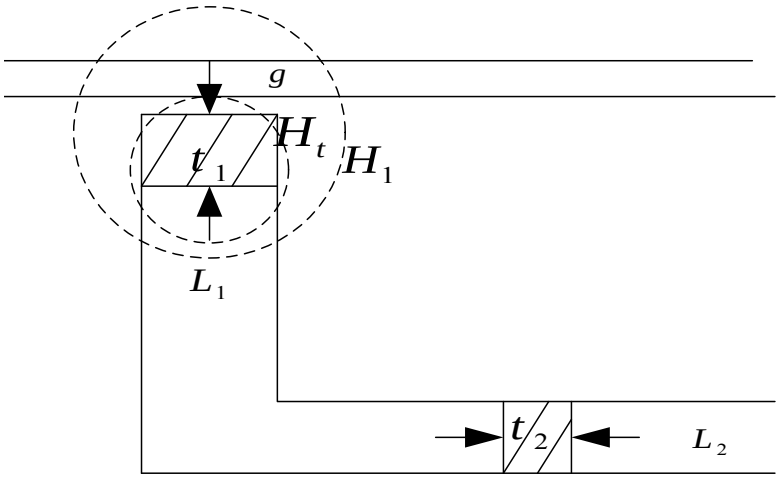

Figure 3.8 Flux pattern for steel bridges

$$R_m = \text{Reluctance of Sections 1 and 2} = \frac{1}{\frac{1}{R_1}+\frac{1}{R_2}} \tag{3.83}$$

where

$$R_1 = \text{Reluctance of Section 1} = \frac{L_1}{\mu_1' 2 l_s h_1} \tag{3.84}$$

$$R_2 = \text{Reluctance of Section 2} = \frac{L_2}{\mu_2' 2 l_s h_2} \tag{3.85}$$

By rearrangement of Equations (3.79)-(3.85), the following equations are obtained.

$$\phi_f = B_r A_g \frac{A_m / A_g}{1+\beta k_l} \tag{3.86}$$

$$B_r = \frac{\phi_r}{A_m} = \frac{h_1 B_{r1} + h_2 B_{r2}}{h_1 + h_2} \tag{3.87}$$

3.4.5 Flux Density Due to the Magnets

The flux density in the air gap due to the magnet is given as

$$B_f = \frac{\phi_f}{A_g} = \frac{B_r\left(\frac{A_m}{A_g}\right)}{1+\beta k_l} \tag{3.88}$$

This density is constant over one pole pitch. The actual tapered flux density is shown in Figure 3.8 and it can be represented by a Fourier series as

$$B_f = \left(\frac{4}{\pi}\right)\left(\frac{\phi_f}{A_g}\right)\sum_{n=1,3,5}^{\infty} k_{fn} \frac{\cos n\frac{P}{2}\phi}{n} \tag{3.89}$$

$$k_{fn} = \frac{\sin n\gamma}{n\gamma} \tag{3.90}$$

where,

$$\gamma = \frac{PL_1}{2D} \tag{3.91}$$

D is the diameter of the machine between two points of air gap and P is the number of poles.

Using the parameters of the machine from Appendix B, the trapezoidal approximation of the flux density of the magnets is obtained as in Figure 3.9. Figure 3.10 gives the Fourier analysis of the waveform for flux density.

3.5 Field Due to the Armature Currents

The previous derivations are based on the flux due to the magnet alone; hence there is no influence of armature currents in air gap. However, the total air gap flux is the summation of the flux due to armature currents and the permanent magnet. The derivations are now focused on the influence of the armature currents on the air gap flux.

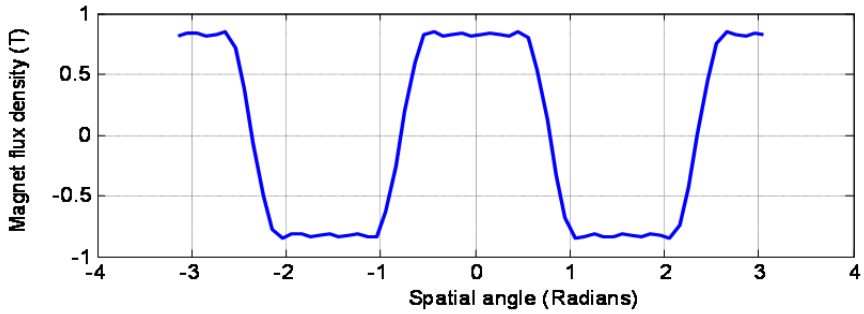

Figure 3.9 Trapezoidal flux density due to magnet

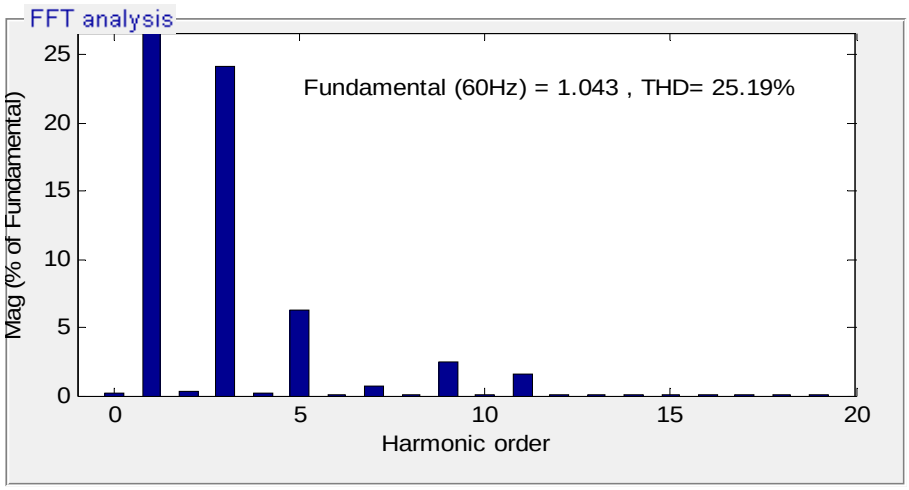

Figure 3.10 Fourier series amplitudes for flux density due to magnet

First, derivation of the flux density in direct axis caused by armature currents is calculated then, the derivation is performed quadrature axis component.

3.5.1 Flux Density in Direct Axis Caused by Armature Currents

The air gap flux density B_{ad} caused by the direct axis armature currents can be obtained from the set of equations similar to the previous Section 3.4 and with the following exceptions:

a. The MMF created by the stator currents is now going to be included with the source of flux given by an amount of the current corresponding to $2F_{dm}\cos(P/2)\theta$.

b. Since the assumption is that the magnets are un-magnetized, the magnet sections has the permeability of 1.

c. Both B_1 and B_2 have the same general directions since the flux in the rotor originates from the stator windings.

d. The flux balance equations should now become,

$$\phi_m = \phi_f + \phi_l, \phi_{ad} = \phi_m + \phi_l \tag{3.92}$$

Hence from the assumptions 'a'-'d', and using the same derivations steps presented in Section 3.4, the equations to be solved are given as

$$\begin{aligned} &H_1'L_1 - H_2'L_2 = 0 \\ &2gH_{ad} + H_1'L_1 = C_d F_{dm} \cos(P/2)\theta \\ &2l_s(h_1B_1' + h_2B_2') + \phi_l' = Dl_s \int_0^{\pi/P} B_{ad}\, d\phi \\ &B_1' = -\mu_1' H_1' \\ &B_2' = -\mu_2' H_2' \end{aligned} \tag{3.93}$$

where,

$$C_d = \frac{4}{\pi} \frac{m/2(\sqrt{2}I_d)Nk_w}{P} \tag{3.94}$$

The flux balance equation given in Equation (3.90) can be rewritten as

$$Dl_s \int_0^{\pi/P} B_{ad}\, d\phi = \phi_m' + \phi_l' = \phi_m' \left(1 + \frac{\phi_l'}{\phi_m'}\right) = \phi_m' k_l \tag{3.95}$$

Here, k_l represents the leakage factor due to armature currents. It has the same form as Equation (3.81).

The magnet flux can now be evaluated by substitution of first and last two equations of (3.93). Hence,

$$R_1 = \text{Reluctance of Section 1} = \frac{L_1}{\mu_1' 2 l_s h_1} \tag{3.96}$$

$$R_2 = \text{Reluctance of Section 2} = \frac{L_2}{\mu_2' 2 l_s h_2} \tag{3.97}$$

Hence, the magnet flux is given by

$$\begin{aligned}\phi_m &= 2 l_s \left(h_1 B_1' + h_2 B_2'\right) \\ &= H_1 L_1' \Big/ \left(\frac{1}{R_1} + \frac{1}{R_2}\right)\end{aligned} \tag{3.98}$$

For the air gap, B_{ad} and H_{ad} have the same value. Using Equations (3.93), (3.94) and (3.95) and solving for H_1,

$$H_1' = \frac{2 C_d F_{dm}}{L_1 \left(1 + \beta k_l\right)} \tag{3.99}$$

Eliminating H_1' from Equation (3.99) and Equation (3.93), and solving for B_{ad},

$$B_{ad} = \frac{C_d \pi F_{dm}}{2g}\left[\cos\left(P/2\right)\theta - \frac{2/\pi}{1 + \beta k_l}\right] \tag{3.100}$$

The air gap field is described by Equation (3.100).

3.5.2 Flux Density in Quadrature Axis Caused by Armature Currents

The quadrature axis flux does not cross the magnet face. Hence, the equation that satisfies for this case is

$$2 g H_{aq} = C_d \pi F_{qm} \sin\left(P/2\right)\theta \tag{3.101}$$

For the air gap, $B_{aq} = H_{aq}$. Hence,

$$B_{aq} = \frac{C_d \pi F_{qm}}{2g}\left[\sin\left(P/2\right)\theta\right] \tag{3.102}$$

3.6 The Total Field and Magnet Operating Point

The total air gap field B_g is the combination of the magnet and armature current fields

$$B_g = B_f + B_{ad} + B_{aq} \tag{3.103}$$

From previous sections,

$$B_f = \frac{\phi_f}{A_g} = \frac{B_r\left(\frac{A_m}{A_g}\right)}{1+\beta k_l} \tag{3.104}$$

$$B_{ad} = \frac{C_d \pi F_{dm}}{2g}\left[\cos(P/2)\theta - \frac{2/\pi}{1+\beta k_l}\right] \tag{3.105}$$

$$B_{aq} = \frac{C_d \pi F_{qm}}{2g}\left[\sin(P/2)\theta\right] \tag{3.106}$$

Adding (3.104), (3.105) and (3.106), the total air gap flux density is given as

$$B_g = B_{gk} + \frac{C_d}{2}\frac{\pi}{g}F\cos\frac{P}{2}(\alpha-\theta)$$

$$B_{gk} = B_r\left(A_m / A_g\right) - 2C\frac{F_{dm}}{g}$$

$$F = \sqrt{F_{dm}{}^2 + F_{qm}{}^2}$$

$$\alpha = \cos^{-1}\frac{F_{dm}}{F} \tag{3.107}$$

From Equation 3.94, the condition for maximum air gap flux density is

$$\alpha = \theta \tag{3.108}$$

Hence, for the maximum air gap flux density in the air gap for IPM machine, the angle between the resultant MMF and d-axis MMF, α should be equal to the considered space angle, θ.

3.7 Simulation Results

To observe the flux density pattern, a computer simulation is performed using the permanent magnet parameters given in Appendix B. For the stator peak current of 10 A, finite element simulation is performed and the flux pattern is shown in Figure 3.11. The variation of air gap flux density along the circumferential angle is shown in Figure 3.12. To observe the resultant flux density due to armature current and magnet flux, the q-axis current is fixed at 8 A and the d-axis current is fixed at 6 A. With the given rated magnet flux density, the resultant plot is obtained and given in Figure 3.13.

Moreover, the simulation is also carried out to study the effect of the flux due to different current angle. A three dimensional plot is performed and shown in Figure 3.14 taking peak stator current as 10 A. Similarly, for the same case, a contour plot is drawn in Figure 3.15 to observe the clear picture of the flux density due to magnet, current angle (alpha) and spatial angle (phi).

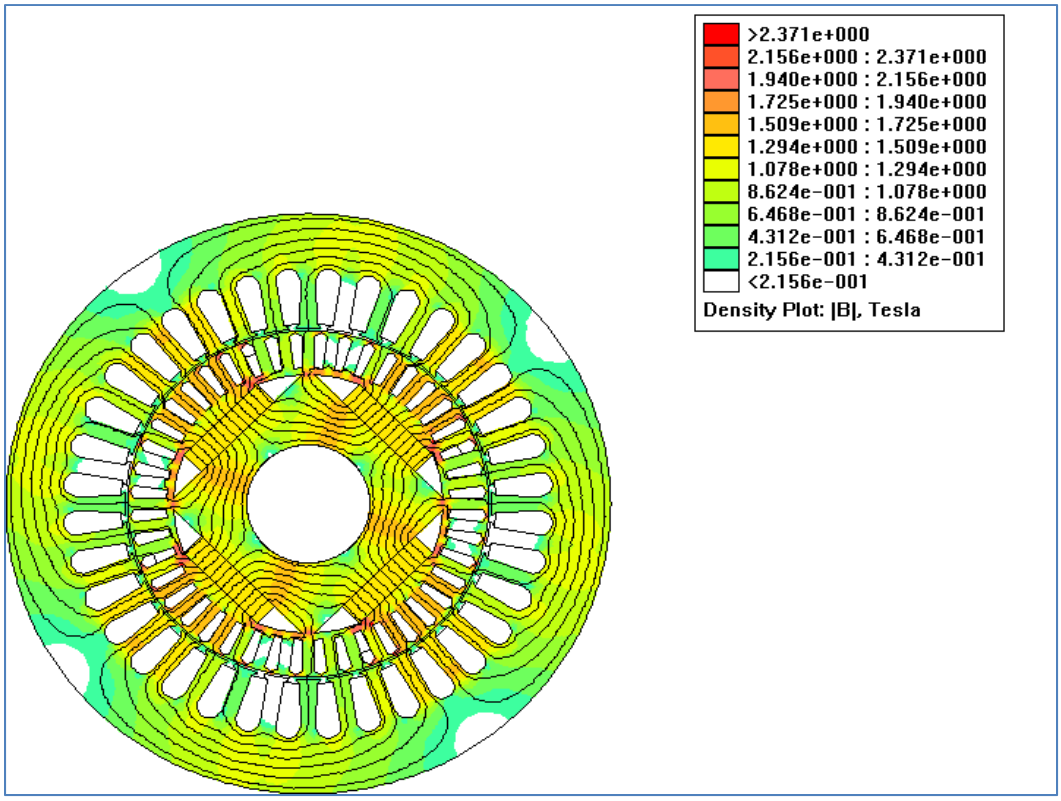

Figure 3.11 Flux patterns for 9-phase IPM machine with rated current

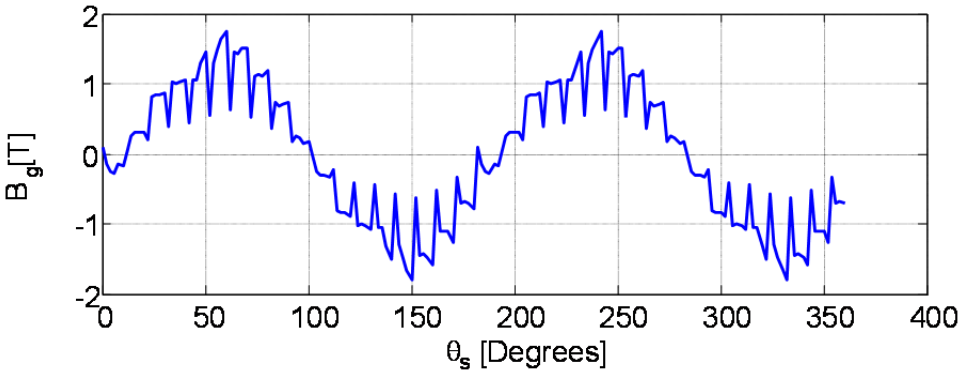

Figure 3.12 Flux density plot for 9-phase IPM machine with rated current

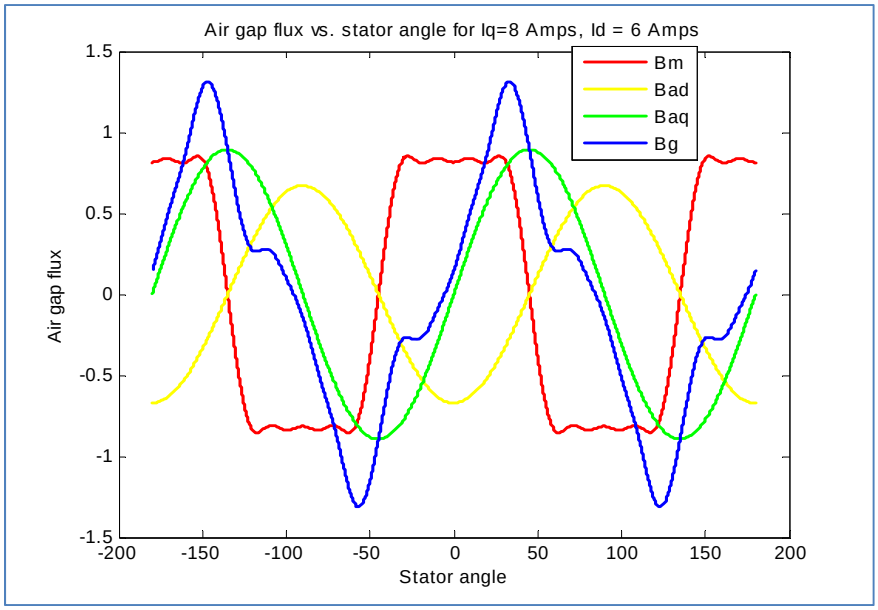

Figure 3.13 Variation of air gap flux density with variation in spatial angle

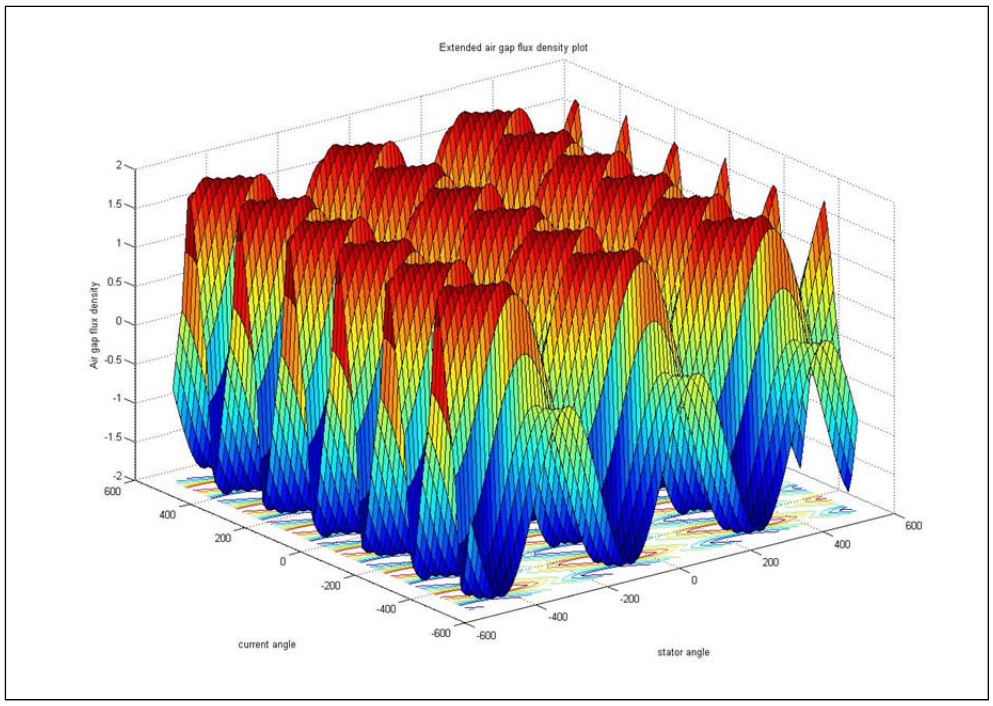

Figure 3.14 Variation of flux density with current angle and spatial angle

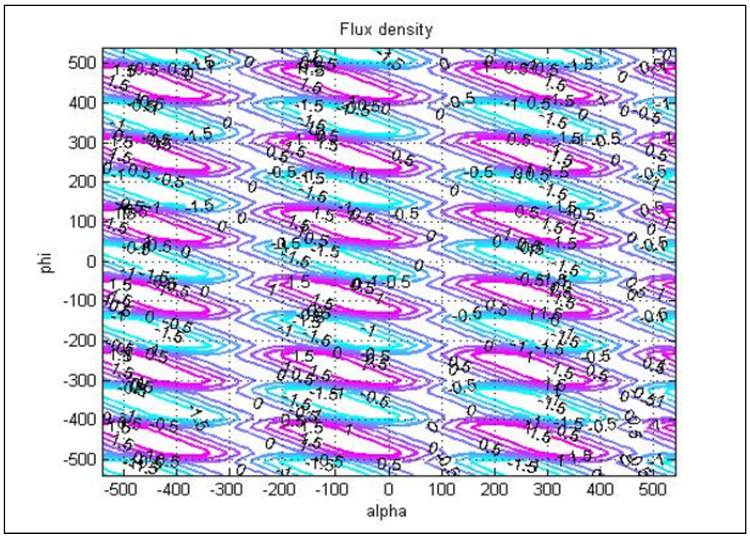

Figure 3.15 Contour plot for 10 A peak current

Figures 3.11-3.15 give some interesting observations in different operating conditions of the 9-phase IPM machine. For peak current of 10 A, the finite element simulation shows the variation of air gap flux density with the circumferential angle. The total flux density in air gap is also obtained with different q and da axis currents in the rated magnet flux condition. With the change of current angle and spatial angle, the 3-dimensional plot in Figure 3.14 gives the sinusoidal variation of the flux density in air gap for peak current of 10 A. From the contour plot, it was observed that the maximum flux density is about 1.5 T which is comparable from the finite element simulation results.

3.8 Conclusion

In this chapter, a comprehensive analysis of 9-phase IPM machine is performed with the inclusion of higher order harmonics. The closed form solution of the model

equations are obtained by using the Fourier series approximation of winding function and air gap function. Similarly, the effect of each harmonic component in the overall torque production is studied without the consideration of damper bars. Similarly, the air gap flux analysis is performed with the analysis of armature reaction and magnet effects. The 2-dimensional finite element plot is drawn to observe the variation of air gap flux density with the circumferential angle. Similarly, variation of the air gap with current angle and spatial angle is also observed under the rated condition for the 9-phase IPM machine. A 3-dimensional analysis is also performed to observe variation of the air gap flux by varying the current angle of the stator windings. Hence, analytical and mathematical methods are applied in this chapter to analyze the 9-phase IPM machine in different operating conditions.

CHAPTER 4

FULL ORDER Q-D MODELING AND SIMULATION OF 9-PHASE IPM MACHINE

4.1 Introduction

This chapter introduces a new technique in modeling of 9-phase IPM machine using the graphical form of the winding functions of stator, rotor damper bars and magnet. The method of transformation is highly applicable in studying performance characteristics of the machine due to reduced numbers of equations. In this chapter, the machine variables are transformed to q-d variables graphically and the equivalent circuit variables of the machine are also derived graphically using corresponding dynamic equations. Firstly, q-d stator winding functions are evaluated in stationary reference frame with harmonics. Secondly, the stationary reference frame transformation is extended to the rotor bars to evaluate the q and d winding functions. Thirdly, self and mutual inductances of stator and rotor circuits are evaluated graphically with the assumption of coupled circuit model of the machine. Finally, with the help of the permanent magnet flux density waveform, the induced voltages of the machine winding is evaluated graphically and the equivalent circuit is reflects the harmonic and inter-harmonic effects. This method gives the solution of machine equations in graphical form avoiding the complex mathematical manipulations.

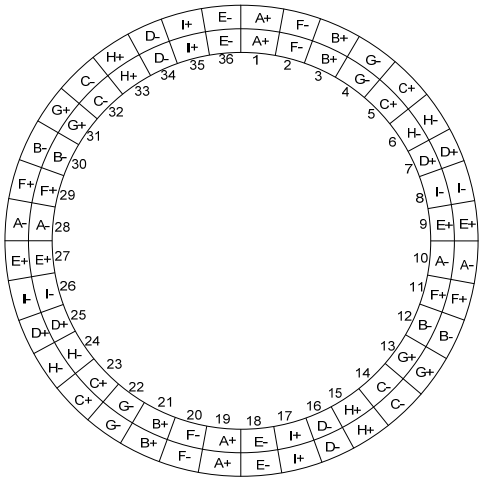

Figure 4.1 Clock diagram of 9-phase IPM machine showing phase distribution

4.2 Stator Winding Functions of 9-Phase IPM Machine

The 9-phase machine to be modeled is a 2 HP 4-pole, full pitched machine having 48 damper bars. The stator slots are dual layered and the number of coils per slot is 56. Figure 4.1 presents the clock diagram of the stator windings showing the phase distribution.

4.2.1 Turn and Winding Functions

The stator turn and winding functions plotted against the circumferential angle of the different phases are shown in Figure 4.2, 4.3 and 4.4. The number of conductors per layer per slot for the stator winding N_s is 28. Since the machine is double layered, the number of conductors per slot is twice N_s. Also as seen in the clock diagram of the machine, only a particular phase having a particular orientation fills up a given slot.

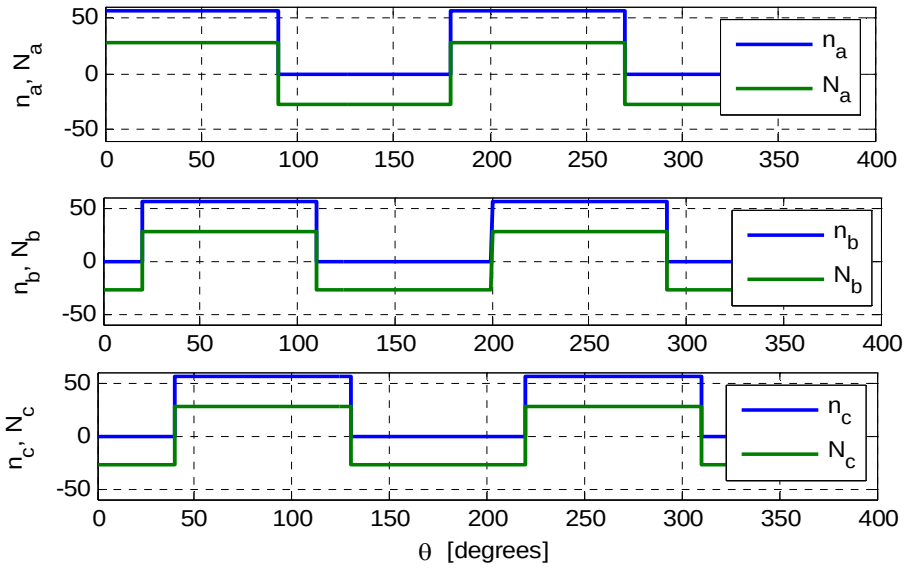

Figure 4.2 Turn and winding functions for phases 'a', 'b', and 'c' of 9-phase IPM machine

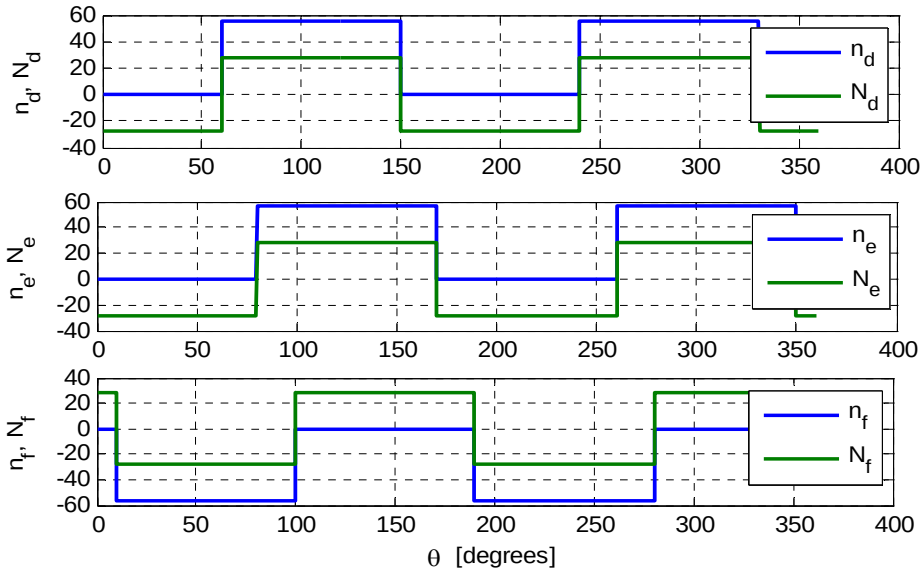

Figure 4.3 Turn and winding functions for phases 'd', 'e' and 'f' of 9-phase IPM machine

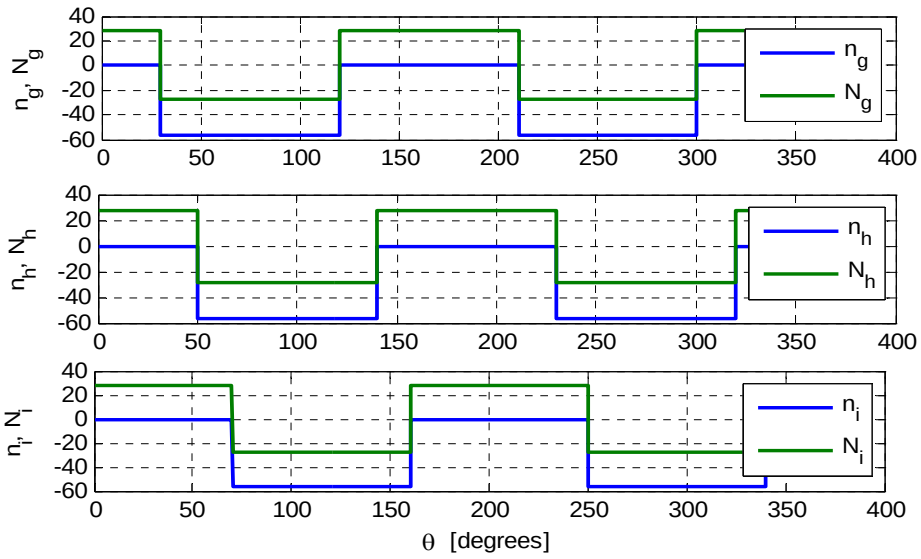

Figure 4.4 Turn and winding functions for phases 'g', 'h' and 'i' of 9-phase IPM machine

4.3 Stationary Reference Frame Transformation of Stator Winding Functions

The winding functions obtained in Section 4.2 are in real variables and to avoid the large number of derivation steps and complex calculations, it is convenient to express these winding functions in any arbitrary reference frame. In this section, the winding functions of Section 4.2 are transformed into the stationary reference frame using the transformation matrix with the inclusion of fundamental and higher order harmonics. The transformation matrix is the same as used in Chapter 3. Figures 4.5-4.12 depict the q and d winding functions transformed from Section 4.2 for each harmonics of the stator winding functions transformed in the stationary reference frame. Similarly, Figure 4.13 shows the zero sequence winding functions of the stator windings obtained from the real variable winding functions in Section 4.2.

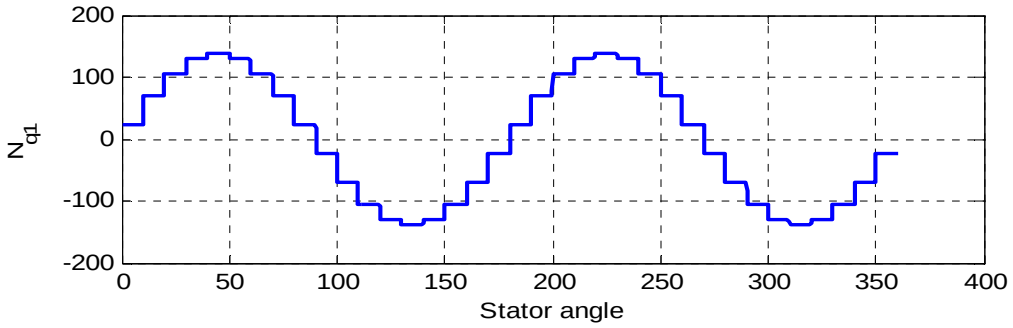

Figure 4.5 q-axis fundamental stator winding function vs. stator angle

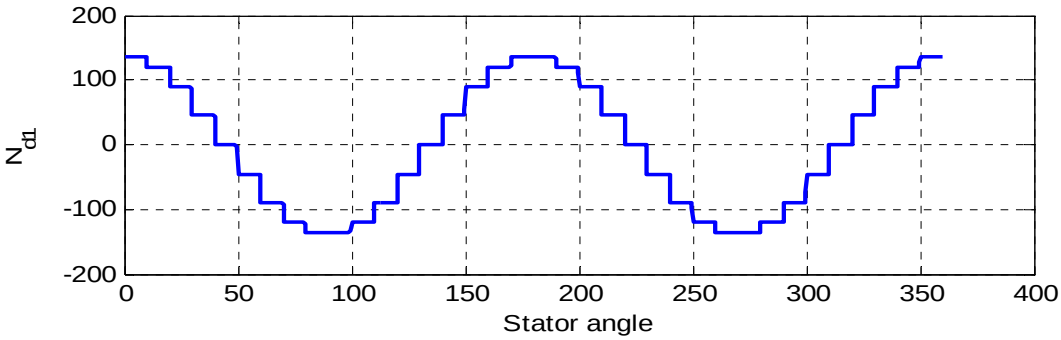

Figure 4.6 d- axis fundamental stator winding function vs. stator angle

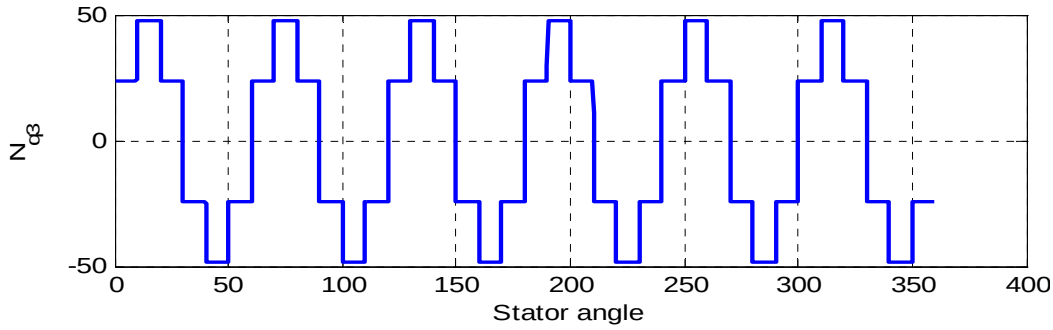

Figure 4.7 q-axis 3rd harmonic stator winding function vs. stator angle

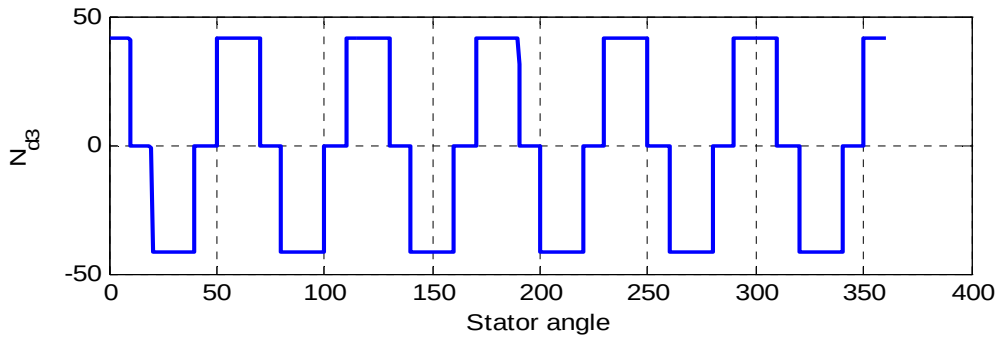

Figure 4.8 d-axis 3rd harmonic stator winding function vs. stator angle

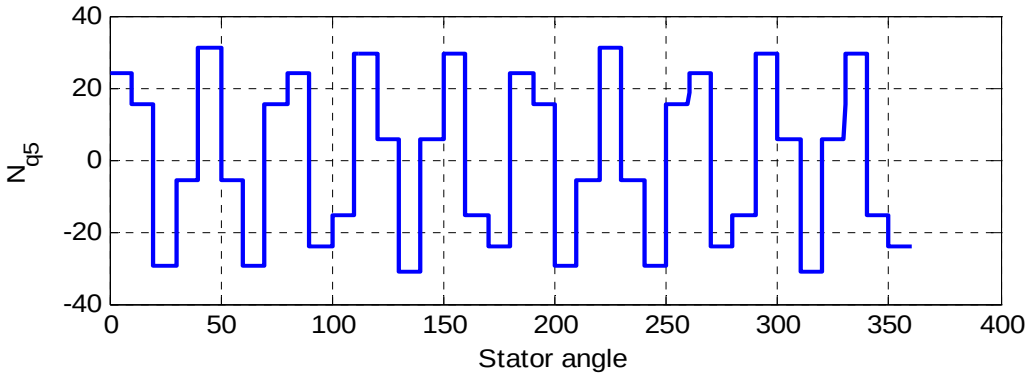

Figure 4.9 q- axis 5th harmonic stator winding function vs. stator angle

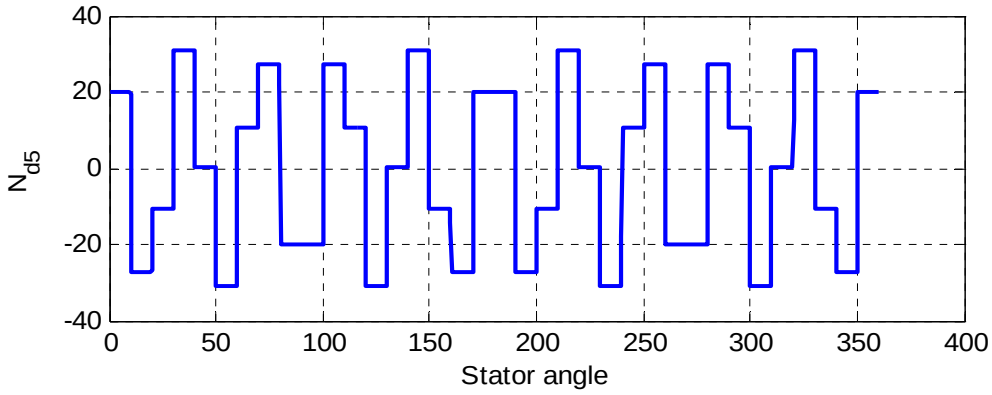

Figure 4.10 d-axis 5th harmonic stator winding function vs. stator angle

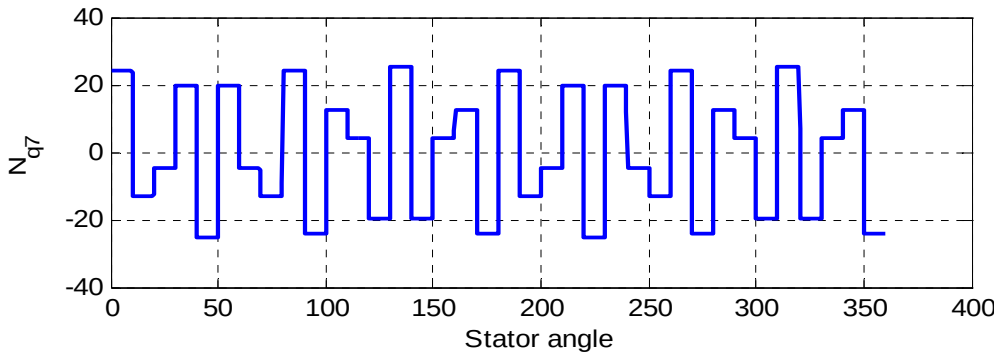

Figure 4.11 q-axis 7th harmonic stator winding function vs. stator angle

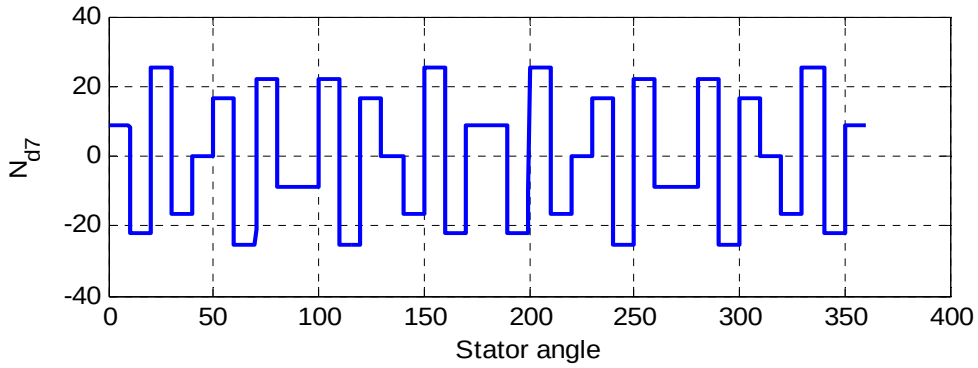

Figure 4.12 d-axis 7th harmonic stator winding function vs. stator angle

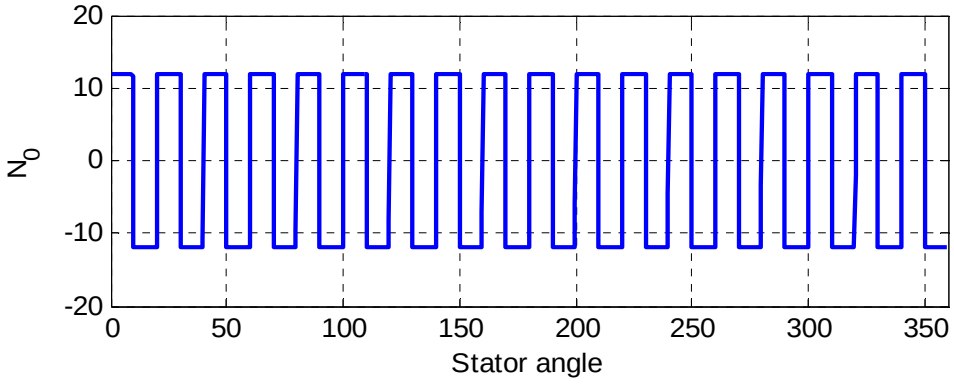

Figure 4.13 zero sequence stator winding function vs. stator angle

4.4 Derivation of Rotor Bar Winding Functions

The cage formed by the damper bars of the IPM machine with *n* (even or odd) bars and two end rings to short circuit all the bars together is considered as *n* identical magnetically coupled circuits. Each circuit is composed of two adjunct rotor bars and segments of the end rings connect two adjacent bars together at both ends of the bars. Each bar and end ring segment of the rotor loop is equivalently represented by a serial connection of a resistor and an inductor as shown in Figure 4.14. From [45], for non-skewed rotor bars, rotor turn and winding function is given in Figure 4.15 and the winding function of the rotor bars is given in Equation (4.1) which is obtained from .the function of Figure 4.15.

$$N_i(\theta)=\begin{cases} -\dfrac{\alpha_r}{2\pi}, 0 \le \theta \le \theta_i \\ 1-\dfrac{\alpha_r}{2\pi}, \theta_i \le \theta \le \theta_i + \alpha_r \\ -\dfrac{\alpha_r}{2\pi}, \theta_i + \alpha_r \le \theta \le 2\pi \end{cases} \tag{4.1}$$

The turn and winding function derived from Equation (4.1) is depicted in Figure 4.15. However, in order to represent the winding function of all damper bars, the first bar is assumed to be started at the origin and plotted against the circumferential angle as shown in Figure 4.16.

4.5 Stationary Reference Frame Transformation of Rotor Winding Functions

Similar to the case of stator winding function, the stationary reference frame transformation is applied to the rotor bars considering the effect of odd order harmonics.

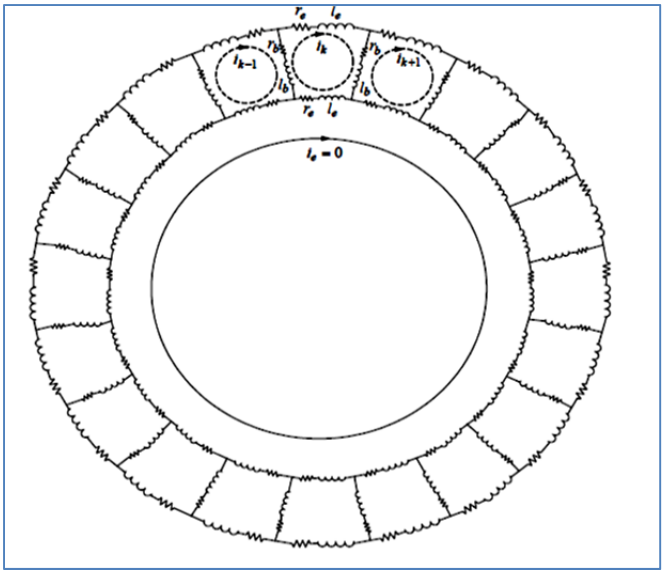

Figure 4.14 Mutually coupled rotor model

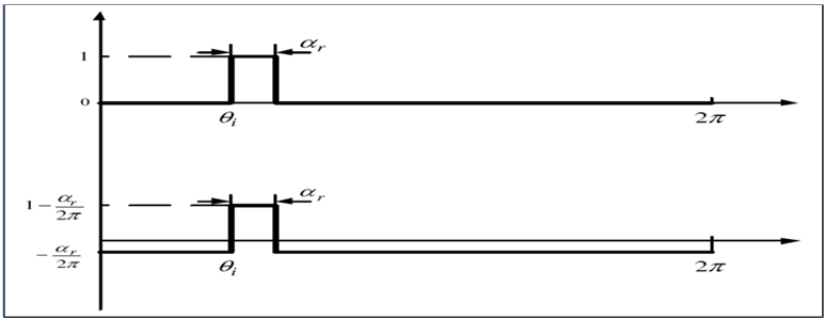

Figure 4.15 Rotor turn and winding function

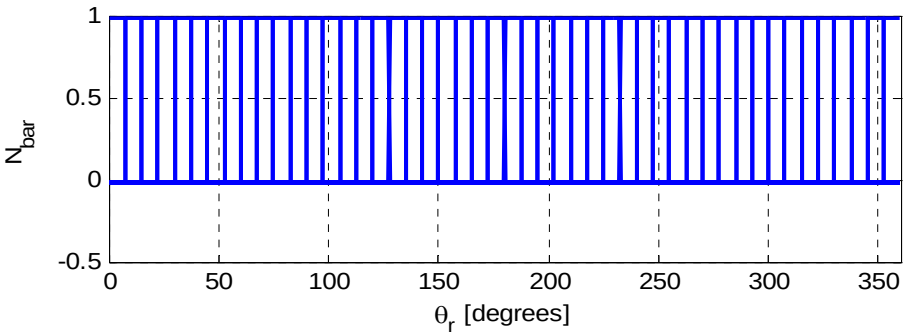

Figure 4.16 Rotor winding functions for each bar

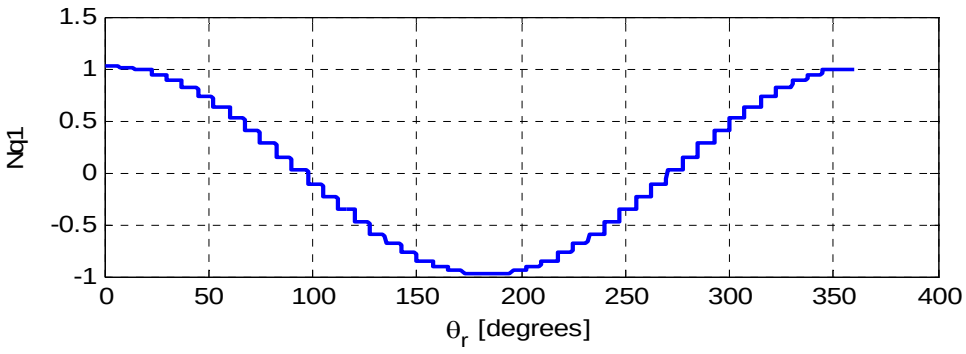

Figure 4.17 q-axis fundamental rotor bar winding function

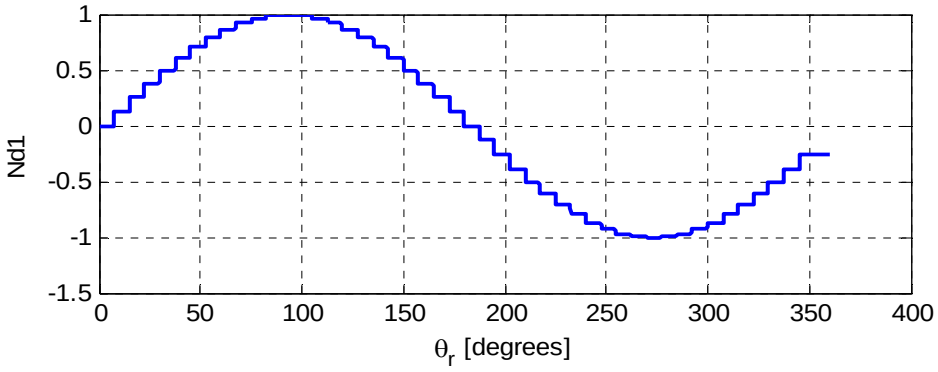

Figure 4.18 d-axis fundamental rotor bar winding function

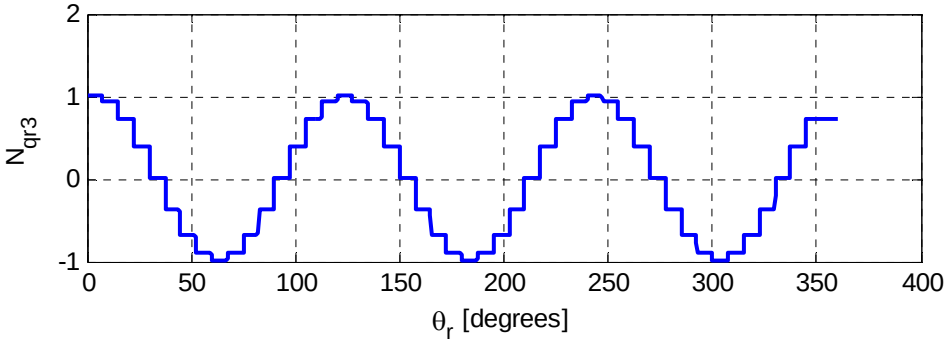

Figure 4.19 q-axis 3rd harmonics rotor bar winding function

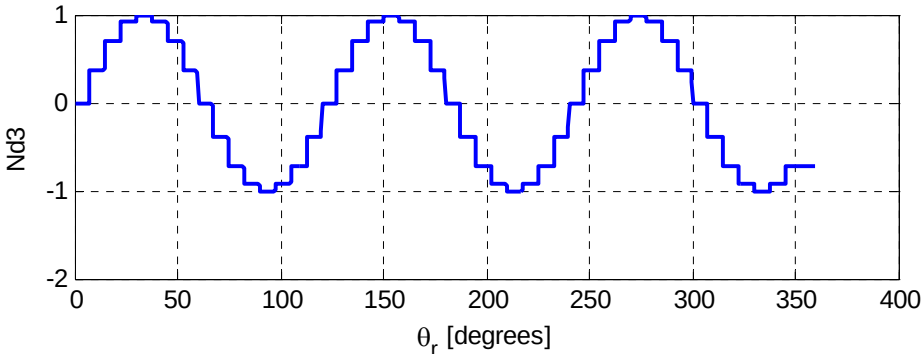

Figure 4.20 d-axis 3rd harmonics rotor bar winding function

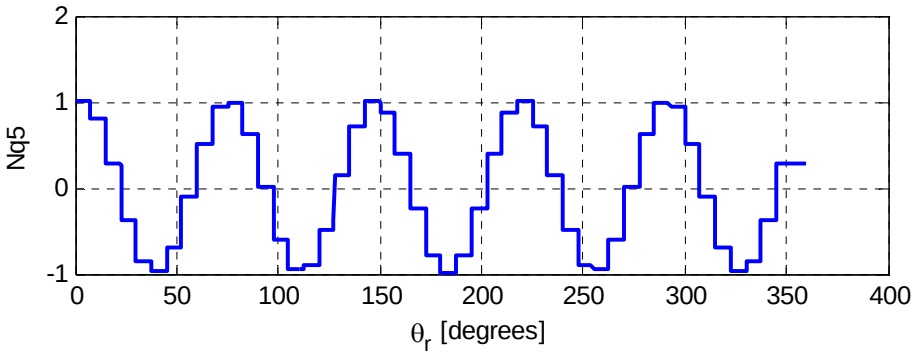

Figure 4.21 q-axis 5th harmonics rotor bar winding function

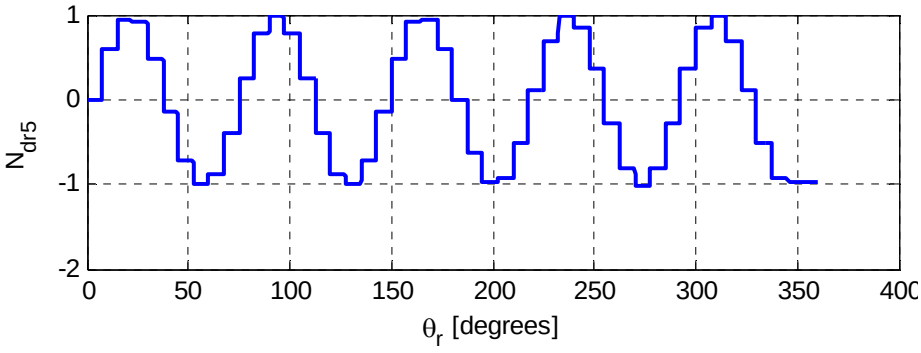

Figure 4.22 d-axis 5th harmonics rotor bar winding function

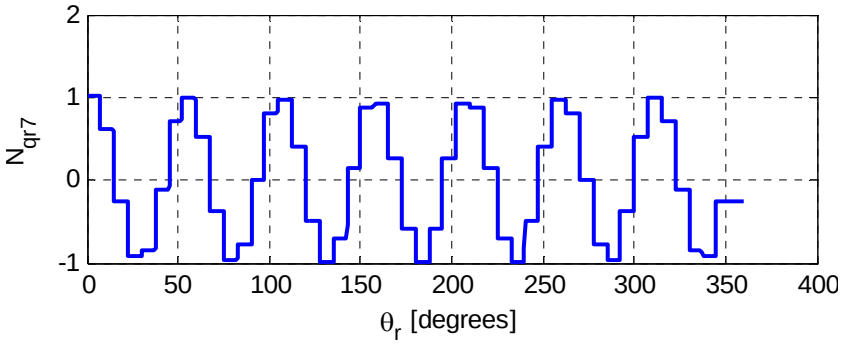

Figure 4.23 q-axis 7th harmonic rotor bar winding function

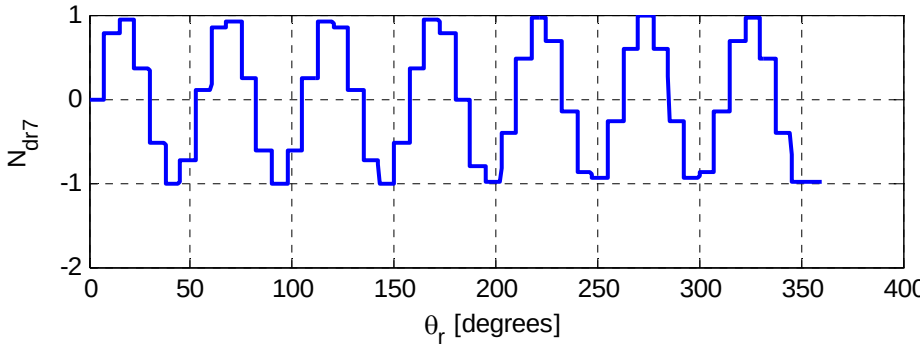

Figure 4.24 d-axis 7th harmonic rotor bar winding function

Considering 'm' number of rotor bars, the order of transformation matrix in this case is n*m where 'n' is corresponding phase number of the machine. Figures 4.17-4.24 show the corresponding plots with variation in rotor angle.

4.6 Derivation of Stator Self-Inductances

After the derivations of the winding functions in stationary reference frame, they are now utilized to determine the q-d parameters in terms of q-d winding functions.

Starting from the basic model equations in real variables, the stator voltage equations are given as

$$V_{abc...is} = r_s i_{abc..is} + p\lambda_{abc..is} \tag{4.2}$$

The stator flux linkage $\lambda_{abc..is}$ is given by the resultant of the flux linkage due to stator currents, rotor currents and magnet flux, i.e.,

$$\lambda_{abc...is} = L_{abc..is} i_{abc...is} + L_{abc..isabc...nr} i_{abc...nr} + \lambda_{abc..im} \tag{4.3}$$

Using reference frame transformation with any arbitrary angle θ in Equation (4.3),

$$T(\theta)\lambda_{abc...is} = \underbrace{T(\theta)L_{abc...is} i_{abc...is}}_{\text{Part I}} + \underbrace{T(\theta)L_{abc..isabc...nr} i_{abc....nr}}_{\text{Part II}} + \underbrace{T(\theta)\lambda_{abc..im}}_{\text{Part III}} \tag{4.4}$$

In Equation (4.3), Part I of the equation defines the flux linkage due to stator currents which gives the derivation of the stator inductances. Similarly, Part II defines the mutual inductances between the stator windings and damper rotor bars. Part III gives the flux induced due to permanent magnet on the stator windings. The self and mutual inductances of the system is obtained from Part I, which is taken into account for derivation of stator self-inductances.

Also, from the properties of the transformation, it can be shown that

$$T(\theta) = T(\theta - \theta_x)T(\theta_x) \tag{4.5}$$

Hence first term in RHS of Equation (4.4) becomes,

$$\begin{aligned} T(\theta)L_{abc...is} i_{abc..is} &= T(\theta - \theta_x)T(\theta_x)L_{abc..is} i_{abc..is} \\ &= T(\theta - \theta_x)T(\theta_x)L_{abc...is}T(\theta_x)^{-1}T(\theta - \theta_x)^{-1} i_{qdoxs} \end{aligned} \tag{4.6}$$

Assume the transformation is to the rotor reference frame, i.e., $\theta = \theta_r$ and $\theta_x = 0$

Hence,

$$T(\theta)L_{abc.....is}i_{abc.....is} = T(\theta_r)\underbrace{T(0)L_{abc....is}T(0)^{-1}}_{\text{Stationary Reference Frame}}T(\theta_r)^{-1}i_{qdoxs} \tag{4.7}$$

As observed in Equation (4.7), the middle terms imply the stationary reference transformation of the stator inductance matrix. According to the basic relation between inductance and winding functions, inductance between 'i' and 'j' is given as

$$L_{ij} = \mu_0 rl\int_0^{2\pi} N_i(\phi)N_j(\phi)g^{-1}(\phi,\theta_r)d\phi \tag{4.8}$$

Hence, for stator phases,

$$L_{aa} = \mu_0 rl\int_0^{2\pi} N_a(\phi)N_a(\phi)g^{-1}(\phi,\theta_r)d\phi \tag{4.9}$$

$$L_{ab} = \mu_0 rl\int_0^{2\pi} N_a(\phi)N_b(\phi)g^{-1}(\phi,\theta_r)d\phi \tag{4.10}$$

The same equation applies for derivation of other self and mutual phase inductances. Now, using Equation (4.9) and (4.10) for the term $T(0)L_{abc....is}T(0)^{-1}$ in Equation (4.7),

$$\begin{aligned} &T(0)L_{abc....is}T(0)^{-1} \\ &= \mu_0 rl\int_0^{2\pi} T(0)\begin{bmatrix} N_a^2 & N_aN_b & N_aN_c & N_aN_d & N_aN_e & N_aN_f & N_aN_g & N_aN_h & N_aN_i \\ N_aN_b & N_b^2 & N_bN_c & N_bN_d & N_bN_e & N_bN_f & N_bN_g & N_bN_h & N_bN_i \\ N_aN_c & N_bN_c & N_c^2 & N_cN_d & N_cN_e & N_cN_f & N_cN_g & N_cN_h & N_cN_i \\ N_aN_d & N_bN_d & N_cN_d & N_d^2 & N_dN_e & N_dN_f & N_dN_g & N_dN_h & N_dN_i \\ N_aN_e & N_bN_e & N_cN_e & N_dN_e & N_e^2 & N_eN_f & N_eN_g & N_eN_h & N_eN_i \\ N_aN_f & N_bN_f & N_cN_f & N_dN_f & N_eN_f & N_f^2 & N_fN_g & N_fN_h & N_fN_i \\ N_aN_g & N_bN_g & N_cN_g & N_dN_g & N_eN_g & N_fN_g & N_g^2 & N_gN_h & N_gN_i \\ N_aN_h & N_bN_h & N_cN_h & N_dN_h & N_eN_h & N_fN_h & N_gN_h & N_h^2 & N_hN_i \\ N_aN_i & N_bN_i & N_cN_i & N_dN_i & N_eN_i & N_fN_i & N_gN_i & N_hN_i & N_i^2 \end{bmatrix}T(0)^{-1} \\ &\times\begin{bmatrix} g^{-1}(\phi,\theta_r) & 0 & 0 & 0 & 0 & 0 & 0 & 0 & 0 \\ 0 & g^{-1}(\phi,\theta_r) & 0 & 0 & 0 & 0 & 0 & 0 & 0 \\ 0 & 0 & g^{-1}(\phi,\theta_r) & 0 & 0 & 0 & 0 & 0 & 0 \\ 0 & 0 & 0 & g^{-1}(\phi,\theta_r) & 0 & 0 & 0 & 0 & 0 \\ 0 & 0 & 0 & 0 & g^{-1}(\phi,\theta_r) & 0 & 0 & 0 & 0 \\ 0 & 0 & 0 & 0 & 0 & g^{-1}(\phi,\theta_r) & 0 & 0 & 0 \\ 0 & 0 & 0 & 0 & 0 & 0 & g^{-1}(\phi,\theta_r) & 0 & 0 \\ 0 & 0 & 0 & 0 & 0 & 0 & 0 & g^{-1}(\phi,\theta_r) & 0 \\ 0 & 0 & 0 & 0 & 0 & 0 & 0 & 0 & g^{-1}(\phi,\theta_r) \end{bmatrix} \end{aligned} \tag{4.11}$$

The given matrix can be resolved as

$$T(0)L_{abc....is}T(0)^{-1} = \mu_0 rl\int_0^{2\pi} T(0)ABT(0)^{-1}C \tag{4.12}$$

where,

$$A=\begin{bmatrix} N_a & N_a & N_a & N_a & N_a & N_a & N_a & N_a & N_a \\ N_b & N_b & N_b & N_b & N_b & N_b & N_b & N_b & N_b \\ N_c & N_c & N_c & N_c & N_c & N_c & N_c & N_c & N_c \\ N_d & N_d & N_d & N_d & N_d & N_d & N_d & N_d & N_d \\ N_e & N_e & N_e & N_e & N_e & N_e & N_e & N_e & N_e \\ N_f & N_f & N_f & N_f & N_f & N_f & N_f & N_f & N_f \\ N_g & N_g & N_g & N_g & N_g & N_g & N_g & N_g & N_g \\ N_h & N_h & N_h & N_h & N_h & N_h & N_h & N_h & N_h \\ N_i & N_i & N_i & N_i & N_i & N_i & N_i & N_i & N_i \end{bmatrix} \tag{4.13}$$

$$B=\begin{bmatrix} N_a & 0 & 0 & 0 & 0 & 0 & 0 & 0 & 0 \\ 0 & N_b & 0 & 0 & 0 & 0 & 0 & 0 & 0 \\ 0 & 0 & N_c & 0 & 0 & 0 & 0 & 0 & 0 \\ 0 & 0 & 0 & N_d & 0 & 0 & 0 & 0 & 0 \\ 0 & 0 & 0 & 0 & N_e & 0 & 0 & 0 & 0 \\ 0 & 0 & 0 & 0 & 0 & N_f & 0 & 0 & 0 \\ 0 & 0 & 0 & 0 & 0 & 0 & N_g & 0 & 0 \\ 0 & 0 & 0 & 0 & 0 & 0 & 0 & N_h & 0 \\ 0 & 0 & 0 & 0 & 0 & 0 & 0 & 0 & N_i \end{bmatrix} \tag{4.14}$$

$$C=\begin{bmatrix} g^{-1}(\phi,\theta_r) & 0 & 0 & 0 & 0 & 0 & 0 & 0 & 0 \\ 0 & g^{-1}(\phi,\theta_r) & 0 & 0 & 0 & 0 & 0 & 0 & 0 \\ 0 & 0 & g^{-1}(\phi,\theta_r) & 0 & 0 & 0 & 0 & 0 & 0 \\ 0 & 0 & 0 & g^{-1}(\phi,\theta_r) & 0 & 0 & 0 & 0 & 0 \\ 0 & 0 & 0 & 0 & g^{-1}(\phi,\theta_r) & 0 & 0 & 0 & 0 \\ 0 & 0 & 0 & 0 & 0 & g^{-1}(\phi,\theta_r) & 0 & 0 & 0 \\ 0 & 0 & 0 & 0 & 0 & 0 & g^{-1}(\phi,\theta_r) & 0 & 0 \\ 0 & 0 & 0 & 0 & 0 & 0 & 0 & g^{-1}(\phi,\theta_r) & 0 \\ 0 & 0 & 0 & 0 & 0 & 0 & 0 & 0 & g^{-1}(\phi,\theta_r) \end{bmatrix} \tag{4.15}$$

Now, applying stationary reference transformation to matrix A, the matrix turns into q-d winding matrix

$$T(0)A=\begin{bmatrix} N_{q1} & N_{q1} & N_{q1} & N_{q1} & N_{q1} & N_{q1} & N_{q1} & N_{q1} & N_{q1} \\ N_{d1} & N_{d1} & N_{d1} & N_{d1} & N_{d1} & N_{d1} & N_{d1} & N_{d1} & N_{d1} \\ N_{q3} & N_{q3} & N_{q3} & N_{q3} & N_{q3} & N_{q3} & N_{q3} & N_{q3} & N_{q3} \\ N_{d3} & N_{d3} & N_{d3} & N_{d3} & N_{d3} & N_{d3} & N_{d3} & N_{d3} & N_{d3} \\ N_{q5} & N_{q5} & N_{q5} & N_{q5} & N_{q5} & N_{q5} & N_{q5} & N_{q5} & N_{q5} \\ N_{d5} & N_{d5} & N_{d5} & N_{d5} & N_{d5} & N_{d5} & N_{d5} & N_{d5} & N_{d5} \\ N_{q7} & N_{q7} & N_{q7} & N_{q7} & N_{q7} & N_{q7} & N_{q7} & N_{q7} & N_{q7} \\ N_{d7} & N_{d7} & N_{d7} & N_{d7} & N_{d7} & N_{d7} & N_{d7} & N_{d7} & N_{d7} \\ N_0 & N_0 & N_0 & N_0 & N_0 & N_0 & N_0 & N_0 & N_0 \end{bmatrix} \tag{4.16}$$

Multiplying Equation (4.16) with $BT(0)^{-1}$ the resulting equation becomes

$$T(0)ABT(0)^{-1}=\underbrace{\begin{bmatrix} N_{q1}^{\,2} & N_{q1}N_{d1} & N_{q1}N_{q3} & N_{q1}N_{d3} & N_{q1}N_{q5} & N_{q1}N_{d5} & N_{q1}N_{q7} & N_{q1}N_{d7} & N_{q1}N_0 \\ N_{q1}N_{d1} & N_{d1}^{\,2} & N_{d1}N_{q3} & N_{d1}N_{d3} & N_{d1}N_{q5} & N_{d1}N_{d5} & N_{d1}N_{q7} & N_{d1}N_{d7} & N_{d1}N_0 \\ N_{q3}N_{q1} & N_{q3}N_{d1} & N_{q3}^{\,2} & N_{q3}N_{d3} & N_{q3}N_{q5} & N_{q3}N_{d5} & N_{q3}N_{q7} & N_{q3}N_{d7} & N_{q3}N_0 \\ N_{d3}N_{q1} & N_{d1}N_{d3} & N_{q3}N_{d3} & N_{d3}^{\,2} & N_{d3}N_{q5} & N_{d3}N_{d5} & N_{d3}N_{q7} & N_{d3}N_{d7} & N_{d3}N_0 \\ N_{q1}N_{q5} & N_{d1}N_{q5} & N_{q3}N_{q5} & N_{d3}N_{q5} & N_{q5}^{\,2} & N_{q5}N_{d5} & N_{q5}N_{q7} & N_{q5}N_{d7} & N_{q5}N_0 \\ N_{q1}N_{d5} & N_{d1}N_{d5} & N_{q3}N_{d5} & N_{d3}N_{d5} & N_{q5}N_{d5} & N_{d5}^{\,2} & N_{d5}N_{q7} & N_{d5}N_{d7} & N_{d5}N_0 \\ N_{q1}N_{q7} & N_{d1}N_{q7} & N_{q3}N_{q7} & N_{d3}N_{q7} & N_{q5}N_{q7} & N_{d5}N_{q7} & N_{q7}^{\,2} & N_{q7}N_{d7} & N_{q7}N_0 \\ N_{q1}N_{d7} & N_{d1}N_{d7} & N_{q3}N_{d7} & N_{d3}N_{d7} & N_{q5}N_{d7} & N_{d5}N_{d7} & N_{q7}N_{d7} & N_{d7}^{\,2} & N_{d7}N_0 \\ N_{q1}N_0 & N_{d1}N_0 & N_{q3}N_0 & N_{d3}N_0 & N_{q5}N_0 & N_{d5}N_0 & N_{q7}N_0 & N_{d7}N_0 & N_0^{\,2} \end{bmatrix}}_{\textbf{Stationary Reference Frame}} \tag{4.17}$$

Recalling Equation (4.12),

$$T(0)L_{abc....is}T(0)^{-1}=\mu_0 rl\int_0^{2\pi}T(0)ABT(0)^{-1}Ci_{qdoxs} \tag{4.18}$$

Equation (4.18) involves the integration of Equation (4.17) from 0 to 2π. If looked closely inside the matrix of (4.17), the integration of product of q and d winding functions will result to value of 0. It is due to the cancellation of the terms after the integration. For example, the graph of N_{q1} given by Figure (4.17) is a cosine function and N_{d1} given by Figure (4.18) is a sine function. If both are multiplied together and the resultant is added from 0 to 2π, it will result in the value of 0. Similar case is true for other integration involving q and d winding functions.

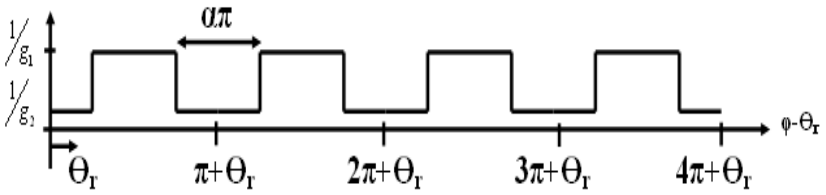

Figure 4.25 Air gap function vs. rotor angle

Recalling Equation (4.7),

$$\begin{aligned} T(\theta)L_{abc.....is}i_{abc.....is} &= T(\theta_r)T(0)L_{abc....is}T(0)^{-1}T(\theta_r)^{-1}i_{qdoxs} \\ &= T(\theta_r)\mu_0 rl\int_0^{2\pi}T(0)ABT(0)^{-1}CT(\theta_r)^{-1}i_{qdoxs} \\ &= L_{qdoxs}i_{qdoxs} \end{aligned} \tag{4.19}$$

The term L_{qdoxs} in Equation (4.19) is the q-d inductance matrix with the inclusion of harmonic components.

From Equation (4.15), the term 'C' defines the matrix due to inverse air gap function which is dependent on rotor angle for the case of IPM machine. Hence, the term L_{qdoxs} in Equation (4.19) is dependent of rotor angle due to the presence of transformation matrix $T(\theta_r)$ and the air gap matrix 'C'. To make the calculation easier, the graphical representation of air gap function is taken which is given in Figure 4.25.

In order to obtain the q-d inductance L_{qdoxs}, the rotor angle is stepped from 0 to 360 degrees and the integration is carried out for Equation (4.19). The inductances are evaluated for each step and plotted from 0 to 360 degrees moving with each step of rotor angle with each harmonics. Applying this method, Figures 4.26-4.29 show the self q and d stator inductances and Figures 4.30-4.35 depict the mutual inductance between corresponding stator harmonics with the variation of rotor angle, θ_r.

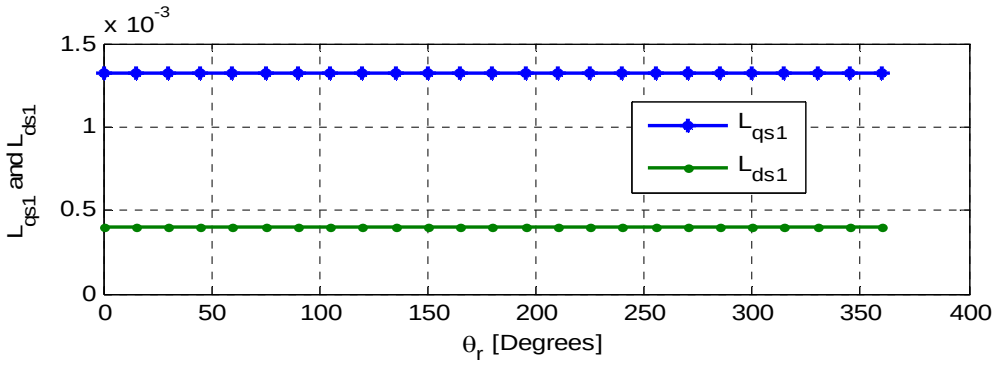

Figure 4.26 Fundamental stator q and d-axis inductances

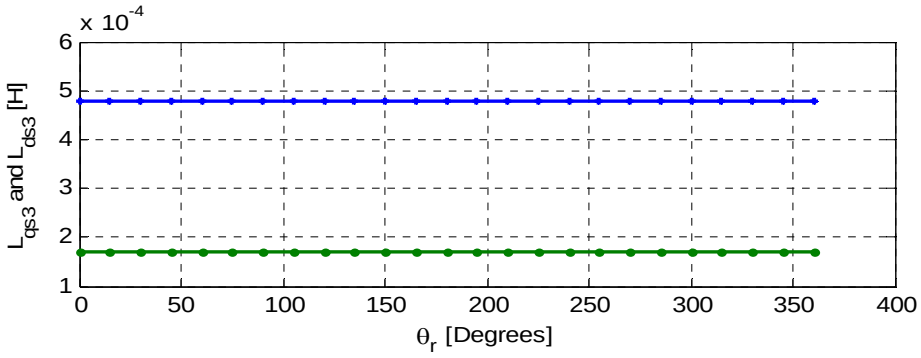

Figure 4.27 3rd harmonic stator q and d-axis inductances

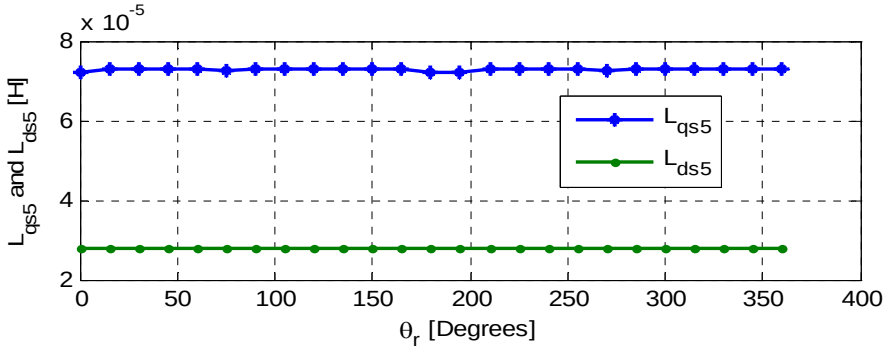

Figure 4.28 5th harmonic stator q and d axis inductances

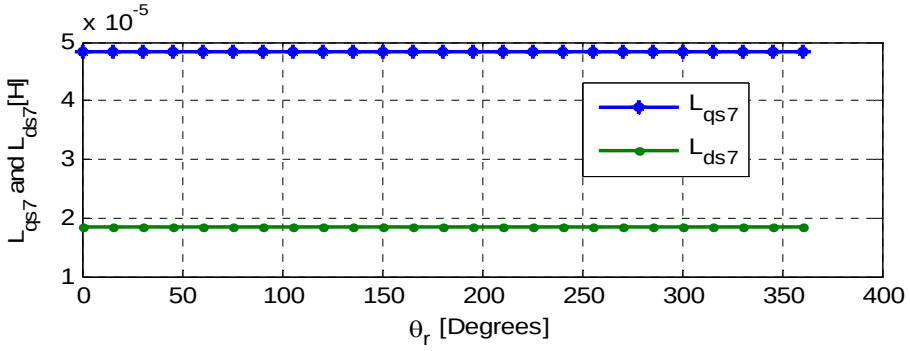

Figure 4.29 7th harmonic stator q and d axis inductances

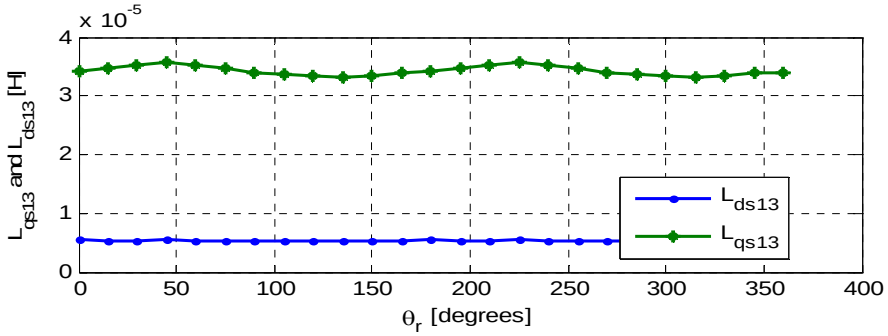

Figure 4.30 Mutual inductance between fundamental and 3rd harmonics

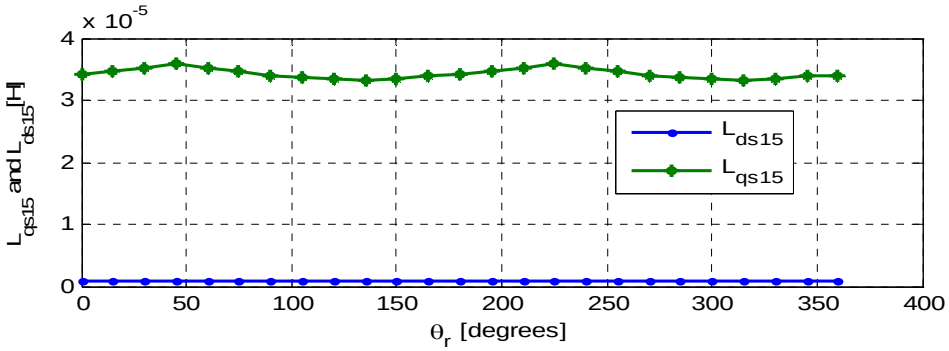

Figure 4.31 Mutual inductance between fundamental and 5th harmonic

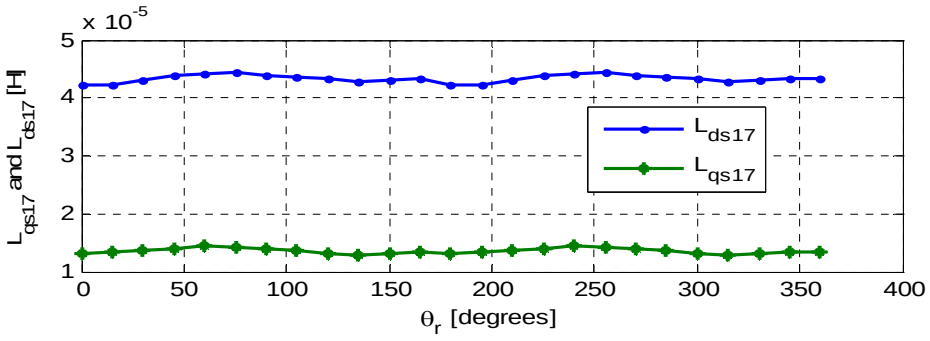

Figure 4.32 Mutual inductance between first and 7th harmonics

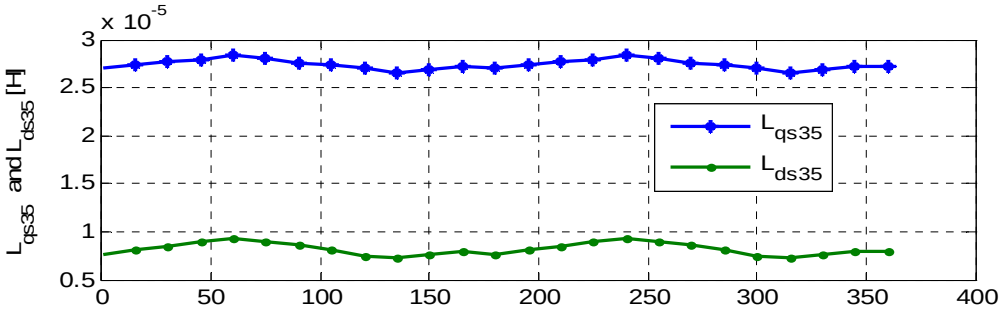

Figure 4.33 Mutual inductance between 3rd and 5th harmonics

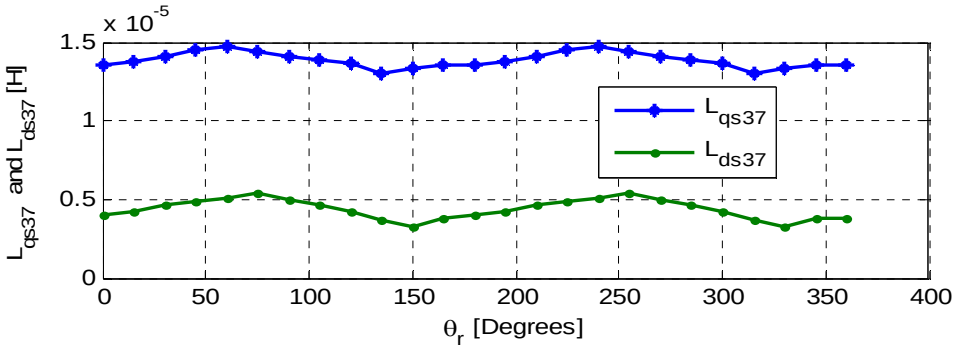

Figure 4.34 Mutual inductance between 3rd and 7th harmonics

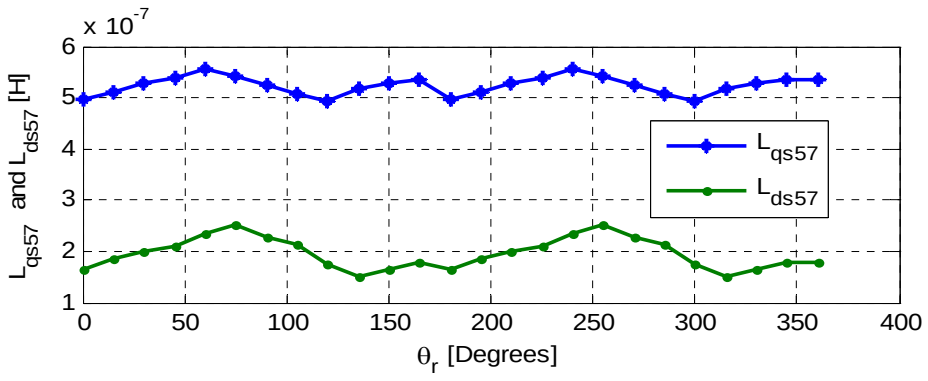

Figure 4.35 Mutual inductance between fifth and 7th harmonics

4.7 Derivation of Rotor Self and Inter Harmonic Inductances

For the derivation of self and inter-harmonic inductances of rotor bars, the reference frame transformation is applied to the rotor flux linkage equations. Similar to the case of the stator inductances, the self and inter-harmonic inductances are obtained graphically using the rotor winding functions and air gap functions.

The voltage equation for rotor is given as

$$V_{abc...nr} = r_r i_{abc..nr} + p\lambda_{abc..nr} \tag{4.20}$$

The rotor flux linkage in real variable form is given as

$$\lambda_{abc...nr} = L_{abc..nr} i_{abc...nr} + L_{abc..isabc...nr} i_{abc...is} \tag{4.21}$$

Multiplying both sides of Equation (4.21) by rotor transformation matrix, $T(\theta - \theta_r)$,

$$T(\theta - \theta_r)\lambda_{abc...nr} = T(\theta - \theta_r)L_{abc..nr} i_{abc...nr} + T(\theta - \theta_r)L_{abc..isabc...nr} i_{abc...is} \tag{4.22}$$

In Equation (4.22), the first term signifies the rotor inductance matrix. Hence, taking this equation,

$$T(\theta - \theta_r)L_{abc..nr}i_{abc...nr} = T(\theta - \theta_r)L_{abc..nr}T(\theta - \theta_r)^{-1}i_{qdor} \tag{4.23}$$

Assuming the rotor reference frame,

$$\theta = \theta_r \tag{4.24}$$

Hence, Equation (4.23) becomes

$$T(\theta - \theta_r)L_{abc..nr}i_{abc...nr} = T(0)L_{abc..nr}T(0)^{-1}i_{qdor} \tag{4.25}$$

This equation is similar to the case of stator circuits except the winding functions now consist of the rotor bars. The integration of the product of q and d axis winding functions is zero. Hence, the same method defined previously is true for this case. As in previous section, the d and q-axis inductances for each harmonic component are determined and plotted with the variation of rotor angle. Figures 4.36-4.39 depict the self-harmonic inductances of the rotor and Figures 4.40-4.45 depict the inter-harmonic inductances of the rotor.

4.8 Mutual Inductance between Corresponding Harmonics of Stator and Rotor

In this section, the derivation of the mutual inductances between stator and rotor is discussed with the help of stationary reference frame transformation of q and d winding functions as derived in Section 4.3.

Applying the transformation for stator flux linkage equations,

$$T(\theta)\lambda_{abc...is} = T(\theta)L_{abc...is}i_{abc...is} + T(\theta)L_{abc..isabc...nr}i_{abc....nr} + T(\theta)\lambda_{abc..im} \tag{4.26}$$

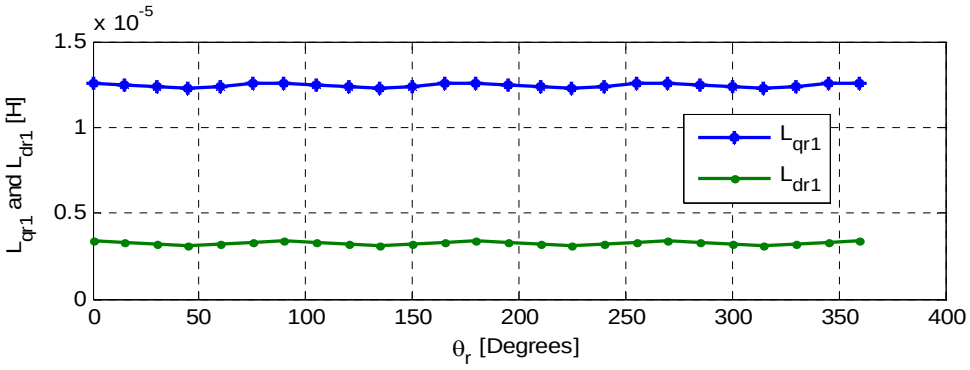

Figure 4.36 Fundamental q and d axis inductances for rotor

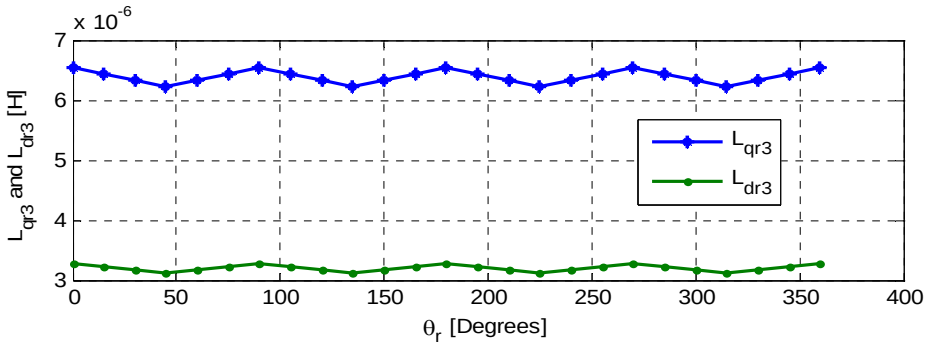

Figure 4.37 3rd harmonic q and d axis inductances for rotor

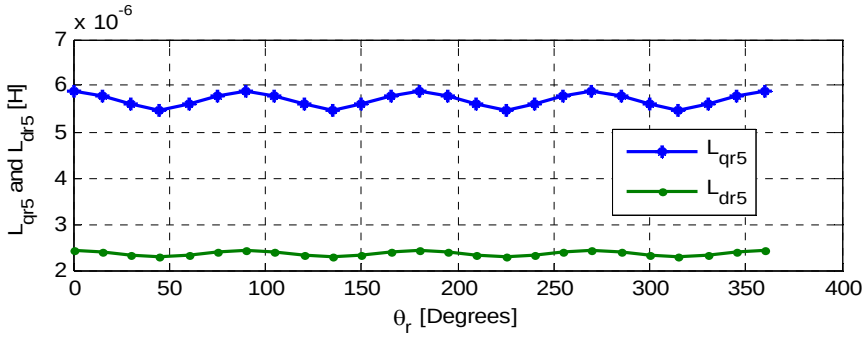

Figure 4.38 5th harmonic q and d axis inductances for rotor

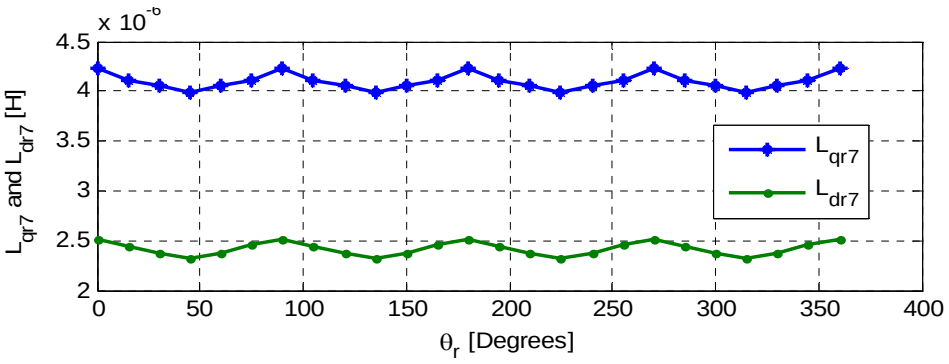

Figure 4.39 7th harmonic q and d axis inductances for rotor

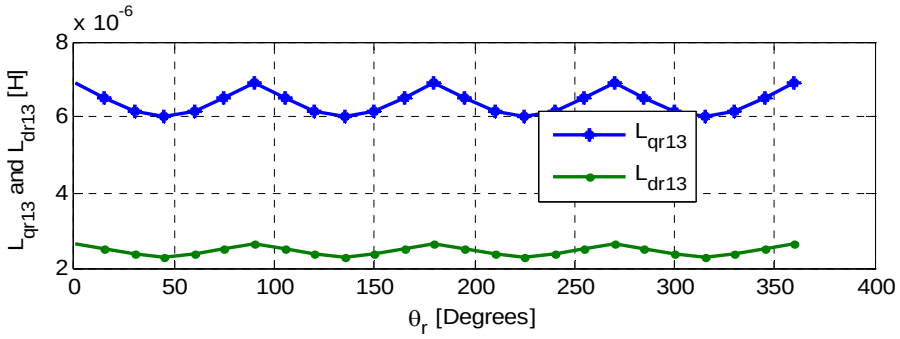

Figure 4.40 Mutual inductance between first and 3rd harmonics for rotor

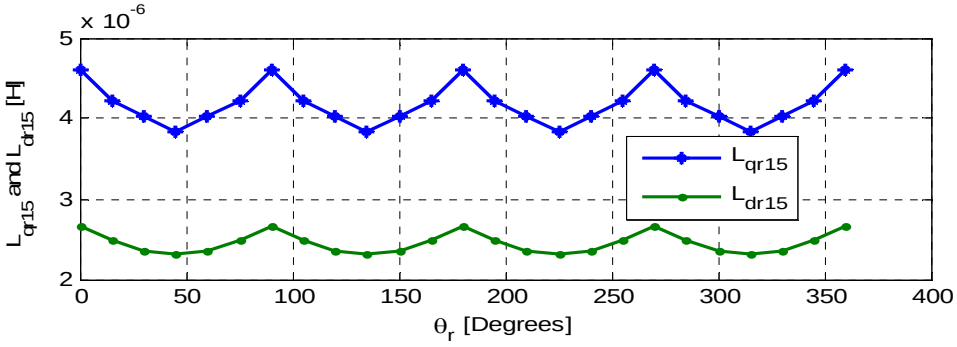

Figure 4.41 Mutual inductance between first and 5th harmonics for rotor

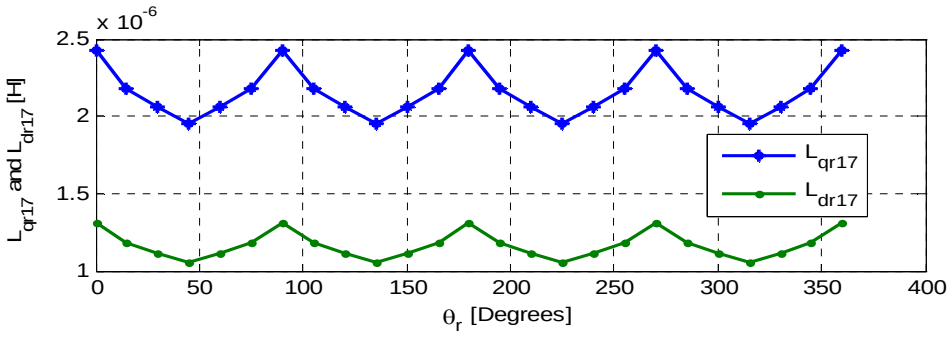

Figure 4.42 Mutual inductance between first and 7th harmonics for rotor

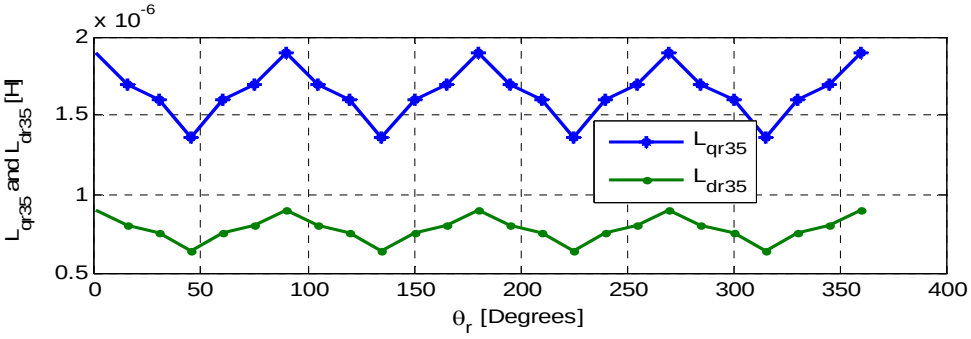

Figure 4.43 Mutual inductance between 3rd and 5th harmonics for rotor

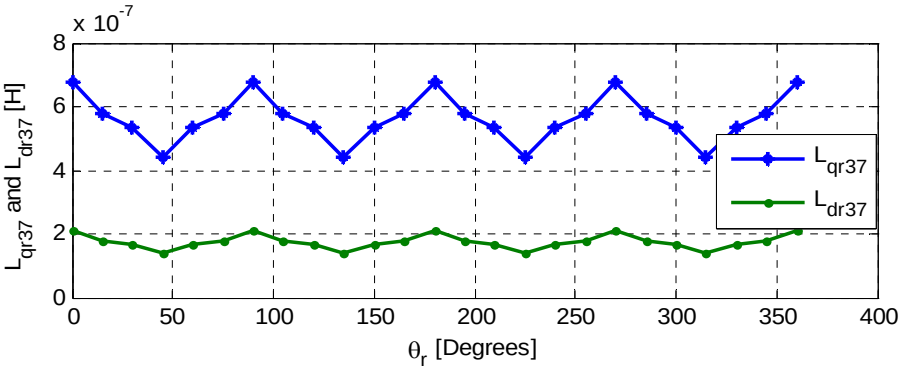

Figure 4.44 Mutual inductance between 3rd and 7th harmonics

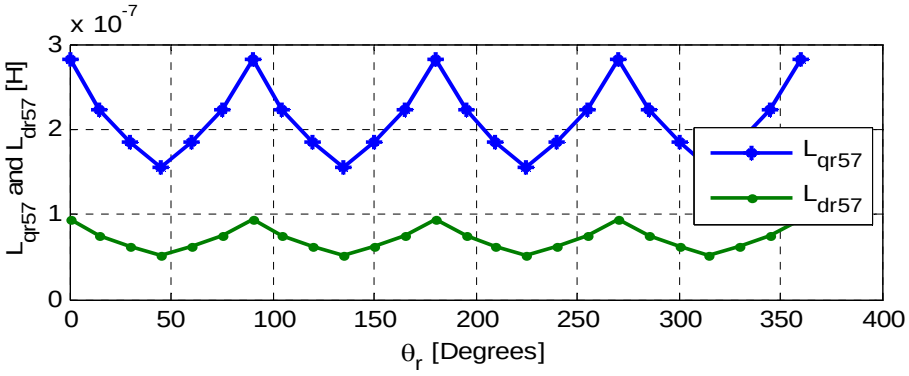

Figure 4.45 Mutual inductance between fifth and 7th harmonics

In order to determine the mutual inductances between stator and rotor, the second term in Equation (4.26) is taken, i.e.,

$$T(\theta)L_{abc..isabc...nr}i_{abc....nr} = T(\theta)L_{abc..isabc...nr}T(\theta-\theta_r)^{-1}i_{qdor} \tag{4.27}$$

Also, $T(\theta) = T(\theta-\theta_x)T(\theta_x)$ (4.28)

Assuming, $\theta_x = 0$, and $\theta = \theta_r$, i.e., rotor reference frame,

$$T(\theta)L_{abc..isabc...nr}i_{abc....nr} = T(\theta-\theta_x)T(\theta_x)L_{abc..isabc...nr}T(\theta-\theta_r)^{-1}i_{qdor} \tag{4.29}$$

If Equation (4.29) is solved in terms of real variables and stationary reference frame transformation is applied, the equation reduces to

$$L_{qdors} = T(\theta_r)\mu_0 rl\int [N_{qdors}]g^{-1}(\phi_s,\theta_r)d\phi_s \tag{4.30}$$

where, $N_{qdors} = \begin{bmatrix} N_{q1s}N_{q1r} & N_{q1s}N_{d1r} & N_{q1s}N_{q3r} & ..... & N_{q1s}N_{0r} \\ N_{d1s}N_{q1r} & N_{d1s}N_{d1r} & N_{d1s}N_{q3r} & ..... & N_{d1s}N_{0r} \\ \vdots & \vdots & \vdots & \vdots & \vdots \\ N_{q1s}N_{0r} & N_{d1s}N_{0r} & N_{q3s}N_{0r} & N_{d3s}N_{0r} & N_{0s}N_{0r} \end{bmatrix}$ (4.31)

Similar to the case of derivations of stator and rotor, the product of q and d winding functions of stator and rotor give rise to zero. Taking into account only the

mutual harmonic terms in Equation (4.31), the mutual harmonic inductances are derived with variation of rotor angle. Figures 4.46-4.49 show the corresponding mutual inductance terms due to corresponding harmonics of stator and rotor bars.

4.9 Induced EMF of the Magnet on Stator Windings

Considering the stator flux linkage equations,

$$T(\theta)\lambda_{abc...is} = T(\theta)L_{abc...is}i_{abc...is} + T(\theta)L_{abc..isabc...nr}i_{abc....nr} + T(\theta)\lambda_{abc..im} \tag{4.32}$$

The 3rd term in above equation defines the flux due to permanent magnet induced on each phase windings of the stator. The flux linkage due to magnet on phase 'a' of IPM machine is given as [2]

$$\lambda_{as} = \int_0^{2\pi} N_a(\phi_s)\int_{\phi_s}^{\phi_s+\pi} B_r(\zeta,\theta_r)rld\zeta d\phi_s \tag{4.33}$$

Here, $B_r(\zeta,\theta_r)$ represents the magnet flux density with the variation of spatial angle. This is derived in Chapter 3 and given in Figure 4.50. In matrix form,

$$\begin{bmatrix}\lambda_{as}\\ \lambda_{bs}\\ \lambda_{cs}\\ \lambda_{ds}\\ \lambda_{es}\\ \lambda_{fs}\\ \lambda_{gs}\\ \lambda_{hs}\\ \lambda_{is}\end{bmatrix} = \frac{rl}{9}\int \begin{bmatrix} N_{as} & N_{as} & N_{as} & N_{as} & N_{as} & N_{as} & N_{as} & N_{as} & N_{as}\\ N_{bs} & N_{bs} & N_{bs} & N_{bs} & N_{bs} & N_{bs} & N_{bs} & N_{bs} & N_{bs}\\ N_{cs} & N_{cs} & N_{cs} & N_{cs} & N_{cs} & N_{cs} & N_{cs} & N_{cs} & N_{cs}\\ N_{ds} & N_{ds} & N_{ds} & N_{ds} & N_{ds} & N_{ds} & N_{ds} & N_{ds} & N_{ds}\\ N_{es} & N_{es} & N_{es} & N_{es} & N_{es} & N_{es} & N_{es} & N_{es} & N_{es}\\ N_{fs} & N_{fs} & N_{fs} & N_{fs} & N_{fs} & N_{fs} & N_{fs} & N_{fs} & N_{fs}\\ N_{gs} & N_{gs} & N_{gs} & N_{gs} & N_{gs} & N_{gs} & N_{gs} & N_{gs} & N_{gs}\\ N_{hs} & N_{hs} & N_{hs} & N_{hs} & N_{hs} & N_{hs} & N_{hs} & N_{hs} & N_{hs}\\ N_{is} & N_{is} & N_{is} & N_{is} & N_{is} & N_{is} & N_{is} & N_{is} & N_{is}\end{bmatrix} \int_{\phi_s}^{\phi_s+\pi} \begin{bmatrix} B_r(\zeta,\theta_r)\\ B_r(\zeta,\theta_r)\\ B_r(\zeta,\theta_r)\\ B_r(\zeta,\theta_r)\\ B_r(\zeta,\theta_r)\\ B_r(\zeta,\theta_r)\\ B_r(\zeta,\theta_r)\\ B_r(\zeta,\theta_r)\\ B_r(\zeta,\theta_r)\end{bmatrix} d\zeta d\phi_s \tag{4.34}$$

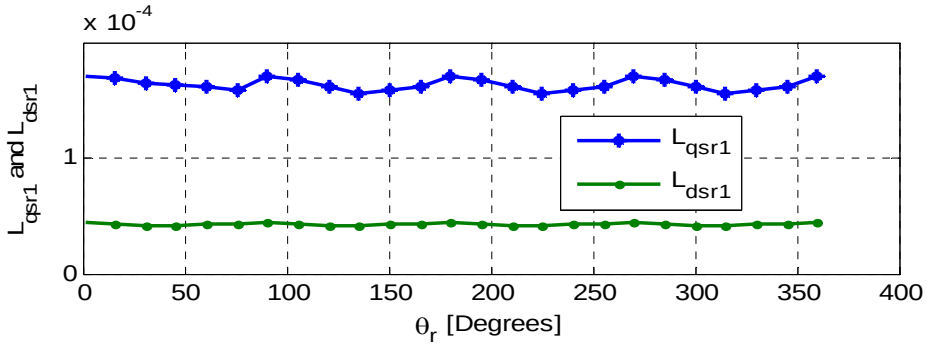

Figure 4.46 Mutual inductance between fundamental of stator and rotor

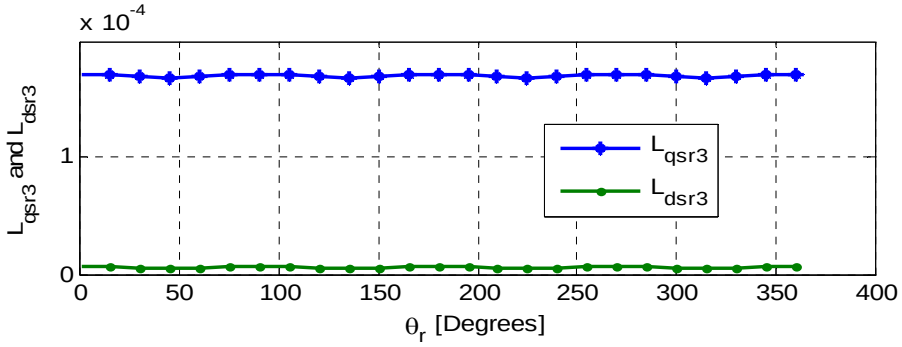

Figure 4.47 Mutual inductance between 3rd harmonics of stator and rotor

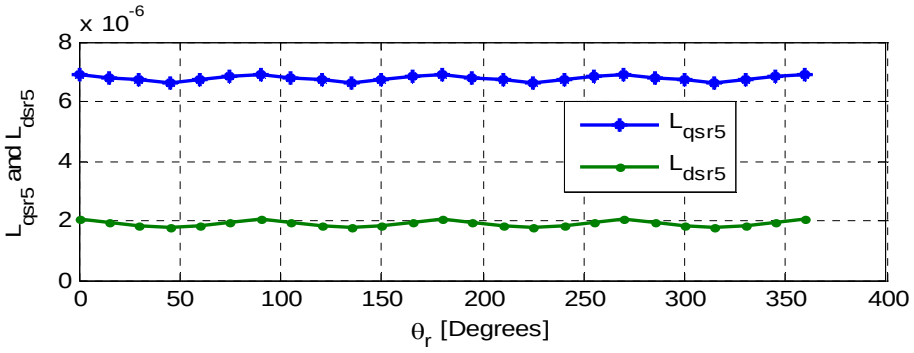

Figure 4.48 Mutual inductance between 5th harmonics of stator and rotor

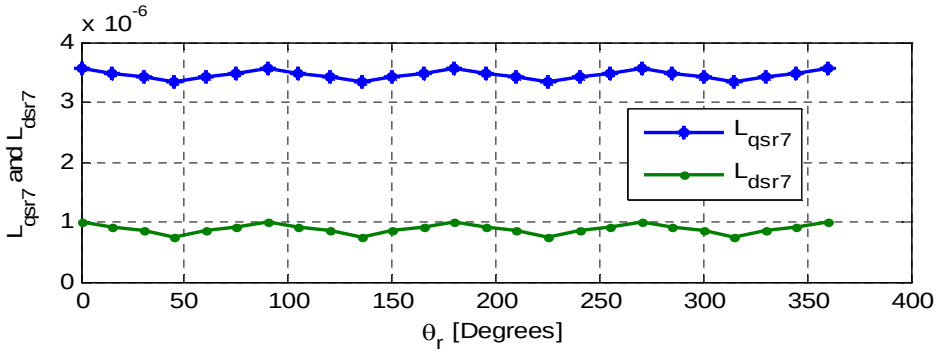

Figure 4.49 Mutual inductance between 7th harmonics of stator and rotor

Multiplying both sides of Equation (4.34) by transformation matrix, $T(\theta)$

$$T(\theta)\begin{bmatrix}\lambda_{as}\\ \lambda_{bs}\\ \lambda_{cs}\\ \lambda_{ds}\\ \lambda_{es}\\ \lambda_{fs}\\ \lambda_{gs}\\ \lambda_{hs}\\ \lambda_{is}\end{bmatrix} = \frac{rl}{9}T(\theta)\int_0^{2\pi}\begin{bmatrix} N_{as} & N_{as} & N_{as} & N_{as} & N_{as} & N_{as} & N_{as} & N_{as} & N_{as}\\ N_{bs} & N_{bs} & N_{bs} & N_{bs} & N_{bs} & N_{bs} & N_{bs} & N_{bs} & N_{bs}\\ N_{cs} & N_{cs} & N_{cs} & N_{cs} & N_{cs} & N_{cs} & N_{cs} & N_{cs} & N_{cs}\\ N_{ds} & N_{ds} & N_{ds} & N_{ds} & N_{ds} & N_{ds} & N_{ds} & N_{ds} & N_{ds}\\ N_{es} & N_{es} & N_{es} & N_{es} & N_{es} & N_{es} & N_{es} & N_{es} & N_{es}\\ N_{fs} & N_{fs} & N_{fs} & N_{fs} & N_{fs} & N_{fs} & N_{fs} & N_{fs} & N_{fs}\\ N_{gs} & N_{gs} & N_{gs} & N_{gs} & N_{gs} & N_{gs} & N_{gs} & N_{gs} & N_{gs}\\ N_{hs} & N_{hs} & N_{hs} & N_{hs} & N_{hs} & N_{hs} & N_{hs} & N_{hs} & N_{hs}\\ N_{is} & N_{is} & N_{is} & N_{is} & N_{is} & N_{is} & N_{is} & N_{is} & N_{is}\end{bmatrix} * \int_{\phi_s}^{\phi_s+\pi}\begin{bmatrix} B_r(\zeta,\theta_r)\\ B_r(\zeta,\theta_r)\\ B_r(\zeta,\theta_r)\\ B_r(\zeta,\theta_r)\\ B_r(\zeta,\theta_r)\\ B_r(\zeta,\theta_r)\\ B_r(\zeta,\theta_r)\\ B_r(\zeta,\theta_r)\\ B_r(\zeta,\theta_r)\end{bmatrix} d\zeta d\phi_s \tag{4.35}$$

From the property of transformation, it can be verified that,

$$T(\theta) = T(\theta - \theta_x)T(\theta_x) \tag{4.36}$$

Hence, RHS of Equation (4.35) becomes

$$= \frac{rl}{9} T(\theta - \theta_x) T(\theta_x) \int_0^{2\pi} \begin{bmatrix} N_{as} & N_{as} & N_{as} & N_{as} & N_{as} & N_{as} & N_{as} & N_{as} & N_{as} \\ N_{bs} & N_{bs} & N_{bs} & N_{bs} & N_{bs} & N_{bs} & N_{bs} & N_{bs} & N_{bs} \\ N_{cs} & N_{cs} & N_{cs} & N_{cs} & N_{cs} & N_{cs} & N_{cs} & N_{cs} & N_{cs} \\ N_{ds} & N_{ds} & N_{ds} & N_{ds} & N_{ds} & N_{ds} & N_{ds} & N_{ds} & N_{ds} \\ N_{es} & N_{es} & N_{es} & N_{es} & N_{es} & N_{es} & N_{es} & N_{es} & N_{es} \\ N_{fs} & N_{fs} & N_{fs} & N_{fs} & N_{fs} & N_{fs} & N_{fs} & N_{fs} & N_{fs} \\ N_{gs} & N_{gs} & N_{gs} & N_{gs} & N_{gs} & N_{gs} & N_{gs} & N_{gs} & N_{gs} \\ N_{hs} & N_{hs} & N_{hs} & N_{hs} & N_{hs} & N_{hs} & N_{hs} & N_{hs} & N_{hs} \\ N_{is} & N_{is} & N_{is} & N_{is} & N_{is} & N_{is} & N_{is} & N_{is} & N_{is} \end{bmatrix} \int_{\phi_s}^{\phi_s+\pi} \begin{bmatrix} B_r(\zeta,\theta_r) \\ B_r(\zeta,\theta_r) \\ B_r(\zeta,\theta_r) \\ B_r(\zeta,\theta_r) \\ B_r(\zeta,\theta_r) \\ B_r(\zeta,\theta_r) \\ B_r(\zeta,\theta_r) \\ B_r(\zeta,\theta_r) \\ B_r(\zeta,\theta_r) \end{bmatrix} d\zeta d\phi_s$$

Again, using the rotor reference frame,

$\theta = \theta_r, \theta_x = 0$, above Equation (4.35) turns into

$$= \frac{rl}{9} T(\theta_r) T(0) \int_0^{2\pi} \begin{bmatrix} N_{as} & N_{as} & N_{as} & N_{as} & N_{as} & N_{as} & N_{as} & N_{as} & N_{as} \\ N_{bs} & N_{bs} & N_{bs} & N_{bs} & N_{bs} & N_{bs} & N_{bs} & N_{bs} & N_{bs} \\ N_{cs} & N_{cs} & N_{cs} & N_{cs} & N_{cs} & N_{cs} & N_{cs} & N_{cs} & N_{cs} \\ N_{ds} & N_{ds} & N_{ds} & N_{ds} & N_{ds} & N_{ds} & N_{ds} & N_{ds} & N_{ds} \\ N_{es} & N_{es} & N_{es} & N_{es} & N_{es} & N_{es} & N_{es} & N_{es} & N_{es} \\ N_{fs} & N_{fs} & N_{fs} & N_{fs} & N_{fs} & N_{fs} & N_{fs} & N_{fs} & N_{fs} \\ N_{gs} & N_{gs} & N_{gs} & N_{gs} & N_{gs} & N_{gs} & N_{gs} & N_{gs} & N_{gs} \\ N_{hs} & N_{hs} & N_{hs} & N_{hs} & N_{hs} & N_{hs} & N_{hs} & N_{hs} & N_{hs} \\ N_{is} & N_{is} & N_{is} & N_{is} & N_{is} & N_{is} & N_{is} & N_{is} & N_{is} \end{bmatrix} \int_{\phi_s}^{\phi_s+\pi} \begin{bmatrix} B_r(\zeta,\theta_r) \\ B_r(\zeta,\theta_r) \\ B_r(\zeta,\theta_r) \\ B_r(\zeta,\theta_r) \\ B_r(\zeta,\theta_r) \\ B_r(\zeta,\theta_r) \\ B_r(\zeta,\theta_r) \\ B_r(\zeta,\theta_r) \\ B_r(\zeta,\theta_r) \end{bmatrix} d\zeta d\phi_s \tag{4.37}$$

Since the integration does not involve the transformation angle, transformation can be brought inside the integration.

$$= \frac{rl}{9} T(\theta_r) \int_0^{2\pi} \underbrace{T(0) \begin{bmatrix} N_{as} & N_{as} & N_{as} & N_{as} & N_{as} & N_{as} & N_{as} & N_{as} & N_{as} \\ N_{bs} & N_{bs} & N_{bs} & N_{bs} & N_{bs} & N_{bs} & N_{bs} & N_{bs} & N_{bs} \\ N_{cs} & N_{cs} & N_{cs} & N_{cs} & N_{cs} & N_{cs} & N_{cs} & N_{cs} & N_{cs} \\ N_{ds} & N_{ds} & N_{ds} & N_{ds} & N_{ds} & N_{ds} & N_{ds} & N_{ds} & N_{ds} \\ N_{es} & N_{es} & N_{es} & N_{es} & N_{es} & N_{es} & N_{es} & N_{es} & N_{es} \\ N_{fs} & N_{fs} & N_{fs} & N_{fs} & N_{fs} & N_{fs} & N_{fs} & N_{fs} & N_{fs} \\ N_{gs} & N_{gs} & N_{gs} & N_{gs} & N_{gs} & N_{gs} & N_{gs} & N_{gs} & N_{gs} \\ N_{hs} & N_{hs} & N_{hs} & N_{hs} & N_{hs} & N_{hs} & N_{hs} & N_{hs} & N_{hs} \\ N_{is} & N_{is} & N_{is} & N_{is} & N_{is} & N_{is} & N_{is} & N_{is} & N_{is} \end{bmatrix}}_{\text{Stationary reference frame}} \int_{\phi_s}^{\phi_s+\pi} \begin{bmatrix} B_r(\zeta,\theta_r) \\ B_r(\zeta,\theta_r) \\ B_r(\zeta,\theta_r) \\ B_r(\zeta,\theta_r) \\ B_r(\zeta,\theta_r) \\ B_r(\zeta,\theta_r) \\ B_r(\zeta,\theta_r) \\ B_r(\zeta,\theta_r) \\ B_r(\zeta,\theta_r) \end{bmatrix} d\zeta d\phi_s \tag{4.38}$$

$$= \frac{rl}{9} T(\theta_r) \int_0^{2\pi} \begin{bmatrix} N_{q1s} & N_{q1s} & N_{q1s} & N_{q1s} & N_{q1s} & N_{q1s} & N_{q1s} & N_{q1s} & N_{q1s} \\ N_{d1s} & N_{d1s} & N_{d1s} & N_{d1s} & N_{d1s} & N_{d1s} & N_{d1s} & N_{d1s} & N_{d1s} \\ N_{q3s} & N_{q3s} & N_{q3s} & N_{q3s} & N_{q3s} & N_{q3s} & N_{q3s} & N_{q3s} & N_{q3s} \\ N_{d3s} & N_{d3s} & N_{d3s} & N_{d3s} & N_{d3s} & N_{d3s} & N_{d3s} & N_{d3s} & N_{d3s} \\ N_{q5s} & N_{q5s} & N_{q5s} & N_{q5s} & N_{q5s} & N_{q5s} & N_{q5s} & N_{q5s} & N_{q5s} \\ N_{d5s} & N_{d5s} & N_{d5s} & N_{d5s} & N_{d5s} & N_{d5s} & N_{d5s} & N_{d5s} & N_{d5s} \\ N_{q7s} & N_{q7s} & N_{q7s} & N_{q7s} & N_{q7s} & N_{q7s} & N_{q7s} & N_{q7s} & N_{q7s} \\ N_{d7s} & N_{d7s} & N_{d7s} & N_{d7s} & N_{d7s} & N_{d7s} & N_{d7s} & N_{d7s} & N_{d7s} \\ N_{0s} & N_{0s} & N_{0s} & N_{0s} & N_{0s} & N_{0s} & N_{0s} & N_{0s} & N_{0s} \end{bmatrix} \int_{\phi_s}^{\phi_s+\pi} \begin{bmatrix} B_r(\zeta,\theta_r) \\ B_r(\zeta,\theta_r) \\ B_r(\zeta,\theta_r) \\ B_r(\zeta,\theta_r) \\ B_r(\zeta,\theta_r) \\ B_r(\zeta,\theta_r) \\ B_r(\zeta,\theta_r) \\ B_r(\zeta,\theta_r) \\ B_r(\zeta,\theta_r) \end{bmatrix} d\zeta d\phi_s \tag{4.39}$$

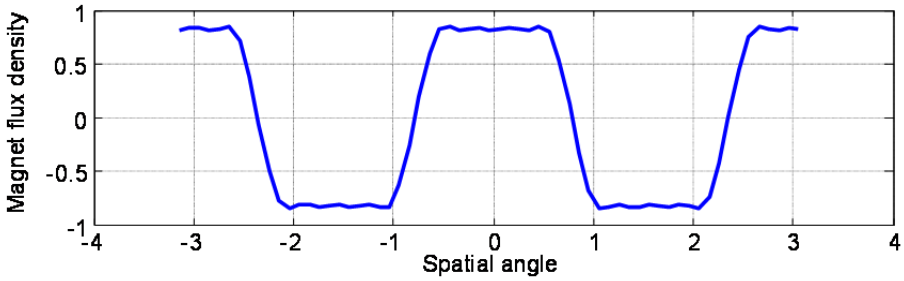

Figure 4.50 Plot of flux density with spatial angle

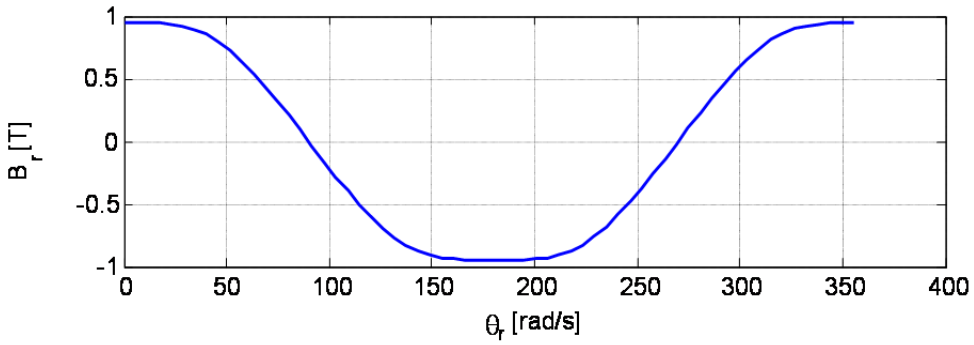

Figure 4.51 Flux density integrated with $\phi_s = 0$

The term inside the second integration is the waveform of the tapered flux density. Since the flux density gives the same value for any range of integration, the integration here is performed for the limits with $\phi_s = 0$. Using this integration, the flux density is as given in Figure 4.51. Solving for the flux linkage of Equation (4.39), it reduces into

$$= \frac{rl}{9} T(\theta_r) \int_0^{2\pi} \begin{bmatrix} 9N_{q1s} B_r(\theta_r) \\ 9N_{d1s} B_r(\theta_r) \\ 9N_{q3s} B_r(\theta_r) \\ 9N_{d3s} B_r(\theta_r) \\ 9N_{q5s} B_r(\theta_r) \\ 9N_{d5s} B_r(\theta_r) \\ 9N_{q7s} B_r(\theta_r) \\ 9N_{d7s} B_r(\theta_r) \\ 9N_{0s} B_r(\theta_r) \end{bmatrix} d\phi_s \tag{4.40}$$

Hence, the fundamental q-axis flux linkage due to magnet is derived as

$$\lambda_{q1ms}=\int_0^{2\pi}\begin{bmatrix} c(\theta_r)\times N_{q1s}(B_r(\theta_r))+c(\theta_r-\alpha)\times N_{d1s}(B_r(\theta_r)) \\ +c(\theta_r-2\alpha)\times N_{q3s}(B_r(\theta_r)) \\ +c(\theta_r-3\alpha)\times N_{d3s}(B_r(\theta_r))+c(\theta_r-4\alpha)\times N_{q5s}(B_r(\theta_r)) \\ +c(\theta_r-5\alpha)\times N_{d5s}(B_r(\theta_r))+c(\theta_r-6\alpha)\times N_{q7s}(B_r(\theta_r)) \\ +c(\theta_r-7\alpha)\times N_{d7s}(B_r(\theta_r))+c(\theta_r-8\alpha)\times N_{0s}(B_r(\theta_r)) \end{bmatrix} d\phi_s \tag{4.41}$$

The plot of the magnet flux linkage with variation in θ_r is given in Figure 4.52.

Since the fundamental q axis flux linkage is very small, the induced voltage due to the q axis flux is almost zero.

Similarly, the fundamental d-axis flux linkage is derived as

$$\lambda_{d1ms}=\int_0^{2\pi}\begin{bmatrix} s(\theta_r)\times N_{q1s}(B_r(\theta_r))+s(\theta_r-\alpha)\times N_{d1s}(B_r(\theta_r))+s(\theta_r-2\alpha)\times N_{q3s}(B_r(\theta_r)) \\ +s(\theta_r-3\alpha)\times N_{d3s}(B_r(\theta_r))+s(\theta_r-4\alpha)\times N_{q5s}(B_r(\theta_r)) \\ +s(\theta_r-5\alpha)\times N_{d5s}(B_r(\theta_r))+s(\theta_r-6\alpha)\times N_{q7s}(B_r(\theta_r)) \\ +s(\theta_r-7\alpha)\times N_{d7s}(B_r(\theta_r))+s(\theta_r-8\alpha)\times N_{0s}(B_r(\theta_r)) \end{bmatrix} \tag{4.42}$$

The graph is obtained for flux linkage as shown in Figure 4.53 and the q-axis induced voltage due to fundamental d-axis flux linkage is given in Figure 4.54

The d-axis 3rd harmonic flux linkage due to magnet is derived as

$$\lambda_{d3ms}=\int_0^{2\pi}\begin{bmatrix} s3(\theta_r)\times N_{q1s}(B_r(\theta_r))+s3(\theta_r-\alpha)\times N_{d1s}B_r(\theta_r)+s3(\theta_r-2\alpha)\times N_{q3s}B_r(\theta_r) \\ +s3(\theta_r-3\alpha)\times N_{d3s}B_r(\theta_r)+s3(\theta_r-4\alpha)\times N_{q5s}(B_r(\theta_r)) \\ +s3(\theta_r-5\alpha)\times N_{d5s}B_r(\theta_r)+s3(\theta_r-6\alpha)\times N_{q7s}B_r(\theta_r) \\ +s3(\theta_r-7\alpha)\times N_{d7s}(B_r(\theta_r))+s3(\theta_r-8\alpha)\times N_{0s}(B_r(\theta_r)) \end{bmatrix} \tag{4.43}$$

The plot of 3rd harmonic d-axis flux linkage is given in Figure 4.55 and plot of q-axis 3rd harmonic induced voltage is depicted in Figure 4.56. Due to the symmetrical transformation, q-axis flux linkage for 3rd harmonic is zero. Hence, d-axis 3rd harmonic induced e.m.f. is also zero.

Similarly, for the 5th harmonics, the d-axis flux linkage is given as

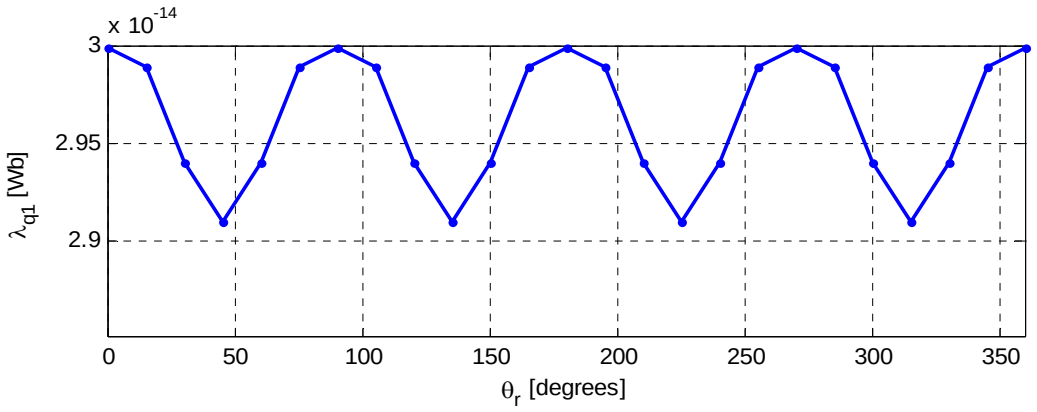

Figure 4.52 Plot of fundamental q-axis flux linkage due to magnet

$$\lambda_{d5ms}=\int_0^{2\pi}\begin{bmatrix} s5(\theta_r)\times N_{q1s}(B_r(\theta_r))+s5(\theta_r-\alpha)\times N_{d1s}(B_r(\theta_r))+s5(\theta_r-2\alpha)\times N_{q3s}(B_r(\theta_r)) \\ +s5(\theta_r-3\alpha)\times N_{d3s}(B_r(\theta_r))+s5(\theta_r-4\alpha)\times N_{q5s}(B_r(\theta_r)) \\ +s5(\theta_r-5\alpha)\times N_{d5s}(B_r(\theta_r))+s5(\theta_r-6\alpha)\times N_{q7s}(B_r(\theta_r)) \\ +s5(\theta_r-7\alpha)\times N_{d7s}(B_r(\theta_r))+s5(\theta_r-8\alpha)\times N_{0s}(B_r(\theta_r)) \end{bmatrix} \tag{4.44}$$

Figure 4.57 depicts the flux linkage due to d axis 5th harmonics. Multiplying this flux linkage by five times the synchronous frequency the q-axis 5th harmonics induced voltage is given in Figure 4.58.

Finally, the q-axis flux linkage for 7th harmonics is given as

$$\lambda_{q7ms}=\int_0^{2\pi}\begin{bmatrix} s7(\theta_r)\times N_{q1s}(B_r(\theta_r))+s7(\theta_r-\alpha)\times N_{d1s}(B_r(\theta_r))+s7(\theta_r-2\alpha)\times N_{q3s}(B_r(\theta_r)) \\ +s7(\theta_r-3\alpha)\times N_{d3s}(B_r(\theta_r))+s7(\theta_r-4\alpha)\times N_{q5s}(B_r(\theta_r)) \\ +s7(\theta_r-5\alpha)\times N_{d5s}(B_r(\theta_r))+s7(\theta_r-6\alpha)\times N_{q7s}(B_r(\theta_r)) \\ +s7(\theta_r-7\alpha)\times N_{d7s}(B_r(\theta_r))+s7(\theta_r-8\alpha)\times N_{0s}(B_r(\theta_r)) \end{bmatrix} \tag{4.45}$$

Figure 4.59 depicts the flux linkage due to d axis and 7th harmonics. Multiplying this flux linkage by seven times the synchronous frequency, the q-axis 7th harmonics induced voltage is obtained as in Figure 4.60.

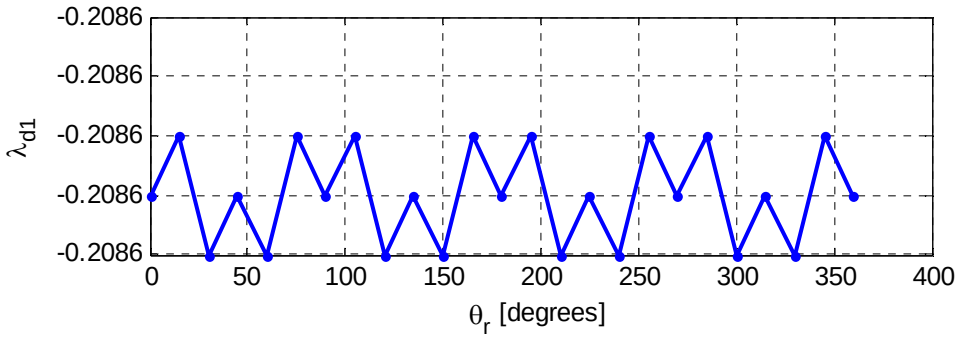

Figure 4.53 Plot of fundamental d-axis flux linkage due to magnet

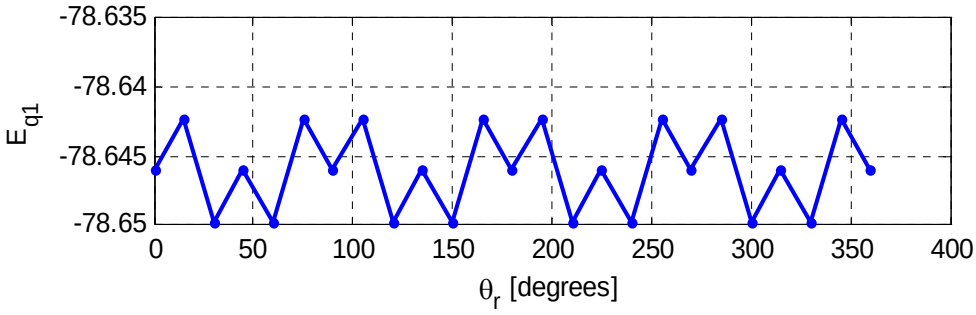

Figure 4.54 Induced EMF due to fundamental d-axis flux linkage

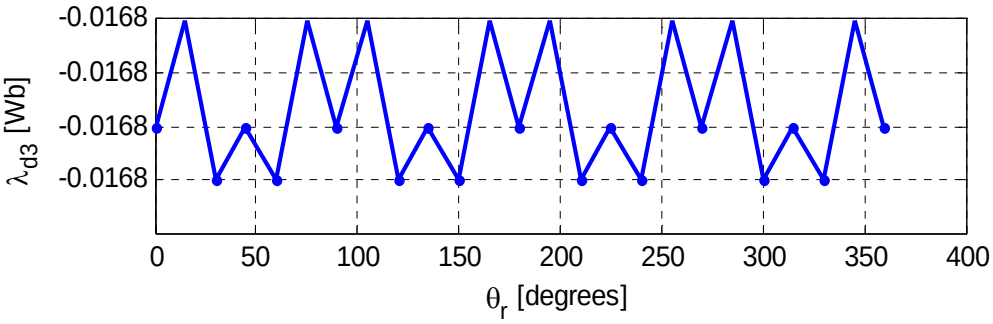

Figure 4.55 Plot of d-axis 3rd harmonic flux linkage

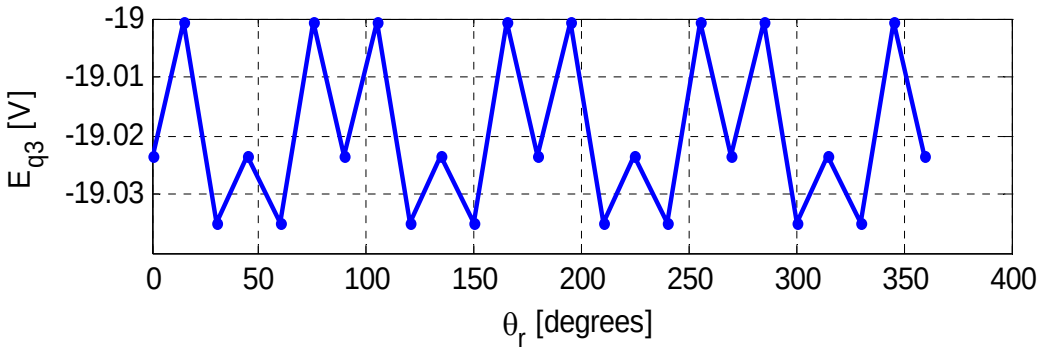

Figure 4.56 Plot of q-axis 3rd harmonic induced voltage

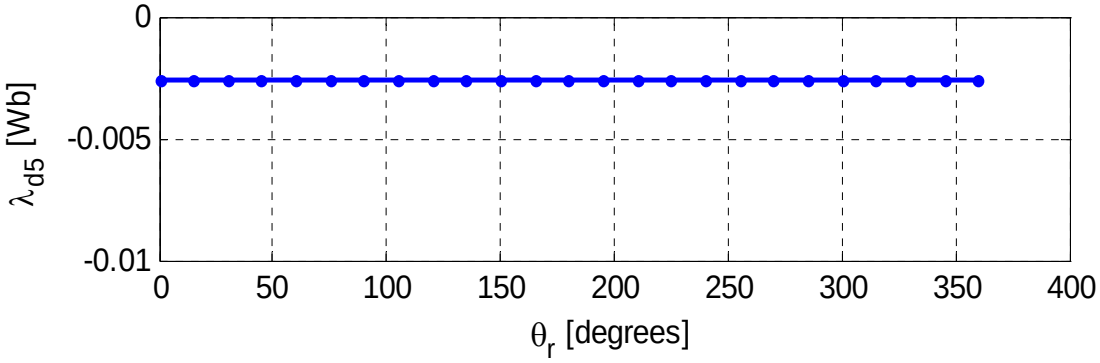

Figure 4.57 Plot of d-axis 5th harmonic flux linkage

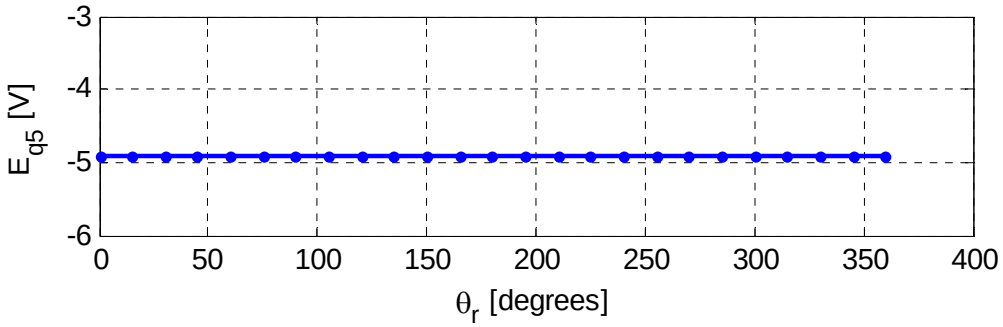

Figure 4.58 Plot of q-axis 5th harmonic induced voltage

4.10 Equivalent Circuit

For the equivalent circuit, the flux and voltage equations are needed in q and d-axis. In case of 9-phase IPM machine with harmonics, the voltage equations are given as

$$
\begin{aligned}
V_{q1s} &= r_s i_{q1s} + \omega\lambda_{d1s} + p\lambda_{q1s} \\
V_{d1s} &= r_s i_{d1s} - \omega\lambda_{q1s} + p\lambda_{d1s} \\
V_{q3s} &= r_s i_{q3s} + 3\omega\lambda_{d3s} + p\lambda_{q3s} \\
V_{d3s} &= r_s i_{d3s} - 3\omega\lambda_{q3s} + p\lambda_{d3s} \\
V_{q5s} &= r_s i_{q5s} + 5\omega\lambda_{d5s} + p\lambda_{q5s} \\
V_{d5s} &= r_s i_{d5s} - 5\omega\lambda_{q5s} + p\lambda_{d5s} \\
V_{q7s} &= r_s i_{q7s} + 7\omega\lambda_{d7s} + p\lambda_{q7s} \\
V_{d7s} &= r_s i_{d7s} - 7\omega\lambda_{q7s} + p\lambda_{d7s} \\
V_{0s} &= r_s i_{0s} + p\lambda_{os}
\end{aligned}
\tag{4.46}
$$

$$
\begin{aligned}
V_{q1r} &= r_r i_{q1r} + (\omega - \omega_r)\lambda_{d1r} + p\lambda_{q1r} \\
V_{d1r} &= r_r i_{d1r} - (\omega - \omega_r)\lambda_{q1r} + p\lambda_{d1r} \\
V_{q3r} &= r_r i_{q3r} + 3(\omega - \omega_r)\lambda_{d3r} + p\lambda_{q3r} \\
V_{d3r} &= r_r i_{d3r} - 3(\omega - \omega_r)\lambda_{q3r} + p\lambda_{d3r} \\
V_{q5r} &= r_r i_{q5r} + 5(\omega - \omega_r)\lambda_{d5r} + p\lambda_{q5r} \\
V_{d5r} &= r_s i_{d5r} - 5(\omega - \omega_r)\lambda_{q5r} + p\lambda_{d5r} \\
V_{q7r} &= r_r i_{q7r} + 7(\omega - \omega_r)\lambda_{d7r} + p\lambda_{q7r} \\
V_{d7r} &= r_r i_{d7r} - 7(\omega - \omega_r)\lambda_{q7r} + p\lambda_{d7r} \\
V_{0r} &= r_r i_{0r} + p\lambda_{or}
\end{aligned}
\tag{4.47}
$$

$$
\begin{aligned}
\lambda_{q1s} &= L_{q1} i_{q1} + L_{13} i_{q3} + L_{15} i_{q5} + L_{17} i_{q7} + L_{q11} i_{q1r} \\
\lambda_{d1s} &= L_{d1} i_{d1} + L_{13} i_{d3} + L_{15} i_{d5} + L_{17} i_{d7} + L_{d11} i_{d1r} + \lambda_{md1} \\
\lambda_{q3s} &= L_{31} i_{q1} + L_{q3} i_{q3} + L_{35} i_{q5} + L_{37} i_{q7} + L_{q33} i_{q3r} \\
\lambda_{d3s} &= L_{31} i_{d1} + L_{d3} i_{d3} + L_{35} i_{d5} + L_{37} i_{d7} + L_{d33} i_{d3r} + \lambda_{md3} \\
\lambda_{q5s} &= L_{51} i_{q1} + L_{53} i_{q3} + L_{q5} i_{q5} + L_{57} i_{q7} + L_{q55} i_{q5r} \\
\lambda_{d5s} &= L_{51} i_{d1} + L_{53} i_{d3} + L_{d5} i_{d5} + L_{57} i_{d7} + L_{d55} i_{d5r} + \lambda_{md5} \\
\lambda_{q7s} &= L_{71} i_{q1} + L_{73} i_{q3} + L_{75} i_{q5} + L_{q7} i_{q7} + L_{q77} i_{q7r} \\
\lambda_{d7s} &= L_{71} i_{d1} + L_{73} i_{d3} + L_{75} i_{d5} + L_{d7} i_{d7} + L_{d77} i_{d7r} + \lambda_{md7}
\end{aligned}
\tag{4.48}
$$

$$
\begin{aligned}
\lambda_{q1r} &= L_{q1r} i_{q1r} + L_{q11} i_{q1s} \\
\lambda_{d1r} &= L_{d1r} i_{d1r} + L_{d11} i_{d1s} \\
\lambda_{q3r} &= L_{q3r} i_{q3r} + L_{q33} i_{q3s} \\
\lambda_{d3r} &= L_{d3r} i_{d3r} + L_{d33} i_{d3s} \\
\lambda_{q5r} &= L_{q5r} i_{q5r} + L_{q55} i_{q5s} \\
\lambda_{d5r} &= L_{d5r} i_{d5r} + L_{d55} i_{d5s} \\
\lambda_{q7r} &= L_{q7r} i_{q7r} + L_{q77} i_{q7s} \\
\lambda_{d7r} &= L_{d7r} i_{d7r} + L_{d77} i_{d7s}
\end{aligned}
\tag{4.49}
$$

4.11 Turns Transformations

The equivalent circuit equations derived in Section 4.10 are simplified using the turn transformations in this section. As the turn and winding functions are used in the derivations of the equivalent circuit parameters, the appropriate ratio of turns makes it easier to transform the rotor or stator harmonic quantities into stator fundamental component to ease the mathematical manipulations.

4.11.1 Rotor Harmonics Turns Transformation

Starting from the rotor voltage equations for 3-phase case,

$$V_{abc....nr} = r_r i_{abc....nr} + p\lambda_{abc....nr} \tag{4.50}$$

Similarly, rotor flux linkage equation is given as

$$\lambda_{abc...nr} = L_{abc...nr} i_{abc...nr} + L_{abc...nrabc...is} i_{abc...is} \tag{4.51}$$

Multiplying both sides of Equation (4.51) by the turns ratio of stator and rotor,

$$\frac{N_s}{N_r}\lambda_{abc....nr} = \frac{N_s}{N_r}L_{abc....nr}i_{abc....nr} + \frac{N_s}{N_r}L_{abc.....nrabc....is}i_{abc.....is} \tag{4.52}$$

$$T(\theta-\theta_r)\frac{N_s}{N_r}\lambda_{abc.....nr} = T(\theta-\theta_r)\frac{N_s}{N_r}L_{abc.....nr}i_{abc.....nr} + T(\theta-\theta_r)\frac{N_s}{N_r}L_{abc....nrabc....is}i_{abc.....is} \tag{4.53}$$

Hence,

$$\begin{aligned}\lambda_{qdor}' &= T(\theta-\theta_r)\left(\frac{N_s}{N_r}\right)^2 L_{abc...nr}i_{abc...nr}' + T(\theta-\theta_r)\frac{N_s}{N_r}L_{abc...nrabcs}i_{abc...is} \\ &= T(\theta-\theta_r)\left(\frac{N_s}{N_r}\right)^2 L_{abc...nr}T(\theta-\theta_r)^{-1}i_{qdor}' + T(\theta-\theta_r)\frac{N_s}{N_r}L_{abc...nrabc....is}T(\theta)^{-1}i_{abc....is}\end{aligned} \tag{4.54}$$

The first part of Equation (4.54) is given as

$$\begin{aligned}&T(\theta-\theta_r)\left(\frac{N_s}{N_r}\right)^2 L_{abc....nr}T(\theta-\theta_r)^{-1}i_{qdor}' \\ &\quad = T(\theta-\theta_r)\frac{N_s{}^2}{N_r{}^2}\frac{\mu_0 rl}{g}\int_0^{2\pi}[N_{abc...nr}]d\phi T(\theta-\theta_r)^{-1}i_{qdor}'\end{aligned} \tag{4.55}$$

where,

$$N_{abc...nr} = \begin{bmatrix} N_{ar}{}^2 & N_{ar}N_{br} & N_{ar}N_{cr} & ..... & N_{ar}N_{nr} \\ N_{br}N_{ar} & N_{br}{}^2 & N_{br}N_{cr} & ..... & N_{br}N_{nr} \\ : & : & : & ..... & : \\ : & : & : & ..... & : \\ N_{nr}N_{ar} & N_{nr}N_{br} & N_{nr}N_{cr} & ..... & N_{nr}{}^2 \end{bmatrix} \tag{4.56}$$

Using rotor reference frame,

$$T(\theta-\theta_r)\frac{N_s{}^2}{N_r{}^2}\frac{\mu_0 rl}{g}\int_0^{2\pi}\begin{bmatrix} N_{ar}{}^2 & N_{ar}N_{br} & N_{ar}N_{cr} & ..... & N_{ar}N_{nr} \\ N_{br}N_{ar} & N_{br}{}^2 & N_{br}N_{cr} & ..... & N_{br}N_{nr} \\ : & : & : & ..... & : \\ : & : & : & ..... & : \\ N_{nr}N_{ar} & N_{nr}N_{br} & N_{nr}N_{cr} & ..... & N_{nr}{}^2 \end{bmatrix} d\phi T(\theta-\theta_r)^{-1}i_{qdor}$$

$$= \frac{N_s{}^2}{N_r{}^2}\frac{\mu_0 rl}{g}T(0)\int_0^{2\pi}\begin{bmatrix} N_{ar}{}^2 & N_{ar}N_{br} & N_{ar}N_{cr} & \ldots\ldots\ldots & N_{ar}N_{nr} \\ N_{br}N_{ar} & N_{br}{}^2 & N_{br}N_{cr} & \ldots\ldots\ldots & N_{br}N_{nr} \\ \vdots & \vdots & \vdots & \ldots\ldots\ldots & \vdots \\ \vdots & \vdots & \vdots & \ldots\ldots\ldots & \vdots \\ N_{nr}N_{ar} & N_{nr}N_{br} & N_{nr}N_{cr} & \ldots\ldots\ldots & N_{nr}{}^2 \end{bmatrix} d\phi T(\theta-\theta_r)^{-1} i_{qdor}' \quad (4.57)$$

$$= \frac{N_s{}^2}{N_r{}^2}\frac{\mu_0 rl}{g}\int_0^{2\pi}\begin{bmatrix} N_{q1r}{}^2 & N_{q1r}N_{d1r} & N_{q1r}N_{q3r} & \ldots\ldots\ldots & N_{q1r}N_{0r} \\ N_{d1r}N_{q1r} & N_{d1r}{}^2 & N_{d1r}N_{q3r} & \ldots\ldots\ldots & N_{d1r}N_{0r} \\ \vdots & \vdots & \vdots & \ldots\ldots\ldots & \vdots \\ \vdots & \vdots & \vdots & \ldots\ldots\ldots & \vdots \\ N_{or}N_{q1r} & N_{or}N_{d1r} & N_{0r}N_{q3r} & \ldots\ldots\ldots & N_{0r}{}^2 \end{bmatrix} d\phi T(\theta-\theta_r)^{-1} i_{qdor}' \quad (4.58)$$

4.11.2 Stator Harmonics Turns Transformations

The expressions derived for rotor-stator mutual turns transformations can also be extended for stator harmonics turns transformations in case of 9-phase machines. Taking the voltage equations for three of the 9-phases,

$$V_{abc....is} = r_s i_{abc....is} + p\lambda_{abc.....is} \quad (4.59)$$

$$\lambda_{abc...is} = L_{abc.....is} i_{abc.....is} + L_{abc.....isabc...nr} i_{abc...nr} \quad (4.60)$$

$$T(\theta)\lambda_{abc.....is} = T(\theta)L_{abc.....is} i_{abc.....is} + T(\theta)L_{abc.....isabc...nr} i_{abc.....nr} \quad (4.61)$$

Multiplying both sides of Equation (4.61) by ratio of harmonic turns,

$$\frac{N_{s1}}{N_{s2}}T(\theta)\lambda_{abc...is} = \left[\frac{N_{s1}}{N_{s2}}\right]^2 T(\theta)L_{abc..is} i_{abc...is}' + \frac{N_{s1}}{N_{s2}}T(\theta)L_{abc..isabc...nr} i_{abc...nr} \quad (4.62)$$

$$\begin{aligned} &\frac{N_{s1}}{N_{s2}}T(\theta)L_{abc..is} i_{abc...is} + \frac{N_{s1}}{N_{s2}}T(\theta)L_{abc..isabc...nr} i_{abc...nr} \\ &= \left[\frac{N_{s1}}{N_{s2}}\right]^2 T(\theta)L_{abc..is}T(\theta)^{-1} i_{qdoxs}' + \frac{N_{s1}}{N_{s2}}T(\theta)L_{abc..isabc...nr}T(\theta-\theta_r)^{-1} i_{qdonr} \end{aligned} \quad (4.63)$$

For evaluating the stator harmonics turns transformations, first term of Equation (4.63) is taken. The inductance matrix $L_{abc..is}$ is the inductance matrix in real variables. It is given as

$$L_{abc..is} = \begin{bmatrix} L_{aa} & L_{ab} & ..... & L_{ai} \\ L_{ba} & L_{bb} & ..... & L_{bi} \\ ... & ... & ... & ... \\ L_{ia} & L_{ib} & .... & L_{ii} \end{bmatrix} \tag{4.64}$$

The inductance matrix in Equation (4.60) consists of self and mutual inductance terms. From definition of inductance,

$$L_{aa} = \mu_0 rl \int_0^{2\pi} N_a(\phi) N_a(\phi) g^{-1}(\phi, \theta_r) d\phi \tag{4.65}$$

$$L_{ab} = \mu_0 rl \int_0^{2\pi} N_a(\phi) N_b(\phi) g^{-1}(\phi, \theta_r) d\phi \tag{4.66}$$

Hence,

$$\begin{aligned} &\left[\frac{N_{s1}}{N_{s2}}\right]^2 T(\theta) L_{abc..is} T(\theta)^{-1} \\ &= \left[\frac{N_{s1}}{N_{s2}}\right]^2 T(\theta) \mu_0 rl \int_0^{2\pi} \begin{bmatrix} {N_a}^2 & N_a N_b & .... & N_a N_i \\ N_b N_a & {N_b}^2 & .... & N_b N_i \\ : & : & .... & : \\ N_i N_a & N_i N_b & .... & {N_i}^2 \end{bmatrix} g^{-1}(\phi, \theta_r) d\phi T(\theta)^{-1} \end{aligned} \tag{4.67}$$

In Equation (4.67), the transformation matrix $T(\theta)$, the winding function matrix and the inverse of the transformation matrix $T(\theta)^{-1}$ gives the winding function in q-d variables as they were derived in previous sections. Proceeding with the derivation, Equation (4.67) can be given as

$$\left[\frac{N_{s1}}{N_{s2}}\right]^2 T(\theta) L_{abc..is} T(\theta)^{-1} = \left(\frac{N_{s1}}{N_{s2}}\right)^2 \mu_0 rl \int [A][C] d\phi \tag{4.68}$$

where, C is the air gap matrix with diagonal terms as air gap function $g^{-1}(\phi, \theta_r)$. Matrix A is given as

$$A = \begin{bmatrix}
N_{q1}^2 & N_{q1}N_{d1} & N_{q1}N_{q3} & N_{q1}N_{d3} & N_{q1}N_{q5} & N_{q1}N_{d5} & N_{q1}N_{q7} & N_{q1}N_{d7} & N_{q1}N_0 \\
N_{q1}N_{d1} & N_{d1}^2 & N_{d1}N_{q3} & N_{d1}N_{d3} & N_{d1}N_{q5} & N_{d1}N_{d5} & N_{d1}N_{q7} & N_{d1}N_{d7} & N_{d1}N_0 \\
N_{q3}N_{q1} & N_{q3}N_{d1} & N_{q3}^2 & N_{q3}N_{d3} & N_{q3}N_{q5} & N_{q3}N_{d5} & N_{q3}N_{q7} & N_{q3}N_{d7} & N_{q3}N_0 \\
N_{d3}N_{q1} & N_{d1}N_{d3} & N_{q3}N_{d3} & N_{d3}^2 & N_{d3}N_{q5} & N_{d3}N_{d5} & N_{d3}N_{q7} & N_{d3}N_{d7} & N_{d3}N_0 \\
N_{q1}N_{q5} & N_{d1}N_{q5} & N_{q3}N_{q5} & N_{d3}N_{q5} & N_{q5}^2 & N_{q5}N_{d5} & N_{q5}N_{q7} & N_{q5}N_{d7} & N_{q5}N_0 \\
N_{q1}N_{d5} & N_{d1}N_{d5} & N_{q3}N_{d5} & N_{d3}N_{d5} & N_{q5}N_{d5} & N_{d5}^2 & N_{d5}N_{q7} & N_{d5}N_{d7} & N_{d5}N_0 \\
N_{q1}N_{q7} & N_{d1}N_{q7} & N_{q3}N_{q7} & N_{d3}N_{q7} & N_{q5}N_{q7} & N_{d5}N_{q7} & N_{q7}^2 & N_{q7}N_{d7} & N_{q7}N_0 \\
N_{q1}N_{d7} & N_{d1}N_{d7} & N_{q3}N_{d7} & N_{d3}N_{d7} & N_{q5}N_{d7} & N_{d5}N_{d7} & N_{q7}N_{d7} & N_{d7}^2 & N_{d7}N_0 \\
N_{q1}N_0 & N_{d1}N_0 & N_{q3}N_0 & N_{d3}N_0 & N_{q5}N_0 & N_{d5}N_0 & N_{q7}N_0 & N_{d7}N_0 & N_0^2
\end{bmatrix} \tag{4.69}$$

Equations (4.68) and (4.69) give the expression of the turns transformations for the stator harmonics.

4.11.3 Turns Transformations for Stator and Rotor Circuits

The rotor and stator harmonic transformations given in Sections 4.11.1 and 4.11.2, respectively are now used as basis for transforming the model equations into the stator side using the appropriate transformations. Starting from the flux linkage equations

$$\lambda_{q1s} = L_{q1} i_{q1} + L_{13} i_{q3} + L_{15} i_{q5} + L_{17} i_{q7} + L_{q11} i_{q1r}$$
$$\lambda_{d1s} = L_{d1} i_{d1} + L_{13} i_{d3} + L_{15} i_{d5} + L_{17} i_{d7} + L_{d11} i_{d1r} + \lambda_{md1}$$
$$\lambda_{q3s} = L_{31} i_{q1} + L_{q3} i_{q3} + L_{35} i_{q5} + L_{37} i_{q7} + L_{q33} i_{q3r}$$

$$
\begin{aligned}
\lambda_{d3s} &= L_{31}i_{d1} + L_{d3}i_{d3} + L_{35}i_{d5} + L_{37}i_{d7} + L_{d33}i_{d3r} + \lambda_{md3} \\
\lambda_{q5s} &= L_{51}i_{q1} + L_{53}i_{q3} + L_{q5}i_{q5} + L_{57}i_{q7} + L_{q55}i_{q5r} \\
\lambda_{d5s} &= L_{51}i_{d1} + L_{53}i_{d3} + L_{d5}i_{d5} + L_{57}i_{d7} + L_{d55}i_{d5r} + \lambda_{md5} \\
\lambda_{q7s} &= L_{71}i_{q1} + L_{73}i_{q3} + L_{75}i_{q5} + L_{q7}i_{q7} + L_{q77}i_{q7r} \\
\lambda_{d7s} &= L_{71}i_{d1} + L_{73}i_{d3} + L_{75}i_{d5} + L_{d7}i_{d7} + L_{d77}i_{d7r} + \lambda_{md7}
\end{aligned}
\tag{4.70}
$$

$$
\begin{aligned}
\lambda_{q1r} &= L_{q1r}i_{q1r} + L_{q11}i_{q1s} \\
\lambda_{d1r} &= L_{d1r}i_{d1r} + L_{d11}i_{d1s} \\
\lambda_{q3r} &= L_{q3r}i_{q3r} + L_{q33}i_{q3s} \\
\lambda_{d3r} &= L_{d3r}i_{d3r} + L_{d33}i_{d3s} \\
\lambda_{q5r} &= L_{q5r}i_{q5r} + L_{q55}i_{q5s} \\
\lambda_{d5r} &= L_{d5r}i_{d5r} + L_{d55}i_{d5s} \\
\lambda_{q7r} &= L_{q7r}i_{q7r} + L_{q77}i_{q7s} \\
\lambda_{d7r} &= L_{d7r}i_{d7r} + L_{d77}i_{d7s}
\end{aligned}
\tag{4.71}
$$

Transforming the rotor harmonic inductances into the stator side using the appropriate transformation ratio with the reference of Equation (4.54), the referred stator inductance can be written as

$$
L_{q1r}' = \left(\frac{N_{q1s}}{N_{q1r}}\right)^2 L_{q1r},\ L_{d1r}' = \left(\frac{N_{d1s}}{N_{d1r}}\right)^2 L_{d1r} \tag{4.72}
$$

$$
L_{q11}' = \left(\frac{N_{q1s}}{N_{q1r}}\right) L_{q11},\ L_{d11}' = \left(\frac{N_{d1s}}{N_{d1r}}\right) L_{d11} \tag{4.73}
$$

$$
L_{q3r}' = \left(\frac{N_{q3s}}{N_{q3r}}\right)^2 L_{q3r},\ L_{d3r}' = \left(\frac{N_{d3s}}{N_{d3r}}\right)^2 L_{d3r} \tag{4.74}
$$

$$
L_{q33}' = \left(\frac{N_{q3s}}{N_{q3r}}\right) L_{q33},\ L_{d33}' = \left(\frac{N_{d3s}}{N_{d3r}}\right) L_{d33} \tag{4.75}
$$

$$
L_{q5r}' = \left(\frac{N_{q5s}}{N_{q5r}}\right)^2 L_{q5r},\ L_{d5r}' = \left(\frac{N_{d5s}}{N_{d5r}}\right)^2 L_{d5r} \tag{4.76}
$$

$$L_{q55}'=\left(\frac{N_{q5s}}{N_{q5r}}\right)L_{q55},\ L_{d55}'=\left(\frac{N_{d5s}}{N_{d5r}}\right)L_{d55} \tag{4.77}$$

$$L_{q7r}'=\left(\frac{N_{q7s}}{N_{q7r}}\right)^2 L_{q7r},\ L_{d7r}'=\left(\frac{N_{d7s}}{N_{d7r}}\right)^2 L_{d7r} \tag{4.78}$$

$$L_{q77}'=\left(\frac{N_{q7s}}{N_{q7r}}\right)L_{q77},\ L_{d77}'=\left(\frac{N_{d7s}}{N_{d7r}}\right)L_{d77} \tag{4.79}$$

$$\begin{gathered}L_{q3}'=\left(\frac{N_{q1s}}{N_{q3s}}\right)^2 L_{q3},\ L_{q5}'=\left(\frac{N_{q1s}}{N_{q5s}}\right)^2 L_{q5},\ L_{q7}'=\left(\frac{N_{q1s}}{N_{q7s}}\right)^2 L_{q7}\\ L_{d3}'=\left(\frac{N_{d1s}}{N_{d3s}}\right)^2 L_{d3},\ L_{d5}'=\left(\frac{N_{d1s}}{N_{d5s}}\right)^2 L_{d5},\ L_{d7}'=\left(\frac{N_{d1s}}{N_{d7s}}\right)^2 L_{d7}\end{gathered} \tag{4.80}$$

$$L_{13}'=\left(\frac{N_{q1s}}{N_{q3s}}\right)L_{13},\ L_{15}'=\left(\frac{N_{q1s}}{N_{q5s}}\right)L_{15},\ L_{17}'=\left(\frac{N_{q1s}}{N_{q7s}}\right)L_{17}$$

$$L_{35}'=\left(\frac{N_{q3s}}{N_{q5s}}\right)L_{35}=\left(\frac{N_{q1s}}{N_{q3s}}\right)\left(\frac{N_{q1s}}{N_{q5s}}\right)L_{35}$$

$$L_{37}'=\left(\frac{N_{q3s}}{N_{q7s}}\right)L_{37}=\left(\frac{N_{q1s}}{N_{q3s}}\right)\left(\frac{N_{q1s}}{N_{q7s}}\right)L_{37} \tag{4.81}$$

$$L_{57}'=\left(\frac{N_{q5s}}{N_{q7s}}\right)L_{57}=\left(\frac{N_{q1s}}{N_{q5s}}\right)\left(\frac{N_{q1s}}{N_{q7s}}\right)L_{57}$$

Similarly, the current transformations between the harmonics

$$\begin{gathered}i_{q3}'=\left(\frac{N_{q3s}}{N_{q1s}}\right)i_{q3},\ i_{q5}'=\left(\frac{N_{q5s}}{N_{q1s}}\right)i_{q5},\ i_{q7}'=\left(\frac{N_{q7s}}{N_{q1s}}\right)i_{q7}\\ i_{d3}'=\left(\frac{N_{d3s}}{N_{d1s}}\right)i_{d3},\ i_{d5}'=\left(\frac{N_{d5s}}{N_{d1s}}\right)i_{d5},\ i_{d7}'=\left(\frac{N_{d7s}}{N_{d1s}}\right)i_{d7}\end{gathered} \tag{4.82}$$

$$i_{q3r}' = \left(\frac{N_{q3r}}{N_{q1s}}\right) i_{q3r},\ i_{q5r}' = \left(\frac{N_{q5r}}{N_{q1s}}\right) i_{q5r},\ i_{q7r}' = \left(\frac{N_{q7r}}{N_{q1s}}\right) i_{q7r}$$

The flux transformations are given as

$$\begin{aligned}
&\lambda_{q3s}' = \left(\frac{N_{q1s}}{N_{q3s}}\right)\lambda_{q3s},\ \lambda_{q5s}' = \left(\frac{N_{q1s}}{N_{q5s}}\right)\lambda_{q5s},\ \lambda_{q7s}' = \left(\frac{N_{q1s}}{N_{q7s}}\right)\lambda_{q7s} \\
&\lambda_{d3s}' = \left(\frac{N_{d1s}}{N_{d3s}}\right)\lambda_{d3s},\ \lambda_{d5s}' = \left(\frac{N_{d1s}}{N_{d5s}}\right)\lambda_{d5s},\ \lambda_{d7s}' = \left(\frac{N_{q1s}}{N_{q7s}}\right)\lambda_{d7s} \\
&\lambda_{q1r}' = \left(\frac{N_{q1s}}{N_{q1r}}\right)\lambda_{q1r},\ \lambda_{q3r}' = \left(\frac{N_{q1s}}{N_{q3r}}\right)\lambda_{q3r},\ \lambda_{q5r}' = \left(\frac{N_{q1s}}{N_{q5r}}\right)\lambda_{q5r},\ \lambda_{q7r}' = \left(\frac{N_{q1s}}{N_{q7r}}\right)\lambda_{q7r} \\
&\lambda_{d1r}' = \left(\frac{N_{d1s}}{N_{d1r}}\right)\lambda_{d1r},\ \lambda_{d3r}' = \left(\frac{N_{d3s}}{N_{d3r}}\right)\lambda_{d3r},\ \lambda_{d5r}' = \left(\frac{N_{d1s}}{N_{d5r}}\right)\lambda_{d5r},\ \lambda_{d7r}' = \left(\frac{N_{d1s}}{N_{d7r}}\right)\lambda_{d7r}
\end{aligned} \tag{4.83}$$

The flux equations after transformation are given as

$$\begin{aligned}
\lambda_{q1s} &= L_{q1} i_{q1} + L_{13} i_{q3}' + L_{15} i_{q5}' + L_{17} i_{q7}' + L_{q11} i_{q1r}' \\
\lambda_{d1s} &= L_{d1} i_{d1} + L_{13} i_{d3}' + L_{15} i_{d5}' + L_{17} i_{d7}' + L_{d11} i_{d1r}' + \lambda_{md1} \\
\lambda_{q3s}' &= L_{31} i_{q1} + L_{q3} i_{q3}' + L_{35} i_{q5}' + L_{37} i_{q7}' + L_{q33} i_{q3r}' \\
\lambda_{d3s}' &= L_{31} i_{d1} + L_{d3} i_{d3}' + L_{35} i_{d5}' + L_{37} i_{d7}' + L_{d33} i_{d3r}' + \lambda_{md3} \\
\lambda_{q5s}' &= L_{51} i_{q1} + L_{53} i_{q3}' + L_{q5} i_{q5}' + L_{57} i_{q7}' + L_{q55} i_{q5r}' \\
\lambda_{d5s}' &= L_{51} i_{d1} + L_{53} i_{d3}' + L_{d5} i_{d5}' + L_{57} i_{d7}' + L_{d55} i_{d5r}' + \lambda_{md5} \\
\lambda_{q7s}' &= L_{71} i_{q1} + L_{73} i_{q3}' + L_{75} i_{q5}' + L_{q7} i_{q7}' + L_{q77} i_{q7r}' \\
\lambda_{d7s}' &= L_{71} i_{d1} + L_{73} i_{d3}' + L_{75} i_{d5}' + L_{d7} i_{d7}' + L_{d77} i_{d7r}' + \lambda_{md7}
\end{aligned} \tag{4.84}$$

$$\begin{aligned}
\lambda_{q1r}' &= L_{q1r} i_{q1r}' + L_{q11} i_{q1s} \\
\lambda_{d1r}' &= L_{d1r} i_{d1r}' + L_{d11} i_{d1s} \\
\lambda_{q3r}' &= L_{q3r} i_{q3r}' + L_{q33} i_{q3s}' \\
\lambda_{d3r}' &= L_{d3r} i_{d3r}' + L_{d33} i_{d3s}' \\
\lambda_{q5r}' &= L_{q5r} i_{q5r}' + L_{q55} i_{q5s}' \\
\lambda_{d5r}' &= L_{d5r} i_{d5r}' + L_{d55} i_{d5s}' \\
\lambda_{q7r}' &= L_{q7r} i_{q7r}' + L_{q77} i_{q7s}' \\
\lambda_{d7r}' &= L_{d7r} i_{d7r}' + L_{d77} i_{d7s}'
\end{aligned} \tag{4.85}$$

Turns ratio transformation of voltage equations

Original Equations

$$
\begin{aligned}
V_{q1s} &= r_s i_{q1s} + \omega\lambda_{d1s} + p\lambda_{q1s} \\
V_{d1s} &= r_s i_{d1s} - \omega\lambda_{q1s} + p\lambda_{d1s} \\
V_{q3s} &= r_s i_{q3s} + 3\omega\lambda_{d3s} + p\lambda_{q3s} \\
V_{d3s} &= r_s i_{d3s} - 3\omega\lambda_{q3s} + p\lambda_{d3s} \\
V_{q5s} &= r_s i_{q5s} + 5\omega\lambda_{d5s} + p\lambda_{q5s} \\
V_{d5s} &= r_s i_{d5s} - 5\omega\lambda_{q5s} + p\lambda_{d5s} \\
V_{q7s} &= r_s i_{q7s} + 7\omega\lambda_{d7s} + p\lambda_{q7s} \\
V_{d7s} &= r_s i_{d7s} - 7\omega\lambda_{q7s} + p\lambda_{d7s} \\
V_{0s} &= r_s i_{0s} + p\lambda_{os}
\end{aligned}
\tag{4.86}
$$

$$
\begin{aligned}
V_{q1r} &= r_r i_{q1r} + (\omega - \omega_r)\lambda_{d1r} + p\lambda_{q1r} \\
V_{d1r} &= r_r i_{d1r} - (\omega - \omega_r)\lambda_{q1r} + p\lambda_{d1r} \\
V_{q3r} &= r_r i_{q3r} + 3(\omega - \omega_r)\lambda_{d3r} + p\lambda_{q3r} \\
V_{d3r} &= r_r i_{d3r} - 3(\omega - \omega_r)\lambda_{q3r} + p\lambda_{d3r} \\
V_{q5r} &= r_r i_{q5r} + 5(\omega - \omega_r)\lambda_{d5r} + p\lambda_{q5r} \\
V_{d5r} &= r_s i_{d5r} - 5(\omega - \omega_r)\lambda_{q5r} + p\lambda_{d5r} \\
V_{q7r} &= r_r i_{q7r} + 7(\omega - \omega_r)\lambda_{d7r} + p\lambda_{q7r} \\
V_{d7r} &= r_r i_{d7r} - 7(\omega - \omega_r)\lambda_{q7r} + p\lambda_{d7r} \\
V_{0r} &= r_r i_{0r} + p\lambda_{or}
\end{aligned}
\tag{4.87}
$$

$$
V_{q3s}' = \left(\frac{N_{q1s}}{N_{q3s}}\right)V_{q3s},\ V_{q5s}' = \left(\frac{N_{q1s}}{N_{q5s}}\right)V_{q5s},\ V_{q7s}' = \left(\frac{N_{q1s}}{N_{q7s}}\right)V_{q7s}
$$

$$
V_{d3s}' = \left(\frac{N_{d1s}}{N_{d3s}}\right)V_{d3s},\ V_{d5s}' = \left(\frac{N_{d1s}}{N_{d5s}}\right)V_{d5s},\ V_{d7s}' = \left(\frac{N_{d1s}}{N_{d7s}}\right)V_{d7s}
\tag{4.88}
$$

$$
V_{q1r}' = \left(\frac{N_{q1s}}{N_{q1r}}\right)V_{q1r},\ V_{q3r}' = \left(\frac{N_{q1s}}{N_{q3r}}\right)V_{q3r},\ V_{q5r}' = \left(\frac{N_{q1s}}{N_{q5r}}\right)V_{q5r},\ V_{q7r}' = \left(\frac{N_{q1s}}{N_{q7r}}\right)V_{q7r}
$$

$$
V_{d1r}' = \left(\frac{N_{d1s}}{N_{d1r}}\right)V_{d1r},\ V_{d3r}' = \left(\frac{N_{d1s}}{N_{d3r}}\right)V_{d3r},\ V_{d5r}' = \left(\frac{N_{d1s}}{N_{d5r}}\right)V_{d5r},\ V_{d7r}' = \left(\frac{N_{d1s}}{N_{d7r}}\right)V_{d7r}
$$

After the transformation

$$
\begin{aligned}
V_{q1s} &= r_s i_{q1s} + \omega\lambda_{d1s} + p\lambda_{q1s} \\
V_{d1s} &= r_s i_{d1s} - \omega\lambda_{q1s} + p\lambda_{d1s} \\
V_{q3s}' &= r_s i_{q3s}' + 3\omega\lambda_{d3s}' + p\lambda_{q3s}' \\
V_{d3s}' &= r_s i_{d3s}' - 3\omega\lambda_{q3s}' + p\lambda_{d3s}' \\
V_{q5s}' &= r_s i_{q5s}' + 5\omega\lambda_{d5s}' + p\lambda_{q5s}' \\
V_{d5s}' &= r_s i_{d5s}' - 5\omega\lambda_{q5s}' + p\lambda_{d5s}' \\
V_{q7s}' &= r_s i_{q7s}' + 7\omega\lambda_{d7s}' + p\lambda_{q7s}' \\
V_{d7s}' &= r_s i_{d7s}' - 7\omega\lambda_{q7s}' + p\lambda_{d7s}'
\end{aligned}
\tag{4.89}
$$

$$
\begin{aligned}
V_{q1r}' &= r_r' i_{q1r}' + (\omega - \omega_r)\lambda_{d1r}' + p\lambda_{q1r}' \\
V_{d1r}' &= r_r' i_{d1r}' - (\omega - \omega_r)\lambda_{q1r}' + p\lambda_{d1r}' \\
V_{q3r}' &= r_r' i_{q3r}' + 3(\omega - \omega_r)\lambda_{d3r}' + p\lambda_{q3r}' \\
V_{d3r}' &= r_r' i_{d3r}' - 3(\omega - \omega_r)\lambda_{q3r}' + p\lambda_{d3r}' \\
V_{q5r}' &= r_r' i_{q5r}' + 5(\omega - \omega_r)\lambda_{d5r}' + p\lambda_{q5r}' \\
V_{d5r}' &= r_r' i_{d5r}' - 5(\omega - \omega_r)\lambda_{q5r}' + p\lambda_{d5r}' \\
V_{q7r}' &= r_r' i_{q7r}' + 7(\omega - \omega_r)\lambda_{d7r}' + p\lambda_{q7r}' \\
V_{d7r}' &= r_r' i_{d7r}' - 7(\omega - \omega_r)\lambda_{q7r}' + p\lambda_{d7r}'
\end{aligned}
\tag{4.90}
$$

The torque equation is given as

$$
\begin{aligned}
T_e = {} & \frac{9P}{4}[(L_{q1} - L_{d1}) i_{q1} i_{d1} + 3(L_{q3} - L_{d3}) i_{q3} i_{d3} \\
& + 5(L_{q5} - L_{d5}) i_{q5} i_{d5} + 7(L_{q7} - L_{d7}) i_{q7} i_{d7} \\
& + 2L_{13}(i_{q1} i_{d3} - i_{d1} i_{q3}) + 6L_{15}(i_{q1} i_{d5} - i_{d1} i_{q5}) \\
& + 6L_{17}(i_{q1} i_{d7} - i_{d1} i_{q7}) + 2L_{35}(i_{q3} i_{d5} - i_{d3} i_{q5}) \\
& + 2L_{57}(i_{q5} i_{d7} - i_{q7} i_{d5}) + 10L_{37}(i_{q3} i_{d7} - i_{q7} i_{d3})] \\
& + \frac{9P}{4}[i_{q1}\lambda_{dm1} + 3i_{q3}\lambda_{dm3} + 5i_{q5}\lambda_{dm5} + 7i_{q7}\lambda_{dm7}]
\end{aligned}
\tag{4.91}
$$

Applying the transformations to refer the variables in Equation (4.82) to stator fundamental component,

$$
\begin{aligned}
T_e = \frac{9P}{4}[(L_{q1} - L_{d1})i_{q1}i_{d1} + 3\left(\left[\frac{N_{q3}}{N_{q1}}\right]^2 L_{q3}' - \left[\frac{N_{d3}}{N_{d1}}\right]^2 L_{d3}'\right)\left[\frac{N_{q1}}{N_{q3}}\right]i_{q3}'\left[\frac{N_{d1}}{N_{d3}}\right]i_{d3}' \\
+ 5\left(\left[\frac{N_{q5}}{N_{q1}}\right]^2 L_{q5}' - \left[\frac{N_{d5}}{N_{d1}}\right]^2 L_{d5}'\right)\left[\frac{N_{q1}}{N_{q5}}\right]i_{q5}'\left[\frac{N_{d1}}{N_{d5}}\right]i_{d5}' \\
+ 7\left(\left[\frac{N_{q7}}{N_{q1}}\right]^2 L_{q7}' - \left[\frac{N_{d7}}{N_{d1}}\right]^2 L_{d7}'\right)\left[\frac{N_{q1}}{N_{q7}}\right]i_{q7}'\left[\frac{N_{d1}}{N_{d7}}\right]i_{d7}' \\
+ 2\left[\frac{N_{q3}}{N_{q1}}\right]L_{13}'\left(i_{q1}\left[\frac{N_{d1}}{N_{d3}}\right]i_{d3}' - i_{d1}\left[\frac{N_{q1}}{N_{q3}}\right]i_{q3}'\right) + 6L_{15}\left(i_{q1}\left[\frac{N_{d1}}{N_{d5}}\right]i_{d5}' - i_{d1}i\left[\frac{N_{q1}}{N_{q5}}\right]i_{q5}'\right) \\
+ 6\left[\frac{N_{q7}}{N_{q1}}\right]L_{17}'\left(i_{q1}\left[\frac{N_{d1}}{N_{d7}}\right]i_{d7}' - i_{d1}\left[\frac{N_{q1}}{N_{q7}}\right]i_{q7}'\right) + \\
2\left[\frac{N_{q3}N_{q5}}{N_{q1}^{\ 2}}\right]L_{35}'\left(\left[\frac{N_{q1}}{N_{q3}}\right]i_{q3}'\left[\frac{N_{d1}}{N_{d5}}\right]i_{d5}' - \left[\frac{N_{d1}}{N_{d3}}\right]i_{d3}'\left[\frac{N_{q1}}{N_{q5}}\right]i_{q5}'\right) \\
+ 2\left[\frac{N_{q5}N_{q7}}{N_{q1}^{\ 2}}\right]L_{57}'\left(\left[\frac{N_{q1}}{N_{q5}}\right]i_{q5}'\left[\frac{N_{d1}}{N_{d7}}\right]i_{d7}' - \left[\frac{N_{q1}}{N_{q7}}\right]i_{q7}'i\left[\frac{N_{d1}}{N_{d5}}\right]i_{d5}'\right) \\
+ 10\left[\frac{N_{q3}N_{q7}}{N_{q1}^{\ 2}}\right]L_{37}'\left(\left[\frac{N_{q1}}{N_{q3}}\right]i_{q3}'\left[\frac{N_{d1}}{N_{d7}}\right]i_{d7}' - \left[\frac{N_{q1}}{N_{q7}}\right]i_{q7}'\left[\frac{N_{d1}}{N_{d3}}\right]i_{d3}'\right)] \\
+ \frac{9P}{4}[i_{q1}\lambda_{dm1} + 3\left[\frac{N_{q1}}{N_{q3}}\right]i_{q3}'\lambda_{dm3} + 5\left[\frac{N_{q1}}{N_{q5}}\right]i_{q5}'\lambda_{dm5} + 7\left[\frac{N_{q1}}{N_{q7}}\right]i_{q7}'\lambda_{dm7}]
\end{aligned}
\tag{4.92}
$$

Equation 4.92 gives the torque equation in terms of the transformed variables referred to the fundamental component of the stator harmonics. The corresponding turns transformations appear in this equation since the equation is taken as derived in Chapter 3. Using the set of Equations (4.89)-(4.90), the equivalent circuit is drawn to accommodate the referred quantities. Figure 4.61 depicts the q-axis equivalent with the inclusion of damper windings. Similarly, Figure 4.62 shows the d-axis equivalent of the system.

4.12 Simulation and Experimental Results

By using MATLAB/Simulink, the developed coupled model was simulated and the results are presented in this section. To validate the coupled circuit model, the computer simulation for the no-load generator mode of operation was undertaken in Figure 4.63.

Shown are the waveforms of the magnet flux density, induced voltage and the phase 'a' induced flux linkage. To validate the simulation results the IPM is run as a generator at no-load with a 115 V, 5hp dc motor acting as a prime mover.

The four induced voltages for stator phases 'A', 'B', 'C' and 'D' are shown in Figure 4.64 (a) and those of phases 'E', 'F', 'G' and 'H' are shown in Figure 4.64 (b) All the induced voltages are due to the presence of the permanent magnets buried in the rotor. The experimental waveforms of Figure 4.64 are in good agreement to the magnet induced voltage of phase 'A' shown in Figure 4.63.

In the computer simulation results, the IPM is run as motor at no-load for 0.5 seconds at which a load torque of 8 Nm is applied. The results for no-load characteristics are shown in Figures 4.65-4.74. Figure 4.65 shows the responses of the rotor speed and Figure 4.66 is the response for the electromagnetic torque. The phase 'a' and phase 'e' currents are shown in Figures 4.67 and 4.68, respectively. Out of the forty eight rotor bars for the damper winding only two (bars 1 and 14) are selected. The rotor bars 1 and 14 currents are shown in Figure 4.69 and 4.70, respectively. The changes of speed, torque, phase 'a' current and phase 'e' currents after applying load at 0.5 secs. are shown in Figures 4.71-4.74.

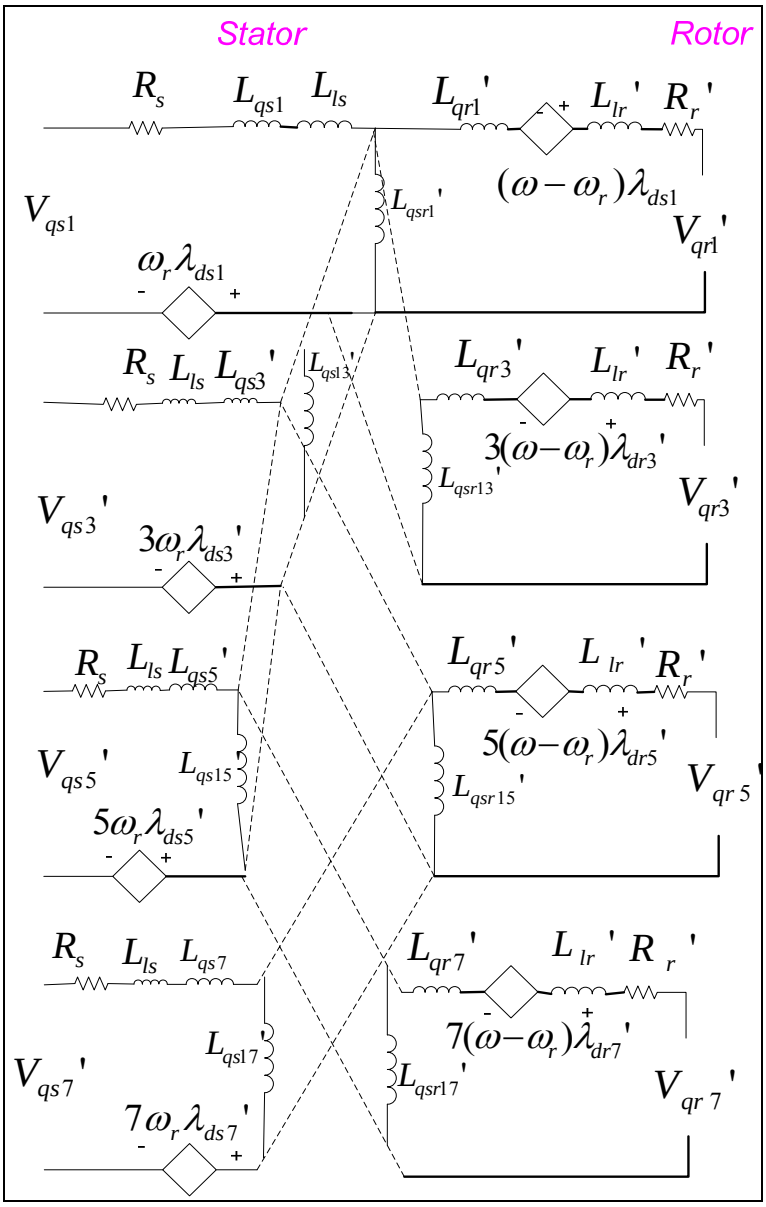

Figure 4.61 q-axis equivalent of the system

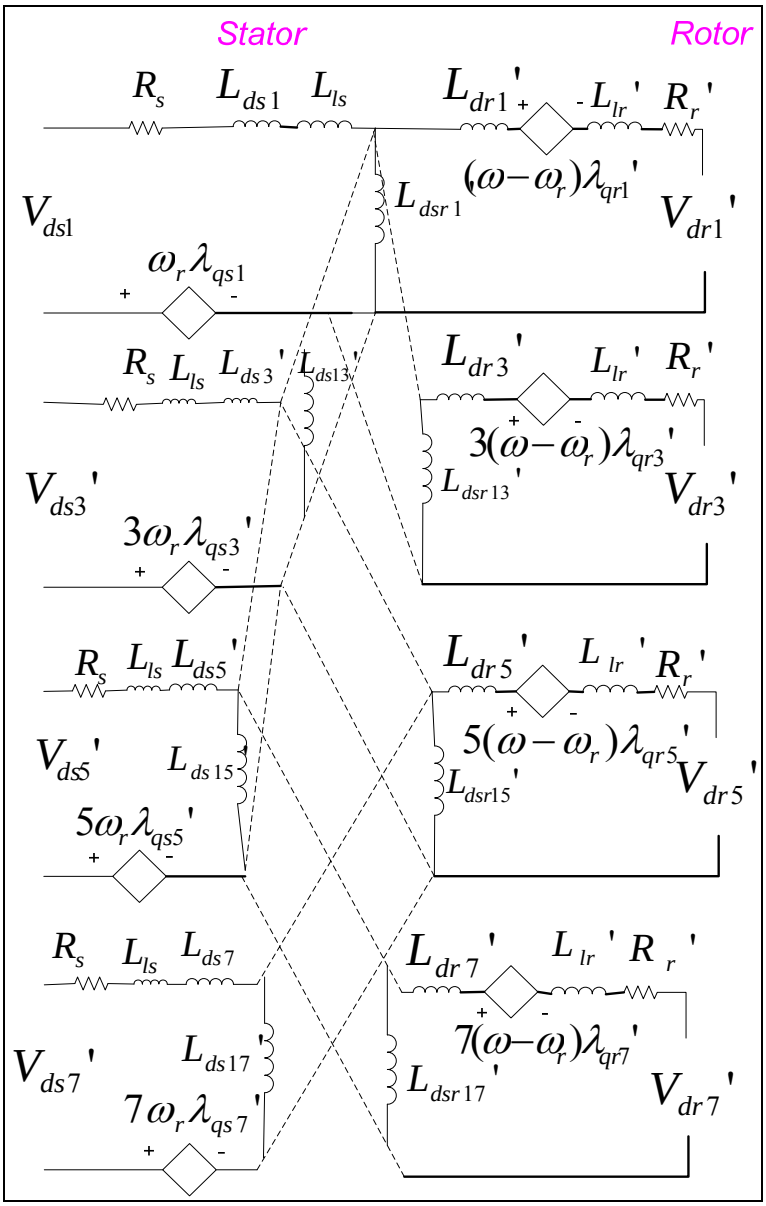

Figure 4.62 d-axis equivalent of the system

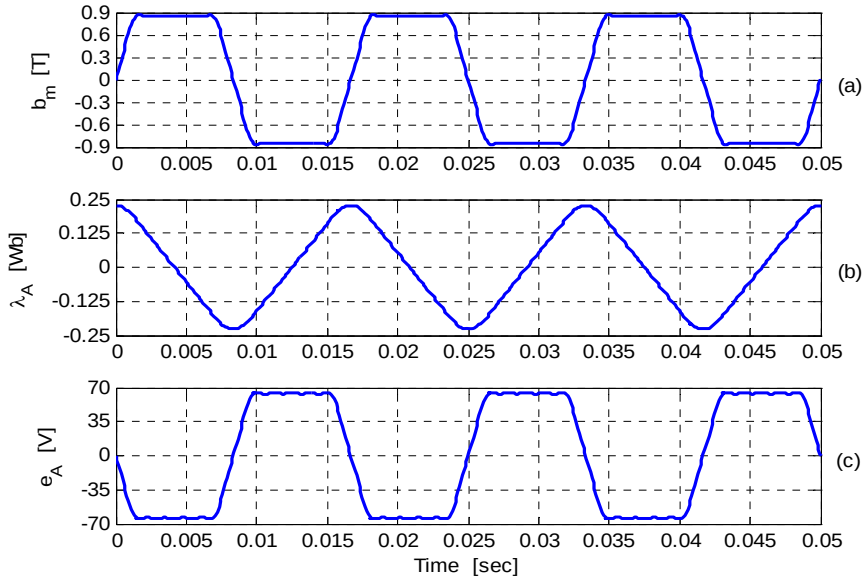

Figure 4.63 Model of the magnet flux density (a) trapezoidal magnet flux density (b) phase 'A' induced flux linkage and (c) phase 'A' induced voltage

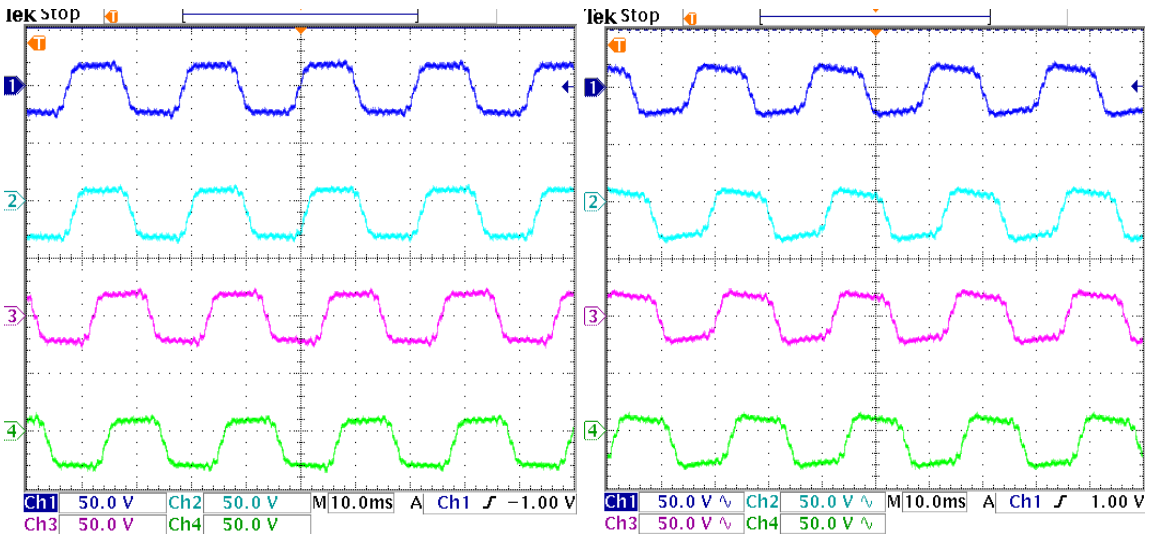

a. b.

Figure 4.64 Induced voltages for phases a. Phases A, B, C, D b. Phases E, F, G, H

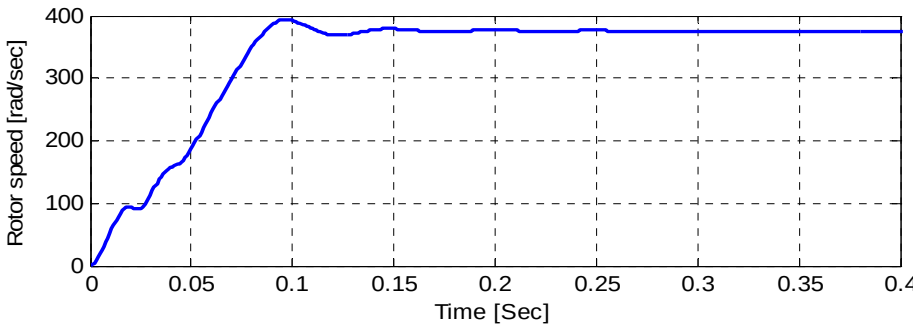

Figure 4.65 Plot of rotor speed vs time

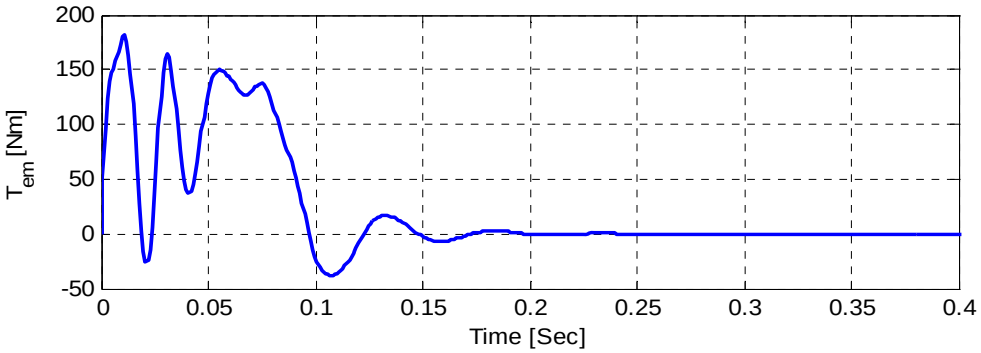

Figure 4.66 Plot of electromagnetic torque vs time

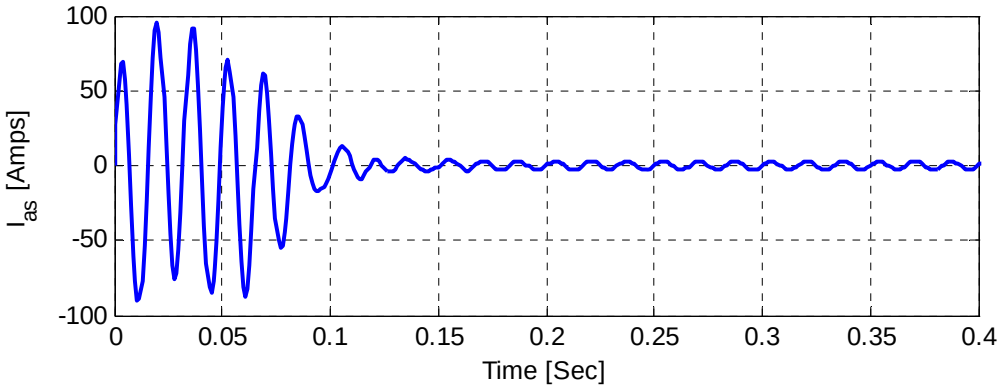

Figure 4.67 Plot of phase 'a' current vs. time

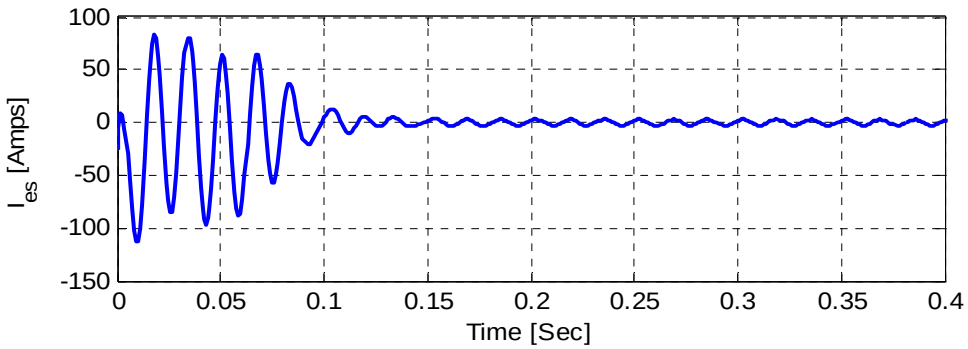

Figure 4.68 Plot of phase 'e' current vs. time

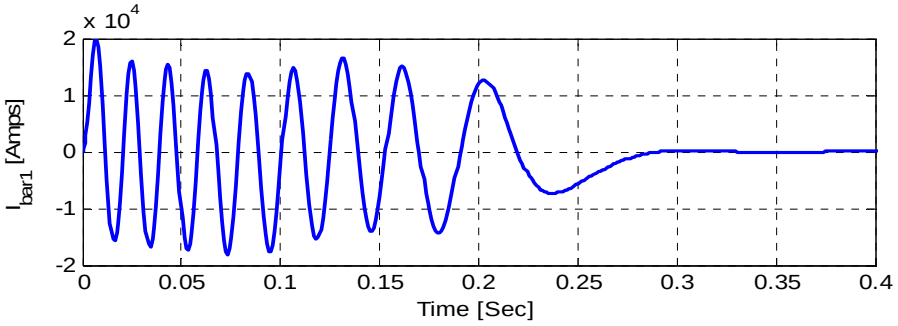

Figure 4.69 Plot of bar 1 current vs. Time

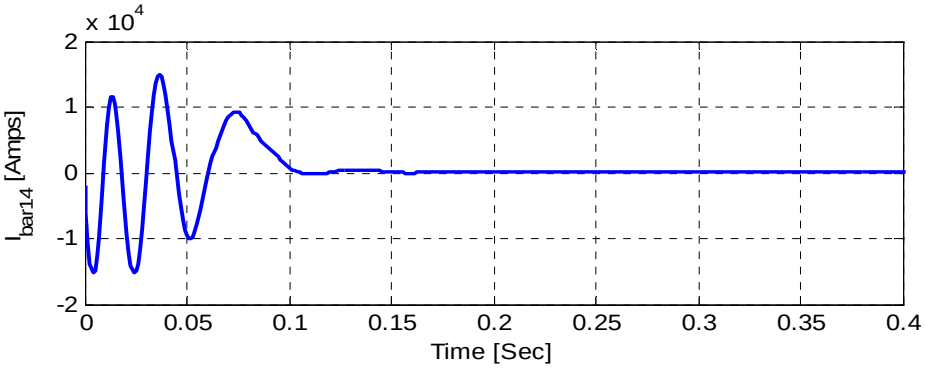

Figure 4.70 Plot of bar 14 current vs. time

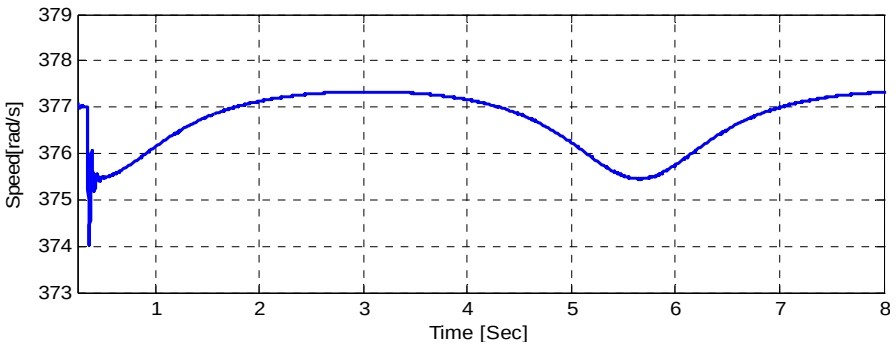

Figure 4.71 Change in speed after load is applied at 0.5 seconds

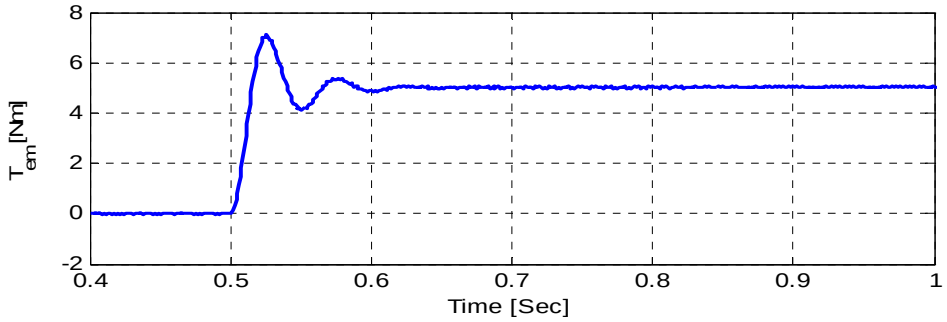

Figure 4.72. Change in electromagnetic torque after load is applied

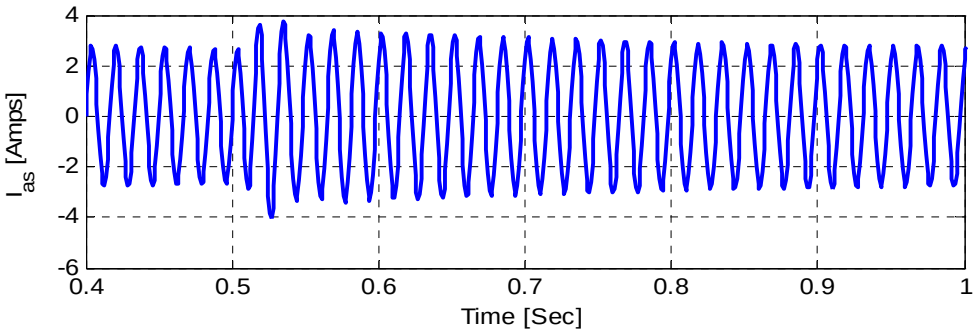

Figure 4.73 Change in phase ‘a’ current after load is applied

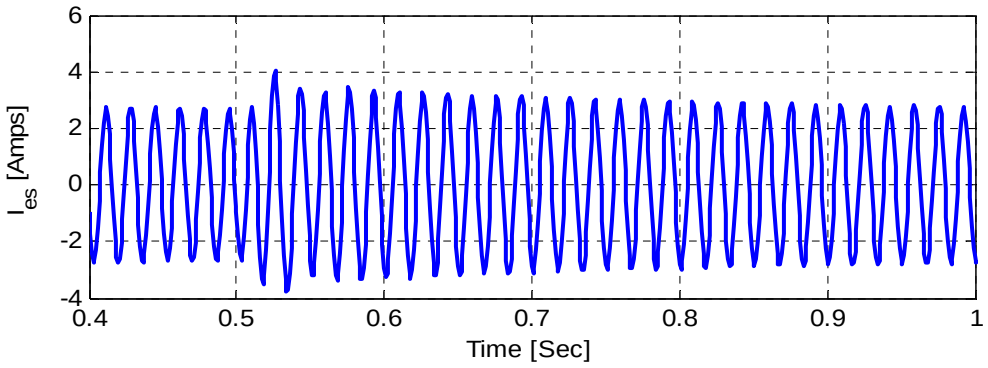

Figure 4.74 Change in phase ‘e’ current after load is applied

4.13 Conclusion

A new modeling technique for multiphase machine is introduced in this chapter where full order model of a 9-phase interior permanent magnet machine is performed graphically using the turn and winding functions of stator. Similarly, the expressions of the machine parameters with the inclusion of higher order harmonics as well as the stator induced voltages from the magnet flux density has been presented in this chapter. The full order coupled model includes the rotor damper windings in which each rotor circuit is considered individually. Simplified models yielding equivalent circuits are presented using the d and q axes winding functions of stator and rotor circuits. Similarly, with the trapezoidal approximation of the magnetic flux density of the permanent magnet, induced voltages are traced with reference frame transformations. The experimental waveforms of the induced voltage are found comparable to the magnet induced voltage of phase ‘A’ shown in Section 4.12. In the simulation results, it can be observed that the model behaves as expected whereby after the load of 8 Nm was applied the rotor speed dropped

momentarily and then returned back to the synchronous speed of 377 rad/s. The currents in the damper winding are also zero at steady-state condition.

CHAPTER 5

THREE MACHINE MODEL OF 9-PHASE IPM MACHINE USING FOURIER SERIES AND FULL ORDER MODEL

5.1 Introduction

The analysis and modeling of the 9-phase machine in previous chapter was performed under the assumption that all the phase of the machine were connected to 9-phase source. However, there is a possibility in case of 9-phase machine that, it can be visualized as a three machines out of which each are connected to 3-phase supply. This connection aids greatly for the fault tolerant and reliable operation of 9-phase machine. This section covers an analysis of such type of configuration of 9-phase machine, where 3-phases are taken to be separately connected to separate 3-phase sources. Firstly, the model equations are derived using the three machine configuration starting from the equations derived in Chapter 3 with the inclusion of magnet flux but excluding the damper bars. Secondly, the contribution of each machine towards the total torque is analyzed using the equivalent circuits. Lastly, full order coupled model is developed graphically with the help of turns and winding functions of the machine for three machine configurations including the damper bars.

5.2 Three Machine Configuration

Figure 5.1 shows the configuration used for the three machine analysis, where N denotes the neutral point of the three machines and a, b, c…i denotes the corresponding

phases of the machine. As observed in Figure 5.1, phases ‘a’, ‘d’ and ‘g’ are connected to a 3-phase source with neutral N_1. Similarly, phases ‘b’, ‘e’ and ‘h’ are connected to another 3-phase source with neutral N_2. Lastly, remaining phases ‘c’, ‘f’ and ‘i’ are also connected to 3rd 3-phase source with neutral point N_3. This configuration is given in tabular form in Table 5.1.

5.2.1 Derivation of Stator q and d Axis Inductances

The stator q and d axis inductances are derived in the three machine configuration in the similar way as described in Chapter 3. However, in this case, only 3-phase transformations are performed, hence no higher order harmonics exists. In order to adjust the transformation matrix, the corresponding phases of Machine I and Machine II are shifted by angle of $\beta = \frac{2\pi}{9}$, hence this effect needs to be included in transformation matrix. The same case is true in the derivation of transformation matrix for Machine III. Keeping these considerations in to account, the transformation matrices are given in Equations (5.1), (5.2) and (5.3), respectively for individual machines.

Machine I

$$T(\theta_1) = \begin{bmatrix} c(\theta+\theta_{01}) & c(\theta+\theta_{01}-\alpha_1) & c(\theta+\theta_{01}+\alpha_1) \\ s(\theta+\theta_{01}) & s(\theta+\theta_{01}-\alpha_1) & s(\theta+\theta_{01}+\alpha_1) \\ 1/2 & 1/2 & 1/2 \end{bmatrix}, \alpha_1 = \frac{2\pi}{3} \tag{5.1}$$

Machine II

$$T(\theta_2) = \begin{bmatrix} c(\theta+\theta_{02}-\beta) & c(\theta+\theta_{02}-\beta-\alpha_2) & c(\theta+\theta_{02}-\beta+\alpha_2) \\ s(\theta+\theta_{02}-\beta) & s(\theta+\theta_{02}-\beta-\alpha_2) & s(\theta+\theta_{02}-\beta+\alpha_2) \\ 1/2 & 1/2 & 1/2 \end{bmatrix}, \alpha_2 = \frac{2\pi}{3}, \beta = \frac{2\pi}{9} \tag{5.2}$$

Table 5.1 Three machine configuration of the machine for analysis

Phase number	Machine I	Machine II	Machine III
a	a_1		
b		a_2	
c			a_3
d	b_1		
e		b_2	
f			b_3
g	c_1		
h		c_2	
i			c_3

Machine III

$$T(\theta_3)=\begin{bmatrix} c(\theta+\theta_{03}-2\beta) & c(\theta+\theta_{03}-2\beta-\alpha_3) & c(\theta+\theta_{03}-2\beta+\alpha_3) \\ s(\theta+\theta_{03}-2\beta) & s(\theta+\theta_{03}-2\beta-\alpha_3) & s(\theta+\theta_{03}-2\beta+\alpha_3) \\ 1/2 & 1/2 & 1/2 \end{bmatrix}, \alpha_3=\frac{2\pi}{3}, \beta=\frac{2\pi}{9} \tag{5.3}$$

where, θ_{01}, θ_{02} and θ_{03} represent the initial rotor angle for corresponding machine configurations.

In derivations of the q-d inductances, the real variable inductance matrix derived in Table 3.1 is used with the exclusion of higher order harmonics. The reason not to include the higher order harmonics is due to the fact that they will be cancelled as transformation matrix is only of 3-phase. Proceeding the same way of derivation, the q and d inductance matrix elements for each of the machine configurations are derived.

The inductance matrix for Machine I can be given as

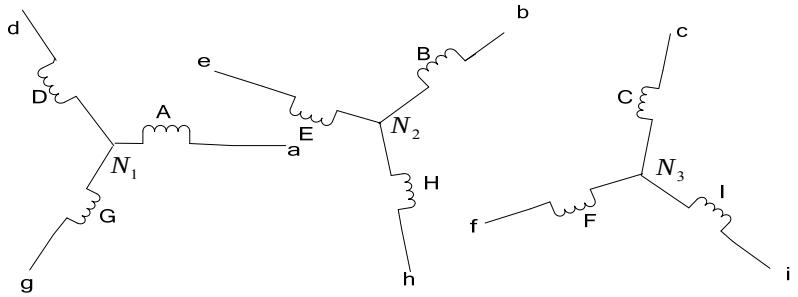

Figure 5.1 Three sets of 3-phase configuration for 9-phase machine

$$L_{q1} = \begin{bmatrix} L_{q11} & L_{d11} & L_{011} \\ L_{q12} & L_{d12} & L_{012} \\ L_{q13} & L_{d13} & L_{013} \end{bmatrix} \tag{5.4}$$

where, L_{q11} defines the q-axis self-inductance of the Machine I and L_{d11} defines the d-axis self-inductance of Machine I. Similarly L_{q12} and L_{d12} defines the q and d axis mutual inductances between Machine I and Machine II, respectively. After the evaluation of the inductances, each element of the matrix of Equation (5.4) are derived as follows:

$$L_{q11} = k[\frac{3}{2}\pi {N_1}^2 a_0 + \frac{3}{2}\frac{\pi {N_1}^2 a_1}{2}\cos(2\theta_{01})] + L_{ls} \tag{5.5}$$

$$L_{d11} = k[\frac{3}{2}\pi {N_1}^2 a_0 - \frac{3}{2}\frac{\pi {N_1}^2 a_1}{2}\cos(2\theta_{01})] + L_{ls} \tag{5.6}$$

$$L_{011} = L_{ls} \tag{5.7}$$

$$L_{q12} = k[\frac{3}{2}\pi {N_1}^2 a_0 \cos(\theta_{01} - \theta_{02}) + \frac{3}{2}\frac{\pi {N_1}^2 a_1}{2}\cos(\theta_{01} + \theta_{02})] \tag{5.8}$$

$$L_{d12} = k[\frac{3}{2}\pi {N_1}^2 a_0 \cos(\theta_{01} - \theta_{02}) - \frac{3}{2}\frac{\pi {N_1}^2 a_1}{2}\cos(\theta_{01} + \theta_{02})] \tag{5.9}$$

$$L_{012} = 0 \tag{5.10}$$

$$L_{q13} = k[\frac{3}{2}\pi N_1^{\,2} a_0 \cos(\theta_{01} - \theta_{03}) + \frac{3}{2}\frac{\pi N_1^{\,2} a_1}{2}\cos(\theta_{01} + \theta_{03})] \tag{5.11}$$

$$L_{d13} = k[\frac{3}{2}\pi N_1^{\,2} a_0 \cos(\theta_{01} - \theta_{03}) - \frac{3}{2}\frac{\pi N_1^{\,2} a_1}{2}\cos(\theta_{01} + \theta_{03})] \tag{5.12}$$

$$L_{013} = 0 \tag{5.13}$$

where, $k = \frac{\mu_0 rl}{4}$

Similar equations also exist for Machine II. Proceeding the same way as Machine I, the self and mutual inductance of Machine II and Machine III are derived as

$$L_{q22} = k[\frac{3}{2}\pi N_1^{\,2} a_0 + \frac{3}{2}\frac{\pi N_1^{\,2} a_1}{2}\cos(2\theta_{02})] + L_{ls} \tag{5.14}$$

$$L_{d22} = k[\frac{3}{2}\pi N_1^{\,2} a_0 - \frac{3}{2}\frac{\pi N_1^{\,2} a_1}{2}\cos(2\theta_{02})] + L_{ls} \tag{5.15}$$

$$L_{022} = L_{ls} \tag{5.16}$$

$$L_{q23} = k[\frac{3}{2}\pi N_1^{\,2} a_0 \cos(\theta_{02} - \theta_{03}) + \frac{3}{2}\frac{\pi N_1^{\,2} a_1}{2}\cos(\theta_{02} + \theta_{03})] \tag{5.17}$$

$$L_{d23} = k[\frac{3}{2}\pi N_1^{\,2} a_0 \cos(\theta_{02} - \theta_{03}) - \frac{3}{2}\frac{\pi N_1^{\,2} a_1}{2}\cos(\theta_{02} + \theta_{03})] \tag{5.18}$$

$$L_{023} = 0 \tag{5.19}$$

$$L_{q33} = k[\frac{3}{2}\pi N_1^{\,2} a_0 + \frac{3}{2}\frac{\pi N_1^{\,2} a_1}{2}\cos(2\theta_{03})] + L_{ls} \tag{5.20}$$

$$L_{d33} = k[\frac{3}{2}\pi N_1^{\,2} a_0 - \frac{3}{2}\frac{\pi N_1^{\,2} a_1}{2}\cos(2\theta_{03})] + L_{ls} \tag{5.21}$$

$$L_{033} = L_{ls} \tag{5.22}$$

Equations (5.5)-(5.22) give an idea about the inductance matrix that comes into play when the three machine arrangement is considered in the 9-phase IPM machine.

Similarly, these equations also demonstrate that the self and mutual inductances are the functions of initial rotor angles. For the simplicity of analysis, assuming that the initial rotor angle is zero and proceed with the derivation

If $\theta_{01} = \theta_{02} = \theta_{03} = 0$, Equations (5.5) to (5.22) turns into

$$L_{q11} = k[\frac{3}{2}\pi N_1^{\,2} a_0 + \frac{3}{2}\frac{\pi N_1^{\,2} a_1}{2}] + L_{ls} \tag{5.23}$$

$$L_{d11} = k[\frac{3}{2}\pi N_1^{\,2} a_0 - \frac{3}{2}\frac{\pi N_1^{\,2} a_1}{2}] + L_{ls} \tag{5.24}$$

$$L_{011} = L_{ls} \tag{5.25}$$

$$L_{q12} = k[\frac{3}{2}\pi N_1^{\,2} a_0 + \frac{3}{2}\frac{\pi N_1^{\,2} a_1}{2}] \tag{5.26}$$

$$L_{d12} = k[\frac{3}{2}\pi N_1^{\,2} a_0 - \frac{3}{2}\frac{\pi N_1^{\,2} a_1}{2}] \tag{5.27}$$

$$L_{012} = 0 \tag{5.28}$$

$$L_{q13} = k[\frac{3}{2}\pi N_1^{\,2} a_0 + \frac{3}{2}\frac{\pi N_1^{\,2} a_1}{2}] \tag{5.29}$$

$$L_{d13} = k[\frac{3}{2}\pi N_1^{\,2} a_0 - \frac{3}{2}\frac{\pi N_1^{\,2} a_1}{2}] \tag{5.30}$$

$$L_{013} = 0 \tag{5.31}$$

$$L_{q22} = k[\frac{3}{2}\pi N_1^{\,2} a_0 + \frac{3}{2}\frac{\pi N_1^{\,2} a_1}{2}] + L_{ls} \tag{5.32}$$

$$L_{d22} = k[\frac{3}{2}\pi N_1^{\,2} a_0 - \frac{3}{2}\frac{\pi N_1^{\,2} a_1}{2}] + L_{ls} \tag{5.33}$$

$$L_{022} = L_{ls} \tag{5.34}$$

$$L_{q23} = k[\frac{3}{2}\pi N_1^{\,2} a_0 + \frac{3}{2}\frac{\pi N_1^{\,2} a_1}{2}] \tag{5.35}$$

$$L_{d23} = k[\pi N_1{}^2 a_0 - \frac{3}{2}\frac{\pi N_1{}^2 a_1}{2}] \tag{5.36}$$

$$L_{023} = 0 \tag{5.37}$$

$$L_{q33} = k[\frac{3}{2}\pi N_1{}^2 a_0 + \frac{3}{2}\frac{\pi N_1{}^2 a_1}{2}] + L_{ls} \tag{5.38}$$

$$L_{d33} = k[\frac{3}{2}\pi N_1{}^2 a_0 - \frac{3}{2}\frac{\pi N_1{}^2 a_1}{2}] + L_{ls} \tag{5.39}$$

$$L_{033} = L_{ls} \tag{5.40}$$

Equations (5.23)-(5.40) also signify an interesting observation that if the zero initial case is assumed, the self and mutual inductances gives the same equations except the leakage terms that comes in effect in case of the self-inductances.

5.2.2 Flux Due to Permanent Magnets

Using the same concept of transformations as derived in Section 5.2.1, the flux due to permanent magnet on each machine can be evaluated. The flux due to permanent magnets is derived as follows with the inclusion of the initial angles:

$$\lambda_{d1m} = \frac{3}{2}\pi B_1 N_1 \cos(\theta_{01}) \tag{5.41}$$

$$\lambda_{q1m} = 0 \tag{5.42}$$

$$\lambda_{01m} = 0 \tag{5.43}$$

$$\lambda_{d2m} = \frac{3}{2}\pi B_1 N_1 \cos(\theta_{02}) \tag{5.44}$$

$$\lambda_{02m} = 0 \tag{5.45}$$

$$\lambda_{d3m} = \frac{3}{2}\pi B_1 N_1 \cos(\theta_{03}) \tag{5.46}$$

$$\lambda_{q3m} = 0 \tag{5.47}$$

$$\lambda_{03m} = 0 \tag{5.48}$$

$$\lambda_{d1m} = \frac{3}{2}\pi B_1 N_1 \tag{5.49}$$

$$\lambda_{q1m} = 0 \tag{5.50}$$

$$\lambda_{01m} = 0 \tag{5.51}$$

$$\lambda_{d2m} = \frac{3}{2}\pi B_1 N_1 \tag{5.52}$$

$$\lambda_{q2m} = 0 \tag{5.53}$$

$$\lambda_{02m} = 0 \tag{5.54}$$

$$\lambda_{d3m} = \frac{3}{2}\pi B_1 N_1 \tag{5.55}$$

$$\lambda_{q3m} = 0 \tag{5.56}$$

$$\lambda_{03m} = 0 \tag{5.57}$$

5.2.3 Voltage and Flux Equations for Each Machine

After the derivation of corresponding inductance and permanent magnet flux, the analysis is performed for voltage and flux equations of each machine. Keeping the same stator resistance in each case and ω as the frequency of fundamental component, the voltage and flux equations for each machine configurations are given as

Machine I

$$V_{q1} = r_s i_{q11} + p\lambda_{q1} + \omega\lambda_{d1}$$

$$V_{d1} = r_s i_{d11} + p\lambda_{d1} - \omega\lambda_{q1} \tag{5.58}$$

$$V_{01} = r_s i_{011} + p\lambda_{01}$$

$$\lambda_{q1} = L_{q11} i_{q11} + L_{q12} i_{q22} + L_{q13} i_{q33}$$

$$\lambda_{d1} = L_{d11} i_{d11} + L_{d12} i_{d22} + L_{d13} i_{d13} \tag{5.59}$$

$$\lambda_{01} = L_{011} i_{011}$$

Machine II

$$V_{q2} = r_s i_{q22} + p\lambda_{q2} + \omega\lambda_{d2}$$

$$V_{d2} = r_s i_{d22} + p\lambda_{d2} - \omega\lambda_{q2} \tag{5.60}$$

$$V_{02} = r_s i_{022} + p\lambda_{02}$$

$$\lambda_{q2} = L_{q12} i_{q11} + L_{q22} i_{q22} + L_{q23} i_{q33}$$

$$\lambda_{d2} = L_{d12} i_{d11} + L_{d22} i_{d22} + L_{d13} i_{d33} \tag{5.61}$$

$$\lambda_{02} = L_{022} i_{022}$$

Machine III

$$V_{q3} = r_s i_{q33} + p\lambda_{q3} + \omega\lambda_{d3}$$

$$V_{d3} = r_s i_{d33} + p\lambda_{d3} - \omega\lambda_{q3} \tag{5.62}$$

$$V_{03} = r_s i_{033} + p\lambda_{03}$$

$$\lambda_{q3} = L_{q13} i_{q13} + L_{q23} i_{q22} + L_{q33} i_{q33}$$

$$\lambda_{d3} = L_{d13} i_{d11} + L_{d23} i_{d22} + L_{d33} i_{d33} \tag{5.63}$$

$$\lambda_{03} = L_{033} i_{033}$$

5.2.4 Torque Equations for Each Machine

After the derivation of flux and voltage equations for each machine configurations, the next step is the derivation of torque. Similar to the case derived before, the electromagnetic torque is derived from the concept of co-energy. In the resulting magnetic circuit, the co-energy stored is given in terms of stator current and magnet flux as

$$W_{co} = \frac{1}{2} I_s{}^t L_{ss} I_s + I_s{}^t \lambda_m \tag{5.64}$$

The electromagnetic torque,

$$T_e = \frac{\partial W_{co}}{\partial \theta_{rm}} \tag{5.65}$$

Taking the partial derivative of equation of co-energy,

$$T_e = \frac{1}{2} I_s{}^t \frac{\partial L_{ss}}{\partial \theta_{rm}} I_s + I_s{}^t \frac{\partial \lambda_m}{\partial \theta_{rm}} \tag{5.66}$$

Since, $\theta_r = \frac{P}{2} \theta_{rm}$

$$T_e = \frac{P}{2} \frac{1}{2} I_s{}^t \frac{\partial L_{ss}}{\partial \theta_r} I_s + \frac{P}{2} I_s{}^t \frac{\partial \lambda_m}{\partial \theta_r} \tag{5.67}$$

Applying transformation to the above equation,

$$T_e = \frac{P}{2} \frac{1}{2} \left[T(\theta)^{-1} I_{qdos} \right]^t \frac{\partial L_{ss}}{\partial \theta_r} T(\theta)^{-1} I_{qdos} + \frac{P}{2} \left[T(\theta)^{-1} I_{qdos} \right]^t \frac{\partial \lambda_m}{\partial \theta_r} \tag{5.68}$$

As observed from Equations (5.23)-(5.40), there is the existence of self-machine inductance as well as mutual machine inductances. This also gives rise to the self-machine torque and mutual machine torque since each of the inductance contributes to

the torque positively. For the analysis, self and mutual torque of each machine configuration is derived separately with the help of the inductance matrix derived in Table 3.1, permanent magnet flux and transformation matrix. The electromagnetic-torque of each machine utilizing this concept can be given as

Machine I

$$T_{e1} = \frac{3P}{4}\frac{1}{2}[I_{q1d101}]^t T(\theta_1)\frac{\partial L_{ss}}{\partial \theta_r}T(\theta_1)^{-1}\left[I_{q1d1o1}\right] \tag{5.69}$$

$$= \frac{3P}{4}[(L_{q11} - L_{d11})i_{q11}i_{d11}] \tag{5.70}$$

Machine II

$$T_{e2} = \frac{3P}{4}\frac{1}{2}[I_{q2d202}]^t T(\theta_2)\frac{\partial L_{ss}}{\partial \theta_r}T(\theta_2)^{-1}\left[I_{q2d2o2}\right] \tag{5.71}$$

$$= \frac{3P}{4}[(L_{q22} - L_{d22})i_{q22}i_{d22}] \tag{5.72}$$

Machine III

$$T_{e3} = \frac{3P}{4}\frac{1}{2}[I_{q3d3o3}]^t T(\theta_3)\frac{\partial L_{ss}}{\partial \theta_r}T(\theta_3)^{-1}\left[I_{q3d3o3}\right] \tag{5.73}$$

$$= \frac{3P}{4}[(L_{q33} - L_{d33})i_{q33}i_{d33}] \tag{5.74}$$

Similarly, due to the existence of the mutual inductance terms, the mutual torques of the machines is also derived as

Machine I and Machine II:

$$T_{e12} = \frac{3P}{4}\frac{1}{2}[I_{q1d1o1}]^t T(\theta_1)\frac{\partial L_{ss}}{\partial \theta_r}T(\theta_2)^{-1}\left[I_{q2d2o2}\right] \tag{5.75}$$

$$= \frac{3P}{4}[(L_{q12} - L_{d12})(i_{q11}i_{d22} + i_{d11}i_{q22})] \tag{5.76}$$

Machine I and Machine III:

$$T_{e13} = \frac{3P}{4}\frac{1}{2}[I_{q1d1o1}]^t T(\theta_1)\frac{\partial L_{ss}}{\partial \theta_r}T(\theta_3)^{-1}\left[I_{q3d3o3}\right] \tag{5.77}$$

$$= \frac{3P}{4}[(L_{q13} - L_{d13})(i_{q11}i_{d33} + i_{d11}i_{q33})] \tag{5.78}$$

Machine II and Machine III:

$$T_{e23} = \frac{3P}{4}\frac{1}{2}[I_{q2d2o2}]^t T(\theta_2)\frac{\partial L_{ss}}{\partial \theta_r}T(\theta_3)^{-1}\left[I_{q3d3o3}\right] \tag{5.79}$$

$$= \frac{3P}{4}[(L_{q23} - L_{d23})(i_{q22}i_{d33} + i_{d22}i_{q33})] \tag{5.80}$$

Finally, the torque is obtained considering the induced magnetic flux due to magnet in each machine configurations.

Machine I and magnet:

$$T_{e1m} = \frac{3}{2}\frac{P}{2}\left[I_{q1d1o1}\right]^t T(\theta_1)\frac{\partial \lambda_m}{\partial \theta_r} \tag{5.81}$$

$$= \frac{3P}{4}\lambda_{d1m}i_{q11} \tag{5.82}$$

Machine II and magnet:

$$T_{e2m} = \frac{3}{2}\frac{P}{2}\left[I_{q2d2o2}\right]^t T(\theta_2)\frac{\partial \lambda_m}{\partial \theta_r} \tag{5.83}$$

$$= \frac{3P}{4}\lambda_{d2m}i_{q22} \tag{5.84}$$

Machine III and magnet:

$$T_{e3m} = \frac{3}{2}\frac{P}{2}\left[I_{q3d3o3}\right]^t T(\theta_3)\frac{\partial \lambda_m}{\partial \theta_r} \tag{5.85}$$

$$= \frac{3P}{4}\lambda_{d3m}i_{q33} \tag{5.86}$$

Now, the total torque is obtained by summation of the individual machine torques and torque due to magnet in each configuration. The final expression for torque is given as

$$\begin{aligned} T_e = \frac{3P}{4}[&(L_{q11}-L_{d11})i_{q11}i_{d11}+(L_{q22}-L_{d22})i_{q22}i_{d22}+(L_{q33}-L_{d33})i_{q33}i_{d33} \\ &+(L_{q12}-L_{d12})(i_{q11}i_{d22}+i_{d11}i_{q22})+(L_{q13}-L_{d13})(i_{q11}i_{d33}+i_{d11}i_{q33}) \\ &++(L_{q23}-L_{d23})(i_{q22}i_{d33}+i_{d22}i_{q33})+\lambda_{d1m}i_{q11}+\lambda_{d2m}i_{q22}+\lambda_{d3m}i_{q33}] \end{aligned} \tag{5.87}$$

Equation (5.87) gives an interesting observation while dealing with the three machine configuration of 9-phase IPM machine. The total torque is summation of individual contribution of each machine, magnets and also due to the mutual interaction between each machine sets. The contribution of particular machine sets to resultant torque can be calculated using the Equations (5.69)-(5.86). It gives the individual contribution towards the total torque when any one of the machine is out of operation.

5.2.5 Equivalent Circuit of the Three Machine Configuration

The equations derived from (5.43) to (5.45) are now utilized in order to derive the equivalent circuit of the machine when operated as three machine configuration. The difference of the equivalent circuit going to be derived from that of the previous chapter is that the source is now reduced to 3-phase compared to 9-phase. Hence, q-d voltage will also be reduced to three to represent each machine configurations. Figure 5.2 shows the equivalent circuit of three machines for the q-axis. Similarly, Figure 5.3 shows the circuit for the d-axis and Figure 5.4 shows the circuit for zero sequence.

In this way, the derivation of the equivalent circuit is performed by taking three machine configuration of the 9-phase machine. This configuration is useful in the case of

operation and control of the machine when there is the availability of three phase inverters only. Comparing to the calculation steps with Chapter 3, it is seen they are highly reduced using three phase analysis. However, there is the demerit of operation in this configuration as the higher order harmonics are not considered in the analysis which implies that the torque improvement is not achievable.

5.3 Full Model of Three Machine Configuration of 9-Phase IPM Machine with Damper Windings

In this section, the full order modeling of the three machine configuration is set forth using the basic equations for winding functions, inductances and flux linkages. This section is similar to the method introduced in Chapter 3, however, q-d stator winding functions are evaluated in stationary reference frame for all machines using respective 3-phase transformation matrix. Secondly, the stationary reference frame transformation is extended to the rotor bars to evaluate the q and d winding functions.

Thirdly, self and mutual inductances of stator and rotor circuits are evaluated graphically with the assumption of coupled circuit model of the machine. Finally, with the help of permanent magnet flux density waveforms, the induced voltage of the machine is evaluated graphically.

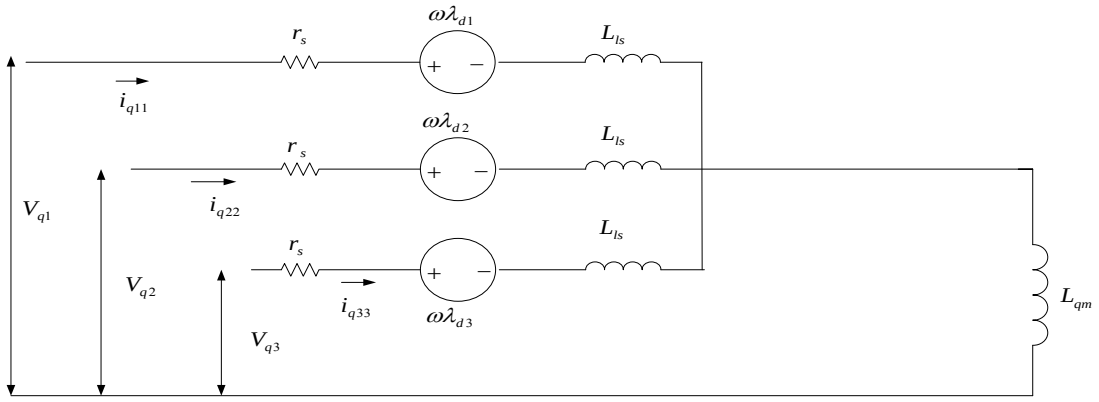

Figure 5.2 Positive sequence model for three machines.

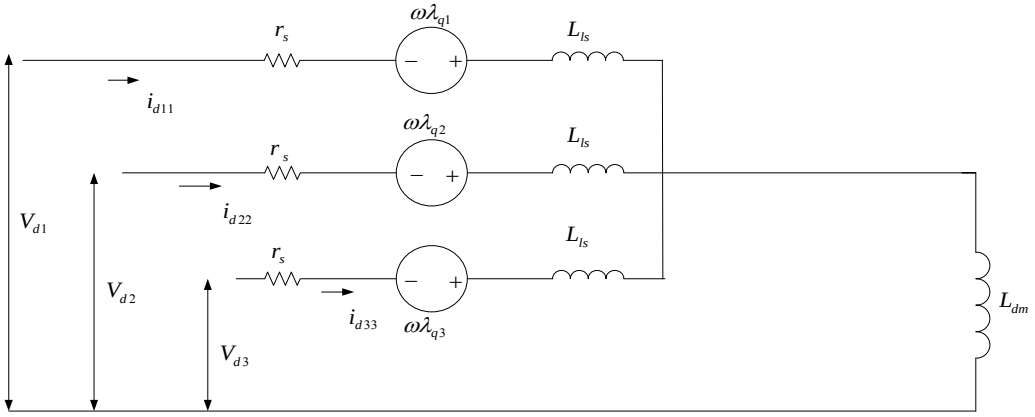

Figure 5.3 Negative sequence model for three machine configuration

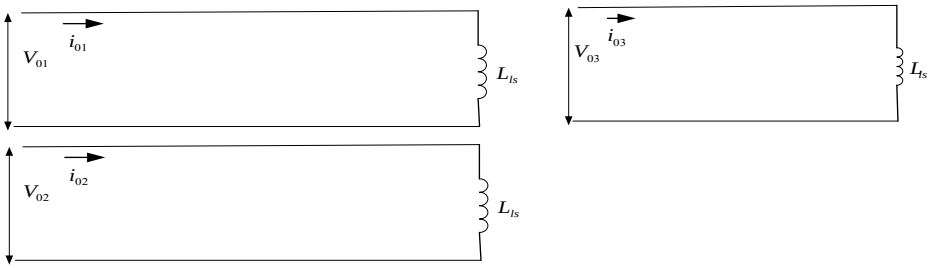

Figure 5.4 Zero sequence model for three machine configuration

The major advantage of this method is that the complexity of long and rigorous mathematical manipulations are reduced significantly as graphical approach is performed and there is no need of calculation of all phase inductances as done in Chapter 3.

5.3.1 Stator Clock Diagram, Turn and Winding Functions

The stator clock diagram, turn and winding functions are similar as derived in Chapter 3. However, in this case, the Machine I comprise phases a,d and g. Similarly, Machine II is made of phases b, e and h and Machine III consists of phases c, f and i. Hence, these are to be taken into account while dealing with the transformations.

5.3.2 Stationary Reference Frame Transformation of Turn and Winding Functions

In this section, the stationary reference frame transformation of the winding functions is discussed. The transformation matrix is same as discussed in previous sections for all machines.

Machine I:

$$T(\theta_1)=\begin{bmatrix} c(\theta+\theta_{01}) & c(\theta+\theta_{01}-\alpha_1) & c(\theta+\theta_{01}+\alpha_1) \\ s(\theta+\theta_{01}) & s(\theta+\theta_{01}-\alpha_1) & s(\theta+\theta_{01}+\alpha_1) \\ 1/2 & 1/2 & 1/2 \end{bmatrix}, \alpha_1=\frac{2\pi}{3} \tag{5.88}$$

Machine II:

$$T(\theta_2)=\begin{bmatrix} c(\theta+\theta_{02}-\beta) & c(\theta+\theta_{02}-\beta-\alpha_2) & c(\theta+\theta_{02}-\beta+\alpha_2) \\ s(\theta+\theta_{02}-\beta) & s(\theta+\theta_{02}-\beta-\alpha_2) & s(\theta+\theta_{02}-\beta+\alpha_2) \\ 1/2 & 1/2 & 1/2 \end{bmatrix}, \alpha_2=\frac{2\pi}{3}, \beta=\frac{2\pi}{9} \tag{5.89}$$

Machine III:

$$T(\theta_3)=\begin{bmatrix} c(\theta+\theta_{03}-2\beta) & c(\theta+\theta_{03}-2\beta-\alpha_3) & c(\theta+\theta_{03}-2\beta+\alpha_3) \\ s(\theta+\theta_{03}-2\beta) & s(\theta+\theta_{03}-2\beta-\alpha_3) & s(\theta+\theta_{03}-2\beta+\alpha_3) \\ 1/2 & 1/2 & 1/2 \end{bmatrix}, \alpha_3=\frac{2\pi}{3}, \beta=\frac{2\pi}{9} \tag{5.90}$$

However, in this analysis, the initial angle is taken to be zero. For the stationary reference frame transformation, the stator winding functions are given in corresponding figures. Figure 5.5 and 5.6 show the q and d-axis stator winding function for Machine I. Similarly, Figure 5.7 and 5.8 show the q and d-axis stator winding function for Machine II. For Machine III, the q and d-axis winding function are given in Figures 5.9 and 5.10. Finally, Figures 5.11, 5.12 and 5.13 show the zero sequence winding functions for corresponding three machines.

5.3.3 Derivation of Rotor Turn and Winding Functions

The rotor winding function is derived in previous chapter and the plot of the winding function for 48 number of bars with rotor angle is given in Figure 5.14.

5.3.4 Stationary Reference Transformation of Rotor Winding Function

In this section, the stationary reference frame transformation of the rotor winding functions is derived using the 3-phase transformation matrix. Figures 5.15, 5.16 and 5.17,

respectively show the q-axis, d-axis and zero-axis winding function with the change of spatial angle of rotor.

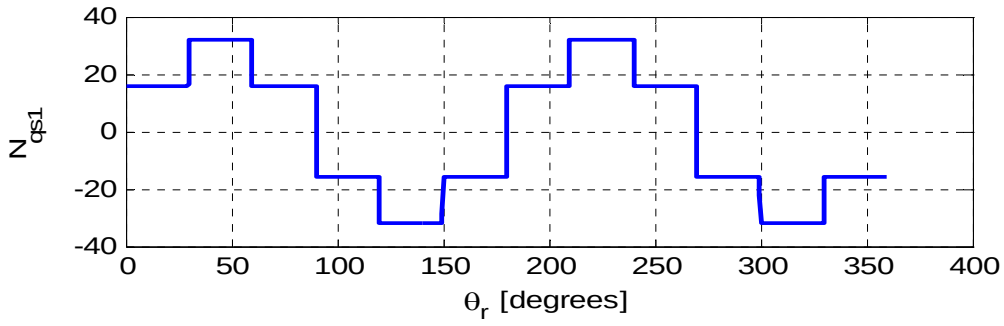

Figure 5.5 q-axis stator winding function for Machine I

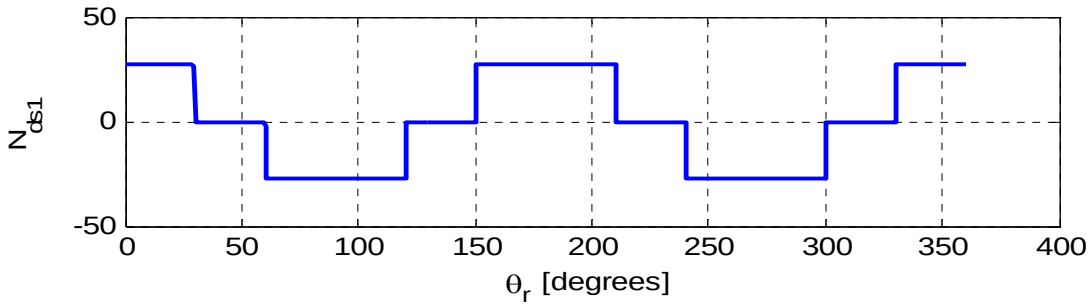

Figure 5.6 d-axis stator winding function for Machine I

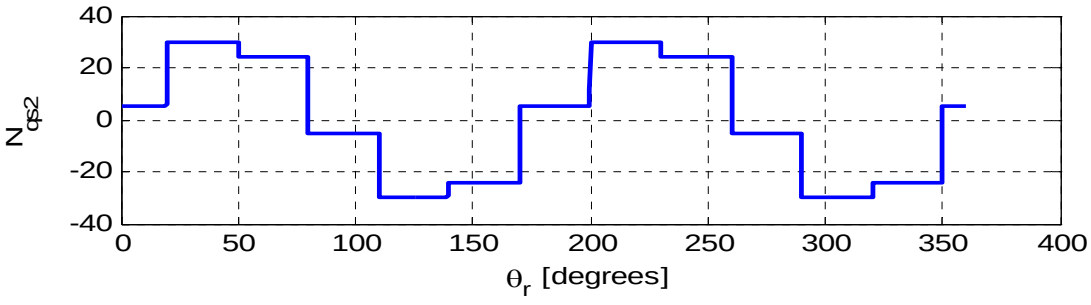

Figure 5.7 q-axis stator winding function for Machine II

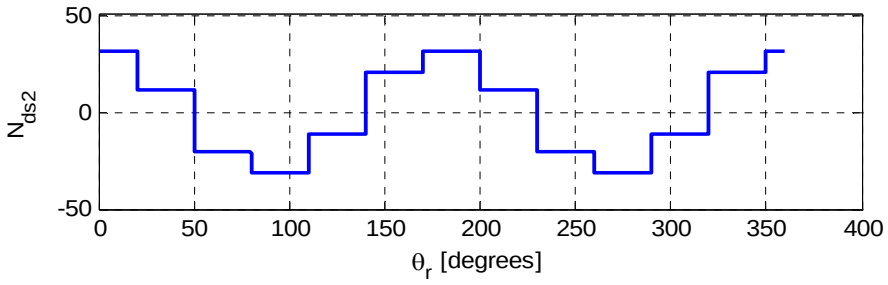

Figure 5.8 d-axis stator winding function for Machine II

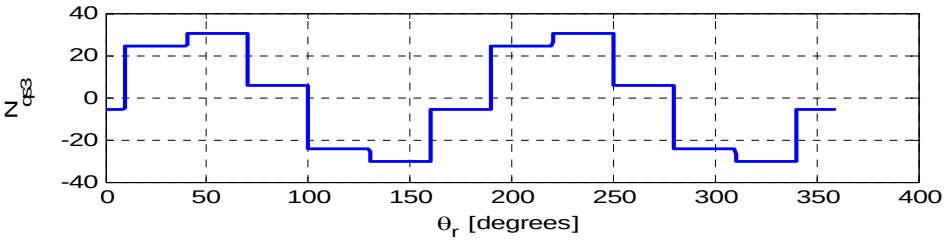

Figure 5.9 q-axis stator winding function for Machine III

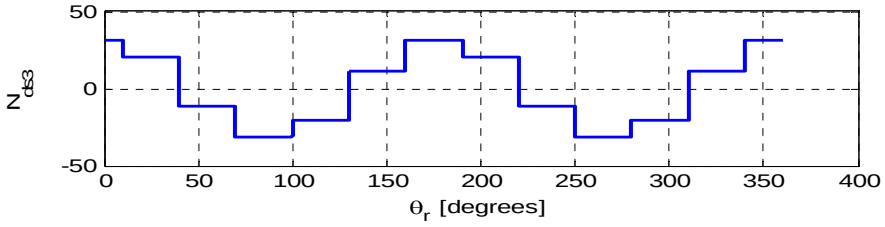

Figure 5.10 d-axis stator winding function for Machine III

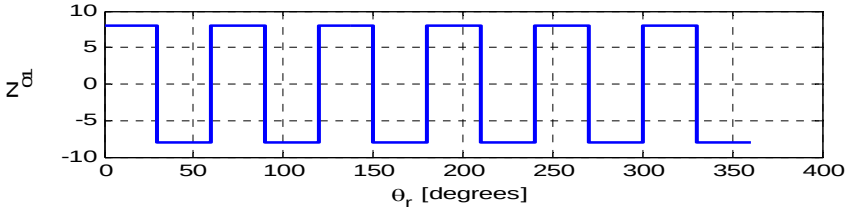

Figure 5.11 Zero-axis stator winding function for Machine I

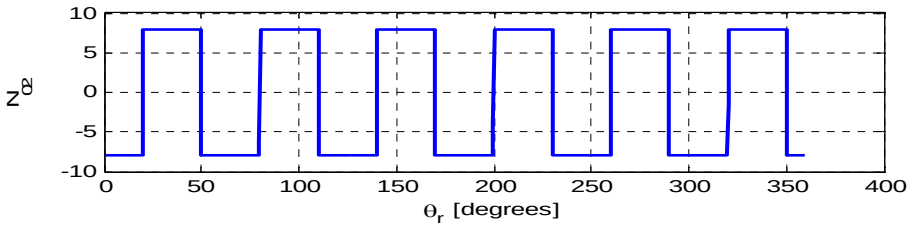

Figure 5.12 Zero-axis stator winding function for Machine II

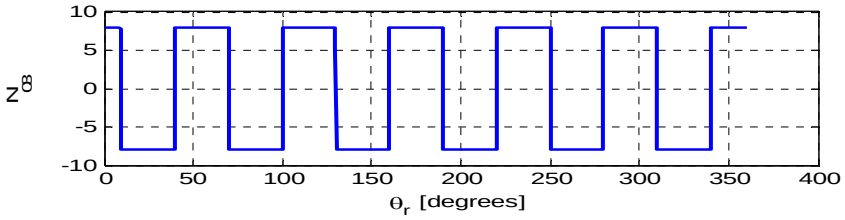

Figure 5.13 Zero-axis stator winding function for Machine III

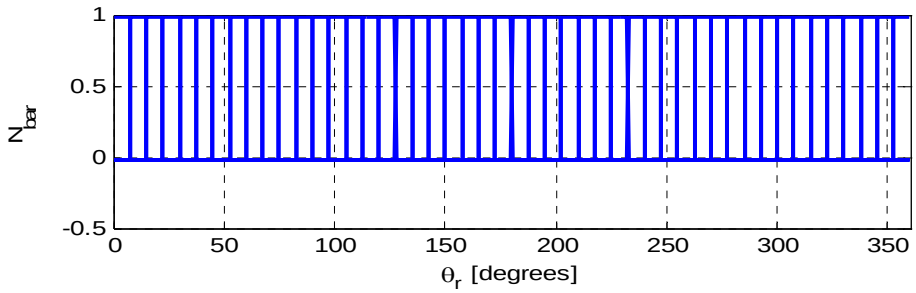

Figure 5.14 Rotor winding function for coupled bars

5.3.5 Derivation of Stator Self-Inductances

After the derivation of the stationary reference frame winding functions, this section describes the use of the derived equations for the derivation of q-d model equations.

The equation of stator flux in real variables is given as

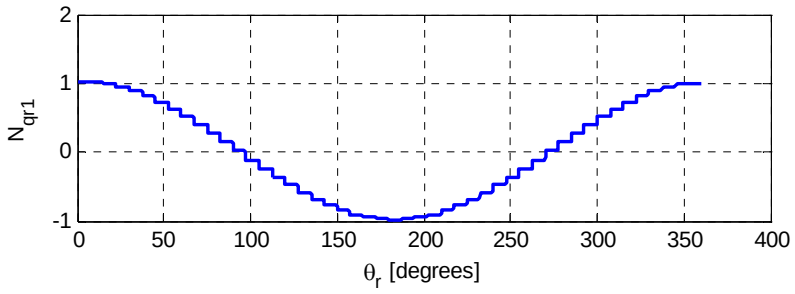

Figure 5.15 q-axis rotor winding function

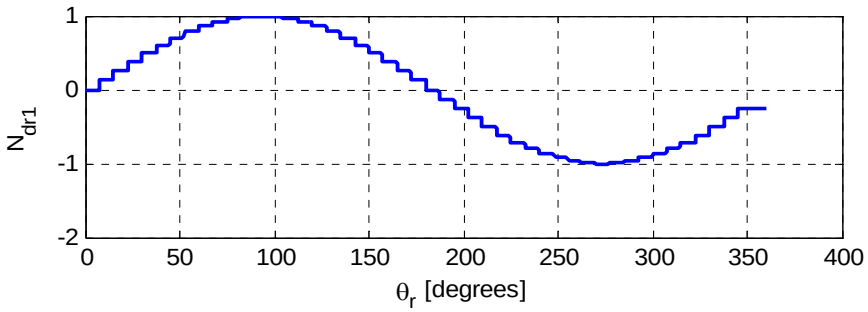

Figure 5.16 d-axis rotor winding function

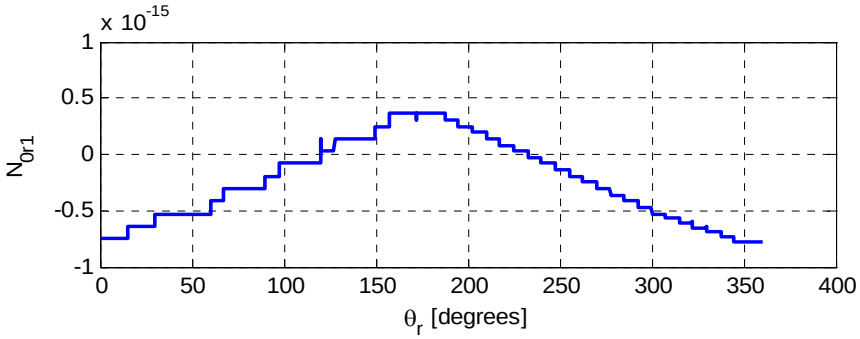

Figure 5.17 zero axis rotor winding function

$$\lambda_{adgs} = L_{adgs} i_{adgs} + L_{adgsbehs} i_{behs} + L_{adgscfis} i_{cfis} + L_{adgsabc\ldots nr} i_{abc\ldots nr} + \lambda_{adgm} \tag{5.91}$$

Using reference frame transformation with angle θ_1 in Equation (5.91),

$$\begin{aligned} T(\theta_1)\lambda_{adgs} &= T(\theta_1)L_{adgs} i_{adgs} + T(\theta_1)L_{adgsbehs} i_{behs} \\ &+ T(\theta_1)L_{adgscfis} i_{cfis} + T(\theta_1)L_{adgsabc\ldots nr} i_{abc\ldots nr} \end{aligned} \tag{5.92}$$

In this section, only the evaluation related to first term of Equation (5.74) is performed for the derivation of self-machine inductances. The second term is the mutual inductance term which is going to be deal later for the derivation of mutual inductances.

Suppose, $T(\theta_1) = T(\theta_1 - \theta_{x1})T(\theta_{x1})$ (5.93)

Hence first term in RHS of Equation (5.75) becomes,

$$\begin{aligned} T(\theta_1)L_{adgs}i_{adgs} &= T(\theta_1 - \theta_{x1})T(\theta_{x1})L_{adgs}i_{adgs} \\ &= T(\theta_1 - \theta_{x1})T(\theta_{x1})L_{adgs}T(\theta_x)^{-1}T(\theta_1 - \theta_{x1})^{-1}i_{qdoxs} \end{aligned} \quad (5.94)$$

Assume the operation in rotor reference mode, i.e., $\theta_1 = \theta_r$ and $\theta_{x1} = 0$

Hence,

$$\begin{aligned} T(\theta)L_{adgs}i_{adgs} &= T(\theta_r)\ \underbrace{T(0)L_{adgs}T(0)^{-1}}_{\text{Stationary Reference Frame}}\ T(\theta_r)^{-1}i_{qdoxs} \\ &= L_{qdoxs}i_{qdoxs} \end{aligned} \quad (5.95)$$

As observed in Equation (5.95), the middle terms imply the stationary reference transformation of the stator inductance matrix. In terms of the winding functions,

$$L_{ij} = \mu_0 rl \int_0^{2\pi} N_i(\phi)N_j(\phi)g^{-1}(\phi,\theta_r)d\phi \quad (5.96)$$

Hence,

$$L_{aa} = \mu_0 rl \int_0^{2\pi} N_a(\phi)N_a(\phi)g^{-1}(\phi,\theta_r)d\phi \quad (5.97)$$

$$L_{ab} = \mu_0 rl \int_0^{2\pi} N_a(\phi)N_b(\phi)g^{-1}(\phi,\theta_r)d\phi \quad (5.98)$$

In the similar way, all inductances can be derived.

Hence, the middle term of Equation (5.95) is given as

$$T(0)L_{adgs}T(0)^{-1}$$

$$= \mu_0 rl\int_0^{2\pi} T(0)\begin{bmatrix} N_a{}^2 & N_aN_d & N_aN_g \\ N_aN_d & N_d{}^2 & N_bN_d \\ N_aN_g & N_gN_d & N_g{}^2 \end{bmatrix} T(0)^{-1} \tag{5.99}$$

$$\times\begin{bmatrix} g^{-1}(\phi,\theta_r) & 0 & 0 \\ 0 & g^{-1}(\phi,\theta_r) & 0 \\ 0 & 0 & g^{-1}(\phi,\theta_r) \end{bmatrix}$$

The given matrix can be resolved as

$$L_{qdoxs} = T(\theta_r)\mu_0 rl\int_0^{2\pi} T(0)ABT(0)^{-1}CT(\theta_r)^{-1} \tag{5.100}$$

where,

$$A=\begin{bmatrix} N_a & N_a & N_a \\ N_d & N_d & N_d \\ N_g & N_g & N_g \end{bmatrix} \tag{5.101}$$

$$B=\begin{bmatrix} N_a & 0 & 0 \\ 0 & N_d & 0 \\ 0 & 0 & N_g \end{bmatrix} \tag{5.102}$$

$$C=\begin{bmatrix} g^{-1}(\phi,\theta_r) & 0 & 0 \\ 0 & g^{-1}(\phi,\theta_r) & 0 \\ 0 & 0 & g^{-1}(\phi,\theta_r) \end{bmatrix} \tag{5.103}$$

Now, multiplying matrix ‘A’ with the stationary reference transformation matrix,

$$T(0)A=\begin{bmatrix} N_{q1} & N_{q1} & N_{q1} \\ N_{d1} & N_{d1} & N_{d1} \\ N_0 & N_0 & N_0 \end{bmatrix} \tag{5.104}$$

Multiplying Equation (5.104) with $BT(0)^{-1}$, the resulting equations is given as

$$T(0)ABT(0)^{-1} = \underbrace{\begin{bmatrix} N_{qs1}^{\ 2} & N_{qs1}N_{ds1} & N_{qs1}N_{0s1} \\ N_{qs1}N_{ds1} & N_{ds1}^{\ 2} & N_{ds1}N_{0s1} \\ N_{qs1}N_{0s1} & N_{ds1}N_{0s1} & N_{0s1}^{\ 2} \end{bmatrix}}_{\textbf{Stationary Reference Frame}} \tag{5.105}$$

The expression of L_{qdoxs} consists of the term 'C', the air gap matrix, which is dependent of rotor angle. Similarly, the transformation matrix is also dependent on rotor angle as seen from Equation (5.100). In the integration of Equation (5.105), the mutual terms containing q-axis and d-axis gives rise to zero similar to the case of 9-phase machine. Recalling the plot of air gap function with the variation of rotor angle, Figure 5.18 shows the variation of air gap function with the rotor angle.

In order to derive the inductances the air gap function is stepped with the variation of rotor angle and inductances are calculated with the help of Equation (5.100). The similar expression can be obtained for other machine configurations. Figures 5.19, 5.20 and 5.21, respectively depict the q and d axis stator inductances for Machine I, Machine II and Machine III. The inductances are plotted with the variation of rotor angle and rotor saliency is observed since d-axis and q-axis inductances are different.

5.3.6 Derivation of Stator Mutual Leakage Inductances

The flux linkage equation for the Machine I is given as

$$\lambda_{adgs} = L_{adgs}\, i_{adgs} + L_{adgsbehs}\, i_{behs} + L_{adgscfis}\, i_{cfis} + L_{adgsabc\,\ldots nr}\, i_{abc\,\ldots nr} + \lambda_{adgm} \tag{5.106}$$

Multiplying both sides by transformation angle $T(\theta_1)$

$$\begin{aligned} T(\theta_1)\lambda_{adgs} = T(\theta_1)L_{adgs}i_{adgs} + T(\theta_1)L_{adgsbehs}i_{behs} + T(\theta_1)L_{adgscfis}i_{cfis} \\ + T(\theta_1)L_{adgsabc\ldots nr}i_{abc\ldots nr} + T(\theta_1)\lambda_{adgm} \end{aligned} \tag{5.107}$$

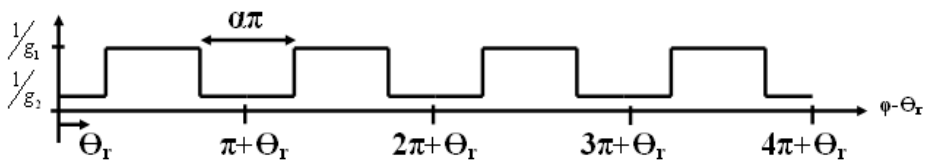

Figure 5.18 Air gap function vs. rotor angle

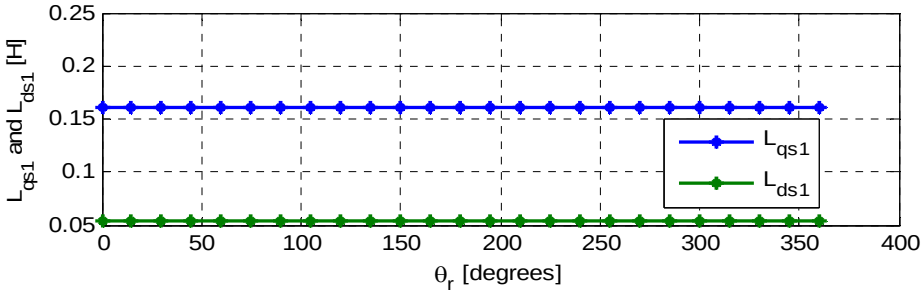

Figure 5.19 q and d-axis stator inductances for Machine I

For the mutual inductance between the machines, the second term is taken into account.

$$T(\theta_1)L_{adgsbeh}i_{behs} = T(\theta_1)L_{adgsbehs}T(\theta_2)^{-1}i_{qdo2s} = L_{qdo12s}i_{qdo2s} \tag{5.108}$$

From the properties of transformation, it can be shown that,

$$T(\theta_1) = T(\theta_1 - \theta_{x1})T(\theta_{x1}) \tag{5.109}$$

$$T(\theta_2) = T(\theta_2 - \theta_{x2})T(\theta_{x2}) \tag{5.110}$$

But,

$$\theta_2 = \theta_1 - \beta \tag{5.111}$$

$$T(\theta_2) = T(\theta_1 - \beta - \theta_{x2})T(\theta_{x2}) \tag{5.112}$$

Substituting this value in Equation (5.92)

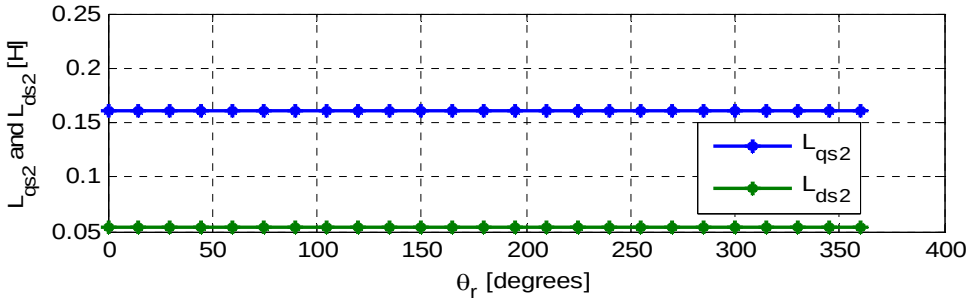

Figure 5.20 q and d-axis stator inductances for Machine II

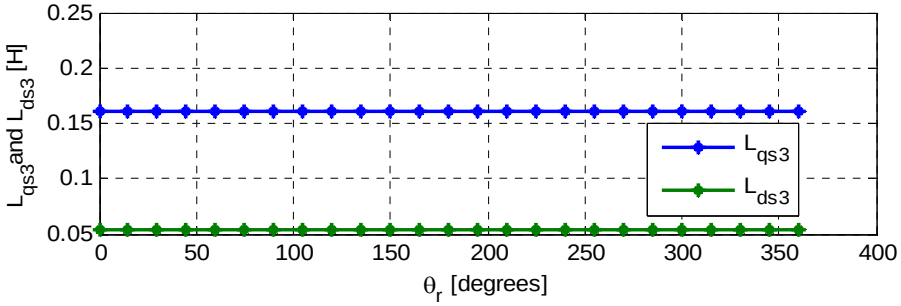

Figure 5.21 q and d-axis stator inductances for Machine III

$$L_{qdo12s} = T(\theta_1 - \theta_{x1})T(\theta_{x1})L_{adgsbehs}T(\theta_{x2})^{-1}T(\theta_1 - \zeta - \theta_{x2}) \tag{5.113}$$

Assuming rotor reference frame,

$$\theta_1 = \theta_r\ ,\ \theta_{x1} = \theta_{x2} = 0 \tag{5.114}$$

$$L_{qdo12s} = T(\theta_r)\underbrace{T(0)L_{adgsbehs}T(0)^{-1}}_{\text{Stationary reference frame}}T(\theta_r - \beta)^{-1} \tag{5.115}$$

$$\begin{aligned} L_{qdo12s} = {} & T(\theta_r)\mu_0 rl\int_0^{2\pi} T(0)\begin{bmatrix} N_aN_b & N_aN_e & N_aN_h \\ N_dN_b & N_dN_e & N_dN_h \\ N_gN_b & N_gN_e & N_gN_h \end{bmatrix}T(0)^{-1}T(\theta_r - \beta)^{-1} \\ & \times\begin{bmatrix} g^{-1}(\phi,\theta_r) & 0 & 0 \\ 0 & g^{-1}(\phi,\theta_r) & 0 \\ 0 & 0 & g^{-1}(\phi,\theta_r) \end{bmatrix} \end{aligned} \tag{5.116}$$

Let Equation (5.116) is represented as

$$L_{qd012s} = \mu_0 rlT(\theta_r)\int_0^{2\pi} T(0)ABT(0)^{-1}T(\theta_r - \beta)^{-1}C \tag{5.117}$$

$$A = \begin{bmatrix} N_a & N_a & N_a \\ N_d & N_d & N_d \\ N_g & N_g & N_g \end{bmatrix} \tag{5.118}$$

$$B = \begin{bmatrix} N_b & 0 & 0 \\ 0 & N_e & 0 \\ 0 & 0 & N_h \end{bmatrix} \tag{5.119}$$

$$T(0)A = \begin{bmatrix} N_{q1} & N_{q1} & N_{q1} \\ N_{d1} & N_{d1} & N_{d1} \\ N_0 & N_0 & N_0 \end{bmatrix} \tag{5.120}$$

$$T(0)ABT(0)^{-1} = \begin{bmatrix} N_{q1}N_{q2} & N_{q1}N_{d2} & N_{q1}N_{02} \\ N_{d1}N_{q2} & N_{d1}N_{d2} & N_{d1}N_{02} \\ N_{01}N_{q2} & N_{01}N_{d2} & N_{01}N_{02} \end{bmatrix} \tag{5.121}$$

$$C = \begin{bmatrix} g^{-1}(\phi,\theta_r) & 0 & 0 \\ 0 & g^{-1}(\phi,\theta_r) & 0 \\ 0 & 0 & g^{-1}(\phi,\theta_r) \end{bmatrix} \tag{5.122}$$

$$L_{qdo12s} = \mu_0 rlT(\theta_r)\int_0^{2\pi} \begin{bmatrix} N_{q1}N_{q2} & N_{q1}N_{d2} & N_{q1}N_{02} \\ N_{d1}N_{q2} & N_{d1}N_{d2} & N_{d1}N_{02} \\ N_{01}N_{q2} & N_{01}N_{d2} & N_{01}N_{02} \end{bmatrix} T(\theta_r - \beta)^{-1} \times \begin{bmatrix} g^{-1}(\phi,\theta_r) & 0 & 0 \\ 0 & g^{-1}(\phi,\theta_r) & 0 \\ 0 & 0 & g^{-1}(\phi,\theta_r) \end{bmatrix} d\phi \tag{5.123}$$

Applying the similar methods derived previously by stepping the rotor angle and evaluating the inductances, the mutual inductance between Machine I and II is derived. Figure 5.22 gives the mutual d and q axis stator inductance between Machine I and

Machine II. Similarly, the mutual inductance between Machine I and Machine III is given in Figure 5.23. The mutual inductance between Machine II and Machine III is depicted in Figure 5.24.

5.3.7 Derivation of Rotor Self-Inductances

The rotor flux linkage in real variable form is given as

$$\lambda_{abc...nr} = L_{abc..nr} i_{abc...nr} + L_{abc..isabc...nr} i_{adgs} \tag{5.124}$$

Multiplying both sides of Equation (5.118) by transformation matrix, $T(\theta_1 - \theta_r)$,

$$T(\theta_1 - \theta_r)\lambda_{abc...nr} = T(\theta_1 - \theta_r)L_{abc..nr} i_{abc...nr} + T(\theta_1 - \theta_r)L_{abc..isabc...nr} i_{adgs} \tag{5.125}$$

For the derivation of rotor self-inductances, only the first term of equation is taken into account. Hence,

$$T(\theta_1 - \theta_r)L_{abc..nr} i_{abc...nr} = T(\theta_1 - \theta_r)L_{abc..nr} T(\theta_1 - \theta_r)^{-1} i_{qdor} \tag{5.126}$$

For rotor reference frame,

$$\theta_1 = \theta_r \tag{5.127}$$

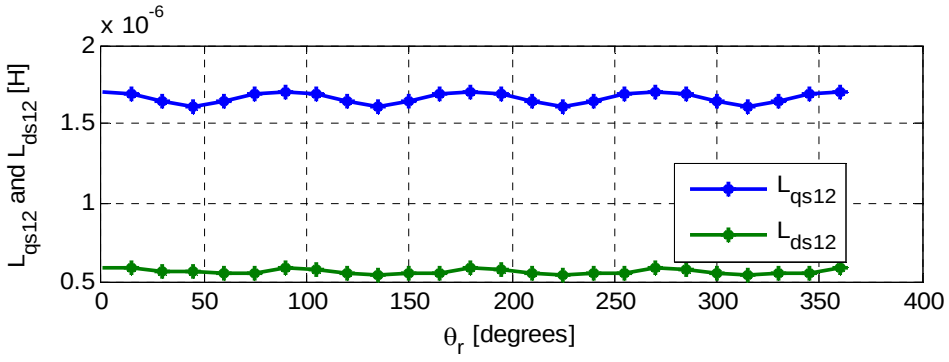

Figure 5.22 Mutual stator leakage inductance between Machine I and Machine II

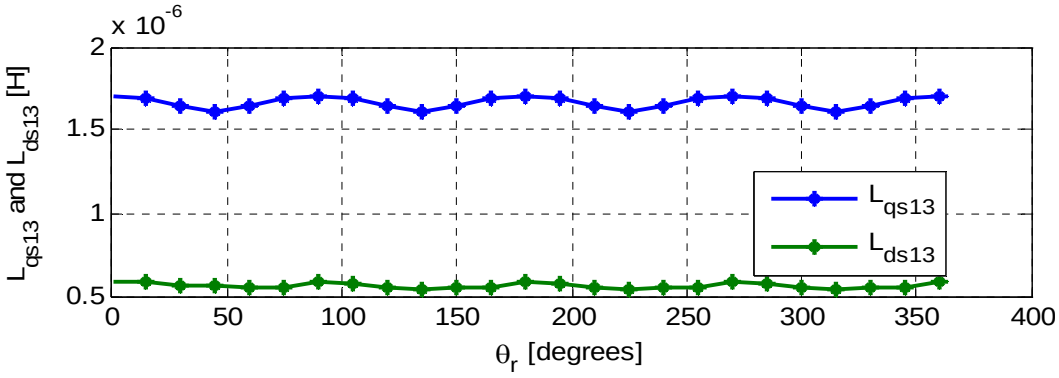

Figure 5.23 Mutual stator leakage inductance between Machine II and Machine III

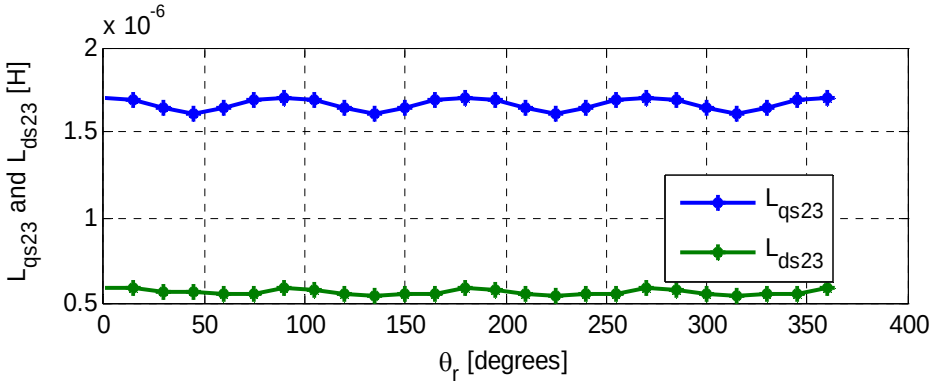

Figure 5.24 Mutual stator leakage inductance between Machine II and Machine III

Hence, above equation becomes

$$T(\theta_1 - \theta_r)L_{abc..nr}\,i_{abc...nr} = T(0)L_{abc..nr}T(0)^{-1}\,i_{qdor} \tag{5.128}$$

This equation is similar to the equation derived in case of the stator circuits except that the inductance now should accommodate the rotor circuits. Hence, the winding functions in stationary reference frame derived are used to evaluate the inductances. Proceeding the same way as derived for the 9-phase case by stepping the rotor angle, the inductances derived for d-q inductance of the rotor circuit are given in Figure 5.25.

5.3.8 Mutual Inductance of Rotor with Other Machines

In the same way, the mutual inductance between the stator of each machine and rotor bars can be determined. The similar method of calculation follows with the adjustment in transformation matrices.

The stator flux linkage after the transformation is given as;

$$T(\theta_1)\lambda_{adgs} = T(\theta_1)L_{adgs}i_{adgs} + T(\theta_1)L_{abc..isabc...nr}i_{abc....nr} + T(\theta_1)\lambda_{adgm} \tag{5.129}$$

Taking the second term in Equation (5.129),

$$T(\theta_1)L_{adgsabc...nr}i_{abc....nr} = T(\theta)L_{adgsabc...nr}T(\theta-\theta_r)^{-1}i_{qdor} \tag{5.130}$$

Suppose, $T(\theta_1) = T(\theta_1-\theta_{x1})T(\theta_{x1})$ (5.131)

Assuming, $\theta_{x1} = 0$, and $\theta_1 = \theta_r$ i.e., rotor reference frame,

$$\begin{aligned} T(\theta_1)L_{abc..isabc...nr}i_{abc....nr} &= T(\theta_1-\theta_x)T(\theta_{x1})L_{adgsabc...nr}T(\theta_1-\theta_r)^{-1}i_{qdor} \\ &= T(\theta_r)T(0)L_{adgsabc..nr}T(0)^{-1}i_{qdor} \\ &= L_{qdors}i_{qdor} \end{aligned} \tag{5.132}$$

If Equation (5.126) is solved in terms of real variables and stationary reference frame transformation is applied, the equation reduces to,

$$L_{qdors} = T(\theta_r)\mu_0 rl\int [N_{qdors}]g^{-1}(\phi_s,\theta_r)d\phi_s \tag{5.133}$$

where,

$$N_{qdors} = \begin{bmatrix} N_{q1s}N_{q1r} & N_{q1s}N_{d1r} & N_{q1s}N_{0r} \\ N_{d1s}N_{q1r} & N_{d1s}N_{d1r} & N_{d1s}N_{0r} \\ N_{q1s}N_{0r} & N_{d1s}N_{0r} & N_{0s}N_{0r} \end{bmatrix} \tag{5.134}$$

Similar to the derivations derived before, the q and d axis mutual inductances between rotor bars and each machine is evaluated with the variation of the rotor angle. Figure 5.26 gives the plot between rotor and Machine I and Figures 5.27 and 5.28 depicts the plot of mutual inductances between rotor and Machine II and III, respectively.

5.3.9 Induced EMF Due to Magnets on Stator Phase Windings

Using the derivation steps as discussed in previous chapter, the transformed flux linkage on stator is given as

$$T(\theta)\lambda_{abc...is} = T(\theta)L_{abc...is}i_{abc...is} + T(\theta)L_{abc..isabc...nr}i_{abc....nr} + T(\theta)\lambda_{abc..im} \tag{5.135}$$

The flux linkage due to magnet on phase 'a' is given as [2]

$$\lambda_{as} = \int_0^{2\pi} N_a(\phi_s)\int_{\phi_s}^{\phi_s+\pi} B_r(\zeta,\theta_r)rld\,\zeta d\phi_s \tag{5.136}$$

In matrix form, for first machine,

$$\begin{bmatrix}\lambda_{as}\\ \lambda_{bs}\\ \lambda_{cs}\end{bmatrix} = \frac{rl}{3}\int \begin{bmatrix}N_{as} & N_{as} & N_{as}\\ N_{ds} & N_{ds} & N_{ds}\\ N_{gs} & N_{gs} & N_{gs}\end{bmatrix}\int_{\phi_s}^{\phi_s+\pi}\begin{bmatrix}B_r(\phi,\theta_r)\\ B_r(\phi,\theta_r)\\ B_r(\phi,\theta_r)\end{bmatrix}d\zeta d\phi_s \tag{5.137}$$

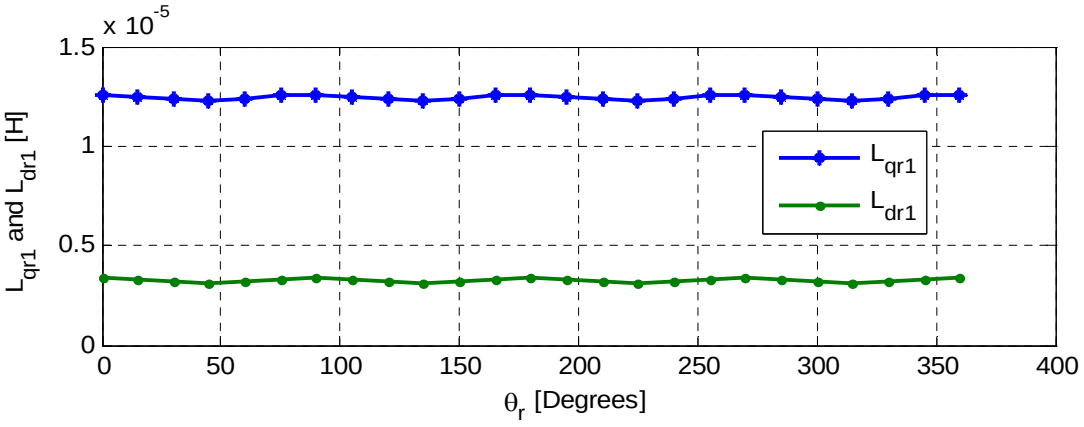

Figure 5.25 Rotor q and d axis inductances

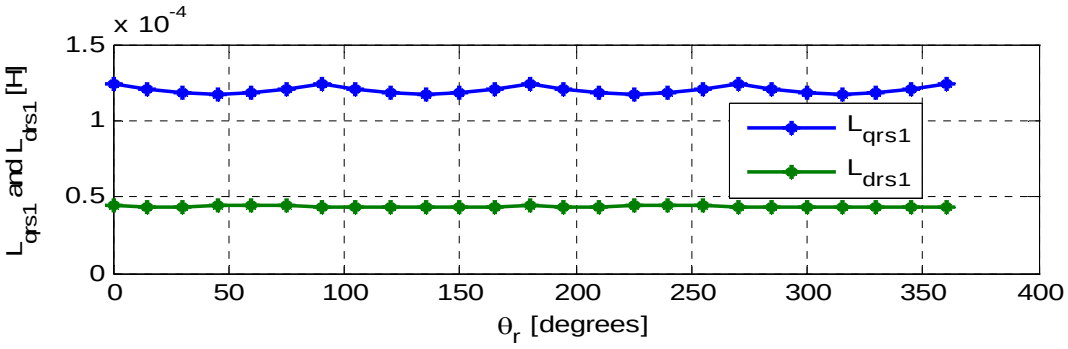

Figure 5.26 Mutual inductances between rotor and Machine I

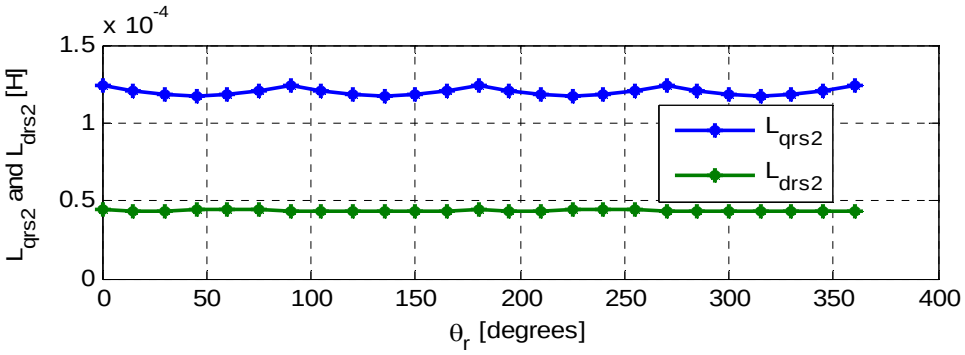

Figure 5.27 Mutual inductances between rotor and Machine II

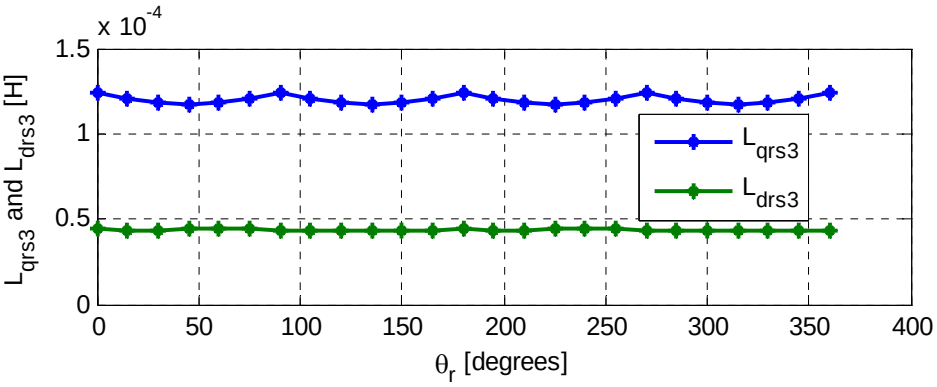

Figure 5.28 Mutual inductances between rotor and Machine III

Multiplying both sides by transformation matrix, $T(\theta_1)$

Let, $T(\theta_1) = T(\theta_1 - \theta_x)T(\theta_x)$ (5.138)

Hence, RHS of above equation becomes

$$= \frac{rl}{3} T(\theta_1 - \theta_x) T(\theta_x) \int_0^{2\pi} \begin{bmatrix} N_{as} & N_{as} & N_{as} \\ N_{ds} & N_{ds} & N_{ds} \\ N_{gs} & N_{gs} & N_{gs} \end{bmatrix} \int_{\phi_s}^{\phi_s+\pi} \begin{bmatrix} B_r(\zeta, \theta_r) \\ B_r(\zeta, \theta_r) \\ B_r(\zeta, \theta_r) \end{bmatrix} d\zeta d\phi_s \quad (5.139)$$

Again, using rotor reference frame, $\theta = \theta_r, \theta_x = 0$, above equation turns into

$$= \frac{rl}{3} T(\theta_r) T(0) \int_0^{2\pi} \begin{bmatrix} N_{as} & N_{as} & N_{as} \\ N_{ds} & N_{ds} & N_{ds} \\ N_{gs} & N_{gs} & N_{gs} \end{bmatrix} \int_{\phi_s}^{\phi_s+\pi} \begin{bmatrix} B_r(\zeta, \theta_r) \\ B_r(\zeta, \theta_r) \\ B_r(\zeta, \theta_r) \end{bmatrix} d\zeta d\phi_s \quad (5.140)$$

Since the integration does not involve the transformation angle, the transformation can be brought inside the integration and apply the transformation. The equation turns into

$$= \frac{rl}{3} T(\theta_r) \int_0^{2\pi} \begin{bmatrix} N_{q1s} & N_{q1s} & N_{q1s} \\ N_{d1s} & N_{d1s} & N_{d1s} \\ N_{0s} & N_{0s} & N_{0s} \end{bmatrix} \int_{\phi_s}^{\phi+\pi} \begin{bmatrix} B_r(\zeta, \theta_r) \\ B_r(\zeta, \theta_r) \\ B_r(\zeta, \theta_r) \end{bmatrix} d\zeta d\phi_s \quad (5.141)$$

The term inside the second integration is the waveform of the tapered flux density. Since the flux density gives the same value for any range of integration, the integration here is performed for the limits with $\phi_s = 0$. Using this integration, the flux density is as given in Figure 5.29. Hence, the equation reduces into,

$$= \frac{rl}{3} T(\theta_r) \int_0^{2\pi} \begin{bmatrix} 3N_{q1s} B_r(\theta_r) \\ 3N_{q1s} B_r(\theta_r) \\ 3N_{q1s} B_r(\theta_r) \end{bmatrix} d\phi_s \quad (5.142)$$

Hence, the fundamental q-axis flux linkage due to magnet is derived as

$$\lambda_{q1ms} = \int_0^{2\pi} \begin{bmatrix} c(\theta_r) \times N_{q1s}(B_r(\theta_r)) + c(\theta_r - \alpha) \times N_{d1s}(B_r(\theta_r)) \\ + c(\theta_r - 2\alpha) \times N_{q3s}(B_r(\theta_r)) \end{bmatrix} d\phi_s \tag{5.143}$$

The q-axis flux linkage is depicted in Figure 5.30. Since the q-axis flux linkage is almost zero, the induced d-axis EMF will also be almost zero. Similarly, fundamental d-axis flux linkage is derived as

$$\lambda_{d1ms} = \int_0^{2\pi} \left[s(\theta_r) \times N_{q1s}(B_r(\theta_r)) + s(\theta_r - \alpha) \times N_{d1s}(B_r(\theta_r)) + s(\theta_r - 2\alpha) \times N_{q3s}(B_r(\theta_r)) \right] \tag{5.144}$$

The plot of d-axis flux linkage with the variation in rotor angle is shown in Figure 5.31 and induced EMF to the stator q-axis is shown in Figure 5.32. Similarly, the flux induced due to magnet in d-axis of Machine II is derived in Figure 5.33 and the induced voltage is derived in Figure 5.34. Similarly, the flux linkage in d-axis of Machine III is shown in Figure 5.35 and induced voltage is shown in Figure 5.36.

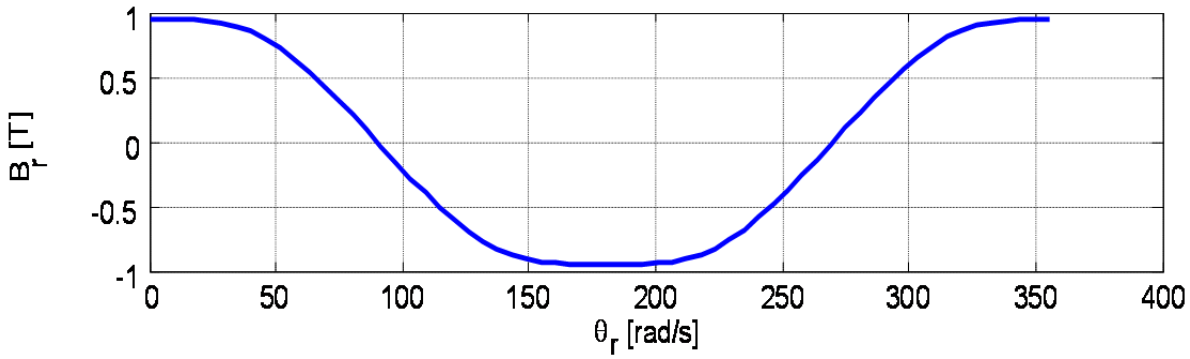

Figure 5.29 Flux density integrated with $\phi_s = 0$

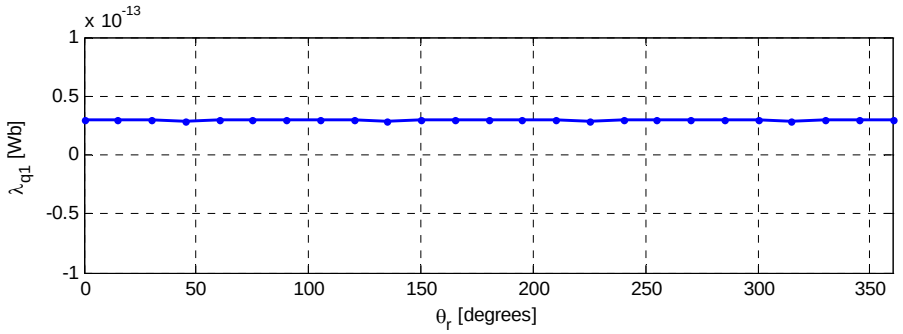

Figure 5.30 q-axis flux linkage between magnet and Machine I

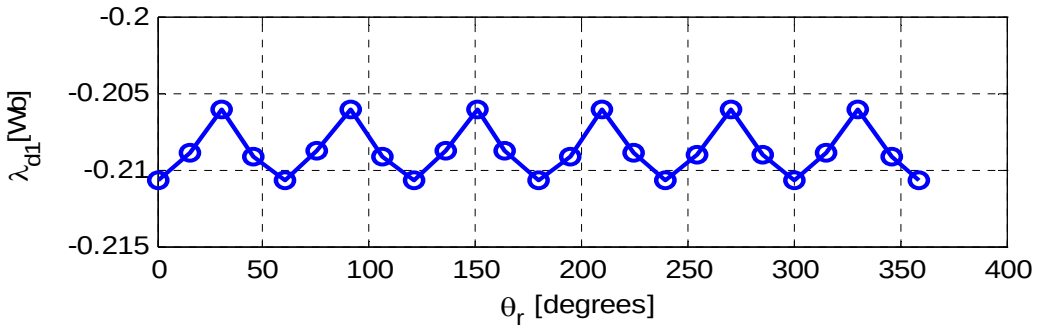

Figure 5.31 d-axis flux linkage between magnet and Machine I

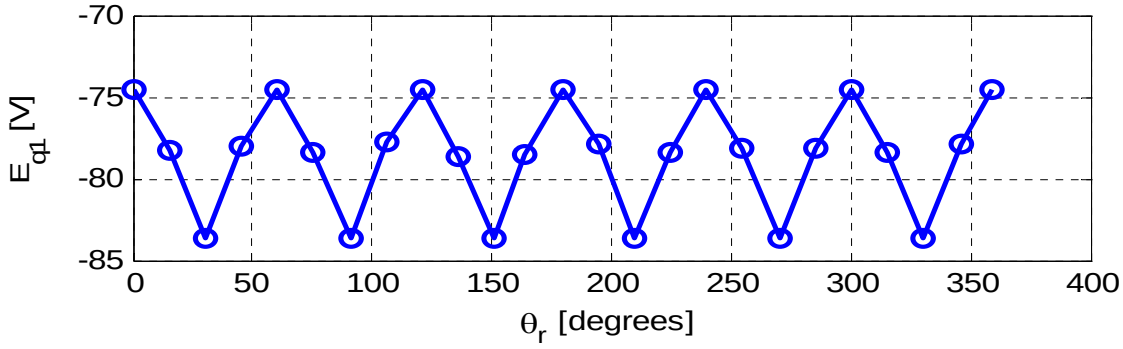

Figure 5.32 q-axis induced voltage between magnet and Machine I

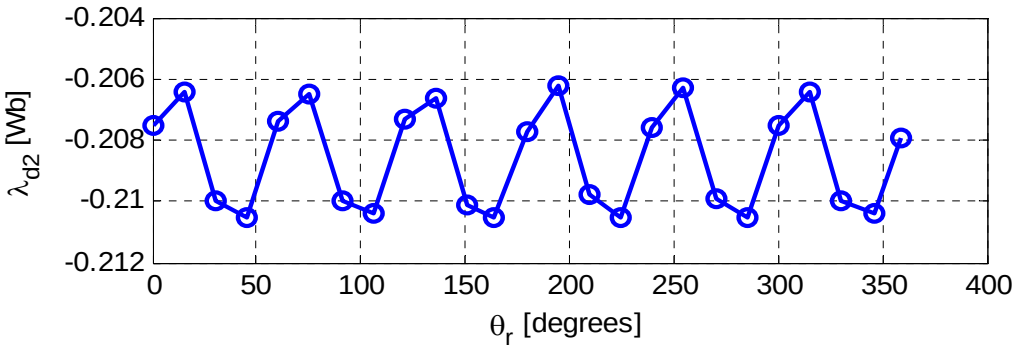

Figure 5.33 d-axis flux linkage between magnet and Machine II

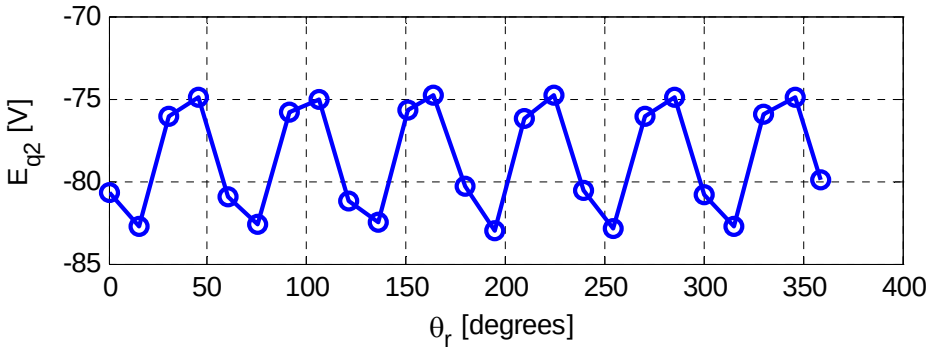

Figure 5.34 d-axis induced voltage between magnet and Machine II

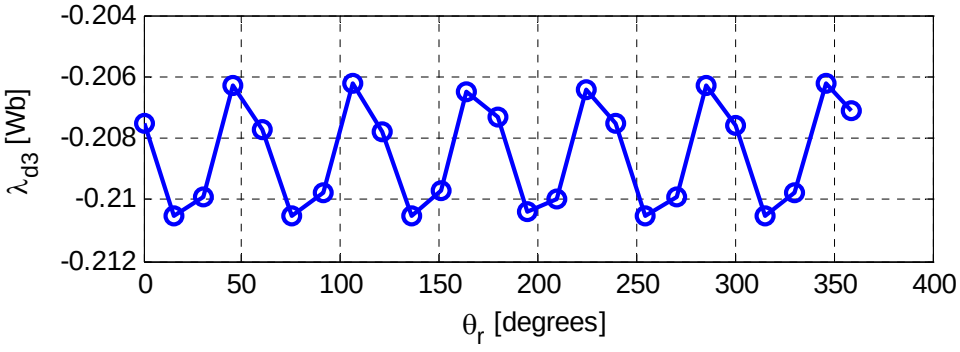

Figure 5.35 d-axis flux linkage between magnet and Machine III

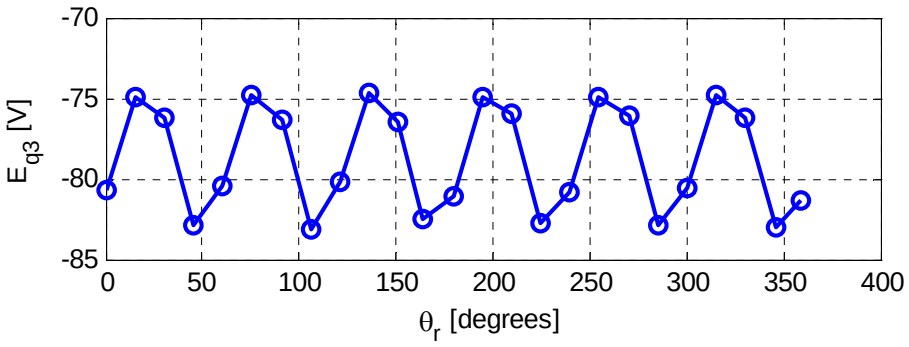

Figure 5.36 q-axis induced voltage between magnet and Machine III

5.4 Conclusion

In this chapter, the model of the three machine configuration of 9-phase IPM machine was performed using the Fourier series of the winding functions as well as the graphical analysis of the coupled d-q circuit model. The equivalent circuit of the machine was analyzed by taking all of the machine performance individually. It was also observed that the resultant torque due to machine is the resultant due to each machine torque and also the mutual torque which arises from the mutual inductance parameters from the machine. The stationary reference frame transformation was used to determine the d-q winding functions and they were also used to derive the performance parameters of the machine with the inclusion of the rotor damper bars. Similarly, the induced flux linkage due to magnet was observed on every machine counterparts when the 9-phase machine is operated as three sets of 3-phase machines. This gives a clear picture of the machine operation when 9-phase machine is operated as 3 sets of 3-phase machines for increased reliability. However, there is no existence of higher order harmonics in the system to get the resultant contribution due to harmonics.

CHAPTER 6

DESIGN AND ANALYSIS OF 9-PHASE INDUCTION MACHINE FOR POLE PHASE MODULATION SCHEME

6.1 Introduction

For the operation of the multiphase induction motor in varying speed/torque operation, pole phase modulation of the motor has been developed in which the change of the number of poles and phases of the stator windings can be done seamlessly. For operation in low speed and high torque, the motor can be operated as 3-phase, 12-pole. In addition for high speed and low torque operation, motor can be operated as 9-phase, 4-pole operation. This chapter presents the pole phase modulated design of the stator windings of a multiphase squirrel cage induction machine using the concepts of turns and winding functions and clock diagrams. The parameter determination of the motor is performed in both configurations using different experimental and estimation techniques. Similarly, the finite element analysis and the full order circuit model simulations are deployed to validate the design. With the development of the finite element field plots, performance comparison of the 4 and the 12-pole stator winding configurations are explored. Coupled circuit model of the configurations are set forth and used to simulate the operation of the motor and demonstrate the possible different operating synchronous speeds.

6.2 Design Strategy for PPM

6.2.1 Design Rule

A general design rule for the PPM is presented in this section. The coil pitch is equal and constant for the two stator winding configurations. Denoting p_1 as the number of poles and m_1 as number of phases and p_2 and m_2 for another set of poles and number of phases for the same machine, the required number of stator slots S, must satisfy the following relationship [54]:

$$S = p_i q_i m_i \tag{6.1}$$

p_i is the number of poles, m_i is the number of phases and q_i is the phase (spread) belt. If the two winding configurations are denoted as i = 1,2, the ratio of the two pole numbers is

$$k = \frac{p_2}{p_1} = \frac{q_1 m_1}{q_2 m_2} \tag{6.2}$$

The constant k is usually chosen such that k <1.

The design procedure is summarized as follows:

a. Select the number of stator slots (S)

b. Select the ratio k

c. Select phase ratio, m_1 / m_2

d. Calculate ratio of phase belt q_1 / q_2

e. Select the coil pitch and connect windings

6.2.2 Design of PPM Using Turn and Winding Functions

In electromagnetic design of electrical machines, turn and winding functions play the major significant role [67, 68]. The parameter estimation, study of air gap flux density and resultant MMF harmonics are made easier by the use of turn and winding functions. However, for this achievement, clock diagram is the initial starting point, where the windings are arranged in the stator slots with the variation of phase sequence and pole numbers [67].

The distribution of phase windings in 36 circumferential slots can be observed in Figure 6.1 in the form of clock diagram. The inner part of the figure shows the distribution for 9-phase, 4-pole whereas the outer part shows the corresponding distribution for 3-phase, 12-pole configuration. After the assignment of this distribution, turn and winding functions of each phase can be drawn by varying the circumferential angle. Figure 6.2 shows the turn and winding function for phases ‘a’, ‘b’, ‘c’ and Figure 6.3 shows the corresponding functions for ‘d’ ‘e’, and ‘f’ phases. Figure 6.4 depicts the turn and winding functions for phases ‘g’, ‘h’ and ‘i’. Similarly, Figure 6.5 shows the turn and winding functions for phases ‘A’, ‘B’ and ‘C’ of 3-phase configuration, respectively.

If any point along the circumference of the graphs in Figures 6.2, 6.3, 6.4 and 6.5 are analyzed, it can be observed that the resultant winding functions of three of the phases in 9-phase configuration gives the winding function of one of phase in 3-phase configuration which is described by Equation (6.3), where WF denotes the winding function of corresponding phases.

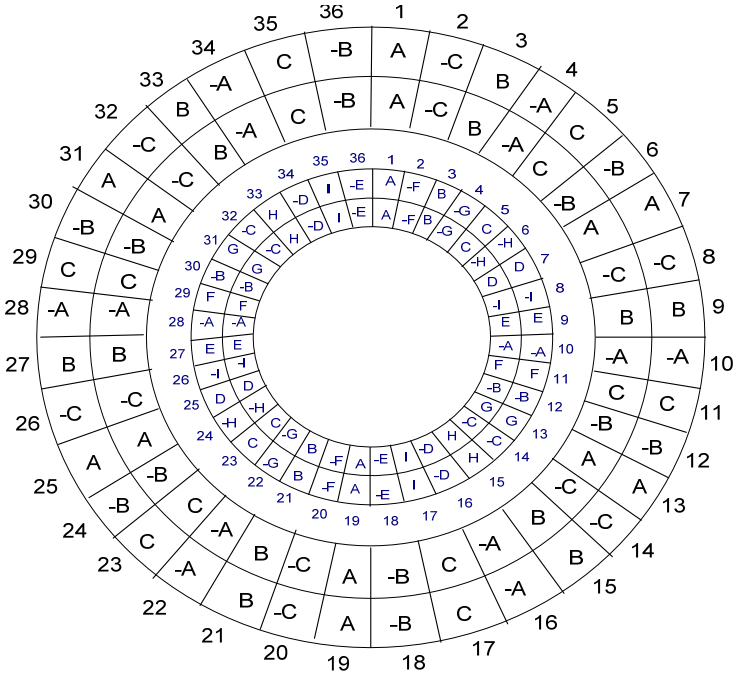

Figure 6.1 Clock diagram for 3-phase, 12-pole (outer) and 9-phase, 4-pole (inner) induction machine

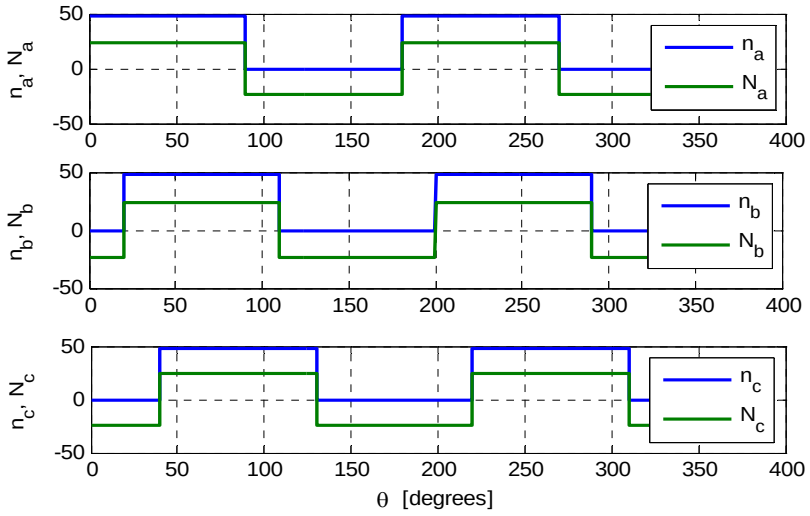

Figure 6.2 Turn and winding functions for phases ‘a’, ‘b’, and ‘c’ of 9-phase induction machine

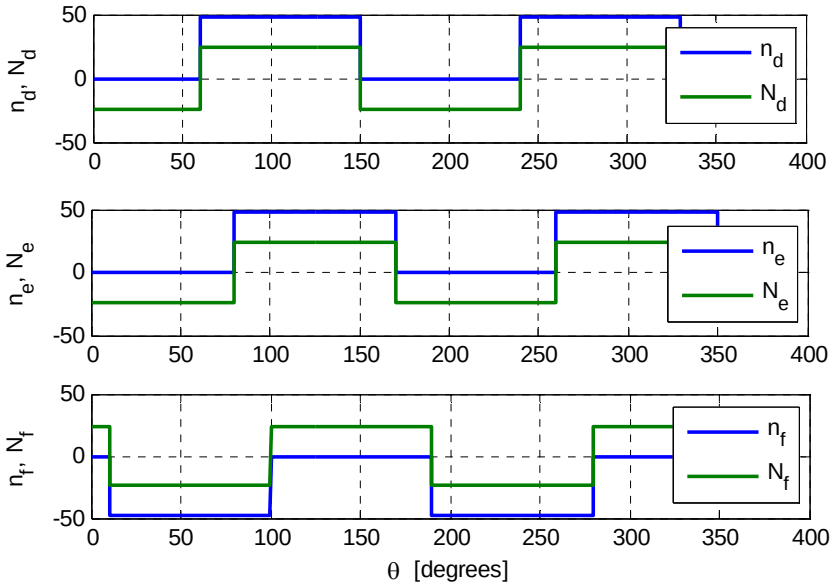

Figure 6.3 Turn and winding functions for phases 'd', 'e' and 'f' of 9-phase induction machine

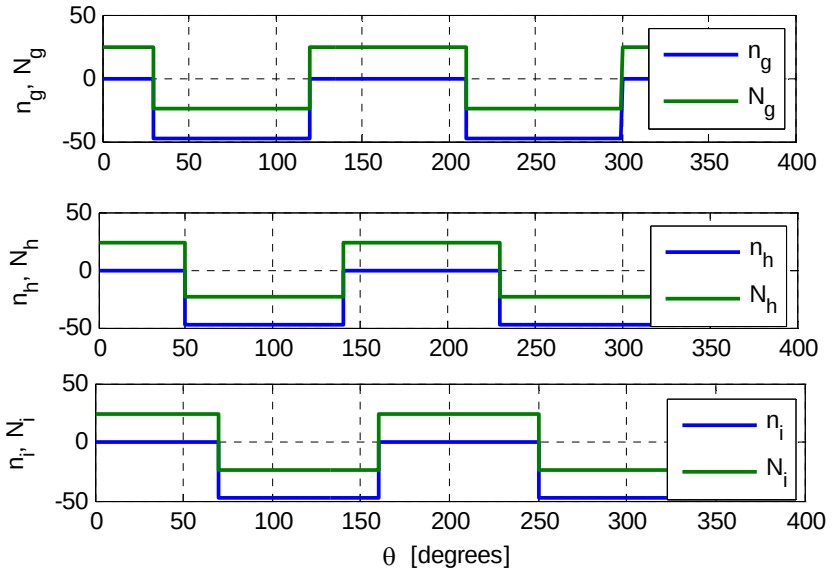

Figure 6.4 Turn and winding functions for phases 'g', 'h' and 'i' of 9-phase induction machine

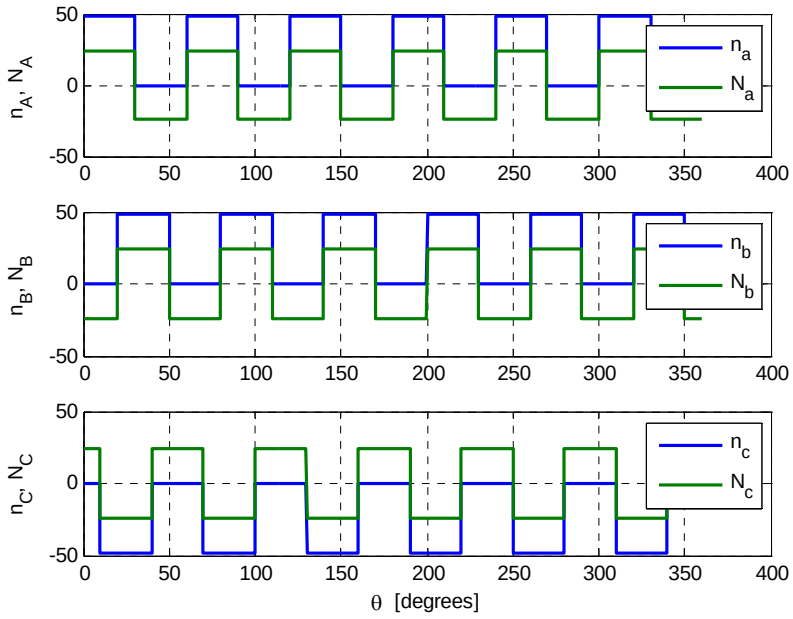

Figure 6.5 Turn and winding functions for phases 'A', 'B' and 'C' of 3-phase induction machine

$$\begin{aligned} WF[a+d+g] &= WF[A] \\ WF[b+e+h] &= WF[B] \\ WF[c+f+i] &= WF[C] \end{aligned} \tag{6.3}$$

6.2.3 Winding Design for PPM

The concept of clock diagram described in Section 6.2 gives the idea to layout the windings in both the configurations. Taking the distribution of phase windings in 9-phase configuration, the winding layout of Figure 6.6 (upper) is designed. Similarly with the distribution of the phases in 3-phase case, the corresponding winding layout of Figure 6.6 (lower) is designed. If the layout in Figure 6.6 is observed as moving through the stator slots, the phase configurations given in Table 6.1 can be derived for the comparison of both operations.

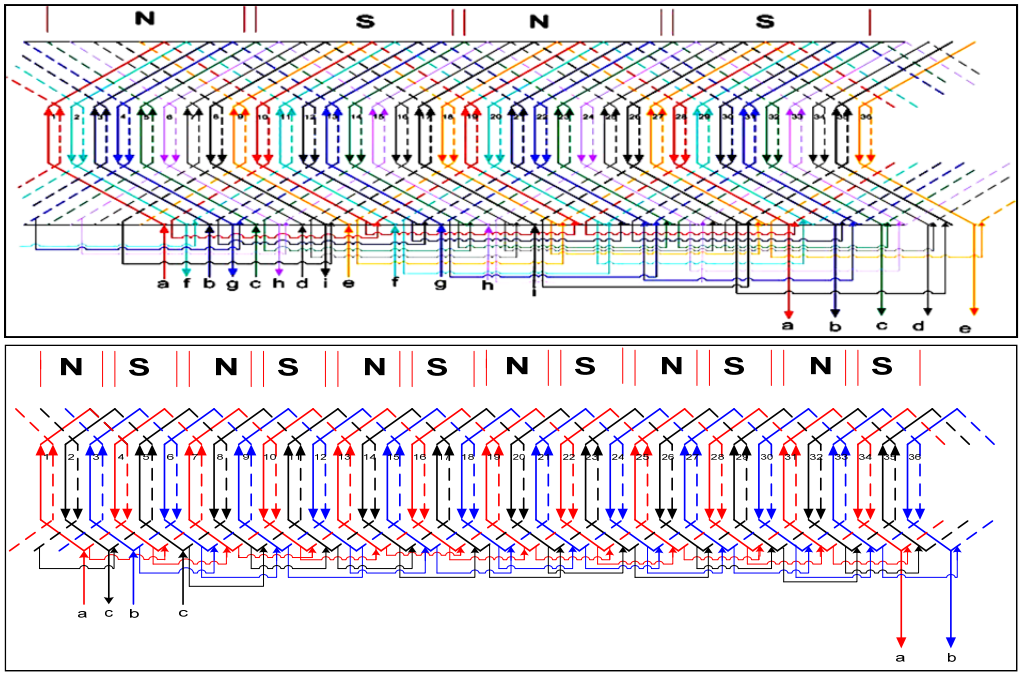

Figure 6.6 Winding layout for 9-phase, 4-pole (upper) and 3-phase, 12-pole (lower)

Table 6.1 Phase configurations for the 3-phase, 12-pole and 9-phase, 4-pole machines.

3-phase, 12-pole	9-phase, 4-pole
A	a
B	b
C	c
A	d
B	e
C	f
A	g
B	h
C	i

The configuration derived using the winding layouts gives us the flexibility to connect three of the windings in 9-phase 12-pole mode to the same source in order to operate as 3-phase, 12-pole mode. However, the source (current/voltage) should be adjusted such that there is existence of continuously rotating MMF for both systems to be in operation.

6.3 Finite Element Realization

Using the stator winding designed for the two configurations in Section 6.2, the two operating modes are analyzed with the finite elements analysis tools, FEMM [41]. For each configuration, the rated current corresponding to the data sheet of motor is injected through the stator windings and the resultant air gap MMF is analyzed in order to observe the corresponding characteristics.

a. 9-phase, 4-pole: The rated current of 2.4 Amperes, corresponding to the stator winding ampere-turns of 9-phase configuration is injected through the windings with the help of the clock diagram given in Figure. (6.1). It should be noted that, the currents are injected with the proper phase shift of $2\pi/9$ as moving through the phase sequences in each of the slots. Figure 6.7 shows the magnetic field pattern of the model when the machine is operating as a 4-pole stator winding. Similarly, Figure 6.8 shows the corresponding air gap flux density with the variation in stator angle.
b. 3-phase, 12-pole: Similar to the case of 9-phase, in 3-phase system, rated current of 7.2 Amperes is injected through each of the stator windings in this

case. However, the phase shift of $2\pi/3$ is adjusted as phase sequence is moved from each of the slots. Figure 6.9 depicts the magnetic field plots after the post processing and in Figure 6.10, the air gap flux density is illustrated. Figures 6.7-6.10 clearly reveal the number of poles for the two stator winding configurations and the nature of the air-gap flux distributions. Hence, it is observed that for the same fundamental MMF injection, the fundamental air-gap flux density of the 3-phase machine is higher with a potential for a higher torque generation as expected.

6.4 Parameter Estimation of 9-phase Induction Machine for Pole Phase Modulation Scheme

In order to determine the induction motor performances (torque, current, efficiency, etc.), the equivalent circuit parameters have to be computed after electromagnetic design of the induction motor. In this section, the two configurations of pole phase modulation are analyzed in terms of determining the equivalent circuit parameter estimation. For the accurate prediction of the parameters, different methods are employed. The conventional experimental test is performed and magnetic analysis is applied with finite elements in order to validate the experimental tests. Comparisons are also made between the machine parameter values obtained using these methods.

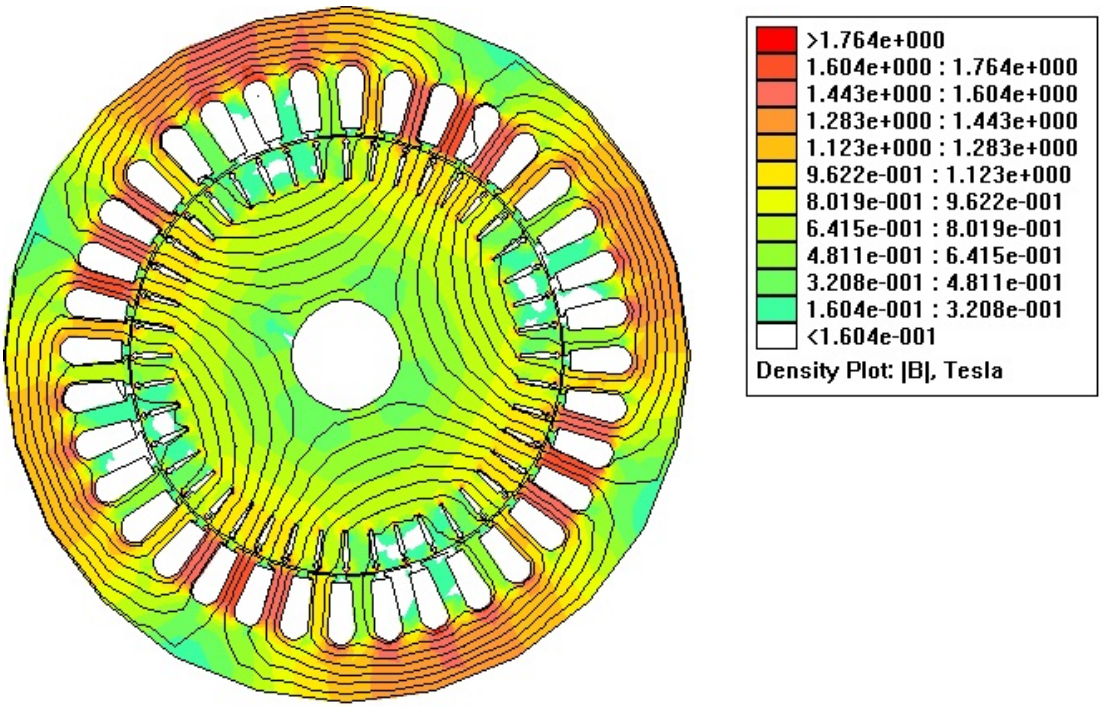

Figure 6.7 Flux density patterns for 9-phase, 4-pole configuration

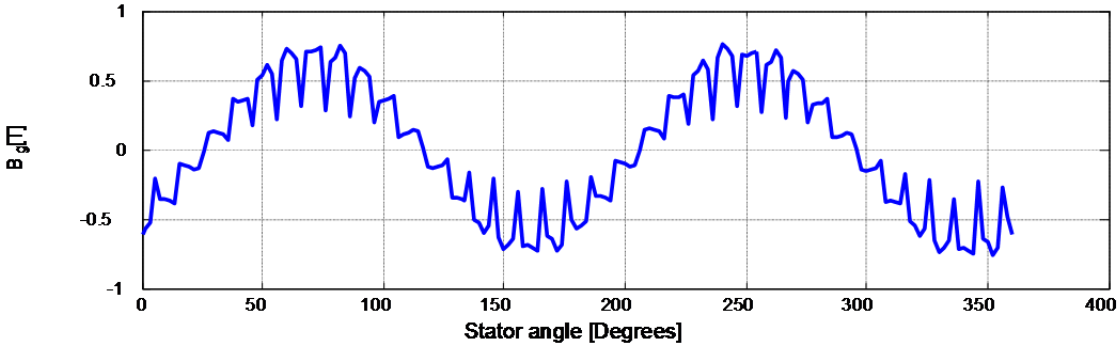

Figure 6.8 Air gap flux of 9-phase, 4-pole machine

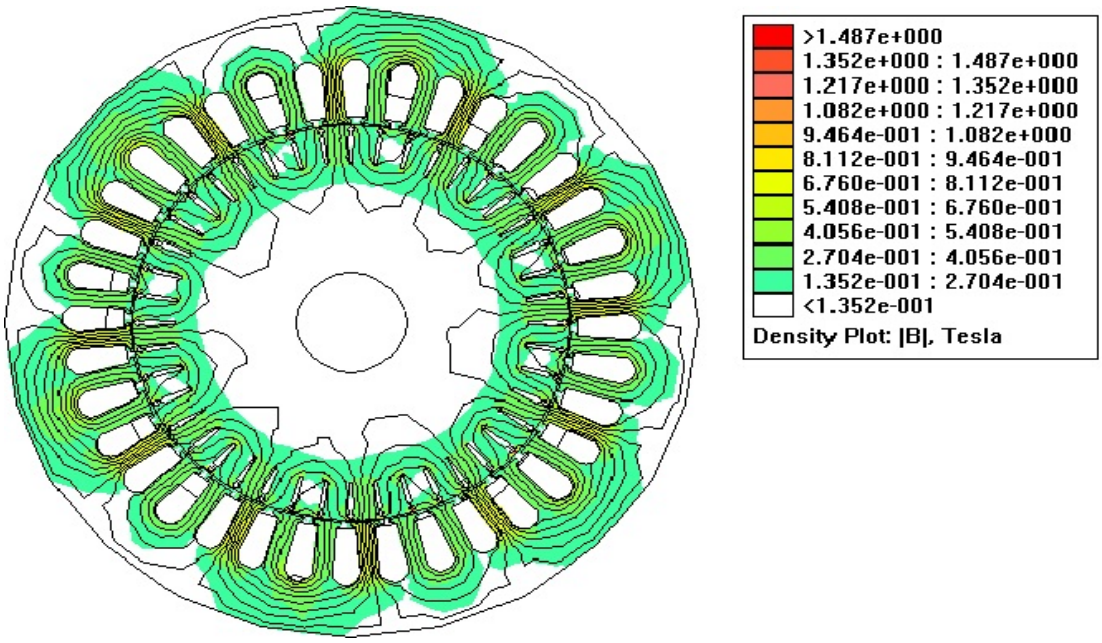

Figure 6.9 Flux density patterns for 3-phase, 12-pole configuration

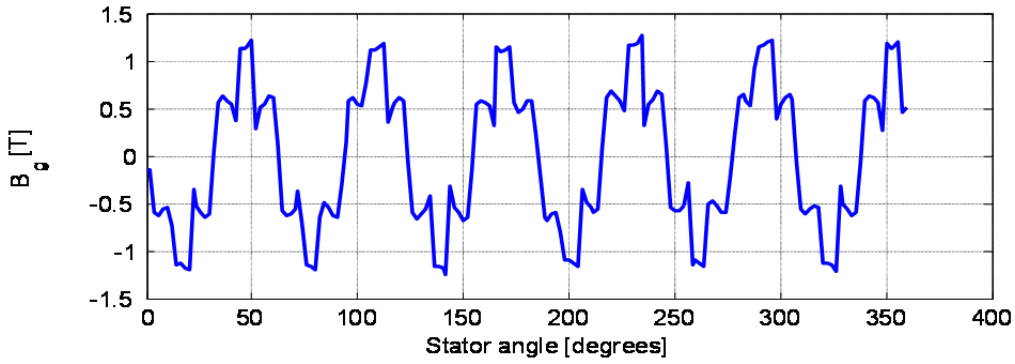

Figure 6.10 Air gap flux plot of 3-phase, 12-pole configuration

6.4.1 Experimental Method

The experimental method incorporates different conventional tests to determine the inductance and resistance parameters of the machine. Figure 6.11 shows the equivalent circuit of the induction machine in terms of those parameters.

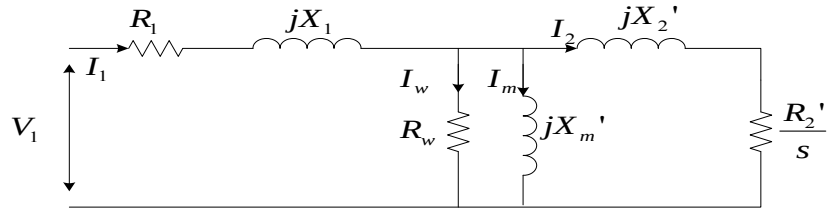

Figure 6.11 Equivalent circuit of induction machine

Conventionally, to determine the parameters of the machine, three tests are performed: DC test, no load test, blocked rotor test.

The DC test is performed to evaluate the stator resistance of the motor. The resistance is defined by applying DC voltage across the stator winding and measuring the current flowing in the circuit.

If V_{dc} is the dc voltage applied across the circuit and I_{dc} is the current flowing through it, the stator resistance is given by Equation (6.4).

$$R_{dc} = \frac{V_{dc}}{I_{dc}} \tag{6.4}$$

The no load test is conducted when the induction motor runs at no load the rotor speed approaches the synchronous speed. The slip is very small in this case. Accordingly, the secondary impedance becomes high compared to magnetizing branch. As a result, the equivalent circuit becomes as in Figure 6.12.

Three observations are taken from the circuit, 3-phase power, $P_{3-ph-NL}$, no load voltage, V_{NL} and no load current, I_{NL}. With these measurements, the no load resistance R_{nl} and no load reactance X_{nl} are computed for varying input voltages.

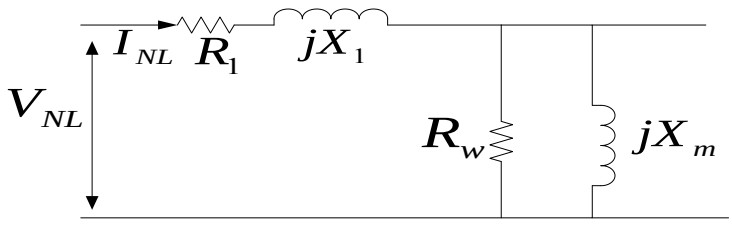

Figure 6.12 No load equivalent circuit

To find the magnetizing inductance and core loss resistance, Equation (6.5) needs to be solved Solving for the no load inductance and resistances in terms of equivalent circuit parameters of Figure 6.12 the following equation needs to be solved:

$$R_{nl} = R_1 + \frac{R_w\left(X_1 + X_m\right)^2}{R_w{}^2 + \left(X_1 + X_m\right)^2}, X_{nl} = \frac{R_w{}^2\left(X_1 + X_m\right)}{R_w{}^2 + \left(X_1 + X_m\right)^2} \tag{6.5}$$

The Blocked Rotor Test is performed when the rotor is prevented from running resulting in the slip being equal to 1. The secondary impedance becomes less than the magnetizing impedance.

Hence the equivalent circuit is given as in Figure 6.13. Three measurements are taken from the circuit, line voltage, V_{BL}, 3-phase power, $P_{3-ph-BL}$, line current, I_{BL}. From the measurements, the short circuit resistance R_{sc} and short circuit reactance X_{sc} is obtained by solving circuit of Figure 6.13.

$$R_{sc} = R_1 + R_2' \tag{6.6}$$

$$X_{sc} = X_1 + X_2' \tag{6.7}$$

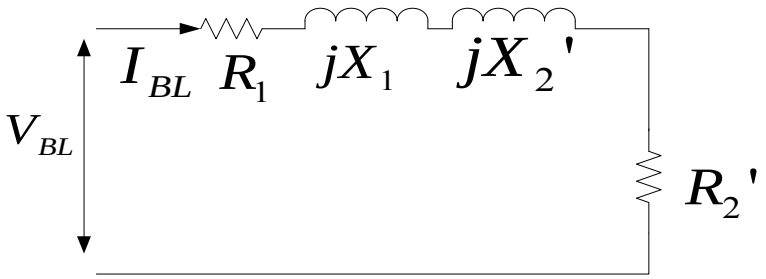

Figure 6.13 Blocked rotor equivalent circuit

Solving Equations (6.4) – (6.7), the no load and locked rotor equivalent parameters are estimated.

6.4.2 Observations and Results from Experimental Methods

For each determined configurations thus considered, no load test and blocked rotor tests are performed to determine the equivalent circuit parameters of the machine.

The DC test is performed to determine the stator resistance that gave DC resistances of 0.99 Ohms in 9-phase, 4-pole and 0.33 Ohms in 3-phase, 12-pole configurations. The conventional two wattmeter method is used for the no load and blocked rotor tests.

Table 6.2 shows the no load observations for 9-phase, 4-pole configuration and Table 6.3 shows locked rotor observations. Figure 6.14 shows the plot of magnetizing inductance vs. mutual flux linkage. Similarly, Figures 6.15 and 6.16 present the plots of sum of leakage inductance and rotor resistance, respectively with change of mutual flux linkage. Table 6.4 shows the no load observations for 3-phase, 12-pole configuration and Table 6.5 presents the locked rotor observations. In Figure 6.17, Magnetizing inductance is plotted in variation with mutual flux linkage.

Table 6.2 No load observation for 9-phase, 4-pole configuration

V_{nl1}	V_{nl2}	I_{nl1}	I_{nl2}	P_1	P_2
252	249	1.44	1.5	245	120
237.4	235.1	1.41	1.35	220	115
221	224	1.27	1.33	190	105
209.5	211.9	1.25	1.2	175	90
195.8	198.14	1.17	1.12	150	80
183.1	181	1.03	1.08	135	70
175.4	173	0.99	1.04	125	65
167.7	165.8	0.95	0.99	115	60
153.7	151.9	0.87	0.91	100	45
139.6	137.7	0.79	0.84	85	40
122.5	120.3	0.72	0.77	70	30
105.3	103.2	0.66	0.71	65	20
90.2	88.4	0.59	0.64	55	15
75.1	73.2	0.53	0.57	45	10
60.2	58.1	0.48	0.52	30	5
45.1	43.6	0.40	0.44	10	5
30.7	28.7	0.34	0.39	5	5
15.3	13.5	0.26	0.32	5	5

Similarly, Figures 6.18 and 6.19 depicts the plot of sum of leakage inductance and rotor resistance, respectively with variation in mutual flux linkage. The magnetizing inductance increases with the increase of mutual flux linkage until the point where magnetic path saturates and it begins to decrease.

Table 6.3 Locked rotor observation for 9-phase, 4-pole configuration

V_1	V_2	I_1	I_2	P_1	P_2
149.5	150	8.7	8.69	500	5
142	144	8.3	8.4	465	5
138.2	139	8.03	8.15	435	5
133.6	134	7.8	7.88	405	5
127.5	128	7.5	7.6	395	5
122	123	7.1	7.2	380	5
118	118.5	6.9	6.8	350	5
113.1	114.2	6.6	6.4	325	5
108.7	109.4	6.29	6.14	295	5
103.2	103.8	5.92	5.77	265	5
V_1	V_2	I_1	I_2	P_1	P_2
98.6	98.3	5.55	5.41	235	5
91.7	92.2	5.14	5.02	205	5
84.9	85.5	4.69	4.58	170	5
77.9	78.4	4.24	4.14	145	5
72.2	72.6	3.86	3.78	120	5
66.8	67.1	3.52	3.44	100	5

Table 6.4 No load observation for 3-phase, 12-pole configuration

V_{nl1}	V_{nl2}	I_1	I_2	P_1	P_2
80.3	80.04	2.75	2.73	130	85
75.4	75.24	2.56	2.55	115	80
69.5	68.97	2.35	2.36	95	75
64.3	64.12	2.23	2.15	80	70
60.6	60.16	2.09	2.07	65	65
55.8	55.38	1.96	1.95	55	60
50.78	50.62	1.83	1.82	45	55
45.95	45.85	1.7	1.7	40	50
39.52	39.43	1.55	1.5	30	45
33.08	32.9	1.45	1.41	20	40

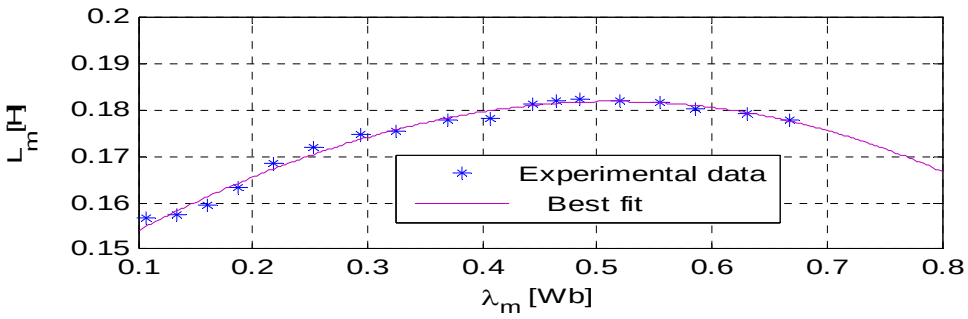

Figure 6.14 Magnetizing inductance vs. mutual flux linkage for 9-phase, 4-pole induction machine

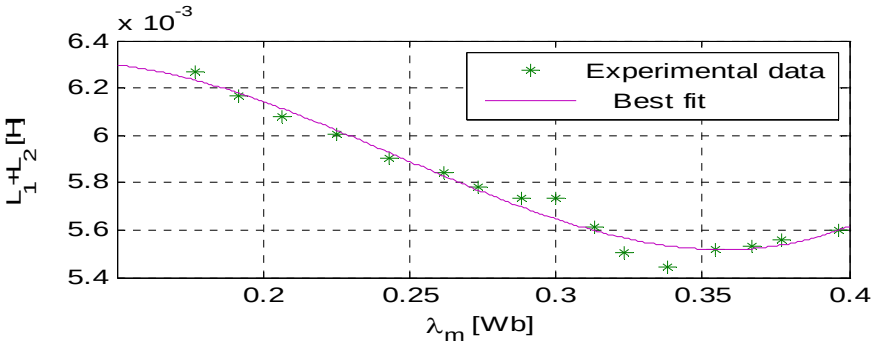

Figure 6.15 Plot of sum of leakage inductance vs. mutual flux linkage for 9-phase, 4-pole induction machine

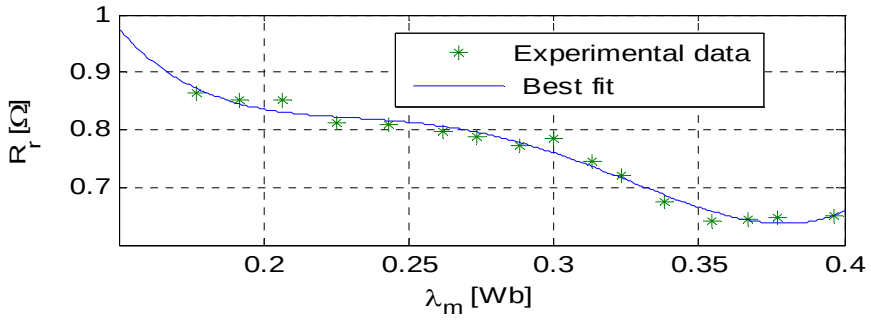

Figure 6.16 Plot of rotor resistance vs. mutual flux linkage for 9-phase, 4-pole induction machine

Table 6.5 Locked rotor observation for 3-phase, 12-pole configuration

Vsc_1	Vsc_2	I_1	I_2	P_1	P_2
43.6	43.5	8.9	8.7	322	15
40.4	40.5	8.1	7.9	275	15
37.3	27.2	7.39	7.21	230	10
34.2	34.1	6.5	6.3	190	5
29.8	29.7	5.6	5.5	140	5
26	25.9	4.82	4.69	105	0
21.1	21.07	3.75	3.69	65	0
14.5	14.5	2.29	2.26	25	0
9.5	9.5	1.26	1.25	15	0

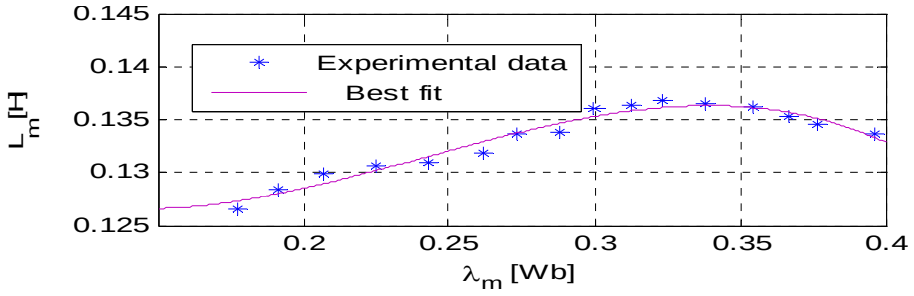

Figure 6.17 Plot of Magnetizing inductance vs. mutual flux linkage for 3-phase, 12-pole induction machine

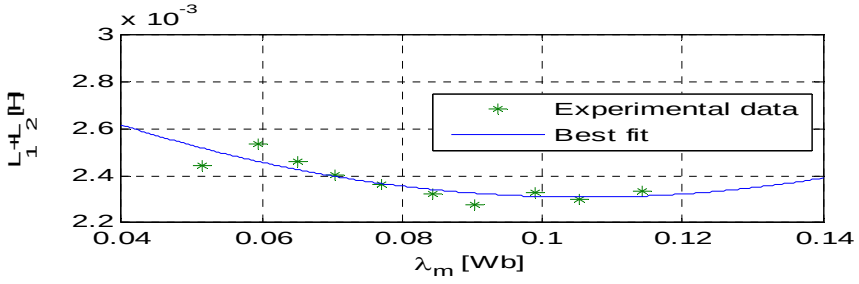

Figure 6.18 Plot of sum of leakage inductance vs. mutual flux linkage for 3-phase, 12-pole induction machine

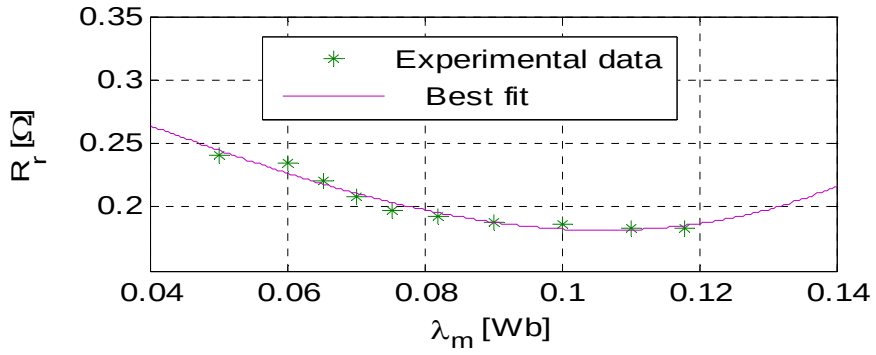

Figure 6.19 Plot of rotor resistance vs. mutual flux linkage for 3-phase, 12-pole induction machine

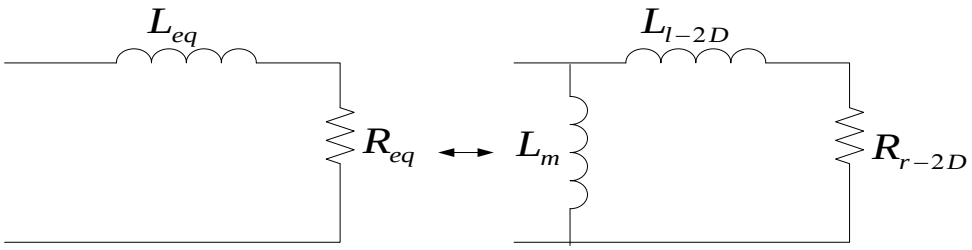

Figure 6.20 Locked rotor equivalent circuit

6.4.3 Finite Element Method

Finite Elements is the method of utilizing the magnetic circuit concept in the form of field analysis. The determination of the parameters using finite elements involves the following steps: [42]

a. For the accurate prediction of iron saturation, the FE simulations are carried out at no-load. (No load test). The frequency is assumed to be zero (rotor reference frame) and magneto static simulations are carried out. In the simulation, the stator currents are assigned within the stator slots. The

magnetizing inductance can be computed from Equation (6.8) with the help of magnetic energy.

$$L_m = \frac{2}{m_s}\left(\frac{2W_m}{I_0^{\,2}}\right) \tag{6.8}$$

where W_m is the magnetic energy extracted from finite elements and I_0 is the injected current.

b. Moreover, the simulation is carried out at locked rotor condition to account the rotor current distribution. The rotor parameters are determined using rotor Joule losses P_{jr} and magnetic energy W_m. The simulations are implemented with varying the frequency such that their effects can be analysed. Equation (6.9) gives the equivalent resistance and inductance parameters in accordance with the locked rotor equivalent circuit of Figure 6.20.

$$R_{eq} = \frac{P_{jr}}{m_s I^2}, \quad L_{eq} = \frac{2}{m_s}\frac{W_m}{I^2} \tag{6.9}$$

The short circuit parameters are evaluated.

$$L_{l,2D} = L_m \frac{L_{eq}\left(L_m - L_{eq}\right) - \left(R_{eq}/\omega_r\right)^2}{\left(L_m - L_{eq}\right)^2 + \left(R_{eq}/\omega_r\right)^2} \tag{6.10}$$

$$R_{r,2D} = R_{eq}\frac{L_m + L_{l,2D}}{L_m - L_{eq}} \tag{6.11}$$

6.4.4 Finite Element Results

The finite element simulation is performed using FEMM and Lua Scripting language. The model is designed using AutoCAD and imported into FEMM for the

analysis. The materials, circuit, blocks and the operating boundaries are specified. The finite element problem is solved using Newton method for both no-load test and blocked rotor. The simulation is carried out as described in previous section for both configurations. Figures 6.21-6.29 illustrate the parameters where the magnetizing inductance is computed over the change of input slot current and mutual flux linkage whereas leakage inductance and rotor resistance is plotted with the change of rotor slip frequency at different currents. As shown in Figure 6.21 and Figure 6.23, the magnetizing inductance decreases with the increase in slot currents due to the armature reaction effects. As shown in Figures 6.25 and 6.26, the leakage inductance increase with the increase of slip frequency until the point where it begins to saturate. Similarly, leakage inductance increases with the increase of current as viewed in Figures 6.25 and 6.26. This is similar for rotor resistance which also increase with the increase of current and slip frequency as shown in Figures 6.28 and 6.29.

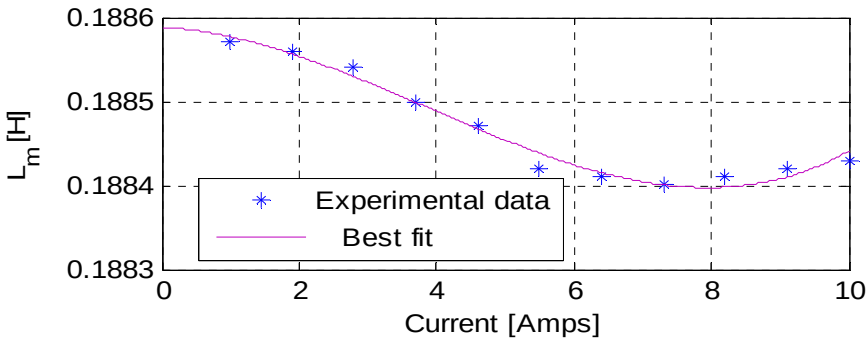

Figure 6.21 Magnetizing inductance vs. current for 9-phase, 4-pole machine

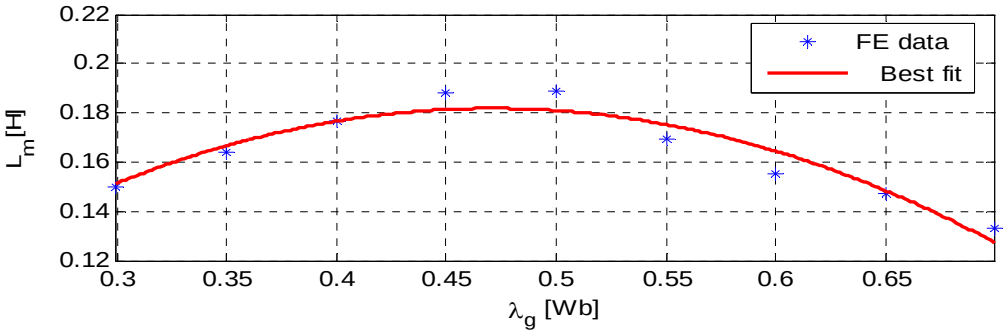

Figure 6.22 Magnetizing inductance vs. air gap flux linkage for 9-phase, 4-pole machine

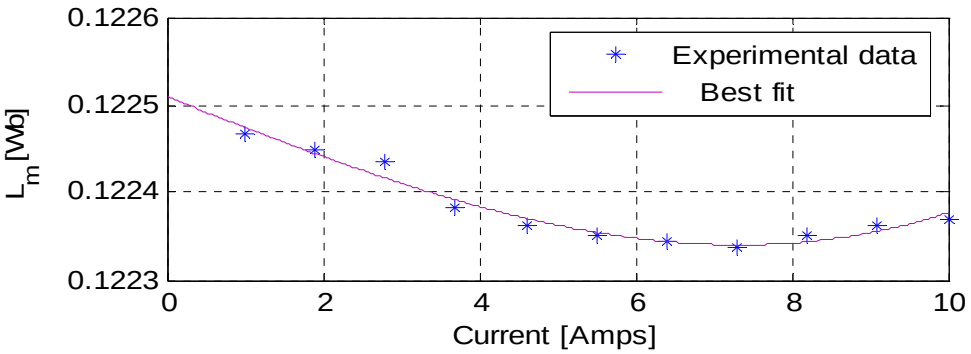

Figure 6.23 Magnetizing inductance vs. current for 3-phase, 12-pole machine

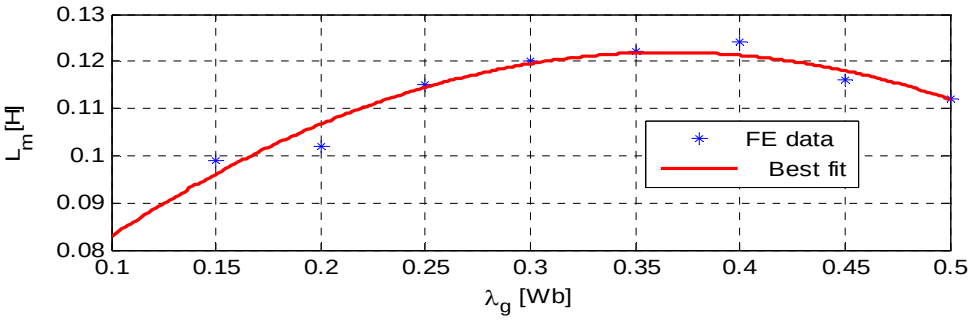

Figure 6.24 Magnetizing inductance vs. air gap flux linkage for 3-phase, 12-pole machine

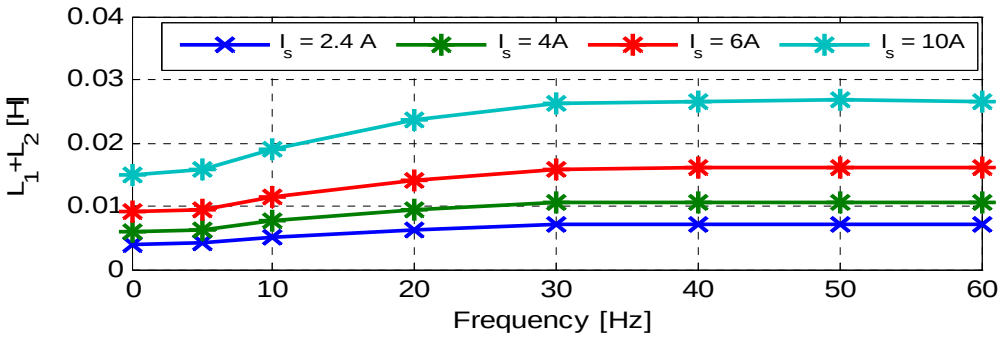

Figure 6.25 Sum of leakage inductance vs. frequency for different peak currents for 9-phase, 4-pole machine

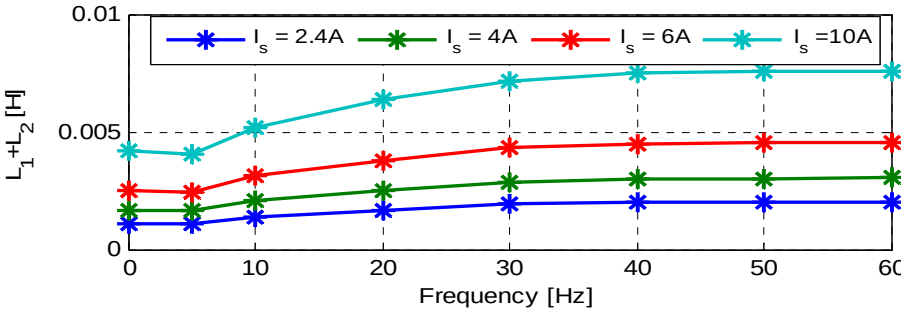

Figure 6.26 Sum of leakage inductance vs. frequency for different peak currents for 3-phase, 12-pole machine

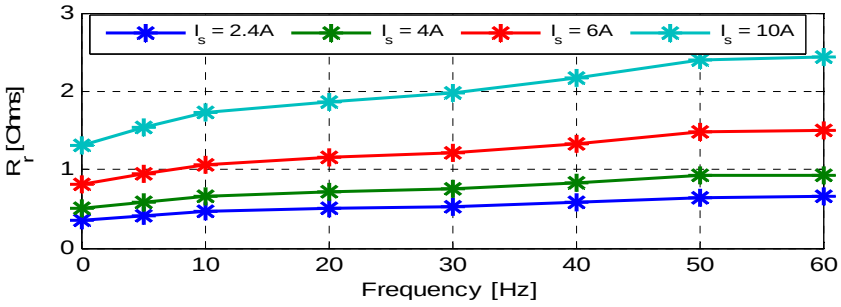

Figure 6.27 Rotor resistance vs. frequency for different peak currents for 9-phase, 4-pole machine

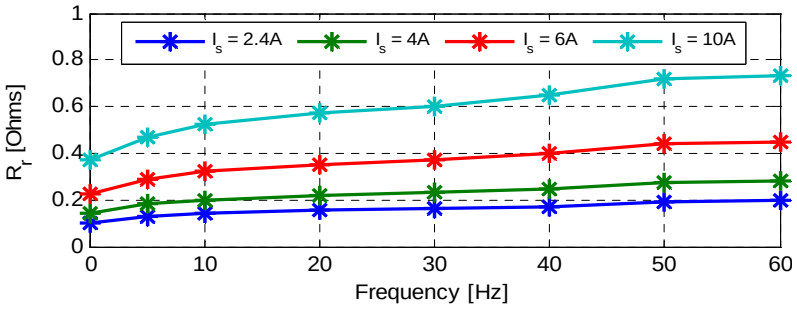

Figure 6.28 Rotor resistance vs. frequency for different peak currents for 3-phase, 12-pole machine

The fundamental component of the winding function for phase 'a' in 9-phase configuration is given as

$$N_s(\omega t) = \frac{2N}{\pi}\sin\omega t = N_s \sin\omega t \tag{6.12}$$

where, N_s is the amplitude of winding function for phase 'a' in 9-phase configuration.

For 3-phase configuration, as depicted in Section (6.1), the resultant MMF of the phases 'a', 'd' and 'g' of 9-phase results in the equivalent MMF of phase 'A' for 3-phase case. Using the resultant of the winding functions of 'a', 'd' and 'g', the winding function for phase 'A' of 3-phase is given as

$$\begin{aligned} N_s(\omega t) &= N\frac{2\left(\sqrt{3}+1\right)}{\pi}[\sin(\omega t+\frac{\pi}{6}] \\ &= N_s'[\sin(\omega t+\frac{\pi}{6}] \end{aligned} \tag{6.13}$$

where, N_s' is the amplitude of winding function for phase 'A' in 3-phase configuration. This amplitude of winding function is utilized in the parameter estimation when dealing with the number of turns per coil side. Now, in order to derive the parameters, some preliminary derivations are performed from the data sheet of the machine.

6.4.5 Preliminary Derivation

In this section, the derivations are performed to get the equivalent dimensions using the parameters from the machine. These parameters are also listed on Appendix C.

Air gap length

$$\begin{aligned} l_g &= 4.754 - 4.75 \\ &= 0.004'' \end{aligned} \tag{6.14}$$

The effective length of stator and rotor:

$$\begin{aligned} l_{ef} &= l_e + 2l_g \\ &= 16.1 + 2 * 0.004 \\ &= 16.108'' \end{aligned} \tag{6.15}$$

The carter coefficient:

$$k_{cs} = \frac{\tau_s}{\tau_s - \frac{2b_0}{\pi}\left\{a\tan\frac{b_0}{2g} - \frac{g}{b_0}\log\left[1+\left(\frac{b_0}{2g}\right)^2\right]\right\}} \tag{6.16}$$

From the given slot details:

$$\begin{aligned} \tau_s &= 0.13 \\ b_0 &= 0.105 \\ g &= 0.004 \end{aligned} \tag{6.17}$$

With these dimensions, the carter coefficient

$$\begin{aligned} k_{cs} &= \frac{0.13}{0.13 - \frac{0.105}{\pi}\left\{a\tan\frac{0.105}{2*0.004} - \frac{0.004}{0.105}\ln\left[1+\left(\frac{0.105}{2*0.004}\right)^2\right]\right\}} \\ &= 1.5011 \end{aligned} \tag{6.18}$$

Since rotor slots are closed type, the Carter's coefficient for rotor, $k_{cr} = 1$

The effective air gap:

$$g_e = k_{cs} k_{cr} l_g$$
$$= 1.5011 * 1 * 0.004 \quad (6.19)$$
$$= 0.0066"$$

Calculation of winding factors

Pitch factor: The pitch of the machine is assumed to be 1.

Hence pitch factor

$$k_{p1} = 1 \quad (6.20)$$

Distribution factor:

Assuming the phase belt to be 60 degrees, the slots per phase belt will be 6 for this machine. The phase belt in per unit of a pole pitch can be expressed by taking the appropriate ratio of slots.

$$\frac{Z}{\tau_p} = \frac{6}{36} = \frac{1}{6} \quad (6.21)$$

Hence,

$$k_{d1} = 0.96$$

Slot opening factor k_{x1}

The slot opening factor is determined using

$$k_{x1} = \frac{\sin(x/2)}{x/2}$$
where (6.22)
$$x = \frac{b_{os}}{\tau_p}\pi = \frac{0.13}{9} * \pi = 0.045$$

Hence

$$k_{x1} = \frac{\sin(0.0225)}{0.0225} = 0.9991 \quad (6.23)$$

Skew factor, k_{s1}

In the calculation, the skew of the stator winding is not supplied, hence

$k_{s1} = 1$

The overall winding factor for the stator winding of the design is given as

$$k_1 = k_{p1} k_{d1} k_{x1} k_{s1} = 1 * 0.96 * 0.9991 * 1 = 0.959 \quad (6.24)$$

Effective radius, $r = 4.7533'$

6.4.6 Magnetizing Inductance of Stator

With the inclusion of harmonics, the magnetizing inductance of the stator is given as

$$L_{msi} = \frac{m_s}{2}\left(\frac{N_{se}}{P}\right)^2 \mu_0 \frac{r l_e}{g_e'} \sum_{h=1}^{\infty}\left(\frac{k_1}{h}\right)^2 \cos(i-1)\frac{2\pi}{m_s} \quad (6.25)$$

where,

$$N_{se} = \frac{4}{\pi} k_1 N_s \quad (6.26)$$

i. For 9-phase, 4-pole,

$$\begin{aligned} &N_s = 24 \\ &m_s = 9 \quad , \; N_{se} = \frac{4}{\pi} 0.959 * 24 = 29.30 \\ &P = 4 \end{aligned} \quad (6.27)$$

Hence, for fundamental component

$$\begin{aligned} L_{ms9\,ph} &= \frac{9}{2}\left(\frac{29.30}{4}\right)^2 \mu_0 \frac{0.12 * 0.408}{0.0001676} \\ &= 0.1888H \end{aligned} \quad (6.28)$$

ii. For 3-phase, 12-pole,

$$N_s = 65.568$$
$$m_s = 3$$
$$P = 12 \qquad , N_{se} = \frac{4}{\pi} 0.959 * 65.568 = 80.06 \tag{6.29}$$

$$L_{ms3ph} = \frac{3}{2}\left(\frac{80.06}{12}\right)^2 \mu_0 \frac{0.12 * 0.408}{0.0001676} \tag{6.30}$$
$$= 0.122H$$

6.4.7 Leakage Inductance of Stator

The leakage inductance of stator is computed using the stator slot configuration. Particularly, it consists of following parts:

Slot leakage inductance

The dimensions of the stator is taken from the machine manual and given in Figure 6.29. Comparing the dimension of the stator and the machine manual,

$$b_0 = 0.105" \qquad d_0 = 0.040" \qquad d_1 = 0.027$$

$$d_2 = 0.027 \qquad d_3 = 0.308 \qquad d_4 = 0.054 \tag{6.31}$$

$$d_5 = 0.308 \qquad d_6 = 0.310" \qquad b_s = 0.310"$$

The specific permeances p_T, p_B and p_{TB} are given as

$$p_T = \mu_0\left[\frac{d_3}{3b_s} + \frac{d_2}{b_s} + \frac{d_1}{b_s - b_0}\log_e\left(\frac{b_s}{b_0}\right) + \frac{d_0}{b_0}\right]$$
$$= \mu_0\left[\frac{0.308}{3 * 0.310} + \frac{0.027}{0.310} + \frac{0.027}{0.310 - 0.105}\log_e\left(\frac{0.310}{0.105}\right) + \frac{0.040}{0.105}\right] \tag{6.32}$$
$$= 1.003 * 10^{-6} H$$

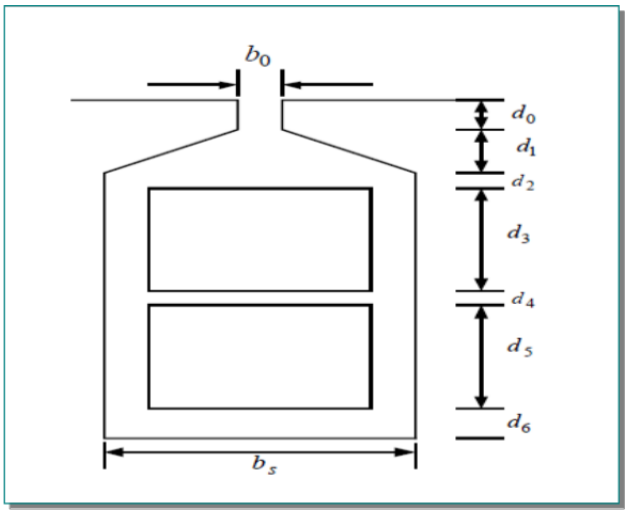

Figure 6.29 Stator slot dimensions for determination of leakage inductance

$$p_B = \mu_0\left[\frac{d_5}{3b_s} + \frac{d_2+d_3+d_4}{b_s} + \frac{d_1}{b_s-b_0}\log_e\left(\frac{b_s}{b_0}\right) + \frac{d_0}{b_0}\right]$$

$$= \mu_0\left[\frac{0.308}{3*0.310} + \frac{0.027+0.308+0.054}{0.310} + \frac{0.027}{0.310-0.105}\log_e\left(\frac{0.310}{0.105}\right) + \frac{0.040}{0.105}\right] \quad (6.33)$$

$$= 2.65*10^{-6}\,H$$

$$p_{TB} = \mu_0\left[\frac{d_3}{2b_s} + \frac{d_2+d_3+d_4}{b_s} + \frac{d_1}{b_s-b_0}\log_e\left(\frac{b_s}{b_0}\right) + \frac{d_0}{b_0}\right]$$

$$= \mu_0\left[\frac{0.308}{2*0.310} + \frac{0.027+0.308+0.054}{0.310} + \frac{0.027}{0.310-0.105}\log_e\left(\frac{0.310}{0.105}\right) + \frac{0.040}{0.105}\right] \quad (6.34)$$

$$= 1.39*10^{-6}\,H$$

Now the inductance per phase is given as

$$L_{phase} = 4m_s N_s^{\,2} l_e \frac{p_s}{S_1} \quad (6.35)$$

where,

$$p_s = \frac{1}{4}\left(p_T + p_B + 2p_{TB}\right)$$
$$= 1.608*10^{-6}\,H/m \quad (6.36)$$

For 9-phase, 4-pole case:

$$L_{phase9} = 4m_s N_s{}^2 l_e \frac{p_s}{S_1}$$
$$= 4(9)(24)^2 (16.1'') \frac{1.608*10^{-6}}{36} \quad (6.37)$$
$$= 0.37mH$$

For 3-phase, 12-pole case:

$$L_{phase3} = 4m_s N_s{}^2 l_e \frac{p_s}{S_1}$$
$$= 4(3)(65.568)^2 (16.1'') \frac{1.608*10^{-6}}{36} \quad (6.38)$$
$$= 0.942mH$$

Zigzag Leakage inductance

For the machine the parameters used to calculate the zigzag leakage inductance:

Stator slot pitch, $\tau_s = \frac{\pi D_{is}}{S} = 0.414'' = 0.0105m$ (6.39)

Stator slot width, $t_1 = \frac{\tau_s}{2} = 0.207'' = 0.00525m$ (6.40)

Since closed type of rotor slot is chosen, the rotor teeth width is equal to the rotor slot width

Hence,

$$t_2 = \frac{\tau_s}{2} = 0.00525m \quad (6.41)$$

The specific permeance corresponding to the zigzag leakage flux is given as

$$p_{zz} = \frac{\mu_0 t_1 t_2 \left(t_1{}^2 + t_2{}^2\right)}{6 g_e t_s{}^3} = 1.64*10^{-6} H/m \quad (6.42)$$

For 9-phase, 4-pole case:

$$L_{zz9} = \frac{4m_s N_s^{\,2}}{S} l_{es} p_{zz} = \frac{4(9)24^2}{36} 16.1 * p_{zz} = 0.138mH \tag{6.43}$$

For 3-phase, 12-pole case:

$$L_{zz3} = \frac{4m_s N_s^{\,2}}{S} l_{es} p_{zz} = \frac{4(3)65.568^2}{36} 16.1 * p_{zz} = 0.961mH \tag{6.44}$$

Skew leakage inductance

Since the number of rotor bars is 44 and rotor slots are skewed, the inductance due to skew is found as

$$L_{lsk} = L_m \left\{ 1 - \left[\frac{\sin(\alpha/2)}{\alpha/2} \right]^2 \right\} \tag{6.45}$$

For 9-phase, 4-pole case:

$$L_{lsk9} = 0.088 \left\{ 1 - \left[\frac{\sin(\pi/44)}{\pi/44} \right]^2 \right\} = 0.149mH \tag{6.46}$$

For 3-phase, 12-pole case:

$$L_{lsk3} = 0.024 \left\{ 1 - \left[\frac{\sin(\pi/44)}{\pi/44} \right]^2 \right\} = 0.0407mH \tag{6.47}$$

The total stator leakage inductance is hence calculated as

$$L_{ls} = L_{lsl} + L_{zz} + L_{lsk} \tag{6.48}$$

For 9-phase, 4-pole case,

$$L_{ls9\,ph} = 0.38 + 0.37 + 0.149 = 0.667mH \tag{6.49}$$

For 3-phase, 12-pole case,

$$L_{ls3\,ph} = 0.942 + 0.961 + 0.0407 = 1.96mH \tag{6.50}$$

Rotor parameters

Rotor slot leakage inductance per bar:

The leakage associated with one rotor bar is computed using the slot dimension again. In rotor bar, particularly the single layered bar is used, hence the specific permeance is given by [40]

$$p_{sl} = \mu_0 \left[\frac{d_{3r}}{3b_{sr}} + \frac{d_{2r}}{b_{sr} - b_{or}} \log_e \left(\frac{b_{sr}}{b_{or}} \right) + \frac{d_{or}}{b_{or}} \right] \tag{6.51}$$

The slot leakage per bar is

$$L_b = n_s{}^2 l_{er} p_{sl} \tag{6.52}$$

where,

$$l_{er} = \frac{l_{es}}{\cos\left(\frac{2\pi}{S_1} \right)} \tag{6.53}$$

$$\begin{aligned} p_{sl} &= \mu_0 \left[\frac{0.604}{3*0.03} + \frac{0.03}{0.06 - 0.03} \log_e \left(\frac{0.03}{0.06} \right) + \frac{0.057}{0.03} \right] \\ &= 9.95*10^{-6} H/m \end{aligned} \tag{6.54}$$

$$l_{er} = \frac{l_{es}}{\cos\left(\frac{2\pi}{S_1} \right)} = 0.0041m \tag{6.55}$$

$$\begin{aligned} L_b &= n_s{}^2 l_{er} p_{sl} \\ &= 1*0.0041*9.95*10^{-6} = 4.11*10^{-8} H \end{aligned} \tag{6.56}$$

For both case of 9-phase, 4-pole machine and 3-phase, 12-pole machine, it is the same.

Rotor end winding inductance per bar

The formula for the end winding inductance per bar of a squirrel cage motor is given by Liwschitz-Garik. The empirical equation is

$$L_{ew} = \mu_0 \left(\frac{4}{9}\right)\left[l_{be} + \kappa \tau_{p2}\right] \tag{6.57}$$

where,

l_{be} : length of the bar from end of core to start of the short circuiting ring

τ_{p2} :rotor pole pitch measured at the middle of the ring

κ :0.18 for P = 2 and 0.09 for P > 2.

Since P > 2,

$$\tau_p = \frac{\pi}{P}\left(D_{or} - 2d_{sr} - d_{re}\right) = \frac{\pi}{4}\left(4.75 - 2*0.801 - 0.06\right) = 3.55'' = 0.09m \tag{6.58}$$

$$L_e = \mu_0 \left(\frac{4}{9}\right)\left(l_{be} + k\tau_{pr(ave)}\right) \tag{6.59}$$

$Here, l_{be} = 0.03''$

Therefore,

$$L_e = \mu_0 \left(\frac{4}{9}\right)\left(l_{be} + k\tau_{pr(ave)}\right) = 5.06*10^{-7} H \tag{6.60}$$

Rotor bar resistance

The length of one rotor bar not including the end ring is

$$l_b = \frac{l_e + 2l_{be}}{\cos\alpha} = 0.414m \tag{6.61}$$

Hence the resistance of one rotor bar is given as

$$r_b = \rho\frac{l_b}{A_b} = \frac{1.6*10^{-8}*0.414}{4.76*10^{-5}} = 1.39*10^{-4} Ohms \tag{6.62}$$

End ring resistance

The tooth pitch at the middle of the end ring can be obtained as

$$\tau_{r2} = \frac{P\tau_{pr(ave)}}{S_r} = 0.00818m \tag{6.63}$$

The resistance of the end winding portion over one rotor slot pitch is,

$$r_e = \rho_{al} \frac{\tau_{r2}}{\alpha_{er}} = 2.74 * 10^{-6} Ohms \tag{6.64}$$

Transformed parameters

For the transformation of parameters from rotor to stator, the following equation is used:

$$T = \frac{4 m_s k_{wsh}{}^2 N_s{}^2}{S_r} \tag{6.65}$$

In case of 9-phase,

$$T = \frac{4 * 9 * 0.959^2 24^2}{44} = 433.4 \tag{6.66}$$

In case of 3-phase,

$$T = \frac{4 * 3 * 0.959^2 65.568^2}{44} = 1078.3 \tag{6.67}$$

6.4.8 Rotor Leakage Inductance

$$L_{be}' = T \left[L_b + \frac{L_e}{2 \sin^2 \left(\frac{P\pi}{S_r} \right)} \right] \tag{6.68}$$

In case of 9-phase,

$$L_{be}' = 433.4 \left[4.11 * 10^{-8} + \frac{5.06 * 10^{-7}}{2 \sin^2 \left(\frac{4 * \pi}{44} \right)} \right] = 0.139 mH \tag{6.69}$$

In case of 3-phase,

$$L_{be}' = 1078.3\left[4.11*10^{-8} + \frac{5.06*10^{-7}}{2\sin^2\left(\frac{12*\pi}{44}\right)}\right] = 0.052mH \tag{6.70}$$

6.4.9 Rotor Resistance

$$R_r' = T\left[R_b + \frac{R_e}{2\sin^2\left(\frac{hP\pi}{S_r}\right)}\right] \tag{6.71}$$

In case of 9-phase,

$$R_r' = 433.4\left[1.39*10^{-4} + \frac{2.74*10^{-6}}{2\sin^2\left(\frac{4\pi}{44}\right)}\right] = 0.67Ohms \tag{6.72}$$

In case of 3-phase,

$$R_r' = 1078.3\left[1.39*10^{-4} + \frac{2.74*10^{-6}}{2\sin^2\left(\frac{12\pi}{44}\right)}\right] = 0.18Ohms \tag{6.73}$$

6.5 Comparison of Parameters using All Methods

Table 6.6 summarizes the parameters obtained under rated current in each methods and Table 6.7 presents the ratio obtained between the 9-phase and 3-phase configurations where k_1, k_2 and k_3 give the ratio for magnetizing inductance, sum of leakage inductances and rotor resistance, respectively. There are more discrepancies in

the ratios especially in the experimental results as expected. The computational and FEM results obtained are comparable since they utilize the same concept of magnetic circuits. The analytical and finite element methods for the determination of the machine parameters have been shown to be adequate and accurate enough for the determination of the parameters of multi-phase machines and other possible connections.

The calculated or measured parameters can now be used for the modelling, analysis and control of the two configurations of the 9-phase induction machine for varying speed-torque requirement.

Table 6.6 Parameters on the rated condition using different methods

Connection	Parameter	Experimental	Computational	FEM
9 ph 4-pole	L_m (H)	0.182	0.188	0.1884
	L_1+L_2 (H)	0.0055	0.0067	0.0065
	R_r (Ω)	0.63	0.67	0.65
3 ph 12-pole	L_m (H)	0.137	0.127	0.123
	L_1+L_2 (H)	0.0021	0.00196	0.0018
	R_r (Ω)	0.15	0.18	0.195

Table 6.7 Comparison of parameters using different methods

Parameter	Experimental	Computational	FEM
k_1	1.32	1.48	1.53
k_2	2.75	3.45	3.61
k_3	4.2	3.72	3.33

6.6 Full Order Modeling and Simulation of 9-phase Induction Machine in Pole Phase Modulation Scheme

6.6.1 Modeling of Stator Winding Circuits

In this section, the coupled full order model of the machine is derived reflecting the distribution of the windings in the stator slots. The turn and winding function concepts are used to calculate the machine parameters with the help of data derived in Section 6.5. Using the clock diagram for 9-phase induction machine as depicted in Figure 6.2, and winding functions of Figures 6.3 and 6.4, the winding functions for each phase of 9-phase induction machine are given as

$$N_a(\theta) = \begin{cases} ns & \mathbf{0} \le \theta \le \dfrac{\pi}{2} \\ -ns & \dfrac{\pi}{2} \le \theta \le \pi \\ ns & \pi \le \theta \le \dfrac{3\pi}{2} \\ -ns & \dfrac{3\pi}{2} \le \theta \le 2\pi \end{cases} \tag{6.74}$$

$$N_b(\theta) = \begin{cases} \text{- ns} & 0 \le \theta \le \dfrac{\pi}{9} \\ \text{ns} & \dfrac{\pi}{9} \le \theta \le \dfrac{11\pi}{18} \\ -\text{ns} & \dfrac{11\pi}{18} \le \theta \le \dfrac{10\pi}{9} \\ \text{ns} & \dfrac{10\pi}{9} \le \theta \le \dfrac{29\pi}{18} \\ -\text{ns} & \dfrac{29\pi}{18} \le \theta \le 2\pi \end{cases} \tag{6.75}$$

$$N_c(\theta)=\begin{cases}\text{- ns} & 0\le\theta\le\dfrac{2\pi}{9}\\ \text{ns} & \dfrac{2\pi}{9}\le\theta\le\dfrac{13\pi}{18}\\ \text{- ns} & \dfrac{13\pi}{18}\le\theta\le\dfrac{11\pi}{9}\\ \text{ns} & \dfrac{11\pi}{9}\le\theta\le\dfrac{31\pi}{18}\\ \text{- ns} & \dfrac{31\pi}{18}\le\theta\le 2\pi\end{cases} \tag{6.76}$$

$$N_d(\theta)=\begin{cases}\text{- ns} & 0\le\theta\le\dfrac{\pi}{3}\\ \text{ns} & \dfrac{\pi}{3}\le\theta\le\dfrac{5\pi}{6}\\ \text{- ns} & \dfrac{5\pi}{6}\le\theta\le\dfrac{4\pi}{3}\\ \text{ns} & \dfrac{4\pi}{3}\le\theta\le\dfrac{11\pi}{6}\\ \text{- ns} & \dfrac{11\pi}{6}\le\theta\le 2\pi\end{cases} \tag{6.77}$$

$$N_e(\theta)=\begin{cases}\text{- ns} & 0\le\theta\le\dfrac{4\pi}{9}\\ \text{ns} & \dfrac{4\pi}{9}\le\theta\le\dfrac{17\pi}{18}\\ \text{- ns} & \dfrac{17\pi}{18}\le\theta\le\dfrac{13\pi}{9}\\ \text{ns} & \dfrac{13\pi}{9}\le\theta\le\dfrac{35\pi}{18}\\ \text{- ns} & \dfrac{35\pi}{18}\le\theta\le 2\pi\end{cases} \tag{6.78}$$

$$N_f(\theta)=\begin{cases}\text{ns} & 0\le\theta\le\dfrac{\pi}{18}\\ \text{-ns} & \dfrac{\pi}{18}\le\theta\le\dfrac{5\pi}{9}\\ \text{ns} & \dfrac{5\pi}{9}\le\theta\le\dfrac{19\pi}{18}\\ \text{-ns} & \dfrac{19\pi}{18}\le\theta\le\dfrac{14\pi}{9}\\ \text{ns} & \dfrac{14\pi}{9}\le\theta\le 2\pi\end{cases} \tag{6.79}$$

$$N_g(\theta)=\begin{cases}\text{ns} & 0\le\theta\le\dfrac{\pi}{6}\\ \text{-ns} & \dfrac{\pi}{6}\le\theta\le\dfrac{2\pi}{3}\\ \text{ns} & \dfrac{2\pi}{3}\le\theta\le\dfrac{7\pi}{6}\\ \text{-ns} & \dfrac{7\pi}{6}\le\theta\le\dfrac{5\pi}{3}\\ \text{ns} & \dfrac{5\pi}{3}\le\theta\le 2\pi\end{cases} \tag{6.80}$$

$$N_h(\theta)=\begin{cases}\text{ns} & 0\le\theta\le\dfrac{5\pi}{18}\\ -\text{ns} & \dfrac{5\pi}{18}\le\theta\le\dfrac{7\pi}{9}\\ \text{ns} & \dfrac{7\pi}{9}\le\theta\le\dfrac{23\pi}{18}\\ -\text{ns} & \dfrac{23\pi}{18}\le\theta\le\dfrac{16\pi}{9}\\ \text{ns} & \dfrac{16\pi}{9}\le\theta\le 2\pi\end{cases} \tag{6.81}$$

$$N_i(\theta)=\begin{cases} \text{ns} & 0\le\theta\le\dfrac{7\pi}{18} \\ -\text{ns} & \dfrac{7\pi}{18}\le\theta\le\dfrac{8\pi}{9} \\ \text{ns} & \dfrac{8\pi}{9}\le\theta\le\dfrac{25\pi}{18} \\ -\text{ns} & \dfrac{25\pi}{18}\le\theta\le\dfrac{17\pi}{9} \\ \text{ns} & \dfrac{17\pi}{9}\le\theta\le 2\pi \end{cases} \tag{6.82}$$

The winding functions thus derived are used to determine the equivalent model of the induction machine. After the winding functions are determined, the self and mutual inductances are calculated using the equations [2]:

$$L_{aa}=\frac{\mu_0 rl}{g}\cdot\int_0^{2\pi} n_a(\theta)\cdot N_a(\theta)\cdot d(\theta) \tag{6.83}$$

$$L_{ab}=\frac{\mu_0 rl}{g}\cdot\int_0^{2\pi} n_a(\theta)\cdot N_b(\theta)\cdot d(\theta) \tag{6.84}$$

6.6.2 Model of the Rotor Squirrel Cage Circuit

The cage formed by the damper bars of the induction machine with *n* bars and two end rings to short circuit all the bars together is considered as *n* identical magnetically coupled circuits. Each circuit is composed of two adjunct rotor bars and segments of the end rings connect two adjacent bars together at both ends. Each bar and end ring segment of the rotor loop is equivalently represented by a serial connection of a resistor and an inductor as shown in Figure (6.30) [45].

The resistance and the inductance of the rotor bar are represented by r_b and l_b, respectively; the resistance and inductance of the partial end winding in the rotor loop are, represented by r_e and l_e, respectively. Three rotor loops are shown in Figure 6.30 and the current flowing through the rotor loops are represented by i_{k-1}, i_k and i_{k+1}, respectively.

Since every rotor loop is treated as an independent phase, a healthy rotor cage having n rotor bars becomes an n phase balanced circuit. The turn function and winding function of a rotor bar considering the skewing is shown in the Figure 6.31 where, α is the ith rotor loop pitch and β is the skew factor. Substituting the turn and winding functions of the ith rotor loop into the general expression for the self-inductance given in Equations (6.83) and (6.84), the self- inductance for the ith rotor loop can be determined.

All the rotor loops have the same self-inductances under the uniform air gap condition, which is given as

$$L_{rr} = \frac{\mu_0 rl}{g_0}\left[\alpha_r - \frac{\beta}{3} - \frac{\alpha_r^{\,2}}{2\pi}\right] \tag{6.85}$$

The mutual inductance between the ith and (i+1)th rotor loop is given as [10]

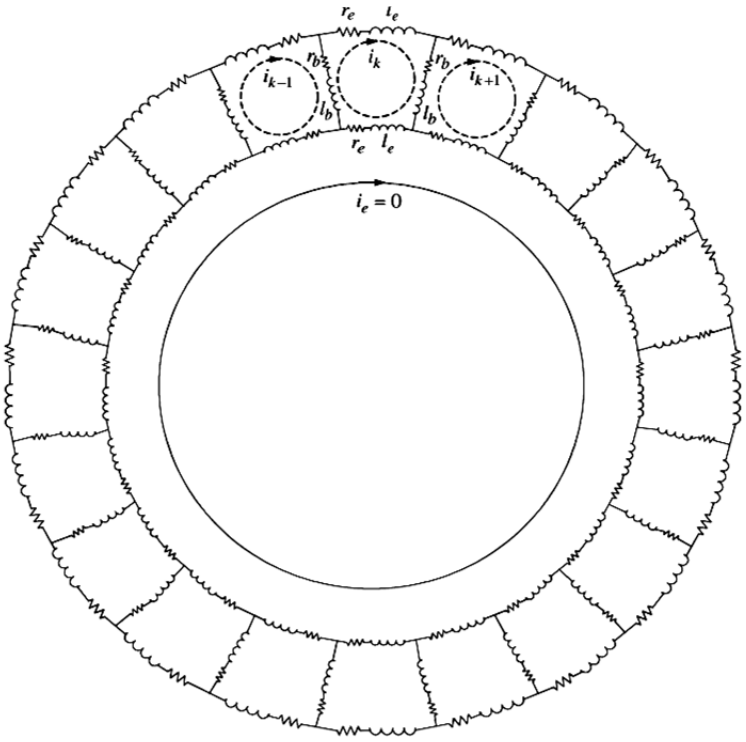

Figure 6.30 Equivalent circuit model of Rotor bars for squirrel cage induction machine

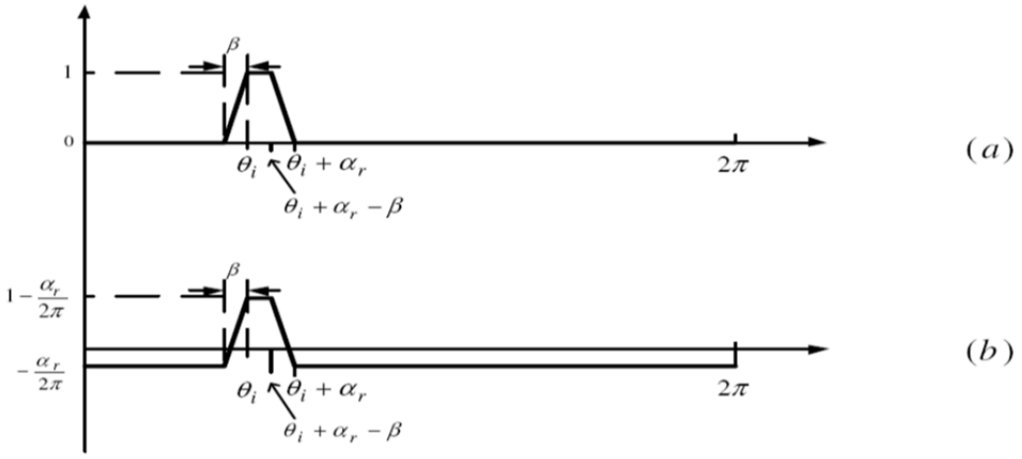

Figure 6.31 Turn and winding functions for equivalent rotor bars

$$L_{rm1} = \frac{\mu_0 rl}{g_0}\left[\frac{\beta}{6} - \frac{\alpha_r{}^2}{2\pi}\right] \tag{6.86}$$

All the mutual inductances between the i-th and the (i+k)th rotor loops have the same values and are given by

$$L_{rm2} = \frac{\mu_0 rl}{g_0}\left[-\frac{\alpha_r{}^2}{2\pi}\right] \tag{6.87}$$

The rotor inductance matrix is given by

$$L_r = \begin{bmatrix} L_{rr}+2(l_b+l_e) & L_{rm1}-l_b & \cdots & L_{rm1}-l_b \\ L_{rm1}-l_b & L_{rr}+2(l_b+l_e) & \cdots & L_{rm2} \\ \vdots & \vdots & \ddots & \vdots \\ L_{rm1}-l_b & L_{rm2} & \cdots & L_{rr}+2(l_b+l_e) \end{bmatrix} \tag{6.88}$$

The rotor resistance matrix can also be formulated using the same model given in Figure 6.30 This matrix is given in Equation (6.89)

$$R_r = \begin{bmatrix} 2(r_b+r_e) & -r_b & \cdots & -r_b \\ -r_b & 2(r_b+r_e) & \cdots & 0 \\ \vdots & \vdots & \ddots & \vdots \\ -r_b & 0 & & 2(r_b+r_e) \end{bmatrix} \tag{6.89}$$

Similarly, the mutual inductance between the stator phase winding and rotor bar can also be formulated.

Using the turn function of rotor bar as derived in Figure 6.31 and winding functions of stator phase windings as derived in Figures 6.2-6.4, the mutual inductance is

$$L_{ij} = \frac{\mu_o rl}{g}\int_0^{2\pi} n_i(\theta)\cdot N_j(\theta)d\theta \tag{6.90}$$

where, ‘i’ denotes the rotor bar number and ‘j’ denotes the stator phase winding number. All the parameters used for this section are derived from Section 6.4.

6.6.3 Voltage and Flux Equations

In this section, the voltage and flux equations used in the modeling of the machine in both configurations are outlined. The voltage equations in real variables for 9-phase machines are

$$V_{abc..is} = r_{abc..is} i_{abc..is} + p\lambda_{abc...is} \tag{6.91}$$

where, $r_{abc..is}$ is a m-dimensional square matrix with the stator resistance values as diagonal element where m is the number of phases The flux linkages, $\lambda_{abc..is}$ is composed of two parts:

$$\lambda_{abc..is} = \lambda_{ss} + \lambda_{sr} = L_{ss} i_{abc..is} + L_{sr} i_{r123..n} \tag{6.92}$$

where, the first term represents the flux linkages due to the stator currents and the second term gives the flux linkages due to the rotor currents.

In Equation (6.92), the self-inductance matrix, L_{ss} and L_{sr} are given by Equation (6.93), where the matrix elements are determined using the turns and winding functions.

$$L_{ss} = \begin{bmatrix} L_{aa} & L_{ab} & .... & L_{ah} & L_{ai} \\ L_{ba} & L_{bb} & .... & L_{bh} & L_{bi} \\ . & . & . & . & . \\ . & . & . & . & . \\ L_{ia} & L_{ib} & .... & L_{ih} & L_{ii} \end{bmatrix} \tag{6.93}$$

$$, L_{sr} = \begin{bmatrix} L_{a1} & L_{a2} & .... & L_{a(n-1)} & L_{an} \\ L_{b1} & L_{b2} & .... & L_{b(n-1)} & L_{bn} \\ . & . & . & . & . \\ . & . & . & . & . \\ L_{i1} & L_{i2} & .... & L_{i(n-1)} & L_{in} \end{bmatrix} \tag{6.94}$$

In the similar way, the rotor voltage equations are given as

$$V_{r123..n} = R_r i_{r123..n} + p\lambda_{r123..n} \tag{6.95}$$

In this case also, R_r is the n by n matrix derived in Equation (6.89). The flux linkage matrix is also composed of two parts.

$$\lambda_{r123..n} = \lambda_{rr} + \lambda_{rs} = L_r i_{r123..n} + L_{rs} i_{abc..i} \tag{6.96}$$

The first term gives the flux linkages due to the rotor currents and second term gives the flux linkages due to the stator currents. The synchronous reference frame transformation is used to transform the above voltage and flux equations into the q-d reference frame to simplify the model and aid in computer simulations.

For the stator and rotor circuits, the transformation matrices are given respectfully as

$$T_s = \frac{2}{m}\begin{pmatrix} \cos(\theta) & \cos\left(\theta - \frac{2\pi}{m}\right) & \cdots & \cos\left(\theta - \frac{2(m-1)\pi}{m}\right) \\ \sin(\theta) & \sin\left(\theta - \frac{2\pi}{m}\right) & \cdots & \sin\left(\theta - \frac{2(m-1)\pi}{m}\right) \end{pmatrix} \tag{6.97}$$

$$T_r = \frac{2}{n}\begin{pmatrix} \cos(\theta - \theta_r) & \cos\left(\theta - \theta_r - \frac{2\pi}{n}\right) & \cdots & \cos\left(\theta - \theta_r - \frac{2(n-1)\pi}{n}\right) \\ \sin(\theta) & \sin\left(\theta - \theta_r - \frac{2\pi}{n}\right) & \cdots & \sin\left(\theta - \theta_r - \frac{2(n-1)\pi}{n}\right) \end{pmatrix} \tag{6.98}$$

where m and n are the numbers of stator phases and rotor bars, respectively. In the coupled circuit model, the analysis is performed in rotor reference frame. i.e., $\omega = \omega_r$.

Hence the transformed voltage and flux equations are

$$\begin{aligned} V_{qs} &= r_{qs} i_{qs} + \omega\lambda_{ds} + p\lambda_{qs} \\ V_{ds} &= r_{ds} i_{ds} + -\omega\lambda_{qs} + p\lambda_{ds} \end{aligned} \tag{6.99}$$

$$\begin{aligned} V_{qr} &= r_{qr} i_{dr} + (\omega - \omega_r)\lambda_{dr} + p\lambda_{qr} \\ V_{dr} &= r_{dr} i_{dr} - (\omega - \omega_r)\lambda_{qr} + p\lambda_{dr} \end{aligned} \tag{6.100}$$

where, $r_{qs}, r_{ds}, r_{qr}, r_{dr}, \omega, \omega_r$ give the q and d axis stator resistances, q and d axis rotor resistances, fundamental speed of stator circuit and fundamental speed of rotor circuit, respectively.

$$\begin{aligned} \lambda_{qs} &= L_{qs} i_{qs} + L_{qsr} i_{qr} \\ \lambda_{ds} &= L_{ds} i_{ds} + L_{dsr} i_{dr} \\ \lambda_{qr} &= L_{qr} i_{qr} + L_{qrs} i_{qs} \\ \lambda_{dr} &= L_{dr} i_{dr} + L_{drs} i_{ds} \end{aligned} \tag{6.101}$$

where, $L_{qs}, L_{ds}, L_{qr}, L_{dr}$ are the q and d axis stator self-inductances and q and d axis rotor self-inductances. Similarly, the mutual inductances between the stator-rotor inductances and rotor-stator inductances are assigned as $L_{qsr}, L_{dsr}, L_{qrs}, L_{drs}$, respectively. These q and d axis inductances are derived after the reference frame transformation of Equations (6.91) - (6.96).

The speed and torque dynamics are given as

$$\begin{aligned} T_e &= \frac{mP}{4}\left[\lambda_{ds} i_{qs} - \lambda_{qs} i_{ds}\right] \\ \frac{2J}{P} p\omega_r &= T_e - T_L \end{aligned} \tag{6.102}$$

6.7 Full Order Model of 9-phase Induction Machine

The stator flux equation in real variable form is given as

$$\lambda_{abc...is} = L_{abc..is} i_{abc...is} + L_{abc..isabc...nr} i_{abc...nr} \tag{6.103}$$

Using reference frame transformation with any arbitrary angle θ in Equation (6.103),

$$T(\theta)\lambda_{abc...is} = T(\theta)L_{abc...is} i_{abc...is} + T(\theta)L_{abc..isabc...nr} i_{abc....nr} \tag{6.104}$$

The flux linkage due to stator currents is given by first term of RHS of Equation (6.104). Hence, derivation of the stator self-inductances only involves the first part of RHS of Equation (6.104).

Suppose, $T(\theta) = T(\theta - \theta_x)T(\theta_x)$ (6.105)

Hence first term in RHS of Equation (4.3) becomes,

$$\begin{aligned} T(\theta)L_{abc...is} i_{abc..is} &= T(\theta - \theta_x)T(\theta_x)L_{abc..is} i_{abc..is} \\ &= T(\theta - \theta_x)T(\theta_x)L_{abc...is}T(\theta_x)^{-1}T(\theta - \theta_x)^{-1} i_{qdoxs} \end{aligned} \tag{6.106}$$

Assume the operation in rotor reference mode, i.e., $\theta = \theta_r$ and $\theta_x = 0$.

Hence,

$$\begin{aligned} T(\theta)L_{abc.....is} i_{abc.....is} &= T(\theta_r)\ \underbrace{T(0)L_{abc....is}T(0)^{-1}}_{\textbf{Stationary Reference Frame}}\ T(\theta_r)^{-1} i_{qdoxs} \\ &= L_{qdoxs} i_{qdoxs} \end{aligned} \tag{6.107}$$

As observed in Equation (6.107), the middle terms imply the stationary reference transformation of the stator inductance matrix. According to the basic relation between inductance and winding functions, inductance between ‘i’ and ‘j’ is given as

$$L_{ij} = \frac{\mu_0 rl}{g}\int_0^{2\pi} N_i(\phi)N_j(\phi)d\phi \tag{6.108}$$

Hence, for stator phases,

$$T(0)L_{abc....is}T(0)^{-1}$$

$$= \frac{\mu_0 rl}{g}\int_0^{2\pi} T(0)\begin{bmatrix} N_a^2 & N_aN_b & N_aN_c & N_aN_d & N_aN_e & N_aN_f & N_aN_g & N_aN_h & N_aN_i \\ N_aN_b & N_b^2 & N_bN_c & N_bN_d & N_bN_e & N_bN_f & N_bN_g & N_bN_h & N_bN_i \\ N_aN_c & N_bN_c & N_c^2 & N_cN_d & N_cN_e & N_cN_f & N_cN_g & N_cN_h & N_cN_i \\ N_aN_d & N_bN_d & N_cN_d & N_d^2 & N_dN_e & N_dN_f & N_dN_g & N_dN_h & N_dN_i \\ N_aN_e & N_bN_e & N_cN_e & N_dN_e & N_e^2 & N_eN_f & N_eN_g & N_eN_h & N_eN_i \\ N_aN_f & N_bN_f & N_cN_f & N_dN_f & N_eN_f & N_f^2 & N_fN_g & N_fN_h & N_fN_i \\ N_aN_g & N_bN_g & N_cN_g & N_dN_g & N_eN_g & N_fN_g & N_g^2 & N_gN_h & N_gN_i \\ N_aN_h & N_bN_h & N_cN_h & N_dN_h & N_eN_h & N_fN_h & N_gN_h & N_h^2 & N_hN_i \\ N_aN_i & N_bN_i & N_cN_i & N_dN_i & N_eN_i & N_fN_i & N_gN_i & N_hN_i & N_i^2 \end{bmatrix} T(0)^{-1}$$

Hence,

$$T(0)L_{abc....is}T(0)^{-1} = \mu_0 rl\int_0^{2\pi} T(0)ABT(0)^{-1} \tag{6.109}$$

where,

$$A = \begin{bmatrix} N_a & N_a & N_a & N_a & N_a & N_a & N_a & N_a & N_a \\ N_b & N_b & N_b & N_b & N_b & N_b & N_b & N_b & N_b \\ N_c & N_c & N_c & N_c & N_c & N_c & N_c & N_c & N_c \\ N_d & N_d & N_d & N_d & N_d & N_d & N_d & N_d & N_d \\ N_e & N_e & N_e & N_e & N_e & N_e & N_e & N_e & N_e \\ N_f & N_f & N_f & N_f & N_f & N_f & N_f & N_f & N_f \\ N_g & N_g & N_g & N_g & N_g & N_g & N_g & N_g & N_g \\ N_h & N_h & N_h & N_h & N_h & N_h & N_h & N_h & N_h \\ N_i & N_i & N_i & N_i & N_i & N_i & N_i & N_i & N_i \end{bmatrix} \tag{6.110}$$

$$B = \begin{bmatrix} N_a & 0 & 0 & 0 & 0 & 0 & 0 & 0 & 0 \\ 0 & N_b & 0 & 0 & 0 & 0 & 0 & 0 & 0 \\ 0 & 0 & N_c & 0 & 0 & 0 & 0 & 0 & 0 \\ 0 & 0 & 0 & N_d & 0 & 0 & 0 & 0 & 0 \\ 0 & 0 & 0 & 0 & N_e & 0 & 0 & 0 & 0 \\ 0 & 0 & 0 & 0 & 0 & N_f & 0 & 0 & 0 \\ 0 & 0 & 0 & 0 & 0 & 0 & N_g & 0 & 0 \\ 0 & 0 & 0 & 0 & 0 & 0 & 0 & N_h & 0 \\ 0 & 0 & 0 & 0 & 0 & 0 & 0 & 0 & N_i \end{bmatrix} \tag{6.111}$$

Now, applying stationary reference transformation to matrix A,

$$T(0)A=\begin{bmatrix} N_{q1} & N_{q1} & N_{q1} & N_{q1} & N_{q1} & N_{q1} & N_{q1} & N_{q1} & N_{q1} \\ N_{d1} & N_{d1} & N_{d1} & N_{d1} & N_{d1} & N_{d1} & N_{d1} & N_{d1} & N_{d1} \\ N_{q3} & N_{q3} & N_{q3} & N_{q3} & N_{q3} & N_{q3} & N_{q3} & N_{q3} & N_{q3} \\ N_{d3} & N_{d3} & N_{d3} & N_{d3} & N_{d3} & N_{d3} & N_{d3} & N_{d3} & N_{d3} \\ N_{q5} & N_{q5} & N_{q5} & N_{q5} & N_{q5} & N_{q5} & N_{q5} & N_{q5} & N_{q5} \\ N_{d5} & N_{d5} & N_{d5} & N_{d5} & N_{d5} & N_{d5} & N_{d5} & N_{d5} & N_{d5} \\ N_{q7} & N_{q7} & N_{q7} & N_{q7} & N_{q7} & N_{q7} & N_{q7} & N_{q7} & N_{q7} \\ N_{d7} & N_{d7} & N_{d7} & N_{d7} & N_{d7} & N_{d7} & N_{d7} & N_{d7} & N_{d7} \\ N_0 & N_0 & N_0 & N_0 & N_0 & N_0 & N_0 & N_0 & N_0 \end{bmatrix} \tag{6.112}$$

Multiplying Equation (4.13) with $BT(0)^{-1}$, the resulting equations is written as

$$T(0)ABT(0)^{-1}=\begin{bmatrix} N_{q1}^{\ 2} & N_{q1d1} & N_{q1q3} & N_{q1d3} & N_{q1q5} & N_{q1d5} & N_{q1q7} & N_{q1d7} & N_{q10} \\ N_{q1d1} & N_{d1}^{\ 2} & N_{d1q3} & N_{d1d3} & N_{d1q5} & N_{d1d5} & N_{d1q7} & N_{d1d7} & N_{d10} \\ N_{q3q1} & N_{q3d1} & N_{q3}^{\ 2} & N_{q3d3} & N_{q3q5} & N_{q3d5} & N_{q3q7} & N_{q3d7} & N_{q30} \\ N_{d3q1} & N_{d1d3} & N_{q3d3} & N_{d3}^{\ 2} & N_{d3q5} & N_{d3d5} & N_{d3q7} & N_{d3d7} & N_{d30} \\ N_{q1q5} & N_{d1q5} & N_{q3q5} & N_{d3q5} & N_{q5}^{\ 2} & N_{q5d5} & N_{q5q7} & N_{q5d7} & N_{q50} \\ N_{q1d5} & N_{d1d5} & N_{q3d5} & N_{d3d5} & N_{q5d5} & N_{d5}^{\ 2} & N_{d5q7} & N_{d5d7} & N_{d50} \\ N_{q1q7} & N_{d1q7} & N_{q3q7} & N_{d3q7} & N_{q5q7} & N_{d5q7} & N_{q7}^{\ 2} & N_{q7d7} & N_{q70} \\ N_{q1d7} & N_{d1d7} & N_{q3d7} & N_{d3d7} & N_{q5d7} & N_{d5d7} & N_{q7d7} & N_{d7}^{\ 2} & N_{d70} \\ N_{q10} & N_{d10} & N_{q30} & N_{d30} & N_{q50} & N_{d50} & N_{q70} & N_{d70} & N_0^{\ 2} \end{bmatrix} \tag{6.113}$$

Again, from Equation (6.107),

$$L_{qdoxs}=T(\theta_r)T(0)L_{abc....is}T(0)^{-1}T(\theta_r)^{-1} \tag{6.114}$$

6.7.1 Derivation of Stator Inductances

The inductances are derived with the help of Equation (6.114). The inductances are calculated and plotted with the change of rotor angle. Since it is an induction machine, it will give constant value of inductances for both q and d-axis. Figures 6.32-6.39 show the self-harmonic inductances of corresponding harmonics.

Proceeding in the same way for the inter-harmonic inductances, Figure 6.40 depict the mutual harmonic inductances between fundamental and 3rd harmonics.

It gives the value of inter-harmonic inductance to be zero. Hence, the inter-harmonic inductance in 9-phase machines is zero. Also, proceeding for the rotor circuits considering each harmonics as in Chapter 4, the q and d axis inductances can be obtained. Figures 6.41-6.48 shows the self-harmonic rotor inductances of corresponding harmonics. Proceeding the same way as Chapter 4, Figures 6.49-6.56 shows the stator-rotor mutual inductances for corresponding harmonics.

6.7.2 Model of the System

Voltage and flux equations for stator

$$
\begin{aligned}
V_{q1s} &= r_s i_{q1s} + \omega\lambda_{d1s} + p\lambda_{q1s} \\
V_{d1s} &= r_s i_{d1s} - \omega\lambda_{q1s} + p\lambda_{d1s} \\
V_{q3s} &= r_s i_{q3s} + 3\omega\lambda_{d3s} + p\lambda_{q3s} \\
V_{d3s} &= r_s i_{d3s} - 3\omega\lambda_{q3s} + p\lambda_{d3s} \\
V_{q5s} &= r_s i_{q5s} + 5\omega\lambda_{d5s} + p\lambda_{q5s} \\
V_{d5s} &= r_s i_{d5s} - 5\omega\lambda_{q5s} + p\lambda_{d5s} \\
V_{q7s} &= r_s i_{q7s} + 7\omega\lambda_{d7s} + p\lambda_{q7s} \\
V_{d7s} &= r_s i_{d7s} - 7\omega\lambda_{q7s} + p\lambda_{d7s} \\
V_{0s} &= r_s i_{0s} + p\lambda_{os}
\end{aligned}
\tag{6.115}
$$

$$
\begin{aligned}
\lambda_{q1s} &= L_{q1s} i_{q1s} + L_{q1sr} i_{q1r} \\
\lambda_{d1s} &= L_{d1s} i_{d1s} + L_{d1sr} i_{d1r} \\
\lambda_{q3s} &= L_{q3s} i_{q3s} + L_{q3sr} i_{q3r} \\
\lambda_{d3s} &= L_{d3s} i_{d3s} + L_{d3sr} i_{d3r} \\
\lambda_{q5s} &= L_{q5s} i_{q5s} + L_{q5sr} i_{q5r} \\
\lambda_{d5s} &= L_{d5s} i_{d5s} + L_{d5sr} i_{d5r} \\
\lambda_{q7s} &= L_{q7s} i_{q7s} + L_{q7sr} i_{q7r} \\
\lambda_{d7s} &= L_{d7s} i_{d7s} + L_{d7sr} i_{d7r}
\end{aligned}
\tag{6.116}
$$

Voltage and flux equations for rotor

$$
\begin{aligned}
V_{q1r} &= r_r i_{q1r} + (\omega - \omega_r)\lambda_{d1r} + p\lambda_{q1r} \\
V_{d1r} &= r_r i_{d1r} - (\omega - \omega_r)\lambda_{q1r} + p\lambda_{d1r} \\
V_{q3r} &= r_r i_{q3r} + 3(\omega - \omega_r)\lambda_{d3r} + p\lambda_{q3r} \\
V_{d3r} &= r_r i_{d3r} - 3(\omega - \omega_r)\lambda_{q3r} + p\lambda_{d3r} \\
V_{q5r} &= r_r i_{q5r} + 5(\omega - \omega_r)\lambda_{d5r} + p\lambda_{q5r} \\
V_{d5r} &= r_s i_{d5r} - 5(\omega - \omega_r)\lambda_{q5r} + p\lambda_{d5r} \\
V_{q7r} &= r_r i_{q7r} + 7(\omega - \omega_r)\lambda_{d7r} + p\lambda_{q7r} \\
V_{d7r} &= r_r i_{d7r} - 7(\omega - \omega_r)\lambda_{q7r} + p\lambda_{d7r} \\
V_{0r} &= r_r i_{0r} + p\lambda_{or}
\end{aligned}
\tag{6.117}
$$

$$
\begin{aligned}
\lambda_{q1r} &= L_{q1r} i_{q1r} + L_{q1sr} i_{q1s} \\
\lambda_{d1r} &= L_{d1r} i_{d1r} + L_{d1sr} i_{d1s} \\
\lambda_{q3r} &= L_{q3r} i_{q3r} + L_{q3sr} i_{q3s} \\
\lambda_{d3r} &= L_{d3r} i_{d3r} + L_{d3sr} i_{d3s} \\
\lambda_{q5r} &= L_{q5r} i_{q5r} + L_{q5sr} i_{q5s} \\
\lambda_{d5r} &= L_{d5r} i_{d5r} + L_{d5sr} i_{d5s} \\
\lambda_{q7r} &= L_{q7r} i_{q7r} + L_{q7sr} i_{q7s} \\
\lambda_{d7r} &= L_{d7r} i_{d7r} + L_{d7sr} i_{d7s}
\end{aligned}
\tag{6.118}
$$

Using the voltage and flux equations in 6.114-6.116, Figure 6.58 shows the Equivalent circuit of the full order model.

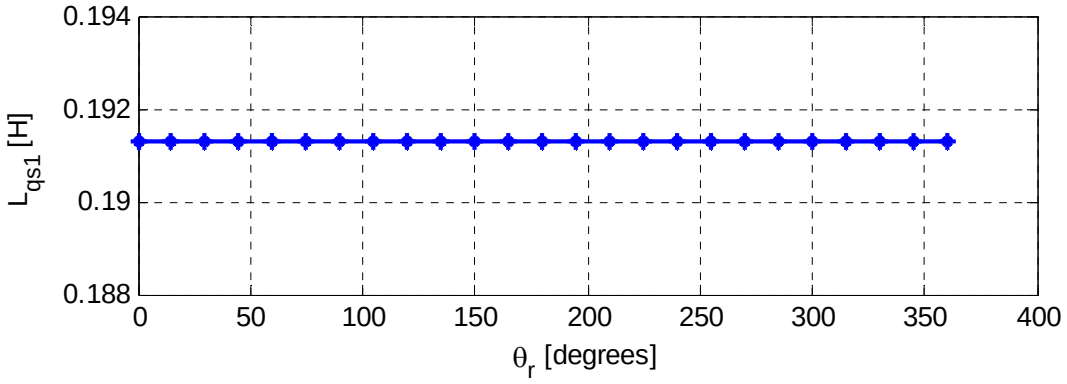

Figure 6.32 q-axis stator fundamental self-inductance of 9-phase induction machine

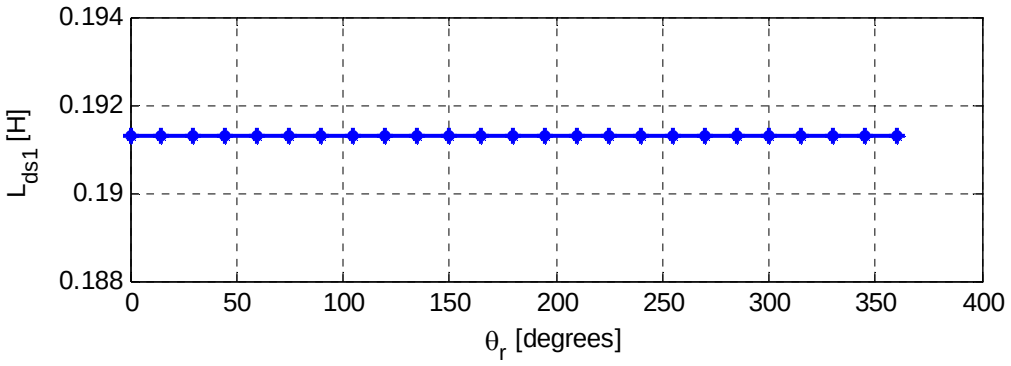

Figure 6.33 d-axis stator fundamental self-inductance of 9-phase induction machine

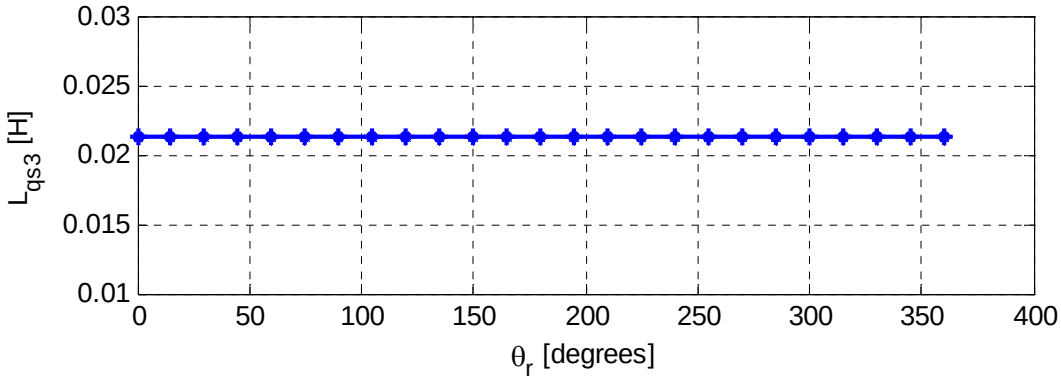

Figure 6.34 q-axis stator 3rd harmonic self-inductance of 9-phase induction machine

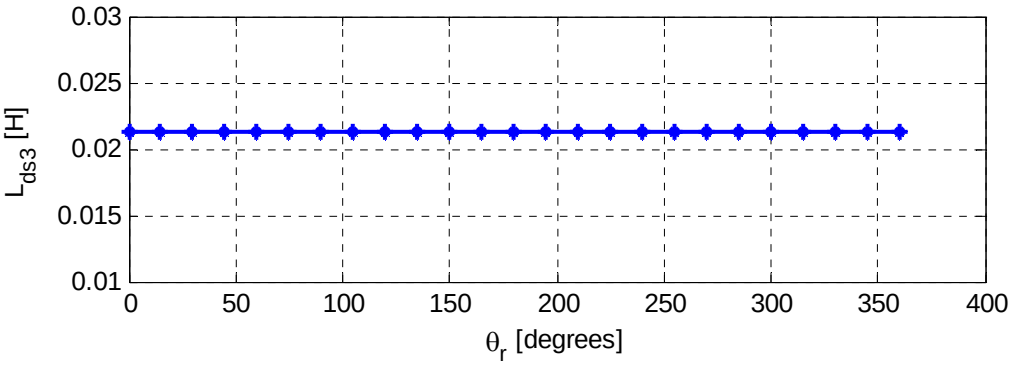

Figure 6.35 d-axis stator 3rd harmonic self-inductance of 9-phase induction machine

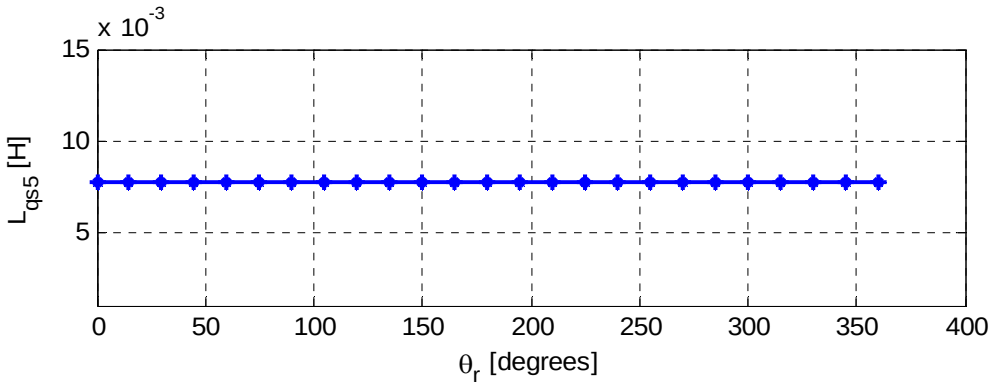

Figure 6.36 q-axis stator 5th harmonic self-inductance of 9-phase induction machine

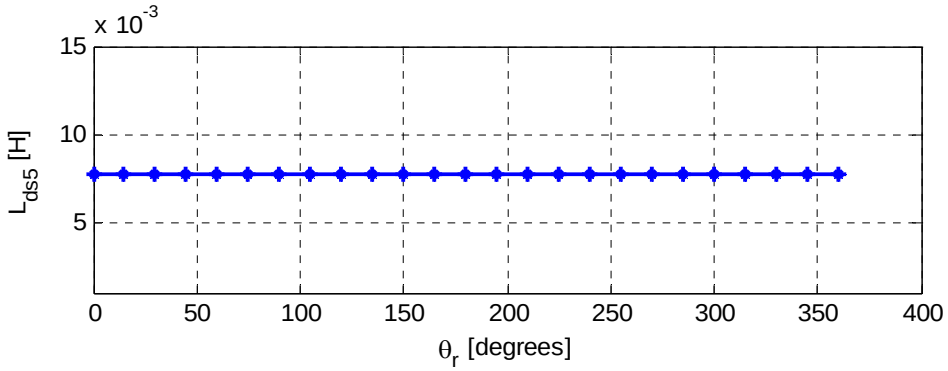

Figure 6.37 d-axis stator 5th harmonic self-inductance of 9-phase induction machine

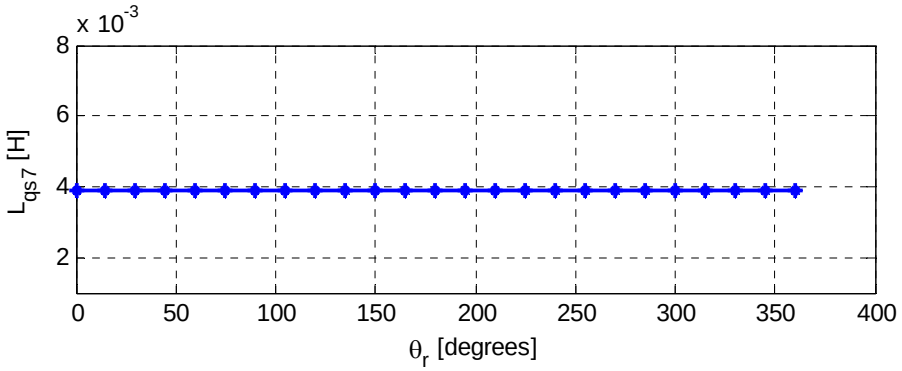

Figure 6.38 q-axis stator 7th harmonic self-inductance of 9-phase induction machine

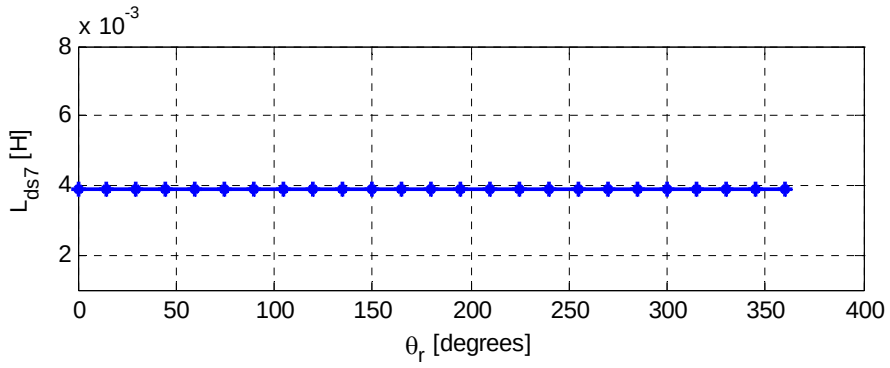

Figure 6.39 d-axis stator 7th harmonic self-inductance of 9-phase induction machine

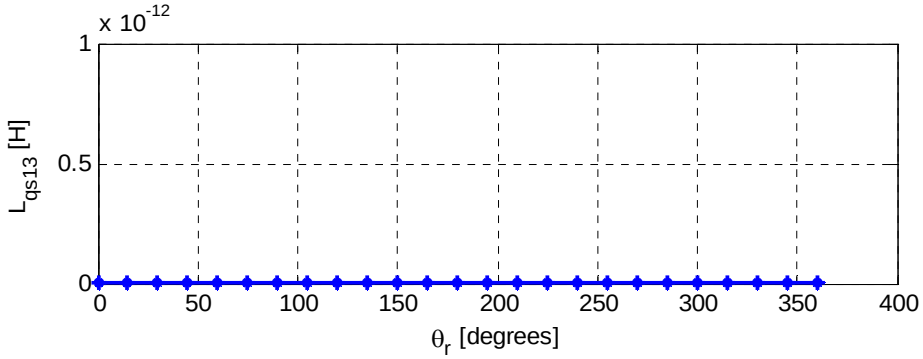

Figure 6.40 q-axis stator fundamental and 3rd harmonic inter-harmonic inductance of 9-phase induction machine

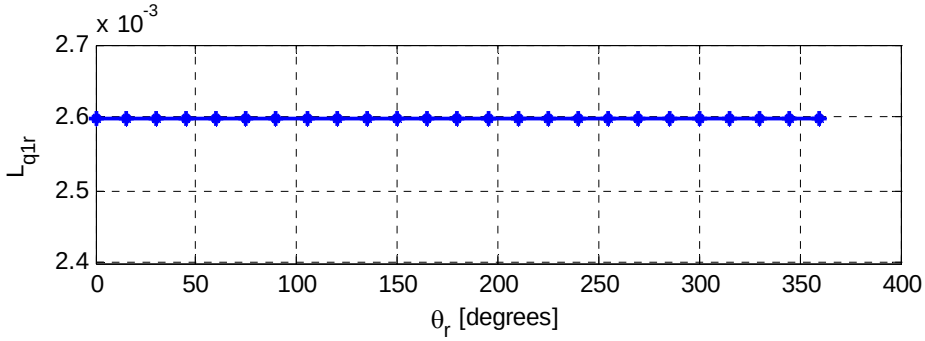

Figure 6.41 q-axis rotor fundamental self-inductance of 9-phase induction machine

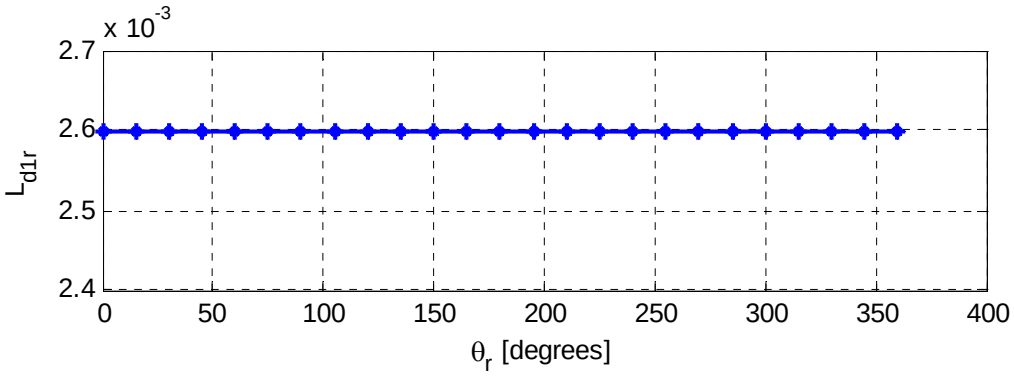

Figure 6.42 d-axis rotor fundamental self-inductance of 9-phase induction machine

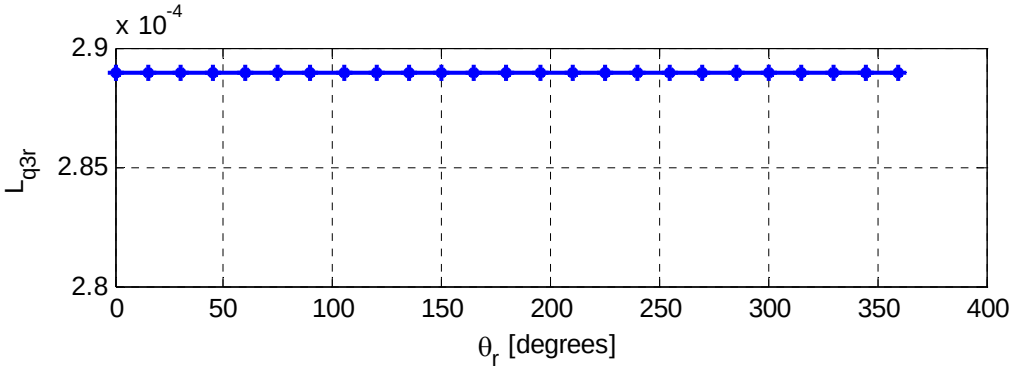

Figure 6.43 q-axis rotor 3rd harmonics self-inductance of 9-phase induction machine

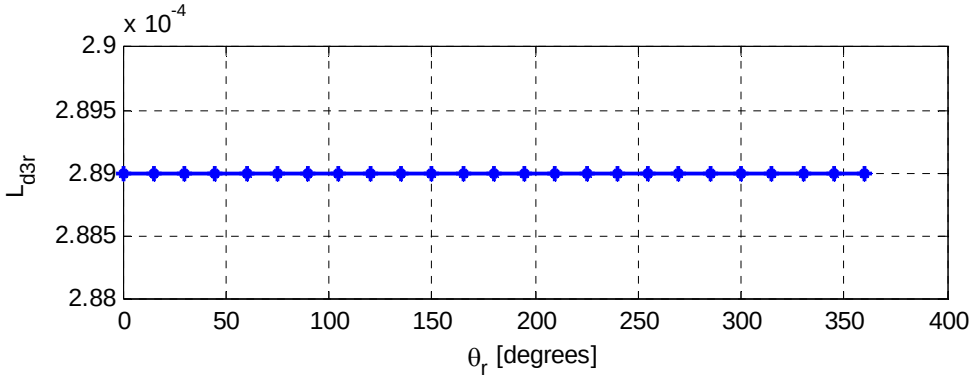

Figure 6.44 d-axis 3rd harmonics rotor self-inductance of 9-phase induction machine

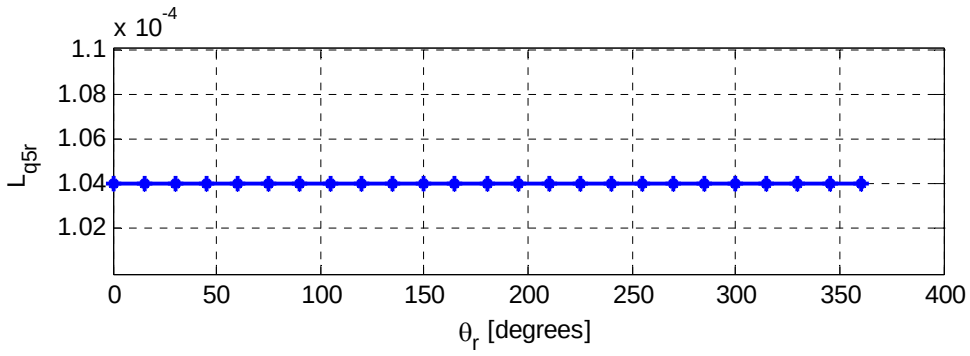

Figure 6.45 q-axis 5th harmonic rotor self-inductance of 9-phase induction machine

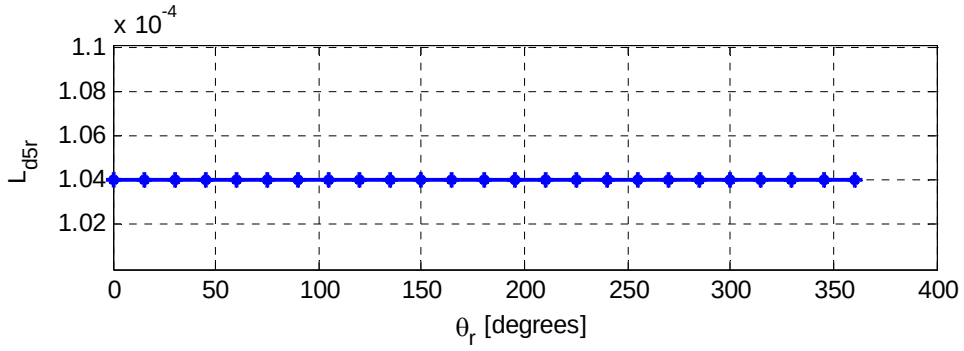

Figure 6.46 d-axis 5th harmonic rotor self-inductance of 9-phase induction machine

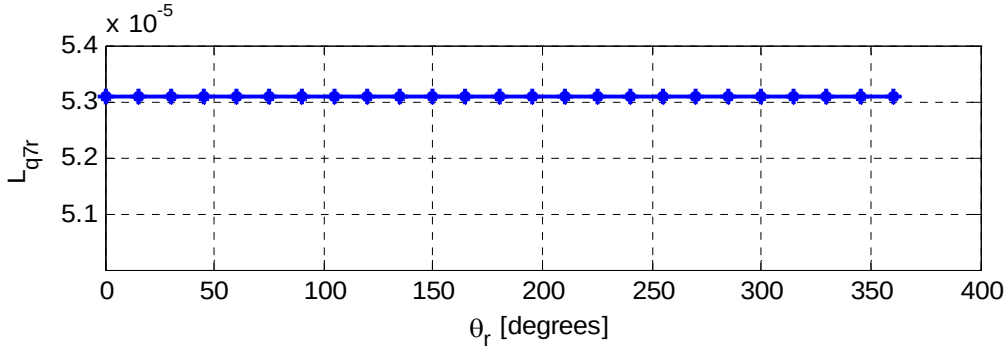

Figure 6.47 q-axis 7th harmonic rotor self-inductance of 9-phase induction machine

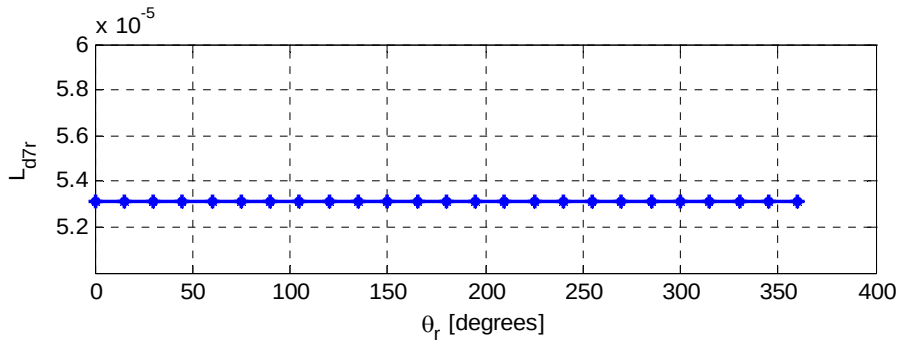

Figure 6.48 d-axis 7th harmonic rotor self-inductance of 9-phase induction machine

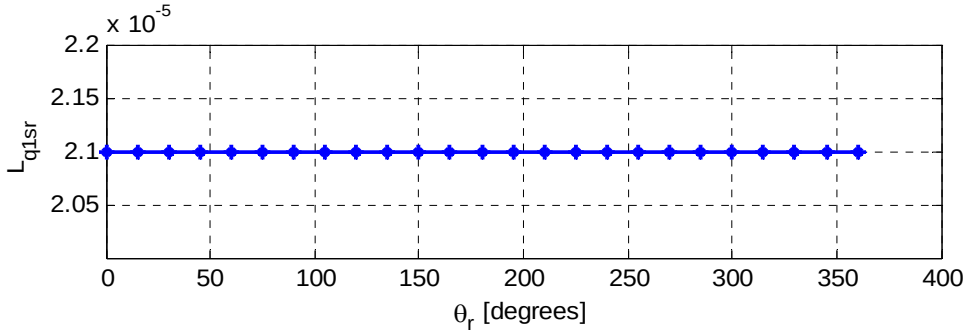

Figure 6.49 q-axis stator-rotor fundamental mutual inductance of 9-phase induction machine

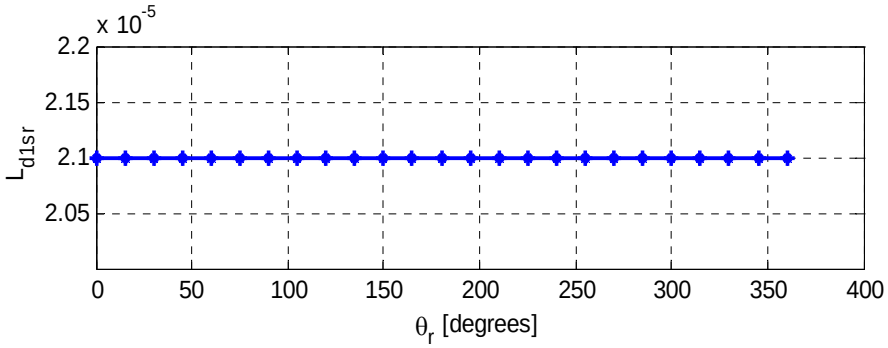

Figure 6.50 d-axis stator-rotor fundamental -inductance of 9-phase induction machine

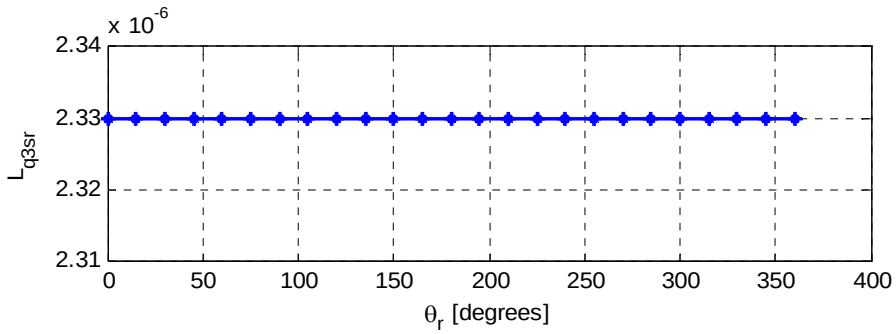

Figure 6.51 q-axis stator-rotor 3rd harmonic -inductance of 9-phase induction machine

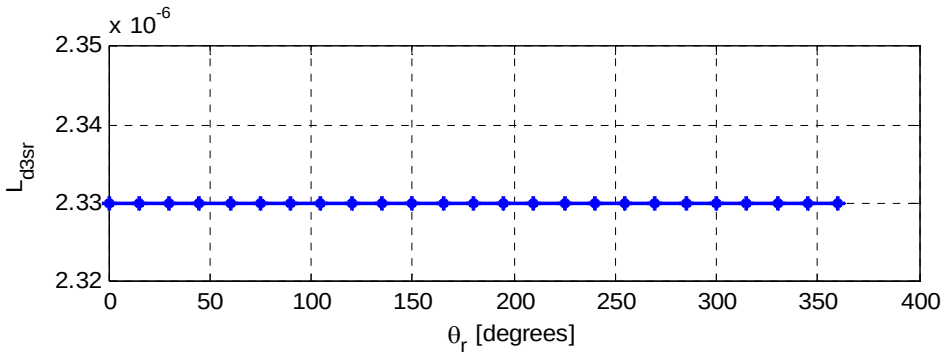

Figure 6.52 d-axis stator-rotor 3rd harmonic inductance of 9-phase induction machine

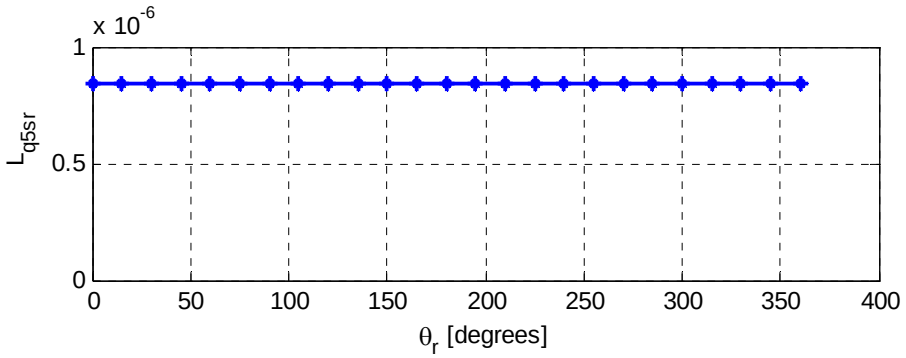

Figure 6.53 q-axis stator-rotor 5th harmonic -inductance of 9-phase induction machine

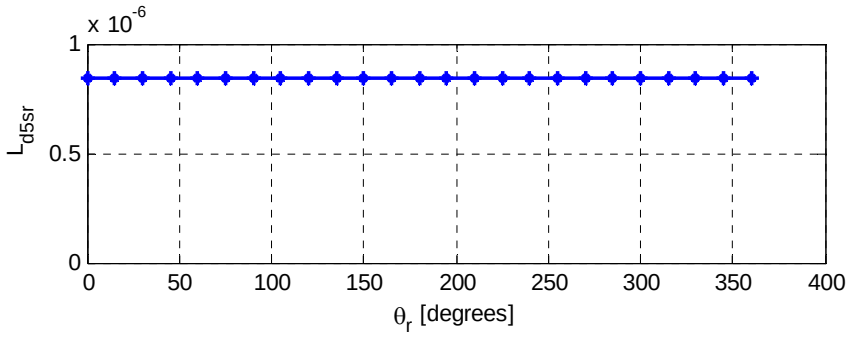

Figure 6.54 d-axis 5th harmonic stator-rotor inductance of 9-phase induction machine

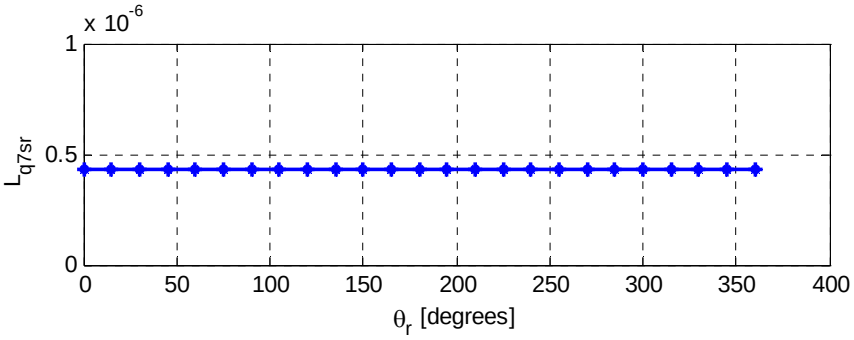

Figure 6.55 q-axis 7th harmonic stator-rotor mutual-inductance of 9-phase induction machine

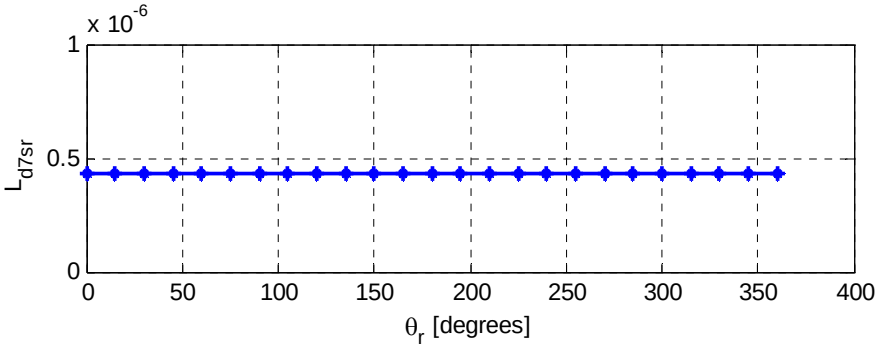

Figure 6.56 d-axis 7th harmonic stator-rotor mutual-inductance of 9-phase induction machine

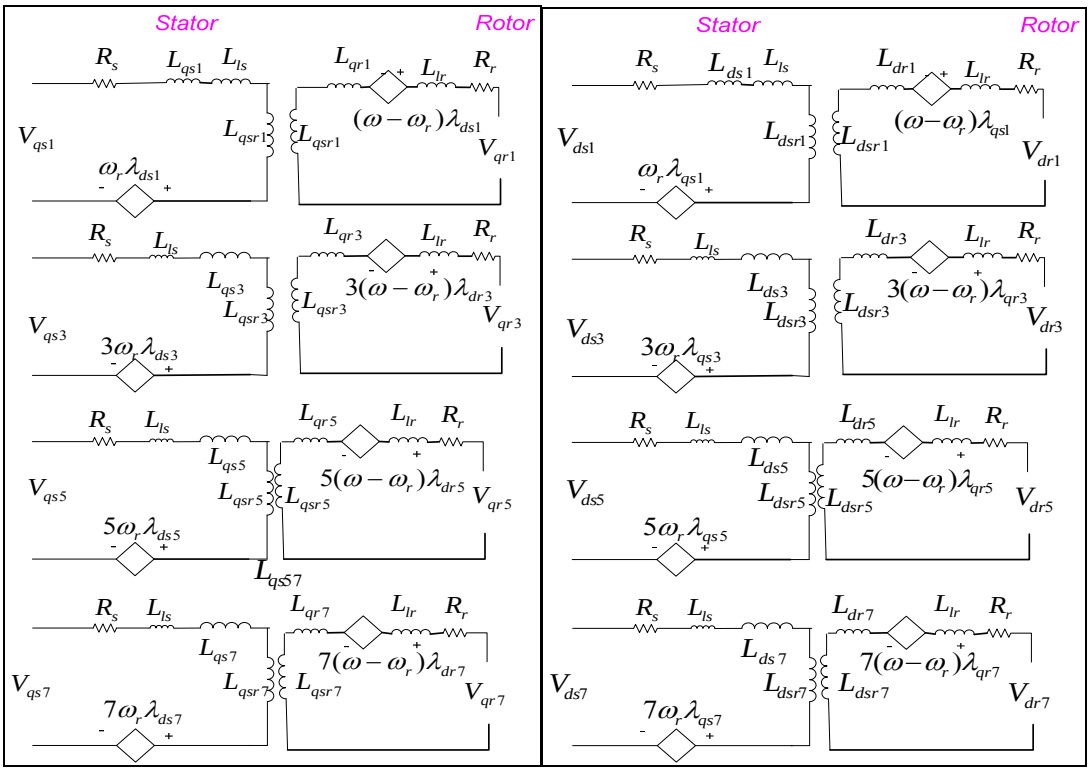

Figure 6.57 (a).q-axis equivalent circuit (b). d-axis equivalent circuit

6.8 Simulation Results

The model equations outlined in Equations (6.91)-(6.102) are derived on the basis of the 9-phase machine. The similar method can be applied to 3-phase machine where, everything is similar except the change in matrix dimensions in inductances and resistances. In both cases, the leakage inductances are inserted using the parameters derived in previous section. The coupled full order simulation is performed using the model described in Section 6.6. The peak phase voltage for each connection is selected such as to have the same stator per turn machine voltage. The machines are supplied by 9 leg and 3 leg inverters with the data and parameters given in Appendix C.

6.8.1 Simulation Results for 9-phase, 4-pole Configuration

The response of the motor with and without a load torque when operated as a 9-phase, 4-pole induction machine configuration is shown in Figures 6.58-6.66. No load characteristics such as the mechanical speed, torque, phase 'a' current and Bar 1 current are shown in Figures. 6.58-6.61, respectively. The change of the operation after a load is applied at 0.5 seconds is shown in Figures 6.62-6.65. The plot of torque with change in speed is shown in Figure 6.66.

6.8.2 Simulation Results for 3-phase, 12-pole Induction Machine Configuration

The dynamics of the motor operating in a 3-phase, 12-pole mode is shown in Figures 6.67-6.75. Figures 6.67-6.70 show the no load mechanical speed, torque, phase 'a' current and Bar 1 current plot, respectively. Similarly, the changes in characteristics after applying a load at 1 sec. are shown in Figures 6.71-6.74, respectively. From Figures 6.59 and 6.68, it is observed that the synchronous speed of the 9-phase, 4-pole induction machine configuration is three times the synchronous speed of the 3-phase, 12-pole configuration. The starting torque for 3-phase mode is higher than 9-phase mode as expected. Additionally, to overcome the high magnitude of MMF to produce 3-phase torque, machine will carry higher current which is also shown in Figure 6.73. The plot of torque with change of speed is shown in Figure 6.75.

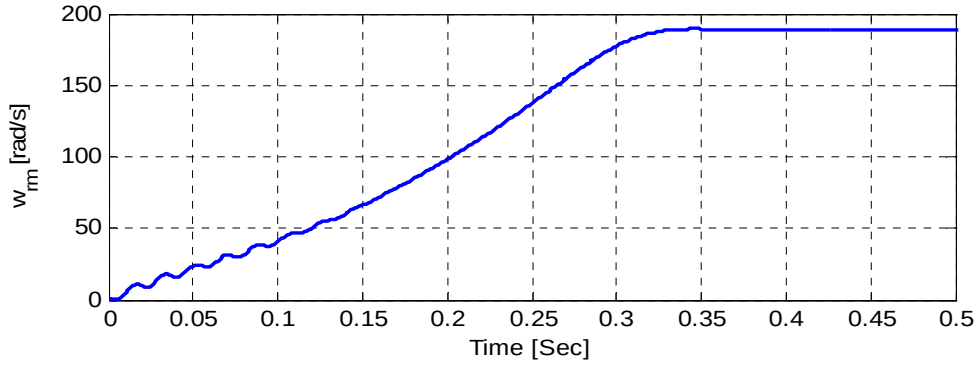

Figure 6.58 Plot of mechanical speed

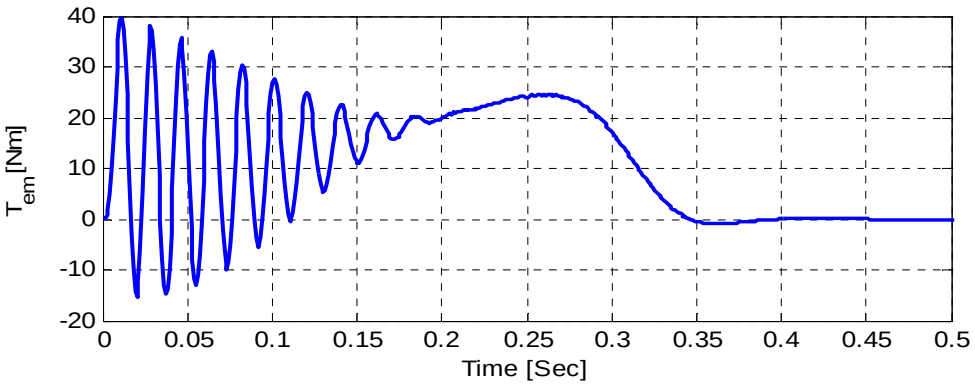

Figure 6.59 Plot of electromagnetic torque

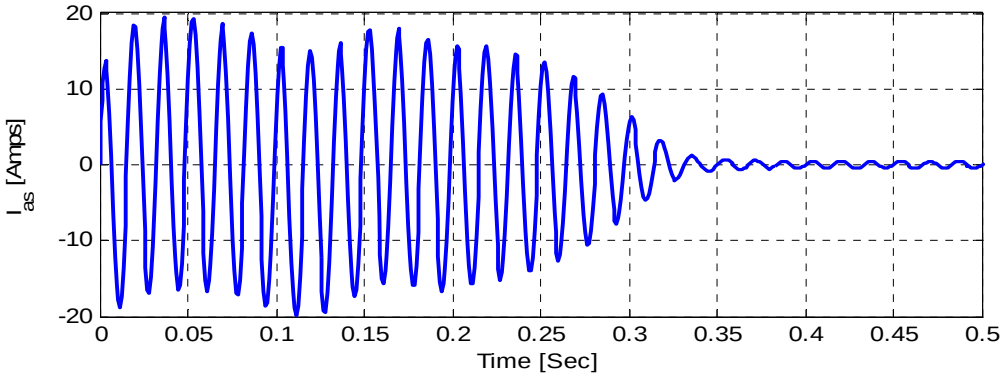

Figure 6.60 Plot of phase a stator current

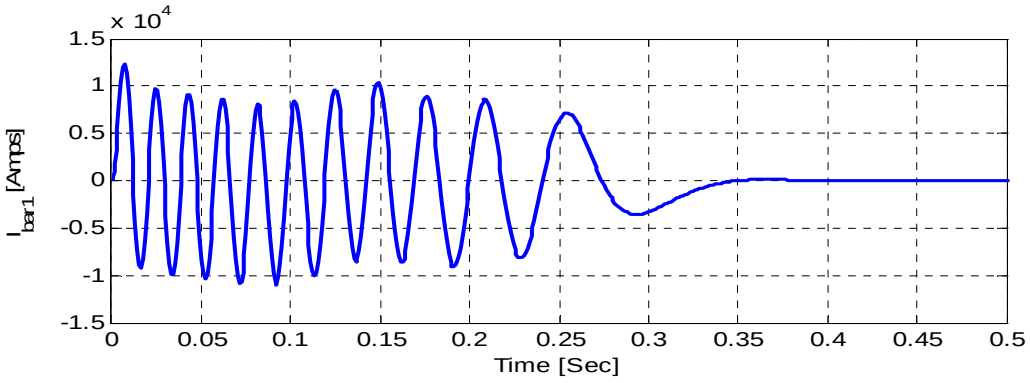

Figure 6.61 Plot of rotor bar 1 current

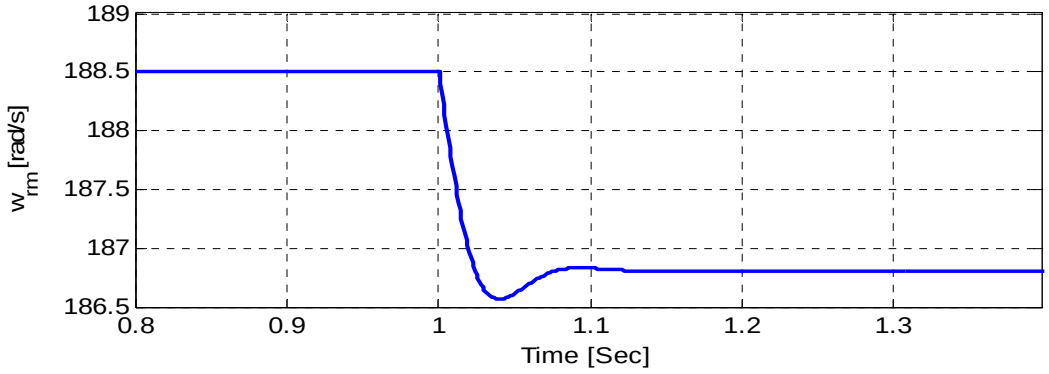

Figure 6.62 Plot of change of mechanical speed with load

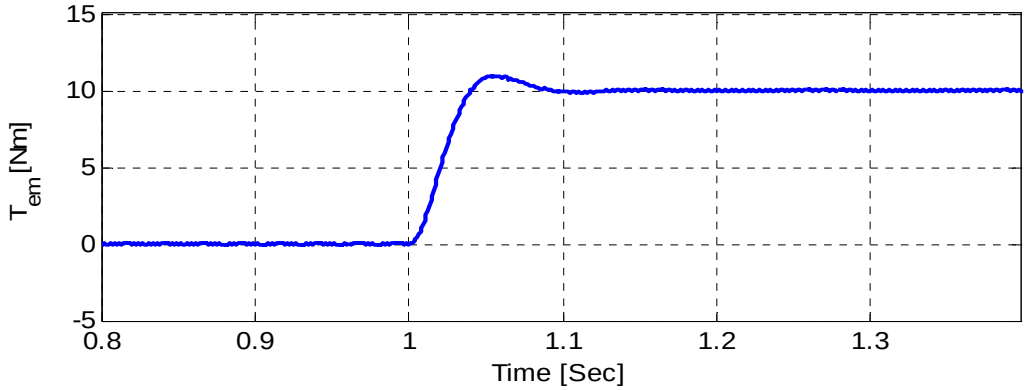

Figure 6.63 Plot of change of electromagnetic torque with load

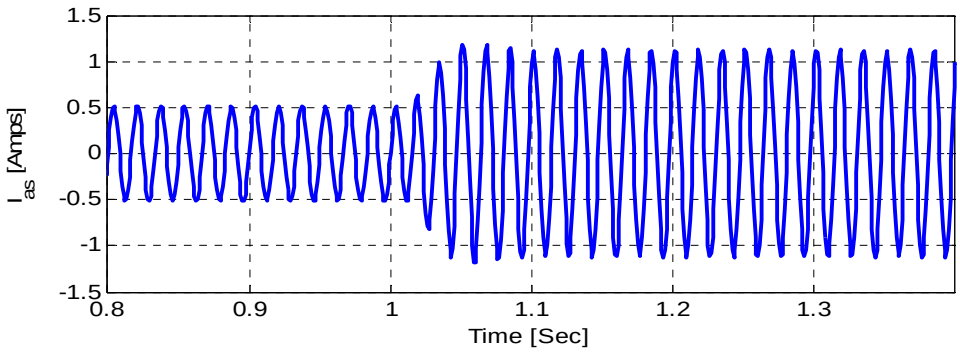

Figure 6.64 Plot of change of phase a stator current with load

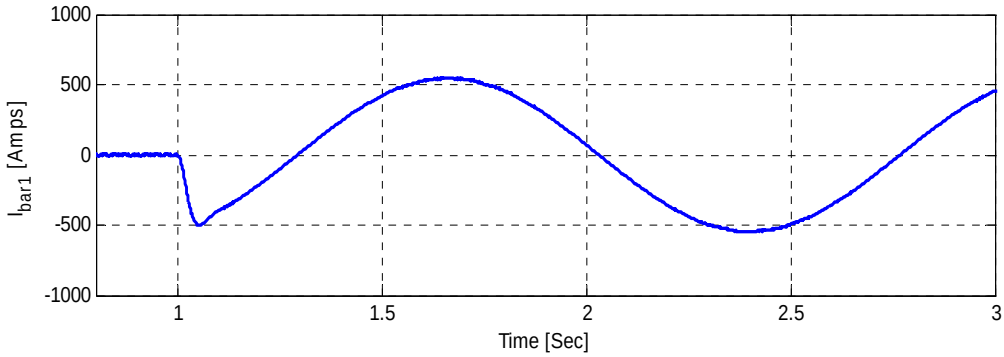

Figure 6.65 Plot of change of rotor bar current with load

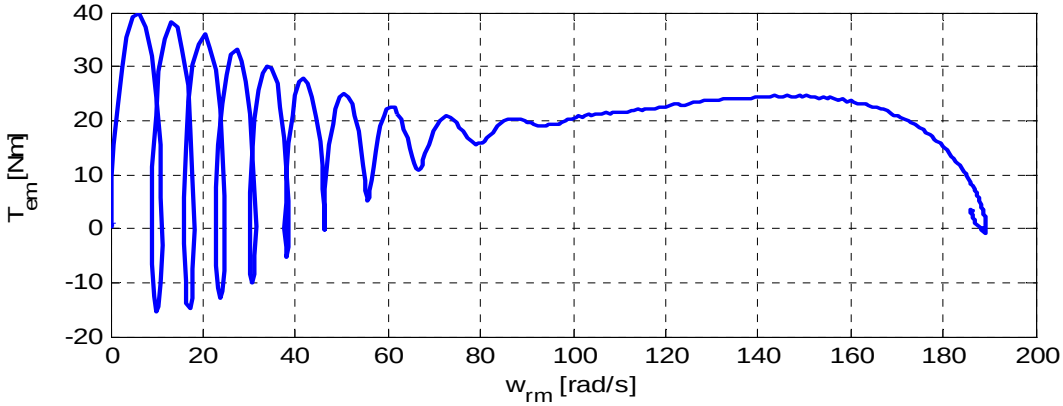

Figure 6.66 Plot of electromagnetic torque vs. mechanical speed

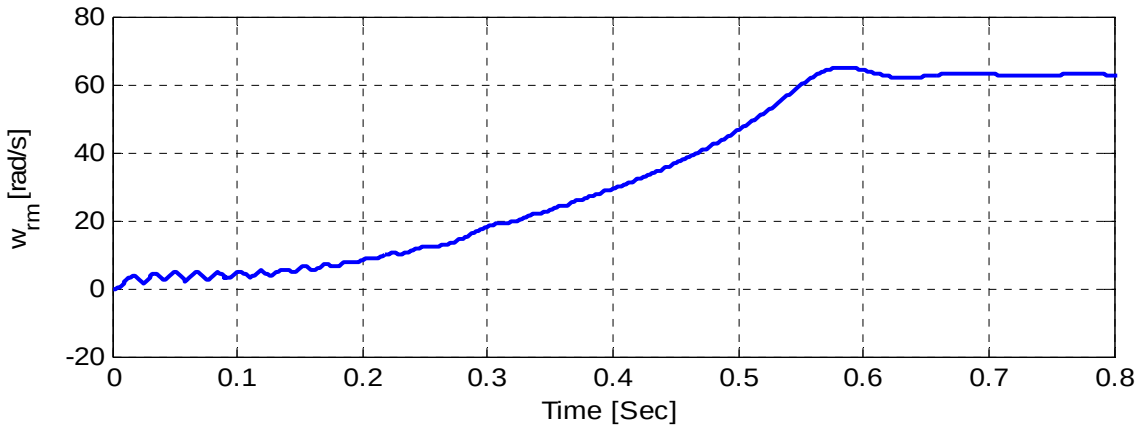

Figure 6.67 Plot of no load mechanical speed

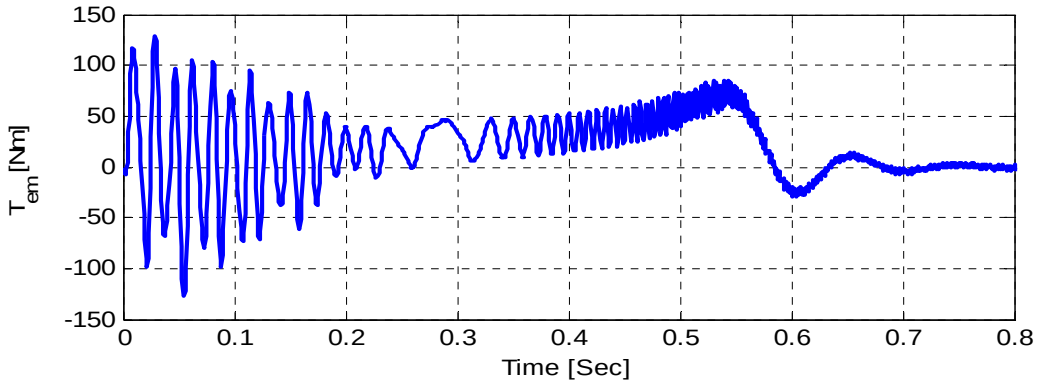

Figure 6.68 Plot of no load electromagnetic torque

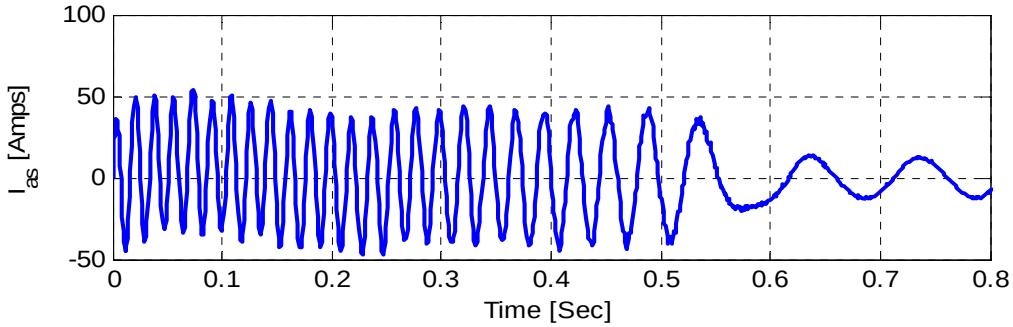

Figure 6.69 Plot of no load phase a current

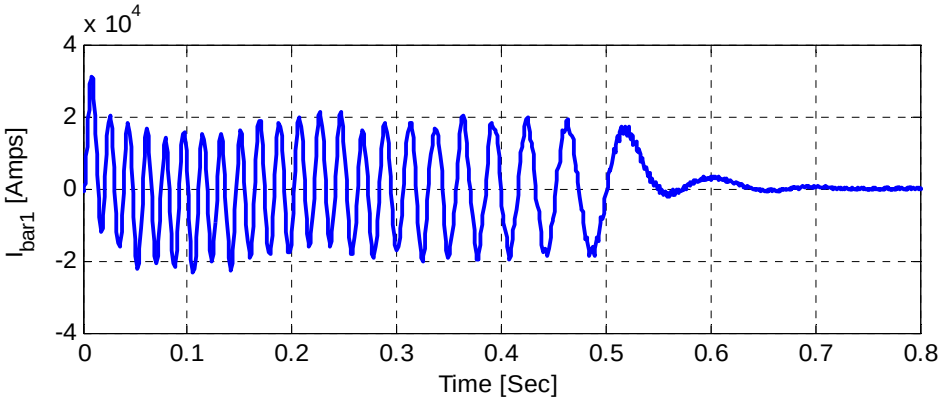

Figure 6.70 Plot of no load bar 1 current

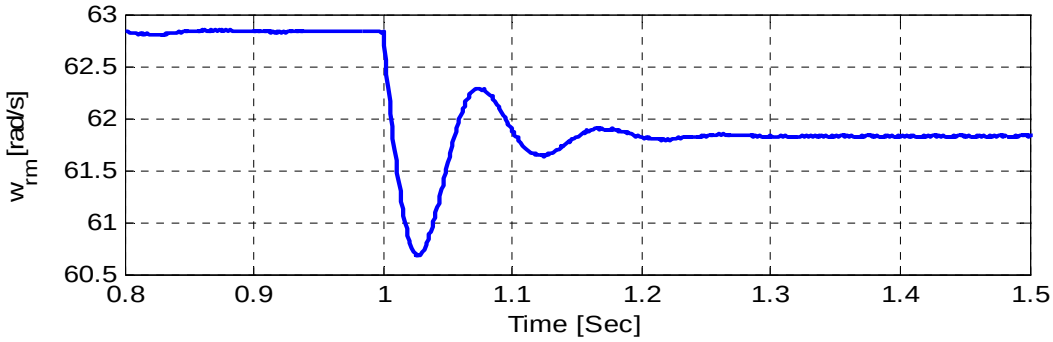

Figure 6.71 Plot of change of mechanical speed with load

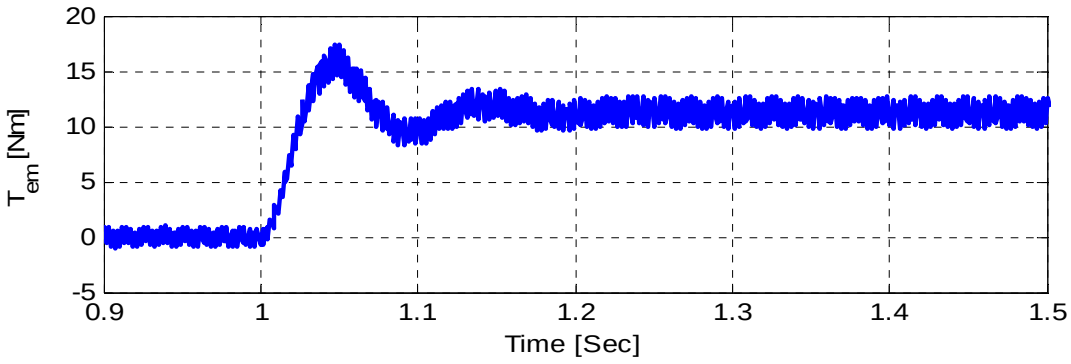

Figure 6.72 Plot of change of electromagnetic torque with load

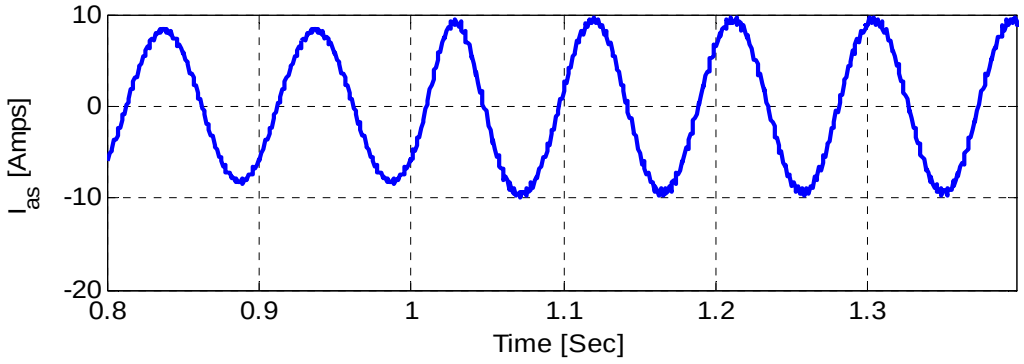

Figure 6.73 Plot of change of phase a current with load

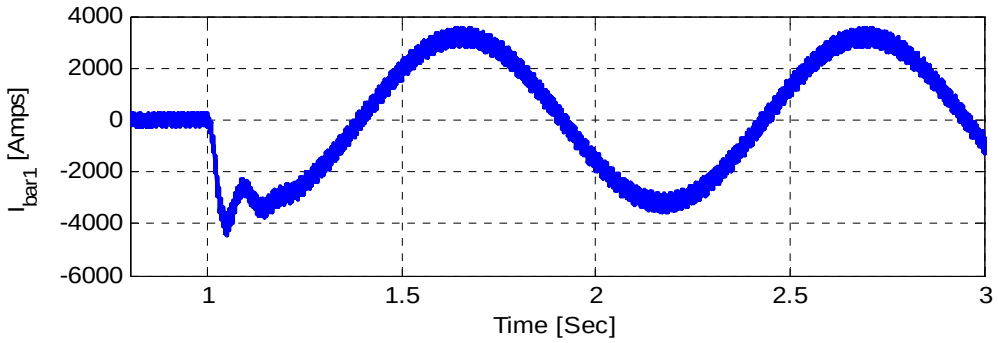

Figure 6.74 Plot of change of bar 1 current with load

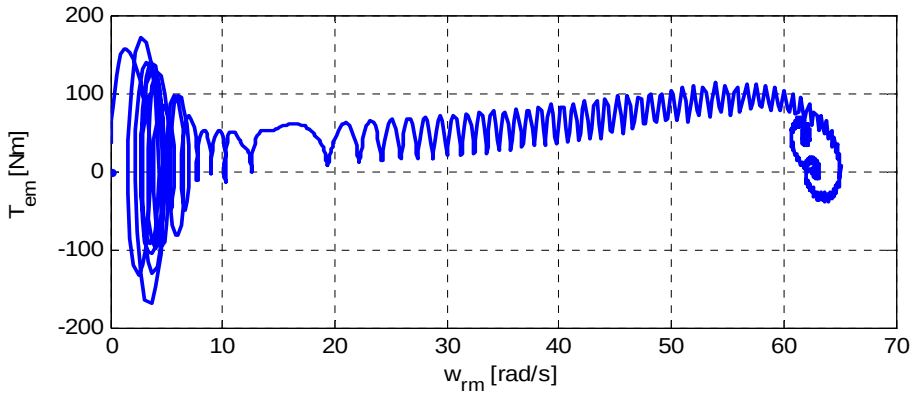

Figure 6.75 Plot of electromagnetic torque vs mechanical speed

6.9 Conclusion

The design, modeling and analysis of multiphase machines for variable speed torque operation using the concept of pole phase modulation is undertaken in this chapter. With the concept of clock diagram, turns and winding functions and winding layouts, the pole phase modulation scheme is effectively analyzed. The observation of the pole changing scheme is demonstrated by air gap plots obtained from the finite element analysis. The parameter estimation of the machine is performed using available techniques and the results are compared. The simulation graphs show the different speeds of operation when the machine is operated as a 9-phase or a 3-phase stator winding configurations. Although the operation of 9-phase, 4-pole seems to be smooth, the 3-phase, 12-pole mode can be utilized for the applications requiring higher starting torques at the expense of higher starting current and larger torque ripple.

CHAPTER 7

THREE MACHINE CONFIGURATION OF 9-PHASE INDUCTION MACHINE INTERFACED WITH 3-PHASE CONVERTERS

7.1 Introduction

Reliability and fault tolerant ability are the major advantages of the multiphase machines. If the number of phases of the machine is multiple of 3, the operation of multiphase machine by breaking it into equivalent 3-phase counterparts is found in literatures from mid-80s with 6-phase machines. The literatures specify such connections with the stator windings grouped into N 3-phase windings, each displaced by 60/N electrical degrees apart, suitable for being separately supplied by a 3-phase inverter [22]. When voltage source inverters are used for the stator windings, all inverters should ideally output 3-phase voltages with identical amplitude shifted by 60/N electrical degrees. Each time this ideal condition is violated, there is the circulation of harmonic currents in stator phases, and it results in torque pulsations.

In this chapter, similar configuration of 9-phase induction machine is analyzed by dividing the stator windings in three groups each with 20 electrical degrees apart. To avoid the harmonic current flow and torque pulsations in the system, the supply voltage from the 3-phase inverters are also managed to have the phase shift of 20 degrees. Figure 7.1 shows the typical configuration of such type of connection with 3-phase windings grouped together to form the individual 3-phase groups. Firstly, the model equations are

derived starting from the real variables for each machine configuration. Secondly, reference frame transformation is performed to transform the real variables equations to synchronous reference frame. Similarly, the q-d axis inductances are derived using full order model by the use of winding functions of stator and rotor. The system is interfaced with the rectifiers in inverters using carrier based PWM and simulation results are also shown to verify the fault tolerant operation of drive in order to accurately determine the torque contribution from each set to the total torque. Additionally, a steady state analysis is performed connecting the 9-phase machine as induction generator in three sets of 3-phase configuration across different loads.

7.2 Dynamic Model for Three Machine Configuration

To realize the three machine scheme, the dynamic model of the machine is presented in this section. The real variable model equations are presented taking into account all the possible self and mutual parameters.

7.2.1 Voltage Equations in Real Variables

From Figure 7.1, it is observed that phases ‘a’, ‘d’ and ‘g’ gives the first machine configuration. Similarly, phases ‘b’, ‘e’ and ‘h’ combine to comprise the second machine and ‘c’, ‘f’ and ‘i’ give the third machine, respectively. Now applying the voltage equations in real variables to each of the sets,

Machine –I

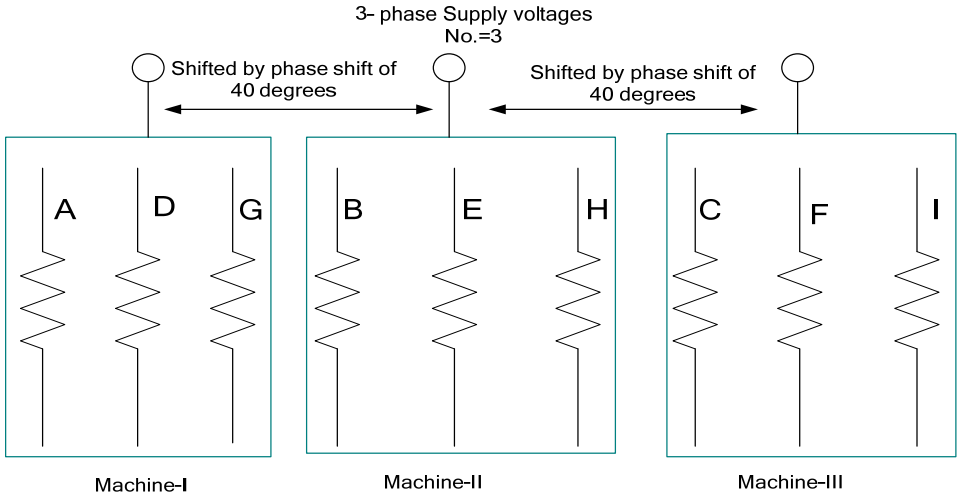

Figure 7.1 Three machine configuration of 9-phase induction machine

$$V_{adg} = r_s i_{adg} + p\lambda_{adg} \tag{7.1}$$

Machine II:

$$V_{beh} = r_s i_{beh} + p\lambda_{beh} \tag{7.2}$$

Machine III:

$$V_{cfi} = r_s i_{cfi} + p\lambda_{cfi} \tag{7.3}$$

Rotor voltage equations:

$$V_{1r} = r_{1r} i_{1r} + p\lambda_{1r}$$

$$V_{2r} = r_{2r} i_{2r} + p\lambda_{2r} \tag{7.4}$$

$$V_{3r} = r_{3r} i_{3r} + p\lambda_{3r}$$

$$V_{nr} = r_{nr} i_{nr} + p\lambda_{nr} \tag{7.5}$$

In the equation sets from (7.1)-(7.5), the symbol ‘V’ correspond to Voltage, ‘λ’ corresponds to flux linkage, ‘r_s’ defines the stator resistance and ‘r_r’defines the rotor

resistance. Similarly, a, b, c…i defines the corresponding phase of the 9-phase induction machine.

7.2.2 Flux Linkage Equations in Real Variables

The three machine sets with three sets of winding each comprise different self and mutual inductance which gives rise to self and mutual flux linkages. The machine with phase numbers ‘a’, ‘d’ and ‘g’ comprise the first machine. Hence, these three windings give rise to self and mutual inductances. This is also true for second and third machine set. However, there is also a mutual inductance that comes into effect between the windings of different machine sets. This inductance gives rise to the mutual flux linkage between the machines which needs to be taken care when deriving the model equations. The flux equations are given in Equation (7.6)-(7.9) reflecting each machine inductances and mutual machine inductances.

$$\lambda_{adg} = L_{adgadg} i_{adg} + L_{adgbeh} i_{beh} + L_{adgcfi} i_{cfi} + L_{adgr} i_{r1..n} \tag{7.6}$$

$$\lambda_{beh} = L_{behadg} i_{adg} + L_{behbeh} i_{beh} + L_{behcfi} i_{cfi} + L_{behr} i_{r1..n} \tag{7.7}$$

$$\lambda_{cfi} = L_{cfiadg} i_{adg} + L_{cfibeh} i_{beh} + L_{cficfi} i_{cfi} + L_{cfir} i_{r1..n} \tag{7.8}$$

Each machine shares the same magnetizing path between stator and rotor. Hence, there exists a rotor flux equation with the mutual inductance between each sets and the rotor. The rotor flux equation in real variables is given as

$$\lambda_{cr1,2,3..n} = L_{radg} i_{adg} + L_{rbeh} i_{beh} + L_{rcfi} i_{cfi} + L_r i_{r1..n} \tag{7.9}$$

The stator inductance matrix in the Equations (7.6)-7.9) is defined in the following section.

7.2.3 Stator and Rotor Inductance Matrix

The flux equations as given in Equations (7.6)-(7.9) consist of the stator and rotor inductance matrix for each configuration. Taking into consideration of all the corresponding phase of the three machine sets, the stator inductance matrix is given as

$$L_{adgadg} = \begin{bmatrix} L_{aa} & L_{ad} & L_{ag} \\ L_{da} & L_{dd} & L_{dg} \\ L_{ga} & L_{gd} & L_{gg} \end{bmatrix} \tag{7.10}$$

$$L_{behbeh} = \begin{bmatrix} L_{bb} & L_{be} & L_{bh} \\ L_{eb} & L_{ee} & L_{eh} \\ L_{hb} & L_{he} & L_{hh} \end{bmatrix} \tag{7.11}$$

$$L_{cficfi} = \begin{bmatrix} L_{cc} & L_{cf} & L_{ci} \\ L_{fc} & L_{ff} & L_{fi} \\ L_{ic} & L_{if} & L_{ii} \end{bmatrix} \tag{7.12}$$

The mutual inductances between each machine sets are derived as

$$L_{adgbeh} = \begin{bmatrix} L_{ab} & L_{ae} & L_{ah} \\ L_{db} & L_{df} & L_{dh} \\ L_{gb} & L_{ge} & L_{gh} \end{bmatrix},\ L_{adgcfi} = \begin{bmatrix} L_{ac} & L_{af} & L_{ai} \\ L_{dc} & L_{df} & L_{di} \\ L_{gc} & L_{gf} & L_{gi} \end{bmatrix}, L_{behadg} = \begin{bmatrix} L_{ba} & L_{bd} & L_{bg} \\ L_{ea} & L_{ed} & L_{eg} \\ L_{ha} & L_{hd} & L_{hg} \end{bmatrix} \tag{7.13}$$

$$L_{behcfi} = \begin{bmatrix} L_{bc} & L_{bf} & L_{bi} \\ L_{ec} & L_{ef} & L_{ei} \\ L_{hc} & L_{hf} & L_{hi} \end{bmatrix},\ L_{cfiadg} = \begin{bmatrix} L_{ca} & L_{cd} & L_{cg} \\ L_{fa} & L_{fd} & L_{fg} \\ L_{ca} & L_{cd} & L_{cg} \end{bmatrix},\ L_{cfibeh} = \begin{bmatrix} L_{cb} & L_{ce} & L_{ch} \\ L_{fb} & L_{fe} & L_{fh} \\ L_{ib} & L_{ie} & L_{ih} \end{bmatrix} \tag{7.14}$$

Similarly, the mutual inductance between each machine sets and rotor bars are calculated as

$$L_{adgr} = \begin{bmatrix} L_{a1} & L_{a2}.... & L_{an} \\ L_{d1} & L_{d2}.... & L_{dn} \\ L_{g1} & L_{g2}.... & L_{gn} \end{bmatrix},\ L_{behr} = \begin{bmatrix} L_{b1} & L_{b2}.... & L_{bn} \\ L_{e1} & L_{e2}.... & L_{en} \\ L_{h1} & L_{h2}.... & L_{hn} \end{bmatrix} \tag{7.15}$$

$$L_{cfir} = \begin{bmatrix} L_{c1} & L_{c2}.... & L_{cn} \\ L_{f1} & L_{f2}.... & L_{fn} \\ L_{i1} & L_{i2}.... & L_{in} \end{bmatrix} \tag{7.16}$$

7.2.4 Transformations

The 3-phase transformation matrix is utilized to perform the synchronous frame transformation of the real variables derived in previous sections. Since each of the machine windings are displaced by some phase shift, it should be reflected in the transformation matrix in each machine set. For the system under consideration, the transformation is performed in rotor reference frame Hence, the transformations are given as

Machine I:

$$T_s(\theta_1) = \begin{bmatrix} c(\theta_r) & c(\theta_r - \alpha_1) & c(\theta_r + \alpha_1) \\ s(\theta_r) & s(\theta_r - \alpha_1) & s(\theta_r + \alpha_1) \\ 1/2 & 1/2 & 1/2 \end{bmatrix}, \alpha_1 = \frac{2\pi}{3} \tag{7.17}$$

Machine II:

$$T_s(\theta_2) = \begin{bmatrix} c(\theta_r - \beta) & c(\theta_r - \beta - \alpha_2) & c(\theta_r - \beta + \alpha_2) \\ s(\theta_r - \beta) & s(\theta_r - \beta - \alpha_2) & s(\theta_r - \beta + \alpha_2) \\ 1/2 & 1/2 & 1/2 \end{bmatrix}, \alpha_2 = \frac{2\pi}{3}, \beta = \frac{2\pi}{9} \tag{7.18}$$

Machine III:

$$T_s(\theta_3)=\begin{bmatrix} c(\theta_r-2\beta) & c(\theta_r-2\beta-\alpha_3) & c(\theta_r-2\beta+\alpha_3) \\ s(\theta_r-2\beta) & s(\theta_r-2\beta-\alpha_3) & s(\theta_r-2\beta+\alpha_3) \\ 1/2 & 1/2 & 1/2 \end{bmatrix}, \alpha_3=\frac{2\pi}{3}, \beta=\frac{2\pi}{9} \tag{7.19}$$

Similarly, the transformation matrix for rotor circuits is given as

$$T_r(\theta_r)=\frac{2}{n}\begin{bmatrix} c(\theta_r) & c(\theta_r-\frac{2\pi}{n}).... & c(\theta_r-\frac{2(n-1)\pi}{n}) \\ s(\theta_r) & s(\theta_r-\frac{2\pi}{n}).... & s(\theta_r-\frac{2(n-1)\pi}{n}) \\ 1/2 & 1/2 & 1/2 \end{bmatrix} \tag{7.20}$$

7.2.5 Derivation of q-d Reference Frame Equations

Applying rotor reference frame transformation matrix of Section 7.2.4 to the voltage equations derived in Section 7.2.2, the derivations of q-d equations are performed. For each machines the following equations define the voltage equations.

For Machine I:

$$\begin{aligned} V_{qs1} &= r_s i_{qs1} + p\lambda_{qs1} + \omega_r \lambda_{ds1} \\ V_{ds1} &= r_s i_{ds1} + p\lambda_{ds1} - \omega_r \lambda_{qs1} \end{aligned} \tag{7.21}$$

For Machine II:

$$\begin{aligned} V_{qs2} &= r_s i_{qs2} + p\lambda_{qs2} + \omega_r \lambda_{ds2} \\ V_{ds2} &= r_s i_{ds2} + p\lambda_{ds2} - \omega_r \lambda_{qs2} \end{aligned} \tag{7.22}$$

For Machine III:

$$\begin{aligned} V_{qs3} &= r_s i_{qs3} + p\lambda_{qs3} + \omega_r \lambda_{ds3} \\ V_{ds3} &= r_s i_{ds3} + p\lambda_{ds3} - \omega_r \lambda_{qs3} \end{aligned} \tag{7.23}$$

Similarly, rotor voltage equations in q-d frame are derived as

$$V_{qdr} = r_{qdrr} i_{qdr} + p\lambda_{qdr} + (\omega - \omega_r)\lambda_{qdr} \tag{7.24}$$

where, r_{qdrr} is the rotor resistance matrix which is derived in Chapter 6 with the help of coupled circuit model. In terms of bar resistance and end ring resistances,

$$r_{qdrr} = T(\theta)\begin{bmatrix} 2(r_b + r_e) & -r_b & \cdots & -r_b \\ -r_b & 2(r_b + r_e) & \cdots & 0 \\ \vdots & \vdots & \ddots & \vdots \\ -r_b & 0 & & 2(r_b + r_e) \end{bmatrix} T(\theta)^{-1} \tag{7.25}$$

The derivations of the flux linkage in q-d reference for stator and rotor are performed in the corresponding sections.

7.2.6 Derivations of q-d Stator and Rotor Flux Equations

The flux linkages using the derivations in previous sections are now transformed into the q-d reference using the corresponding transformation matrix for each machine sets. The flux linkage terms for each stator sets and rotor sets are given as

$$\begin{aligned} \lambda_{abc} &= L_{abcabc} i_{abc} + L_{abcdef} i_{def} + L_{abcghi} i_{ghi} + L_{abcr} i_{r1-n} \\ \lambda_{def} &= L_{defdef} i_{def} + L_{defabc} i_{abc} + L_{defghi} i_{ghi} + L_{defr} i_{r1-n} \\ \lambda_{ghi} &= L_{ghighi} i_{ghi} + L_{ghiabc} i_{abc} + L_{ghidef} i_{def} + L_{ghir} i_{r1-n} \\ \lambda_{r1-n} &= L_{rabc} i_{abc} + L_{rdef} i_{def} + L_{rghi} i_{ghi} + L_{rr1-n} \end{aligned} \tag{7.26}$$

Multiplying Equation (7.26) by the corresponding transformation matrix of each machine sets,

$$\begin{aligned} \lambda_{qds1} = {} & T_s(\theta_1) L_{adgadg} T_s(\theta_1)^{-1} i_{qds1} + T_s(\theta_1) L_{adgbeh} T_s(\theta_2)^{-1} i_{qds2} \\ & + T_s(\theta_1) L_{adgcfi} T_s(\theta_3)^{-1} i_{qds3} + T_s(\theta_1) L_{adgr} T_s(\theta_1 - \theta_r)^{-1} i_{qdr} \end{aligned} \tag{7.27}$$

$$\lambda_{qds2} = T_s(\theta_2)L_{behbeh}T_s(\theta_2)^{-1}i_{qds2} + T_s(\theta_2)L_{behadg}T_s(\theta_1)^{-1}i_{qds1} + T_s(\theta_2)L_{behcfi}T_s(\theta_3)^{-1}i_{qds3} + T_s(\theta_2)L_{behr}T_s(\theta_2-\theta_r)^{-1}i_{qdr} \quad (7.28)$$

$$\lambda_{qds3} = T_s(\theta_3)L_{cfiadg}T_s(\theta_1)^{-1}i_{qds1} + T_s(\theta_3)L_{cfibeh}T_s(\theta_1)^{-1}i_{qds1} + T_s(\theta_3)L_{cficfi}T_s(\theta_3)^{-1}i_{qds3} + T_s(\theta_3)L_{cfir}T_s(\theta_3-\theta_r)^{-1}i_{qdr} \quad (7.29)$$

$$\lambda_{qdr} = T_r(\theta_1-\theta_r)L_{radg}T_s(\theta_1)^{-1}i_{qds1} + T_r(\theta_2-\theta_r)L_{rbeh}T_s(\theta_2)^{-1}i_{qds2} + T_s(\theta_3-\theta_r)L_{rcfi}T_s(\theta_3)^{-1}i_{qds3} + T_r(\theta_r)L_rT_r(\theta_r)^{-1}i_{qdr} \quad (7.30)$$

Equations (7.27-7.30) corresponds to the flux linkage equations due to the self inductance of the individual machines, mutual inductances to other 3-phase counterparts and mutual inductances to rotor circuit. These equations can be written in q-d reference form as

$$\begin{aligned}
\lambda_{qds1} &= L_{qds1}i_{qds1} + L_{qds1qds2}i_{qds2} + L_{qds1qds3}i_{qds3} + L_{qds1qdr}i_{qdr}\\
\lambda_{qds2} &= L_{qds2}i_{qds2} + L_{qds1qds2}i_{qds1} + L_{qds1qds3}i_{qds3} + L_{qds2qdr}i_{qdr}\\
\lambda_{qds3} &= L_{qds3}i_{qds3} + L_{qds3qds2}i_{qds2} + L_{qds1qds3}i_{qds1} + L_{qds3qdr}i_{qdr}\\
\lambda_{qdr} &= L_{qdr}i_{qdr} + L_{qds1qdr}i_{qds1} + L_{qds2qdr}i_{qds2} + L_{qds3qdr}i_{qds3}
\end{aligned} \quad (7.31)$$

Using Equations (7.28) (7.18)-(7.20) the q-axis equivalent circuit of the three machine configuration is drawn in Figure 7.2. Similarly, the d-axis equivalent circuit is shown in Figure 7.3.

7.3 Derivation of Full Order q-d Model of Three Machine Configuration for 9-Phase Induction Machine

The full order q-d model developed in Chapter 5 for IPM machine in three machine configuration is extended in this section for the case of 9-phase induction

machine. The real variable turn and winding function of stator and rotor circuit is taken from Chapter 6 and transformed into stationary reference frame by the method similar to Chapter 5.

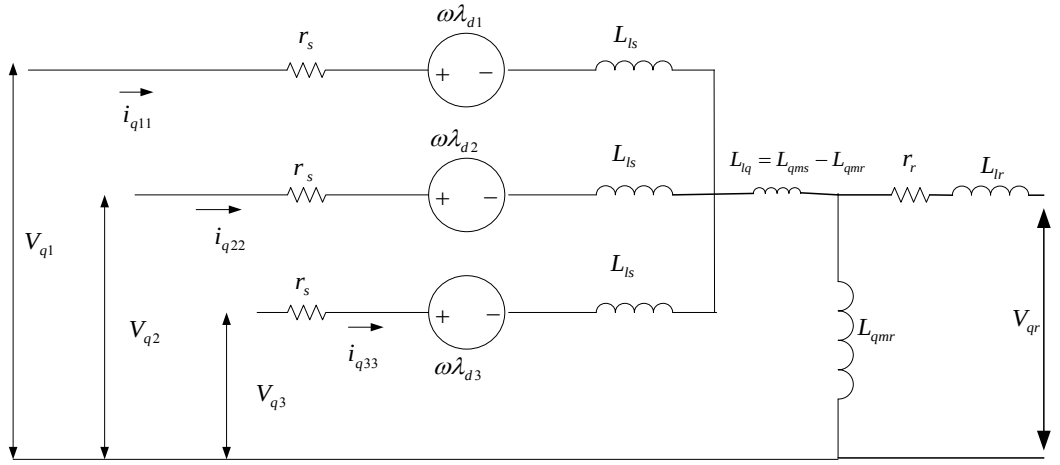

Figure 7.2 q-axis equivalent diagram

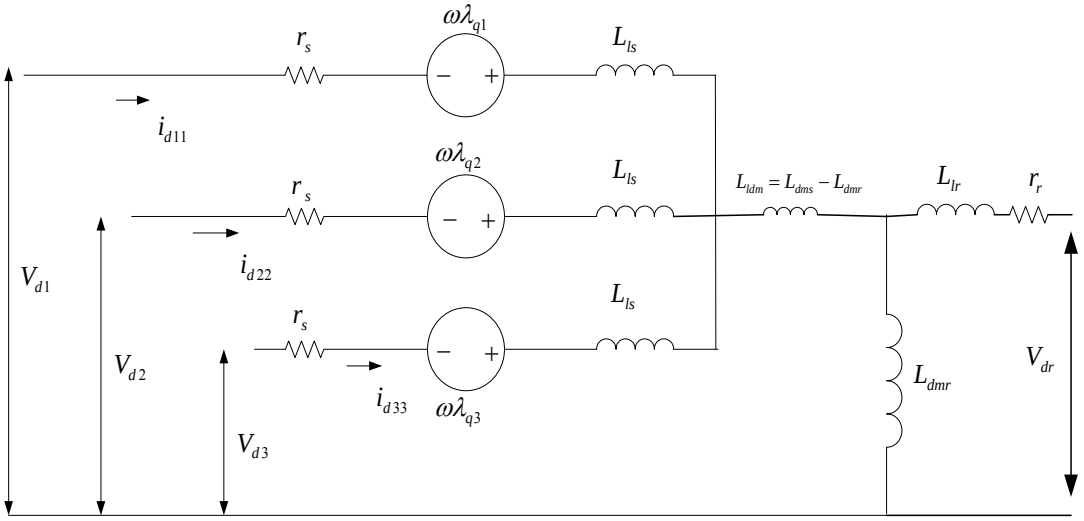

Figure 7.3 d axis equivalent diagram

Each parameter is evaluated in rotor reference and with the variation of rotor angle. However, in this case the air gap is constant, hence saliency factor is unity. The results for self and mutual inductance for each machine and rotor bars are derived in the following section.

7.3.1 Derivation of Self-Machine Inductances

In this section, the self-machine inductance is derived with the variation of rotor angle using the q-d winding function derived using the winding functions given in Chapter 6. Figures 7.4, 7.5 and 7.6 depict the self q and d-axis inductances due to Machine I, Machine II and Machine III, respectively. Similarly, Figure 7.7 shows the q and d axis inductance of rotor bars. Similarly, Figures 7.8, 7.9 and 7.10 show the q and d axis mutual inductances between rotor and corresponding machines, respectively. Finally, Figures 7.11, 7.12 and 7.13 depict the mutual inductances between Machine I and Machine II, Machine I and Machine III and Machine II and Machine III, respectively.

As observed from Figures 7.4-7.13 the q and d axis inductances have the same value. This is true in case of induction machines since it has constant air gap and it has the saliency factor of unity.

7.3.2 Derivation of Torque and Speed Equation

In order to make the derivation easier for each machine configuration, Torque equation is derived from the Power Balance Equation.

For Machine I:

$$V_{qds1} = r_s i_{qds1} + p\lambda_{qds1} - j\omega_r \lambda_{qds1} \tag{7.32}$$

Multiplying both sides by i_{qds1}^{*},

$$V_{qds1} i_{qds1}^{*} = r_s i_{qds1} i_{qds1}^{*} + p\lambda_{qds1} i_{qds1}^{*} - j\omega_r \lambda_{qds1} i_{qds1}^{*} \tag{7.33}$$

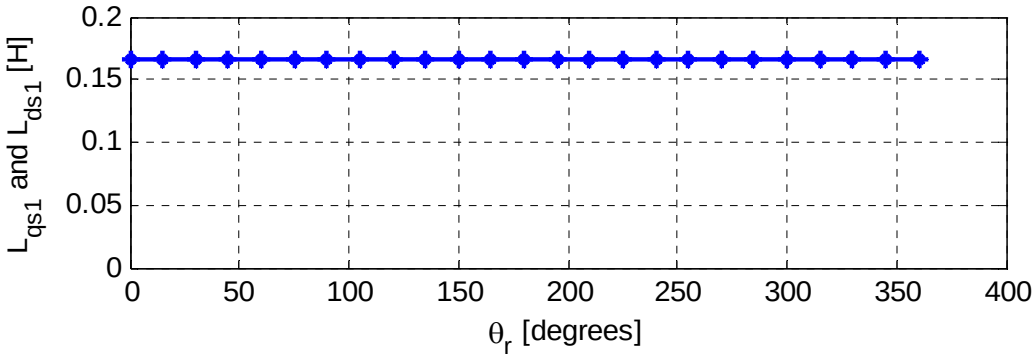

Figure 7.4 q and d axis inductance for Machine I

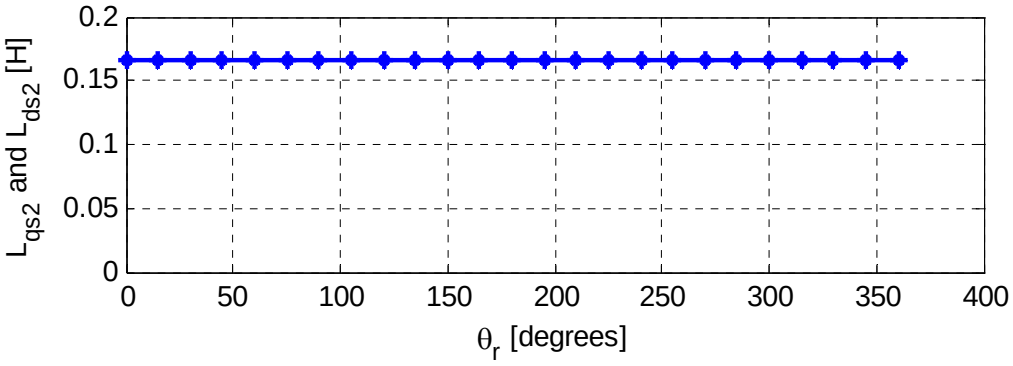

Figure 7.5 q and d axis inductance for Machine II

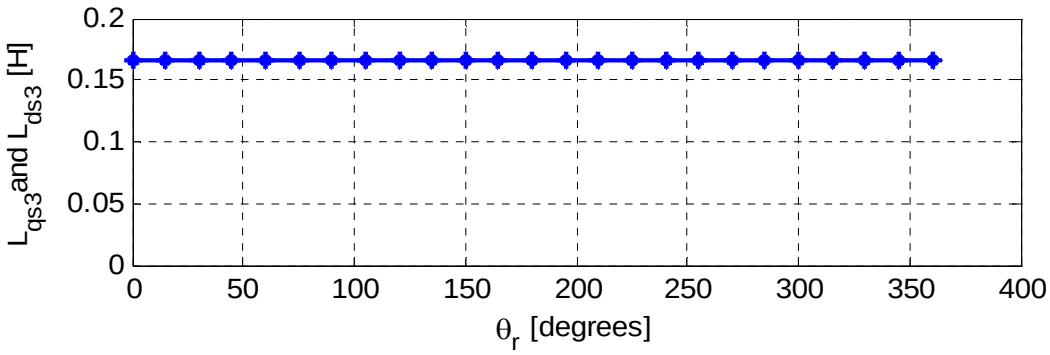

Figure 7.6 q and d axis inductance for Machine III

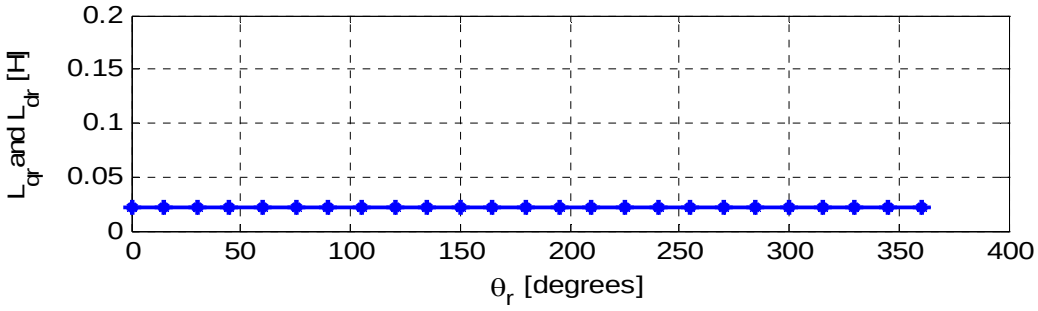

Figure 7.7 q and d axis inductances of rotor bars

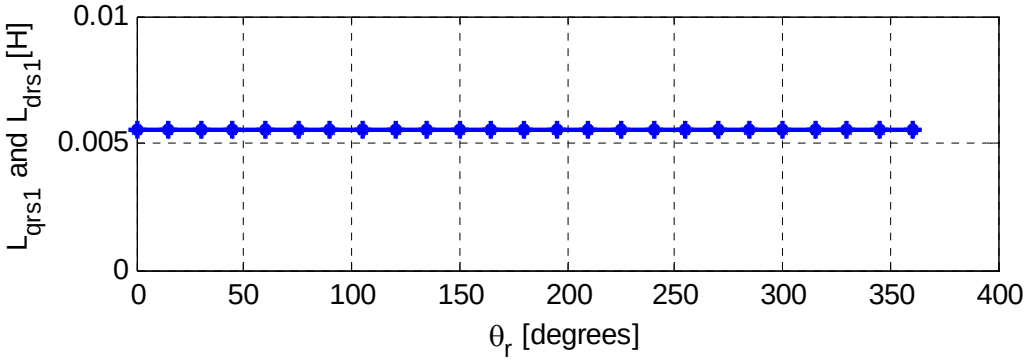

Figure 7.8 Mutual q and d axis inductances between rotor and Machine I

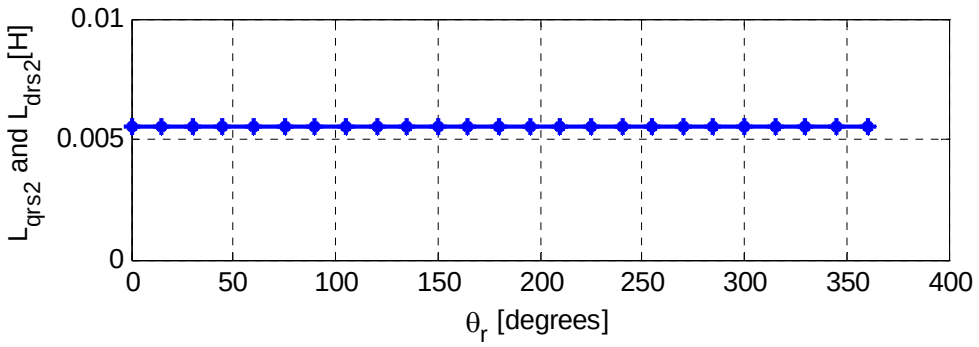

Figure 7.9 q and d axis mutual inductance between rotor and Machine II

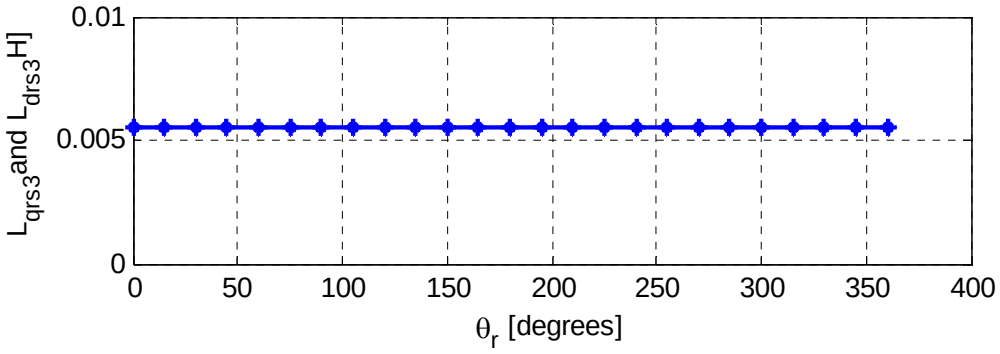

Figure 7.10 q and d axis mutual inductance between rotor and Machine III

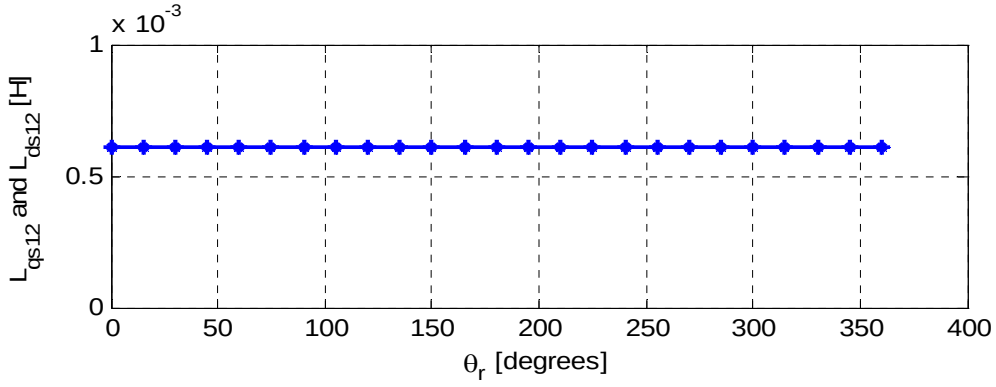

Figure 7.11 q and d axis mutual inductance between Machine I and Machine II

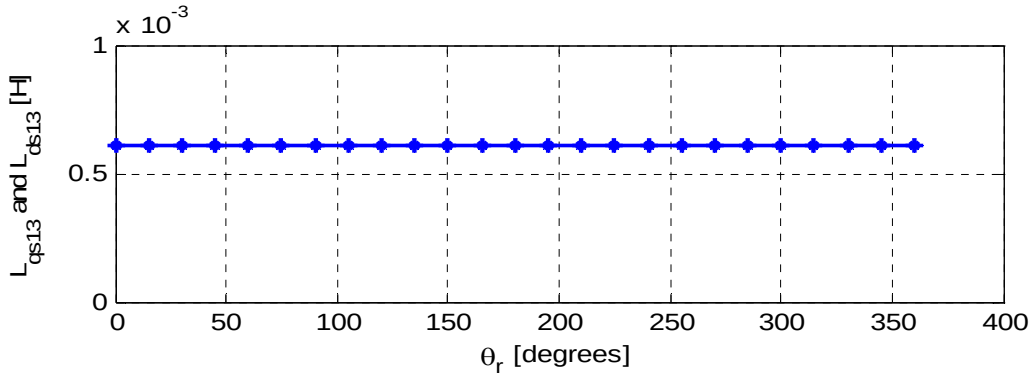

Figure 7.12 q and d axis mutual inductance between Machine I and Machine III

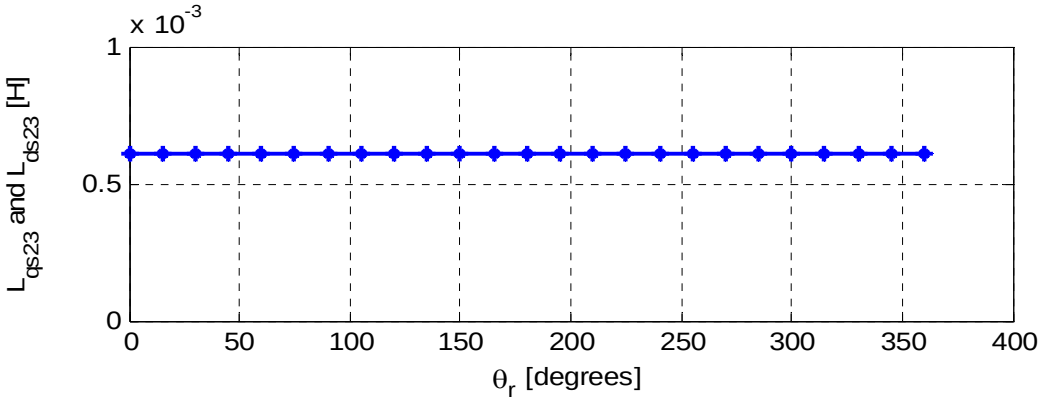

Figure 7.13 q and d axis mutual inductance between Machine I and Machine III

Multiplying both sides by 3/2,

$$\frac{3}{2}V_{qds1}i_{qds1}^{*} = \frac{3}{2}r_s i_{qds1}i_{qds1}^{*} + \frac{3}{2}p\lambda_{qds1}i_{qds1}^{*} - \frac{3}{2}j\omega_r\lambda_{qds1}i_{qds1}^{*} \tag{7.34}$$

In Equation (7.34), the term on LHS gives the total power of the system. Similarly, the first expression in the RHS implies the power loss and the last expression of LHS implies the power due to electromagnetic torque. i.e.,

$$P_t = -\frac{3}{2} j\omega_r \lambda_{qds1} i_{qds1}^{*}$$
$$= -\frac{3}{2}\frac{P}{2}\omega_e \lambda_{qds1} i_{qds1}^{*} \tag{7.35}$$

From the relationship between Power and Electromagnetic torque, the total electromagnetic torque developed in the system is given by

$$T_e = \mathrm{Im}\, ag(\frac{P_t}{\omega_e}) \tag{7.36}$$

Solving Equation (7.36),

$$T_{e1} = \frac{3P}{4}[\lambda_{ds1} i_{qs1} - \lambda_{qs1} i_{ds1}] \tag{7.37}$$

Similarly, torque developed due to Machine II and Machine III are given as

$$T_{e2} = \frac{3P}{4}[\lambda_{ds2} i_{qs2} - \lambda_{qs2} i_{ds2}] \tag{7.38}$$

$$T_{e3} = \frac{3P}{4}[\lambda_{ds3} i_{qs3} - \lambda_{qs3} i_{ds3}] \tag{7.39}$$

The total torque is the resultant of the torque developed due to Machine I, Machine II and Machine III.

$$p\omega_r = \frac{P}{2J}(T_e - T_L) \tag{7.40}$$

where,

P = Number of Poles

J = Moment of Inertia

T_e = Resultant of Electromagnetic Torque = T_{e1}+ T_{e2}+ T_{e3}

7.4 Interfacing of 9-phase Induction Machine with 3-phase Converters

In this section, the 9-phase machine model thus presented is interfaced with 3-phase converters. Figure 7.14 depicts the system diagram of the system in which the 3-phase rectifiers and converters are connected to corresponding 3-phases of the 9-phase machine.

The 3-phase supply is connected to each of the Rectifiers 1, 2 and 3 which are connected to Inverters 1, 2 and 3. Inverter 1 provides 3-phase power to windings ‘a’, ‘d’ and ‘g’ of the 9-phase machine. Similarly, windings ‘b’, ‘e’, ‘h’ and ‘c’, ‘f’ and ‘I’ are fed by Inverters 2 and 3, respectively. Both rectifier and inverter utilize the carrier based modulation scheme with modulation index of 0.8 each. Similarly, the 3-phase supply is of 120 Volts peak with 60 Hz.

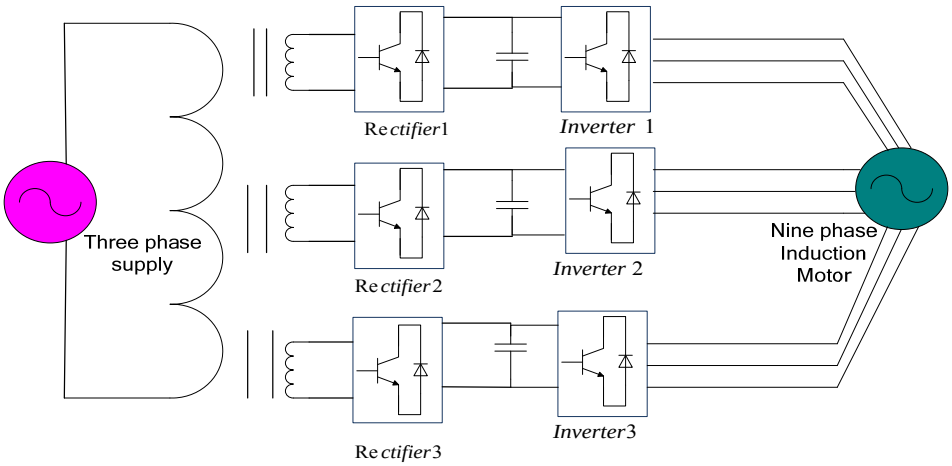

Figure 7.14 Connection of 9-phase motor as three sets of 3-phase machines

The inductance and resistance of the input side of the rectifier is taken as 5 mH and 0.5 Ohms respectively.

If S_{apr} , S_{dpr} , S_{gpr} defines the switching functions for each phases of the Rectifier 1, and i_{as1}, i_{ds1}, i_{gs1}, defines the current input towards the rectifier, then the rectifier model is given as

$$\begin{aligned} i_0 &= S_{apr} i_{as1} + S_{dpr} i_{ds1} + S_{gp} i_{gs1} \\ pV_d &= \frac{1}{C_0}(i_0 - i_d) \end{aligned} \tag{7.41}$$

where, V_d is the dc voltage output of the rectifier, C_0 is the dc link capacitor, i_0 is the current flowing out of the capacitor and i_d is the output current of the rectifier.

Similarly, the boost rectifier voltage equations in real variables for Rectifier 1:

$$\begin{aligned} V_{an} &= \frac{V_d}{2}(2S_{ap} - 1) \\ V_{dn} &= \frac{V_d}{2}(2S_{dp} - 1) \\ V_{gn} &= \frac{V_d}{2}(2S_{gp} - 1) \end{aligned} \tag{7.42}$$

$$\begin{aligned} pi_{as} &= \frac{1}{L_1}[V_{a0} - ri_{as} - V_{an} - V_{no}] \\ pi_{ds} &= \frac{1}{L_1}[V_{do} - ri_{ds} - V_{dn} - V_{no}] \\ pi_{gs} &= \frac{1}{L_1}[V_{go} - ri_{gs} - V_{gn} - V_{no}] \end{aligned} \tag{7.43}$$

The neutral voltage,

$$V_{no} = -\frac{1}{3}(V_{an} + V_{dn} + V_{gn}) \tag{7.44}$$

The inverter equations for Inverter 1 are given as

$$V_{as} = \frac{V_{dc}}{3}\left[2S_{ap} - S_{dp} - S_{gp}\right]$$
$$V_{ds} = \frac{V_{dc}}{3}\left[2S_{dp} - S_{ap} - S_{gp}\right] \quad (7.45)$$
$$V_{gs} = \frac{V_{dc}}{3}\left[2S_{gp} - S_{dp} - S_{ap}\right]$$

Similar equations exist for Rectifiers 2, 3 and Inverters 2 and 3.

7.5 Simulation Results

Using the parameters derived using the three machine configuration and parameters from Appendix C, the full order simulation of the machine was performed using MATLAB/ Simulink. The transient and steady state graphs of the system are given in Figures 7.15 – 7.25. Figure 7.15 shows the plot of speed for no load condition of the system. Similarly, Figures 7.16, 7.17, and 7.18 show the plot of no load torque, phase 'a' current and DC link voltage, respectively. To find the contribution of each machine in total torque, the steady state torque is plotted in Figures 7.19-7.21, respectively. The total torque is given in Figure 7.22. Similarly, Figures 7.23-7.25 depict the plot of steady state inverter currents under no load condition for each machine systems. Finally, Figure 7.26 depicts the phase 'a' inverter voltage for first machine configuration.

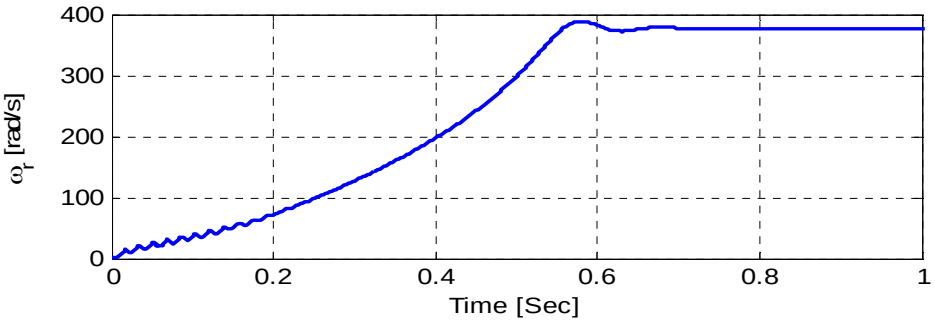

Figure 7.15 Plot of speed under no load

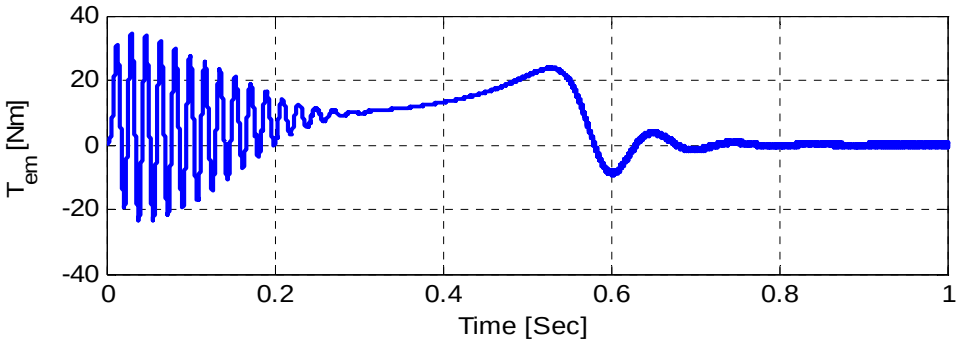

Figure 7.16 Plot of electromagnetic torque

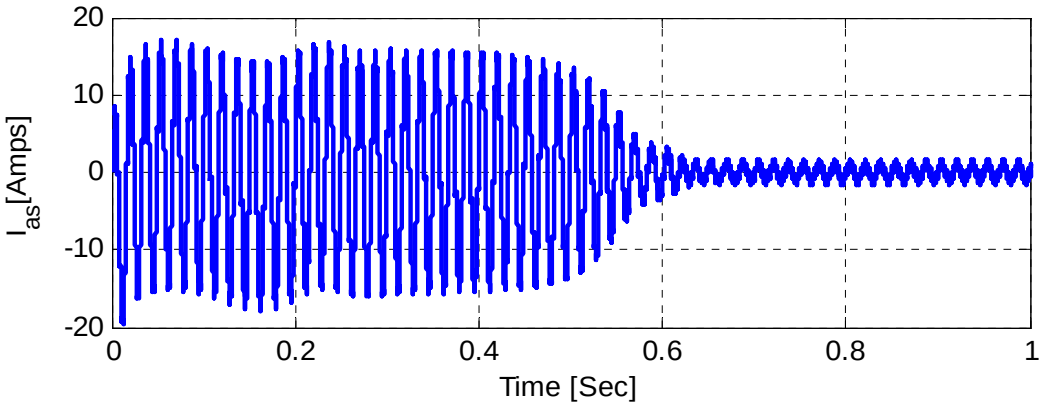

Figure 7.17 Plot of phase ‘a’ current

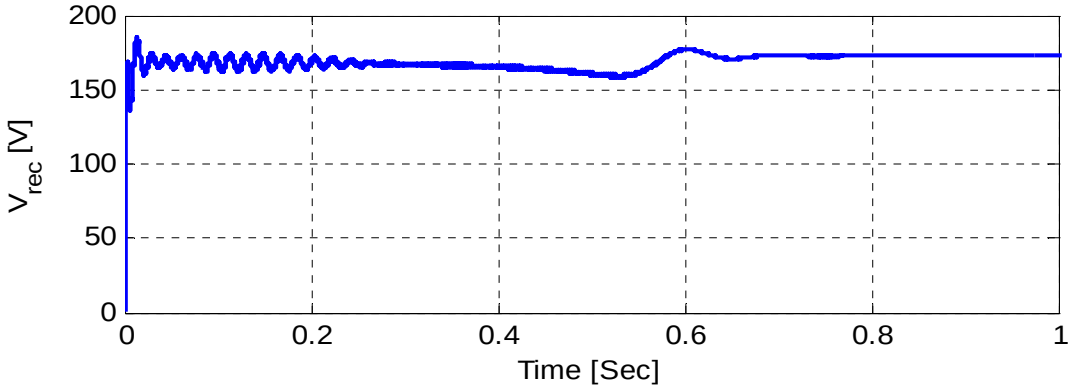

Figure 7.18 Plot of DC link Voltage

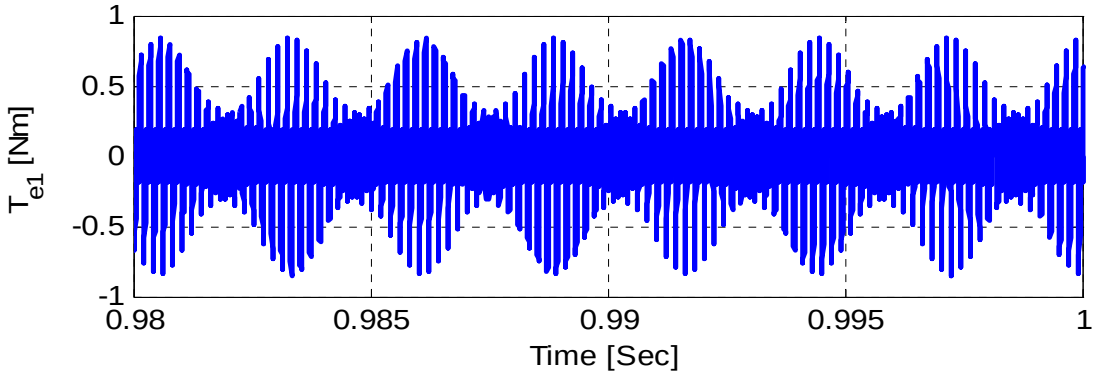

Figure 7.19 Steady state plot of Machine I torque

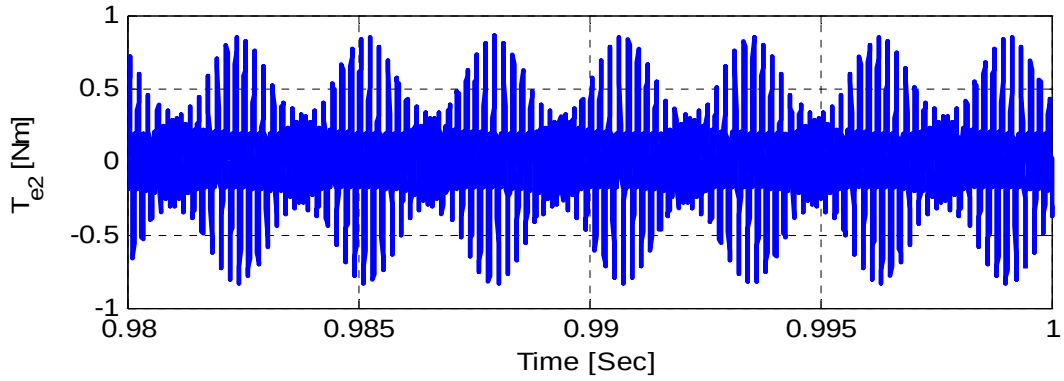

Figure 7.20 Steady state plot of Machine II torque

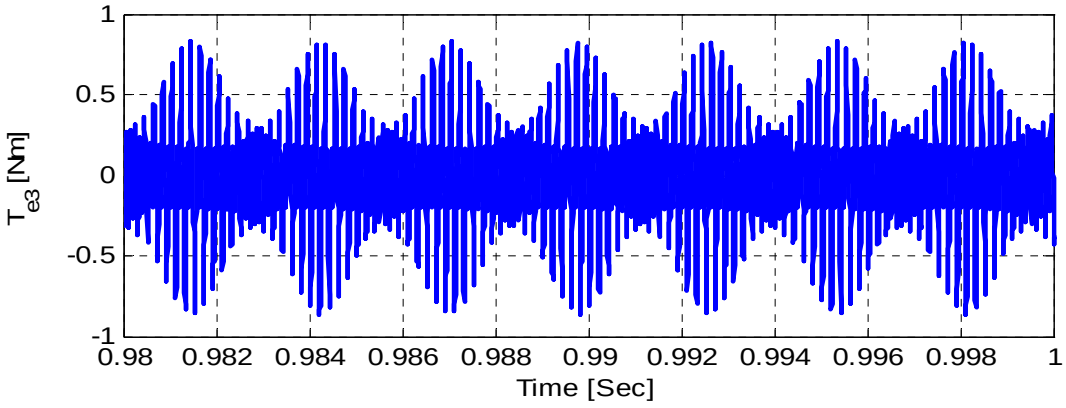

Figure 7.21 Steady state plot of Machine III torque

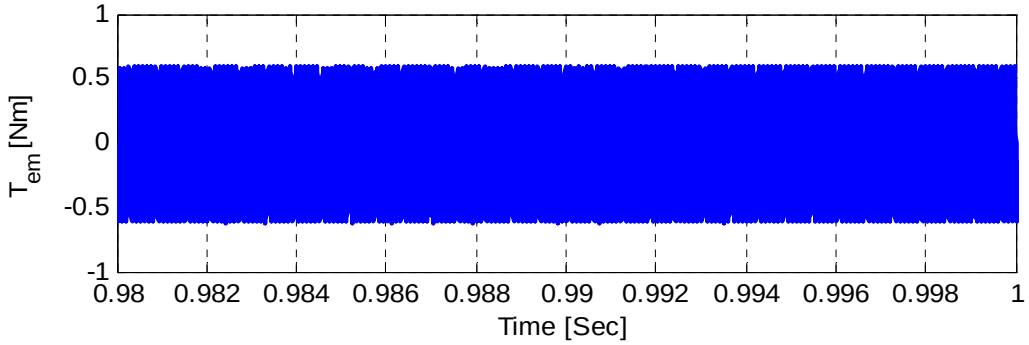

Figure 7.22 Steady state plot of Total machine torque

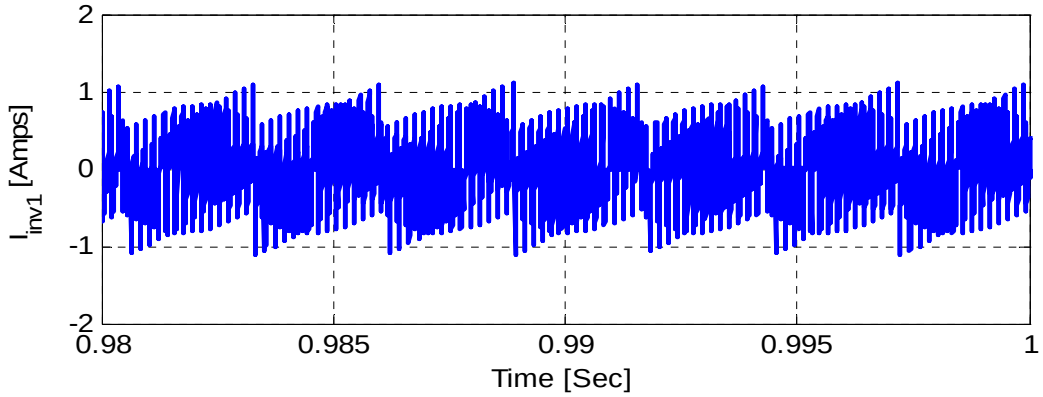

Figure 7.23 Steady state plot of Inverter 1 current

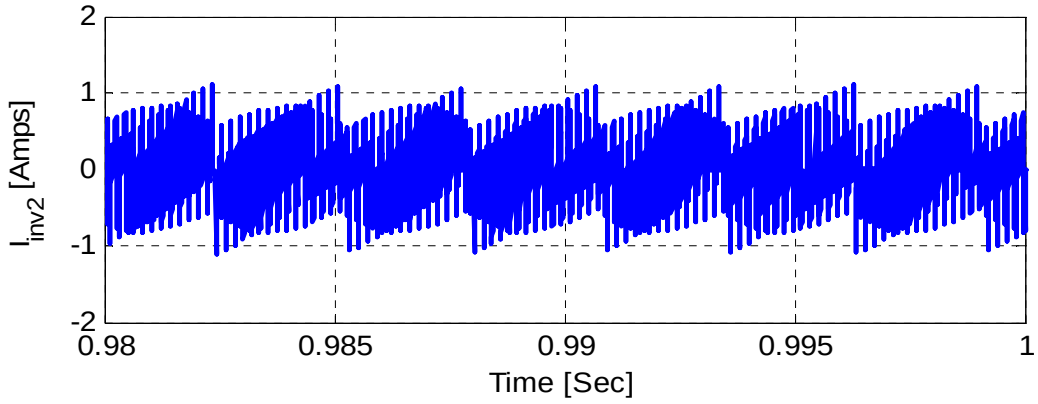

Figure 7.24 Steady state plot of Inverter 2 current

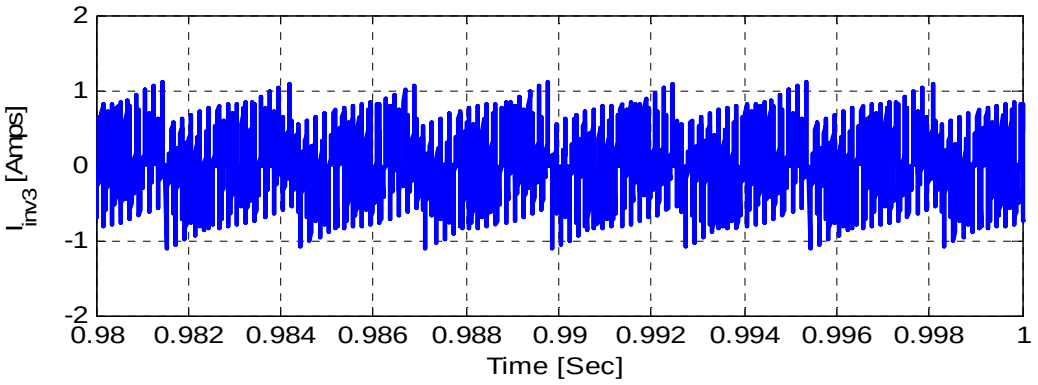

Figure 7.25 Steady state plot of Inverter 3 current

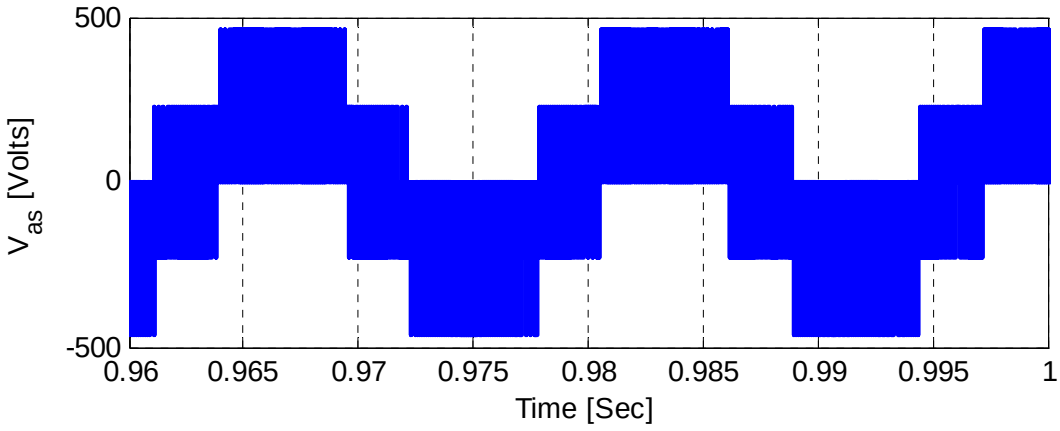

Figure 7.26 Steady state plot of phase 'a' voltage

An interesting observation can be inferred from Figures 7.19-7.21 where plot of individual torque is shown for each machine configuration. The reliability of 9-phase machine can be explained from these graphs. Although the system is coupled, if the machine is driven by three sets of voltages, the torque response from each set equally contributes to the total torque. If any one of the set is out of operation, the remaining sets still perform good operation which also signifies the fault tolerant operation of 9-phase induction machine.

7.6 Steady State Analysis of 9-phase Induction Generator Operated as Three Sets of 3-phase Machines

A particular case of the three machine configuration is discussed in this section, where the machine is connected as a generator to the 3-phase rectifier and different R-L loads. The model equations in steady state are solved to observe the steady state characteristics of the system. The model is illustrated in Figure 7.27.

Neglecting the mutual machine inductances as they are of very small value, the model equations in steady state are given as

Rectifier and load:

$$r_s I_{qds1} - j\omega_e L_s i_{qds1} - j\omega_e L_m \left(I_{qds2} + I_{qds3}\right) - j\omega_e L_{mr} i_{qdr} - \frac{M_{qds}}{2} V_{dc} = 0 \tag{7.46}$$

$$\frac{3}{4}\mathrm{Re}\left(M_{qds} I_{qds}^{\ *}\right) - \frac{V_{dc}}{R_{o1}} = 0 \tag{7.47}$$

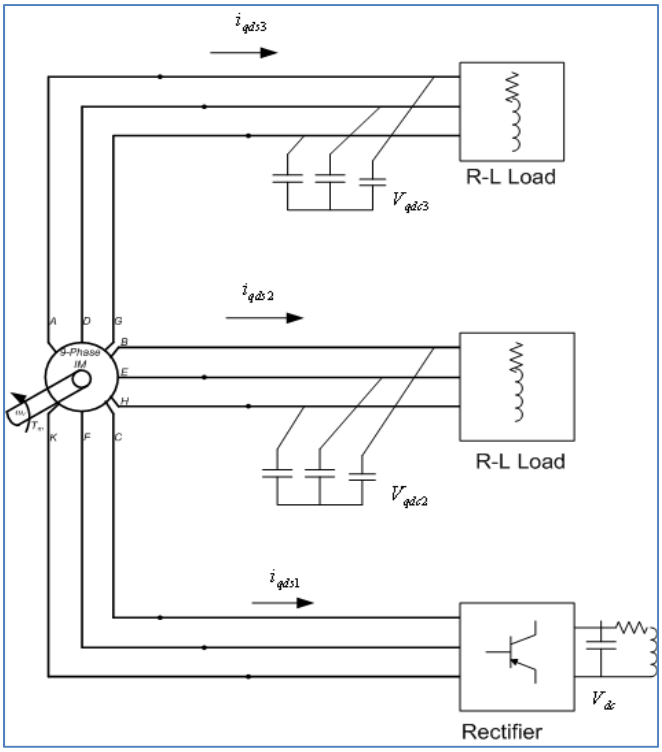

Figure 7.27 3-phase generator connected to rectifier and different loads

where, M is the modulation index, r_s is the stator resistance, L_s is the stator inductance, L_m is the mutual inductance, R_{01} is the load resistance of the rectifier and ω_e is the reference frequency of transformation.

System 2 and load:

$$r_s I_{qds2} - j\omega_e L_s i_{qds2} - j\omega_e L_m \left(I_{qds1} + I_{qds3}\right) - j\omega_e L_{mr} i_{qdr} - V_{qdc2} = 0 \tag{7.48}$$

$$-I_{qds2} - I_{qdl2} - j\omega_e C_{p2} V_{qdc2} = 0 \tag{7.49}$$

$$V_{qdc2} - r_{o2} I_{qdl2} + j\omega_e L_{o2} I_{qdl2} = 0 \tag{7.50}$$

where, V_{qdc2} is the q-d voltage across capacitor C_{p2} of system 2, L_{02} is the load inductance of System 2 and L_{mr} is the mutual inductance between rotor and machine sets.

Similarly, the same equations also apply for System 3 which are given as

$$r_s I_{qds3} - j\omega_e L_s i_{qds3} - j\omega_e L_m \left(I_{qds2} + I_{qds1}\right) - j\omega_e L_{mr} i_{qdr} - V_{qdc2} = 0 \tag{7.51}$$

$$-I_{qds3} - I_{qdl3} - j\omega_e C_{p3} V_{qdc3} = 0 \tag{7.52}$$

$$V_{qdc3} - r_{o3} I_{qdl3} + j\omega_e L_{o3} I_{qdl3} = 0 \tag{7.53}$$

Rotor voltage equations:

$$r_r I_{qdr} - j(\omega_{so}) L_r I_{qdr} - j\omega_{so} L_{mr} \left[I_{qds1} + I_{qds2} + I_{qds3}\right] = 0 \tag{7.54}$$

Now, solving system 2

$$r_r I_{qdr} - j(\omega_{so}) L_r I_{qdr} - j\omega_{so} L_{mr} \left[I_{qds1} + I_{qds2} + I_{qds3}\right] = 0 \tag{7.55}$$

$$V_{qdc2} - r_{o2} I_{qdl2} + j\omega_e L_{o2} I_{qdl2} = 0 \tag{7.56}$$

$$I_{qdl2} = \frac{V_{qdc2}}{r_{o2} - j\omega_e L_{o2}} \tag{7.57}$$

$$V_{qdc2} = \frac{-I_{qds2}}{j\omega_e C_{p2} + \dfrac{1}{r_{o2} - j\omega_e L_{o2}}} \tag{7.58}$$

Similarly, solving System 3,

$$V_{qdc2} = \frac{-I_{qds2}}{j\omega_e C_{p2} + \dfrac{1}{r_{o2} - j\omega_e L_{o2}}} \tag{7.59}$$

Solving the Rotor Voltage equation,

$$I_{qdr} = -\frac{j\omega_{so} L_{mr} \left[I_{qds1} + I_{qds2} + I_{qds3}\right]}{r_r - j\omega_{so} L_r} \tag{7.60}$$

Using substitutions from Equations (7.60), (7.58) and (7.59) and eliminating the variables such that only term with I_{qds1} appears,

$$AI_{qds1} + B\frac{\left\{-I_{qds1}\left(B - \frac{B^2}{A-T}\right)\right\}}{A - S - \frac{B^2}{A-T}} + B\left\{-I_{qds1}B\left(1 - \frac{B - \frac{B^2}{A-T}}{A - S - \frac{B^2}{A-T}}\right)\right\} - \frac{M_{qds1}}{2}V_{dc} = 0 \quad (7.61)$$

where,

$$A = r_s - j\omega_e L_s + \frac{\omega_e L_m r^2 \omega_{so}}{r_r - j\omega_{so} L_r} \quad (7.62)$$

$$B = \frac{\omega_e L_m r^2 \omega_{so}}{r_r - j\omega_{so} L_r} \quad (7.63)$$

$$S = \frac{1}{j\omega_e C_{p2} + \frac{1}{r_{02} - j\omega_e L_{02}}} \quad (7.64)$$

$$T = \frac{1}{j\omega_e C_{p3} + \frac{1}{r_{03} - j\omega_e L_{03}}} \quad (7.65)$$

Solving the Equation (7.61) and separating I_{qds1} such that

$$I_{qds1}K + \frac{M_{qds1}V_{dc}}{2} = 0 \quad (7.66)$$

$$I_{qds1} = \frac{M_{qds1}}{2K}V_{dc} \quad (7.67)$$

From the rectifier current equation,

$$\frac{3}{4}\mathrm{Re}\left(M_{qds}{I_{qds1}}^*\right) = \frac{V_{dc}}{R_{01}} \quad (7.68)$$

$$\frac{3}{4}\mathrm{Re}\left(M_{qds}{}^{*}I_{qds1}\right)=\frac{V_{dc}}{R_{01}} \tag{7.69}$$

Hence

$$\frac{3}{8}\left|M_{qds}\right|^{2}\mathrm{Re}\left(\frac{1}{K}\right)=\frac{1}{R_{01}} \tag{7.70}$$

Equation (7.70) gives an interesting observation relating modulating index of the converter to the other parameters. It shows that the modulating index is not dependent of output voltage but it depends on the load dynamics.

To study the steady state plot, modulation index is plotted for varying speed above the synchronous speed with different load resistances of 30, 40, 50, 60 and 70 Ohms. The variation is shown in Figure 7.28.

In this way, the behavior of the system is studied at steady state. The variation of Modulation index with speed above the synchronous speed can be regarded as the starting point for the further analysis of the system.

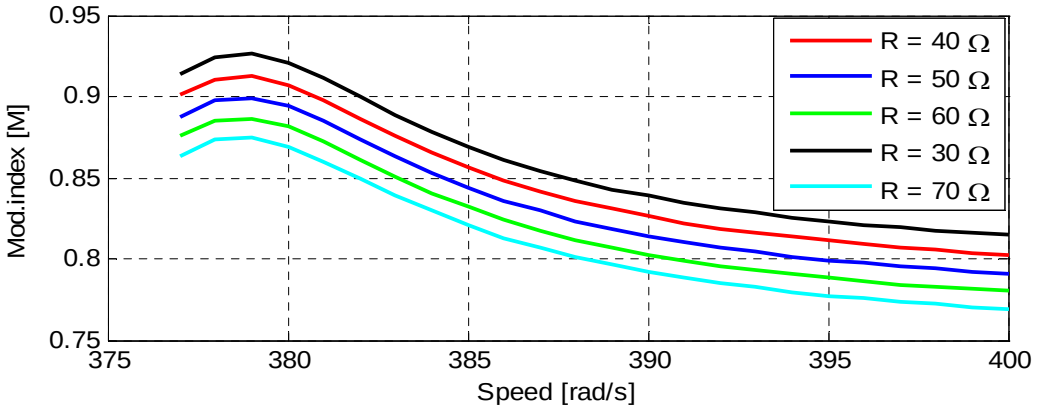

Figure 7.28 Variation of modulation index with the variation in speed

7.7 Conclusion

In this chapter, the three machine configuration of 9-phase induction machine was analyzed in rotor reference frame using the model equations and interfacing with power electronics converters. The contribution of each machine torque towards the total torque in the system is analyzed which signifies the fault tolerant operation and reliability of the system. The parameters of the machine are evaluated using the full order q-d model. The simulation results show that the torque due to individual machine is significant if one or two of the machine will lose power from the system. Hence, a good reliability is obtained from this kind of configuration. The steady state results when operated as a generator shows the inter-coupling of each machine variables when the 9-phase machine is used as generator.

CHAPTER 8

TORQUE CAPABILITY OF 9-PHASE INDUCTION MACHINE OPERATED IN DIFFERENT CONNECTION SCHEMES

8.1 Introduction

As discussed in Chapter 6, for the extended speed/torque capability, a 9-phase induction machine can be operated as 3-phase machine by rearranging the stator windings which is commonly referred as Pole Phase Modulation technique (PPM). Similarly, there exist other connection schemes in case of 9-phase machines as described in Chapter 1. In this chapter, a vector controlled 9-phase induction machine performance is computed using finite element approach when the machine designed for 9-phase, 4-pole operation is operated as pole phase modulation scheme. In order to realize the induction motor performance in any configurations, the finite elements simulations are carried out on the rotor flux reference frame. This approach is applicable for the design of the variable speed multiphase drives for the precise prediction of the controlled performance. Firstly, the vector control scheme using finite elements is discussed with the governing equations. Secondly modeling of the stator and rotor circuits for studying rotor field orientation in finite element software, FEMM is discussed. Finally, the torque capability of the machine is observed performing the simulation of the machine in both operating modes of pole phase modulation using the parameters derived in Chapter 5. Finally, the torque capability of the machine is observed in different connection schemes.

8.2 Vector Control Scheme

In this section, the equations of the motor will be written in the reference frame fixed to rotor flux to realize the vector control scheme. Figure 8.1 describes the field oriented vector control scheme for 9-phase induction motor using finite elements. The reference rotor flux is aligned with the d-axis and corresponding q and d axis currents are estimated with the help of magneto-static simulations. With the help of the Park transformation, the q-d currents are transformed to natural variables and imposed on the slots of the model. The simulation of the finite element model is carried out such that the reference flux is aligned only on d-axis and q-axis rotor flux is zero, which gives the steady state d-axis rotor current to be zero. The similar method can be employed for the 3-phase, 12-pole case with the adjustment in the Park transformation matrix.

The dynamic equations of the motor will be written in the q-d rotor reference frame. The equations are then referred to rotor reference frame to satisfy the field oriented conditions. As these equations only have the fundamental components, they are similar for both nine and 3-phase configuration [41].

Stator and rotor voltage equations:

$$\begin{aligned} V_{qs} &= r_s i_{qs} + p\lambda_{qs} + \omega_r \lambda_{ds} \\ V_{ds} &= r_s i_{ds} + p\lambda_{ds} - \omega_r \lambda_{qs} \end{aligned} \tag{8.1}$$

$$\begin{aligned} V_{qr} &= r_r i_{qr} + p\lambda_{qr} + (\omega - \omega_r)\lambda_{dr} = 0 \\ V_{dr} &= r_r i_{dr} + p\lambda_{dr} - (\omega - \omega_r)\lambda_{qr} = 0 \end{aligned} \tag{8.2}$$

Stator and rotor flux equations:

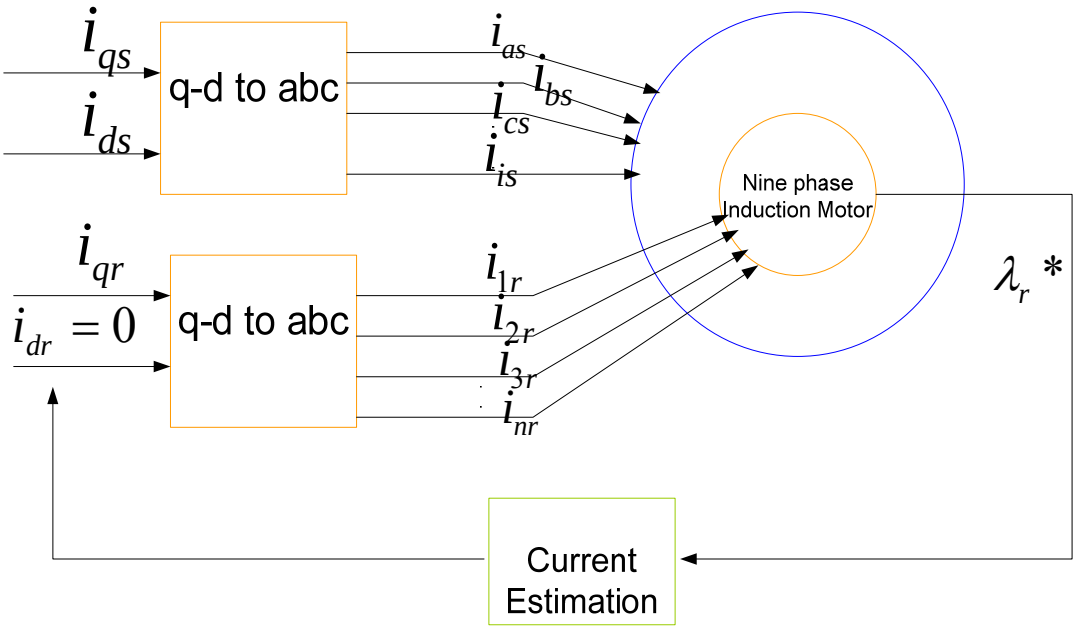

Figure 8.1 Finite element based field oriented scheme for 9-phase induction motor

$$\begin{aligned}
\lambda_{qs} &= L_s i_{qs} + L_m i_{qr} \\
\lambda_{ds} &= L_s i_{ds} + L_m i_{dr} \\
\lambda_{qr} &= L_r i_{qr} + L_m i_{qs} \\
\lambda_{dr} &= L_r i_{dr} + L_m i_{dr}
\end{aligned} \tag{8.3}$$

Under field oriented conditions, the reference frame is chosen such that the d-axis is parallel to the rotor flux, λ_r *. In other words, only d-axis component of rotor flux exists and q-axis component is kept to be zero , i.e.,

$$\lambda_{qr} = 0 \tag{8.4}$$

$$\lambda_{dr} = \lambda_r * \tag{8.5}$$

Assuming the squirrel cage rotor, from Equation (8.2), at steady state,

$$i_{dr} = 0 \tag{8.6}$$

The slip speed, ω_{sl}, which is the difference of stator frequency and rotor frequency is given as

$$\omega_{sl} = \omega - \omega_r = -\frac{R_r i_{rq}}{\lambda_{dr}} \tag{8.7}$$

Using Equations (8.4)-(8.7) in Equation (8.3),

$$\lambda_{dr} = L_m i_{ds}\,,\; i_{qr} = -\frac{L_m i_{qs}}{L_r} \tag{8.8}$$

$$\begin{aligned}\lambda_{ds} &= L_s i_{ds} = L_s i_{qs} + L_m i_{qr} \\ &= \left(L_s - \frac{L_m{}^2}{L_r} \right) i_{qs}\end{aligned} \tag{8.9}$$

This follows that, only varying the q-axis stator current the variation of q-axis rotor current can be performed. Finally the torque equation is given as

$$T = \frac{mP}{4}\frac{L_m}{L_r}\lambda_r * i_{qs} \tag{8.10}$$

where, m is the number of phases and P is the number of poles.

Hence, as seen in Equations (8.1)-(8.10), under the field oriented condition, only the variation of q-axis current and d-axis current are sufficient to determine the variation of other variables.

8.3 Modeling of Stator Circuit in FEM

The finite element simulation is performed using FEMM in aid of the Lua Scripting language. The stator and rotor model is performed using Autocad and imported into FEMM for the analysis. The materials of the model, circuits, blocks and the operating boundary conditions are specified. Newton method is used to solve the finite

element problem. In the modelling of the 36 slot stator for both configurations, a slot matrix is derived from the clock diagram of the model. The outer part of Figure 8.2 shows the clock diagram for 3-phase model and inner part shows the diagram for 9-phase model. After the winding matrix is defined, the stator current should be imposed on each simulation. For imposing the current, the q and d axis current is first transferred into a, b, c currents using Park transformation as described in Section (8.2).

8.4 Modeling of Rotor Circuit in FEM

The modelling of the rotor circuit is performed in q-d reference frame and the winding matrix is determined assuming that the rotor is a 9-phase or 3-phase winding corresponding to the 9-phase or 3 phase induction machine. It is rearranged using the d-q transformation assuming a sine-wave conductor distribution. Such an assumption yields a sinusoidally distributed current in the rotor slots. As the rotor winding matrix is already in q-d frame, there is no need of transforming the q-d rotor currents into natural variables. For the determination of this matrix, the following Equations (8.11) and (8.12) are utilized.

$$k_{rd} = \sin(p\alpha_i),\ k_{rq} = \cos(p\alpha_i) \tag{8.11}$$

where,

$$\alpha_i = \frac{2i-1}{2}\left(\frac{2\pi}{Q_r}\right) \tag{8.12}$$

Q_r is the number of rotor bars in the model and p is the number of poles.

Assuming sinusoidally distributed windings the winding matrix for 9-phase, 4-pole motor is reported in Table (8.1).

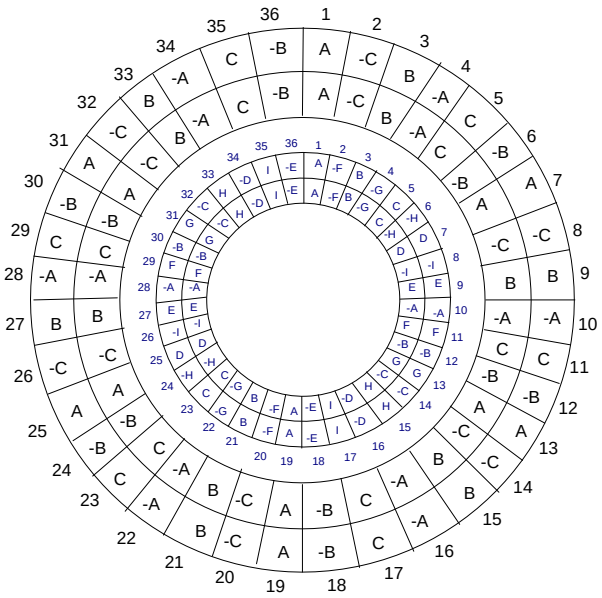

Figure 8.2 Clock diagram for 9-phase, 4-pole (inner) and 3-phase, 12-pole (outer) induction machine

Table 8.1 Rotor winding matrix for 44-slot induction machine

Slot number	k_{rd}	k_{rq}
1	0.142	0.989
2	0.415	0.909
3	0.654	0.755
4	0.841	0.54
5	0.959	0.281
6	1	0
7	0.959	-0.281
8	0.841	-0.540
9	0.654	-0.755
10	0.415	-0.909
11	0.142	-0.989

Table 8.1 cont'd Rotor winding matrix for 44-slot induction machine

Slot number	k_{rd}	k_{rq}
12	-0.142	-0.989
13	-0.415	-0.909
14	-0.654	-0.755
15	-0.841	-0.54
16	-0.959	-0.281
17	-1	0
18	-0.959	0.281
19	-0.841	0.54
20	-0.654	0.755
21	-0.415	0.909
22	-0.142	0.989
23	0.142	0.989
24	0.415	0.909
25	0.654	0.755
26	0.841	0.54
27	0.959	0.281
28	1	0
29	0.959	-0.281
30	0.841	-0.54
31	0.654	-0.755
32	0.415	-0.909
33	0.142	-0.989
34	-0.142	-0.989
35	-0.415	-0.909
36	-0.654	-0.755
37	-0.841	-0.54
38	-0.959	-0.281
39	-1	0

Table 8.1 cont'd Rotor winding matrix for 44-slot induction machine

Slot number	k_{rd}	k_{rq}
40	-0.959	0.281
41	-0.841	0.54
42	-0.654	0.755
43	-0.415	0.909
44	-0.142	0.989

Similar to the 9-phase, 4-pole rotor matrix, similar type of matrix also exists for 3-phase, 12-pole configuration as the elements of the table are dependent on the pole and number of phases from Equation (8.12)-(8.14). The assignment of rotor currents is carried out in the same way of the assignment of the stator currents. However, for this assignment, there is no need of transformation to d-q reference as they are already calculated in d-q reference in Table 8.1.

8.5 Torque Capability of Induction Motor in Pole Phase Modulation

In this section, the realization of the vector control of induction motor when operated as pole phase modulation is observed and the different variables are analyzed that aids for the torque capability of the machine in both configurations. An induction motor has three region of operation as shown in Figure 8.3. According to the scheme described in the Section 8.2, the simulation of the machine needs to be performed in the rotor reference frame by aligning the rotor flux to d axis, then each region of operation

needs to be investigated. The regions of operation of an induction motor under vector control scheme are given as follows:

a. Constant Torque Region: In this region of operation, the rotor flux producing torque is kept constant, and speed is increased from zero to base speed. The q and d axis currents are also constant which gives the constant slip. The rated stator current is drawn under this condition. The machine voltage increases from zero to maximum allowable voltage. This is indicated by the constant part of Figure 8.3.

In order to evaluate the transition frequency solution of the model equations needs to be performed.

$$\begin{aligned} V_{qs} &= r_s i_{qs} + p\lambda_{qs} + \omega_r \lambda_{ds} \\ V_{ds} &= r_s i_{ds} + p\lambda_{ds} - \omega_r \lambda_{qs} \end{aligned} \tag{8.13}$$

Ignoring the stator resistance,

$$\begin{aligned} V_{qs} &= \omega_r \lambda_{ds} \\ V_{ds} &= -\omega_r \lambda_{qs} \end{aligned} \tag{8.14}$$

Also, under rotor field Orientation,

$$\lambda_{qs} = L_s i_{qs} + L_m i_{qr} = \left(L_s - \frac{{L_m}^2}{L_r} \right) i_{qs} \tag{8.15}$$

Squaring and adding,

$$\begin{aligned} {V_{qs}}^2 + {V_{ds}}^2 &= (\omega_r \lambda_{ds})^2 + (\omega_r \lambda_{qs})^2 \\ {V_s}^2 &= {\omega_r}^2 {L_s}^2 {i_{ds}}^2 + {\omega_r}^2 {L_\sigma}^2 {i_{qs}}^2 \end{aligned} \tag{8.16}$$

Hence, the transition frequency is,

$$\omega_B = \frac{V_s}{\sqrt{{L_s}^2 {i_{ds,rated}}^2 + {L_\sigma}^2 \left[{I_s}^2 - {i_{ds,rated}}^2 \right]}} \tag{8.17}$$

b. Field Weakening Region I: After the transition frequency, ω_B the machine attains the Field Weakening region. Here, the rotor flux begins to decrease with the increase of speed. The current constraint is still valid and voltage enters into the constant region.

To evaluate the d and q axis current in this region, starting from the basic dynamic equations of the machine in steady state and adding q and d axis voltages in steady state,

$$\begin{aligned} V_{qs}^{\ 2} + V_{ds}^{\ 2} &= (\omega_r \lambda_{ds})^2 + (\omega_r \lambda_{qs})^2 \\ V_s^{\ 2} &= \omega_r^{\ 2} L_s^{\ 2} i_{ds}^{\ 2} + \omega_r^{\ 2} L_\sigma^{\ 2} i_{qs}^{\ 2} \\ i_{ds}^{\ 2} + i_{qs}^{\ 2} &= I_s^{\ 2} \end{aligned} \tag{8.18}$$

Eliminating the above two equations in terms of i_{qs} and i_{ds}

$$\begin{aligned} i_{qs} &= \sqrt{\frac{\omega^2 L_s^{\ 2} I_s^{\ 2} - V_s^{\ 2}}{\omega^2 L_s^{\ 2} - \omega^2 L_\sigma^{\ 2}}} \\ i_{ds} &= \sqrt{\frac{V_s^{\ 2} - \omega^2 L_\sigma^{\ 2} I_s^{\ 2}}{\omega^2 L_s^{\ 2} - \omega^2 L_\sigma^{\ 2}}} \end{aligned} \tag{8.19}$$

For each value of the rotor speed, currents i_{qs} and i_{ds} are injected such that the flux weakening is obtained. The torque decreases as speed increase.

c. Field Weakening Region II: In this region, the current constraint no longer holds true. Similarly, in this case, the phase voltage is not enough to supply the rated current. As a result of which, torque and flux both will decrease and current limit is not satisfied. The stator q-axis current and d-axis currents both decrease with speed. This is shown as region III in Figure 8.3.

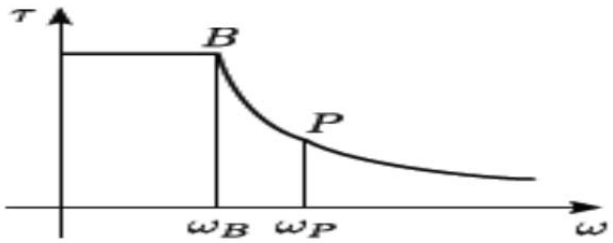

Figure 8.3 Regions of operation of induction motor

8.6 Simulation Results for Pole Phase Modulation

With the help of the model described in Section 8.3 and the algorithm described in Section 8.2, finite element simulation is carried out to verify the controlled performance of pole phase modulated machine in FO condition. The simulation is first carried out for the 9-phase, 4-pole configuration under the rated conditions. With the equivalent rating for operating the machine in 3-phase, 12-pole configuration, the simulations are again carried out. The variables are plotted with respect to the mechanical speed of the motor. Figure 8.4 depicts the q-axis current as mechanical speed changes from 0 to 3000 rad/s. The three regions of operation can be observed from the graph for both 3-phase and 9-phase configurations. The variation of d-axis current with variation of mechanical speed is depicted in Figure 8.5. Similarly, Figure 8.6 describes the variation of variation of input current with the variation of speed for both configurations. The variation of rotor flux with the change of speed is shown in Figure 8.7. Similarly, Figure 8.8 shows the torque capability graph when operated in both configurations. The output power variation in both configurations is shown in Figure 8.9 and total loss in the system is depicted in Figure 8.10. In order to observe the variation of parameters, the parameters

are plotted with variation of electrical speed. Figure 8.11 shows the magnetizing inductance with the change in speed and Figure 8.12 and 8.13 show leakage inductance and rotor resistance of system, respectively.

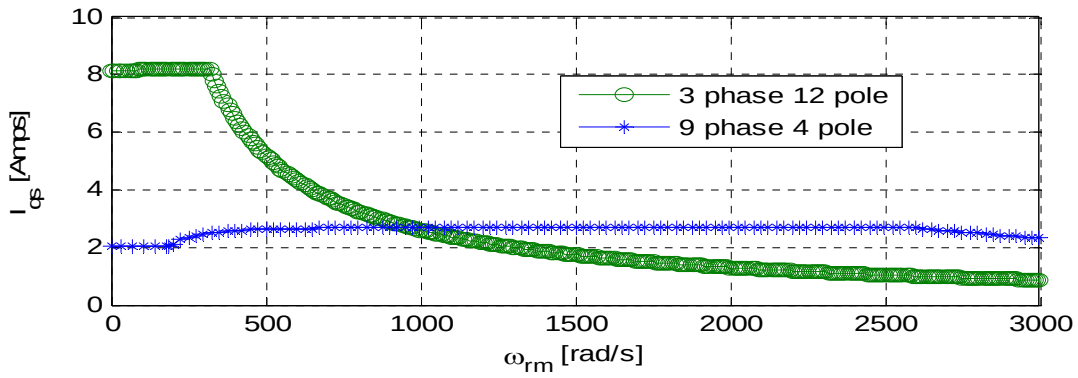

Figure 8.4 q-axis current vs. mechanical speed

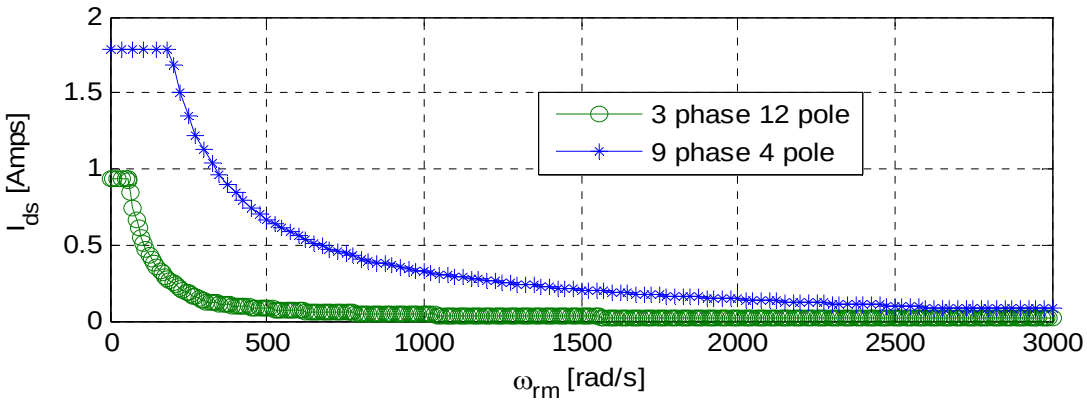

Figure 8.5 Variation of d-axis current vs mechanical speed

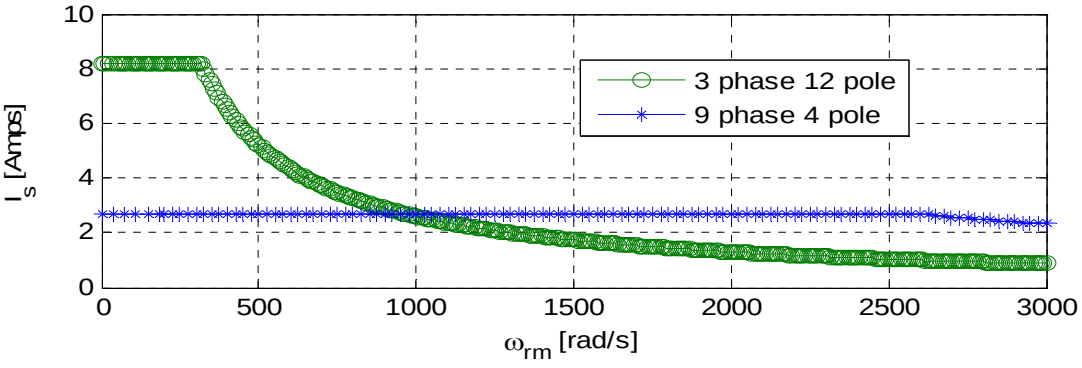

Figure 8.6 Variation of total peak current vs mechanical speed

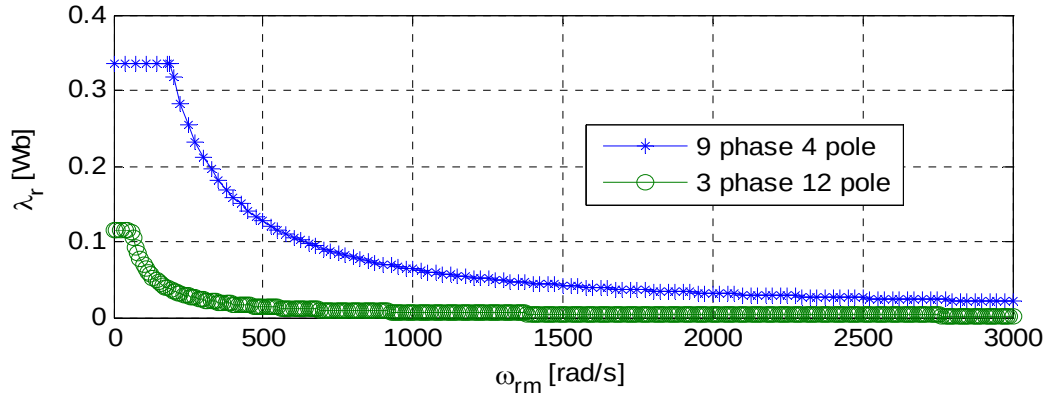

Figure 8.7 Variation of rotor flux vs mechanical speed

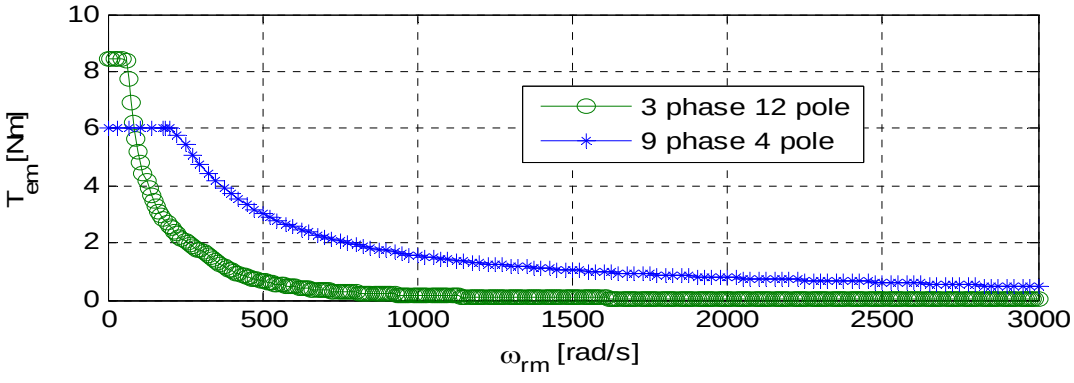

Figure 8.8 Variation of total electromagnetic torque vs speed

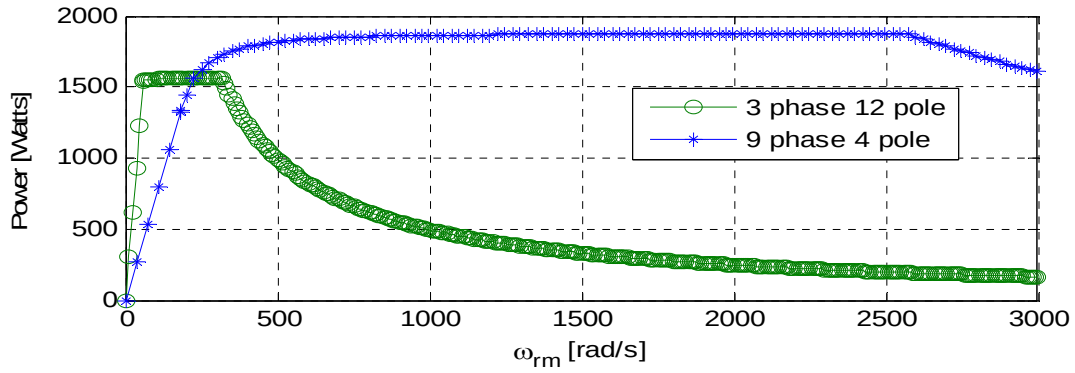

Figure 8.9 Variation of output power vs mechanical speed

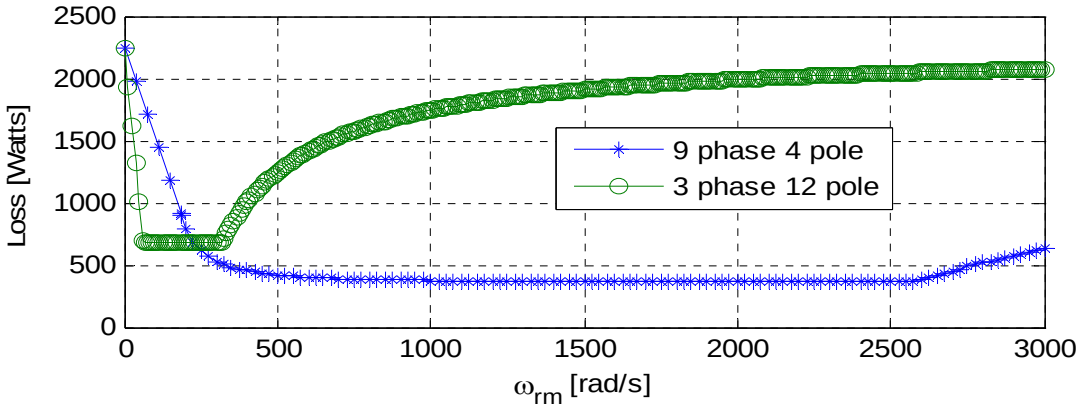

Figure 8.10 Variation of total loss vs mechanical speed

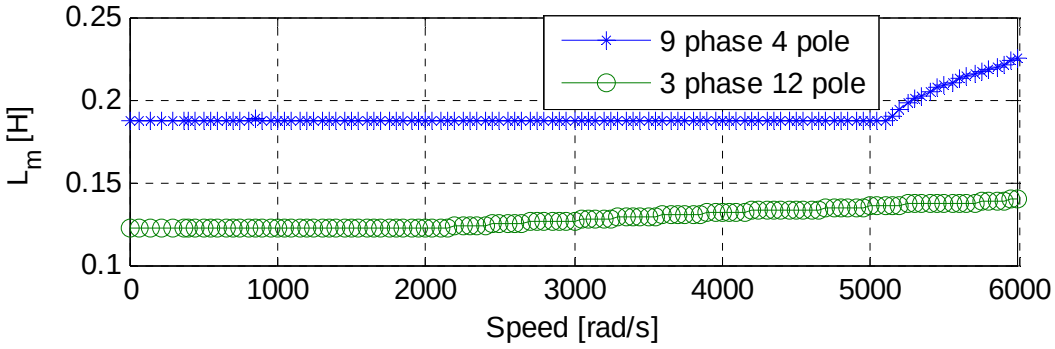

Figure 8.11 Variation of magnetizing inductance with electrical speed

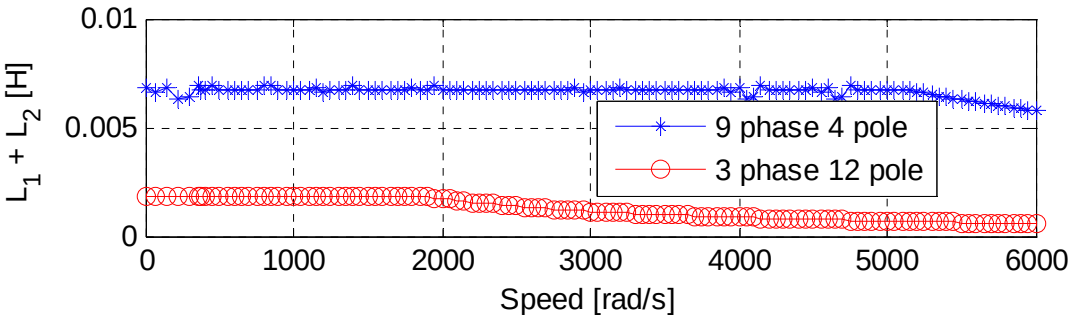

Figure 8.12 Variation of sum of leakage inductance with electrical speed

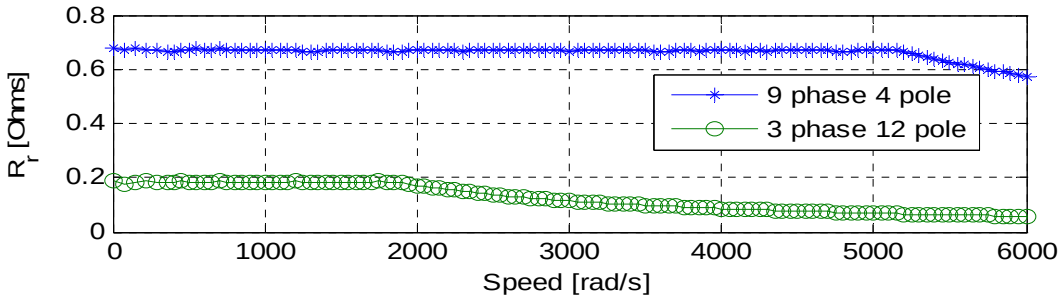

Figure 8.13 Variation of rotor resistance with electrical speed

From the set of Figures 8.4-8.13, the torque capability of the pole phase modulated induction machine can be realized. According to the principle of pole phase modulation, 9 phase machine is utilized as 3-phase, 12-pole configuration in low speeds and for high torque applications whereas it is operated in 9-phase, 4-pole operation for high speed and low torque applications. It corresponds to the observation given in Figure 8.8, where the torque capability graph of the pole phase modulated system is visualized. Until the base speed of the 3-phase configuration, machine can be operated as 3-phase and as it beings to follow the flux weakening path, the 9-phase configuration will result in

higher torque production than 3-phase. This gives an idea of flux weakening control of the 9-phase induction machine when it is operated in pole phase modulation.

8.7 Torque Capability of the 9-phase Induction Machine in Different Connections

In this section, different connections of the 9-phase induction machine are analyzed in terms of the realization of the rotor field orientation using finite elements. As described in Chapter 1, the 9-phase machine can be connected in five different configurations with the varying phase voltages across the windings. Figure 8.14 shows these possible configurations with respective phase voltages. However, finite element simulation involves the current injection in the respective slots. Hence, during the injection of the rated current, the phase current needs to be calculated with the help of the circuit configuration. It is observed that, if I_m has is the maximum voltage amplitude for Connection 1, the maximum current for Connection 2 is $0.684I_m$ and so on. This observation corresponds to the equation derived in Chapter 1 for different connections. After the rated current is evaluated for each configuration, the current is injected inside respective slots using the LUA scripting language. The model of stator circuit, rotor circuit and rotor field orientation are performed as described in previous section with the adjustment in the injected current.

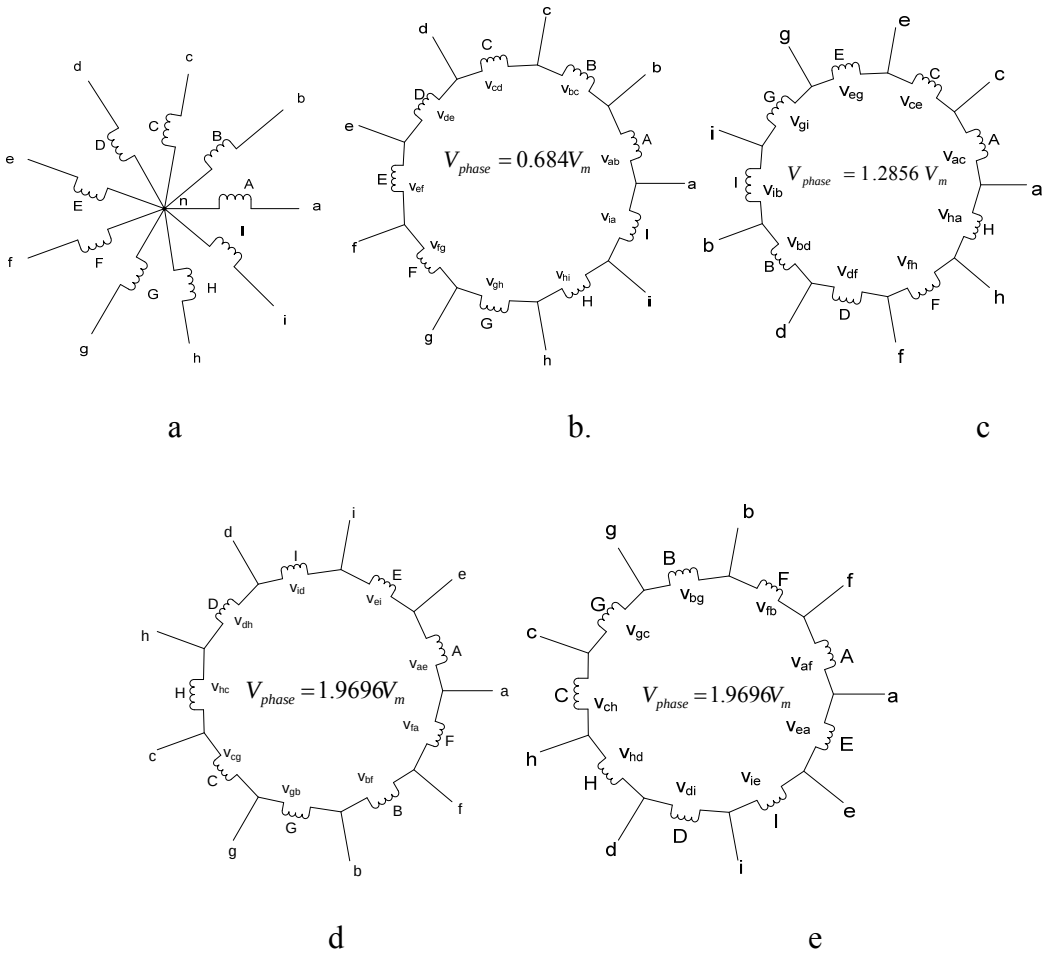

Figure 8.14 Stator connections of 9-phase induction machine a. Star connection b. Connection 1 c. Connection 2 d. Connection 3 e. Connection 4

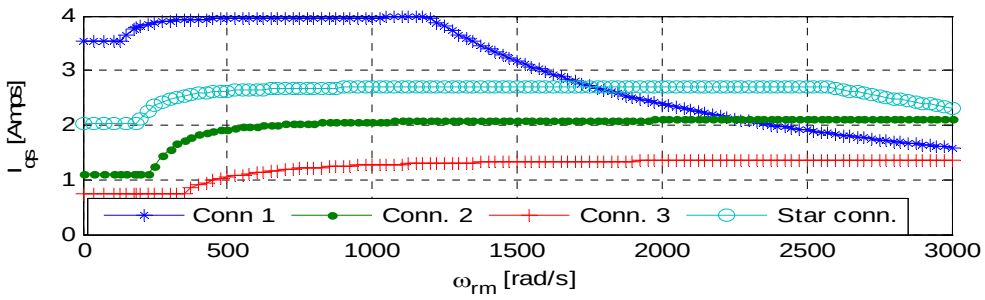

Figure 8.15 Variation of q-axis current vs. mechanical speed

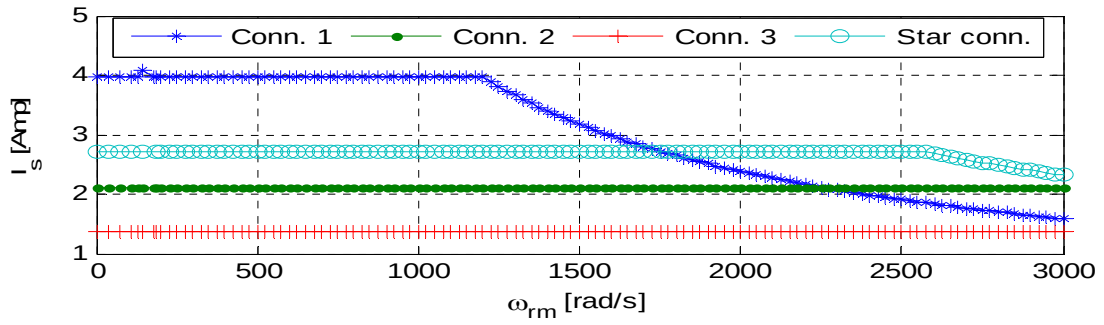

Figure 8.16 Variation of d-axis current vs. mechanical speed

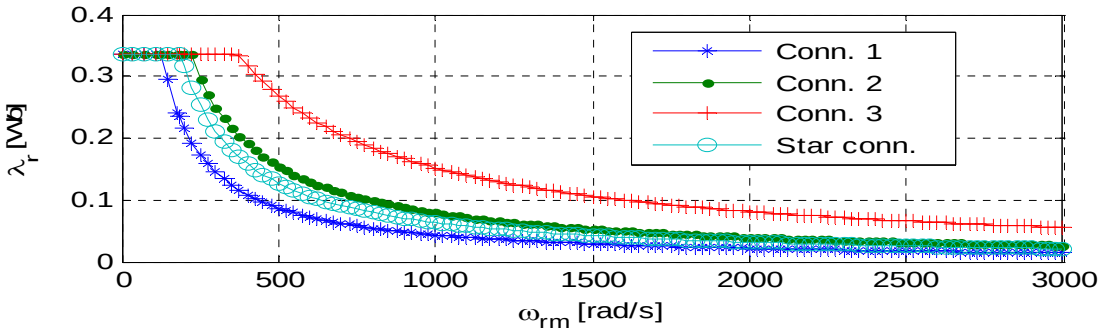

Figure 8.17 Variation of rotor flux vs. mechanical speed

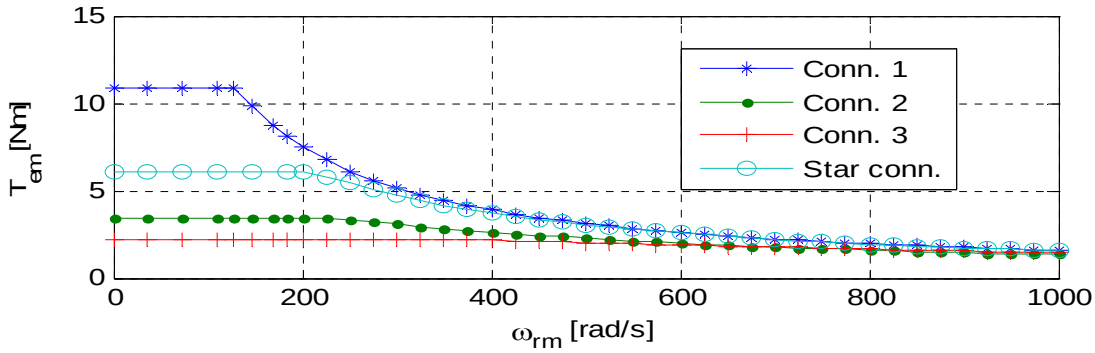

Figure 8.18 Variation of electromagnetic torque vs. mechanical speed

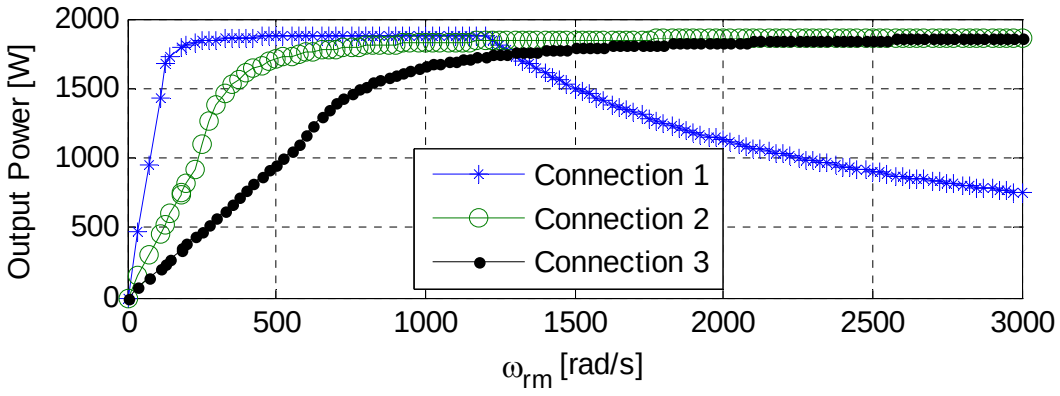

Figure 8.19 Variation of output power vs. mechanical speed

From the set of Figures 8.15-8.19, different connection scheme implies the use of 9-phase induction machine in different configuration with the variation in torque capability and performance of the drive. From the torque graph of Figure 8.18, the transition of the connection can be performed to operate the machine in different torque operations in Field weakening regions.

8.8 Conclusion

In this chapter, a finite element based analysis is presented to study the torque capability for different stator winding connection schemes of 9-phase induction machine. Different regions of operation in Field Weakening operations are also observed with the help of performance graphs. Interesting results verify of the operation of the pole phase modulated drive in different operations to get the required torque capability. Similarly, different regions of operation in different connection schemes also show the flexibility of

operation of the 9-phase induction machine for different operations with different torque requirements.

CHAPTER 9

SWITCHING SIGNAL GENERATION USING C6713 DSP AND XILINX SPARTAN 3E FPGA

9.1 Introduction

In this chapter, progress made in the 9-phase switching signal generation using the interfacing of C6713 DSP and Xilinx Spartan 3E FPGA is presented. The actual PWM signals generated through EMIF interfacing of DSP and FPGA are presented. Similarly, the output voltage and current are also presented first by driving a small resistor and later, driving a 9-phase induction motor.

9.2 Operation of C6713 DSK Starter Kit

The 6713 DSP Starter Kit (DSK) is a low-cost platform which lets customers develop applications for Texas Instruments C67X DSP family. The primary features of the DSK are [77]

a. 225 MHz TMS320C6713 Floating Point DSP

b. AIC23 Stereo Codec

c. Four Position User DIP Switch and Four User LEDs

d. On-board Flash and SDRAM

Figure 9.1 illustrates the C6713 DSK with all the components labelled.

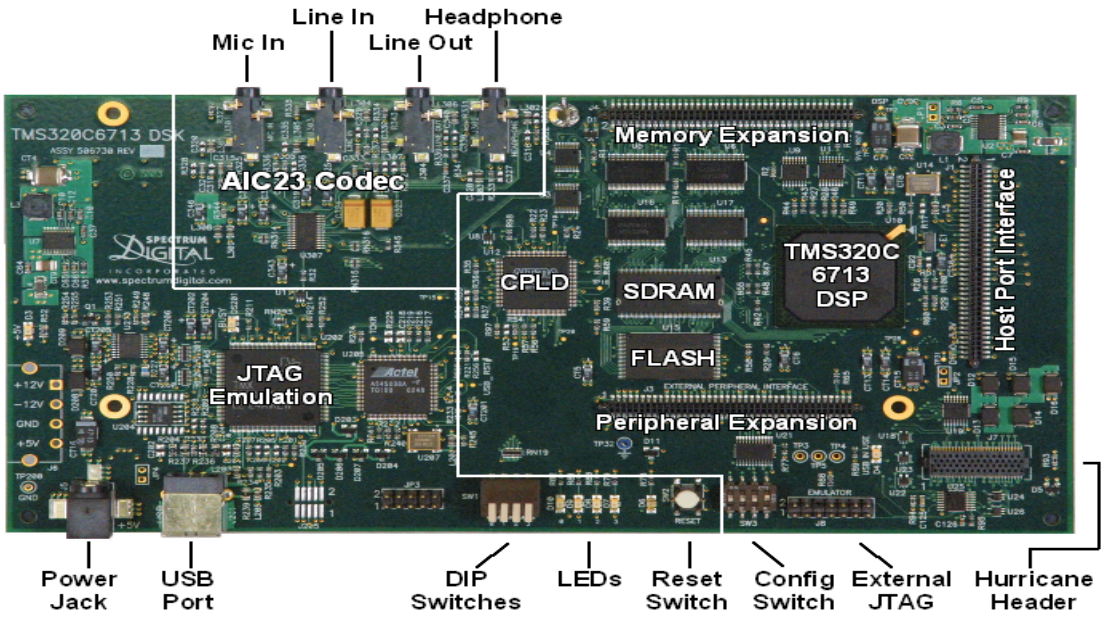

Figure 9.1 Components of C6713 DSK

The peripherals of C6713 DSK include a multi-channel buffered serial ports (McBSPs), 32-bit external memory interface (EMIF) with integrated SDRAM controller , two on-board timers and an enhanced DMA controller (EDMA). The advantage of using C6713 is that it has a significant amount of internal memory so many applications will have all code and data on-chip. The synchronous and asynchronous memories are connected through the EMIF. The daughter card modules can also be added since the EMIF signals are also brought out to standard TI expansion bus connectors. The DSK also consists of on-board codec called the AIC23. Codec stands for coder/decoder which codes analog input samples into a digital format for the DSP to process, then it also decode data coming out of the DSP to generate the processed analog output. Digital data is sent to and from the codec on McBSP1.

9.2.1 Memory Map of C6713 DSK

The major advantage of using the C6713 family of DSPs is that it has a large byte addressable address space. Program data and code can be placed anywhere in the unified address space. Addresses are always 32-bits wide. The memory map shows the address space of a generic C6713 processor on the left with specific details of how each region is used on the right. By default, the internal memory sits at the beginning of the address space. Portions of the internal memory can be reconfigured in software as L2 cache rather than fixed RAM. The EMIF has 4 separate addressable regions called chip enable spaces (CE0-CE3). The SDRAM occupies CE0 while the Flash and CPLD share CE1. CE2 and CE3 are generally reserved for daughter cards. Figure 9.2 depicts the memory map of C6713 DSP [77].

9.3 Operation of Xilinx Spartan 3E FPGA

The Spartan-3E family of Field-Programmable Gate Arrays (FPGAs) is specifically designed to meet the needs of high volume, cost-sensitive consumer electronic applications.

The new features of the Spartan-3E family improve the system performance and cost of configuration is also reduced. These Spartan-3E FPGA enhancements deliver more functionality and bandwidth than was previously possible, setting new standards in the programmable logic industry. [76]

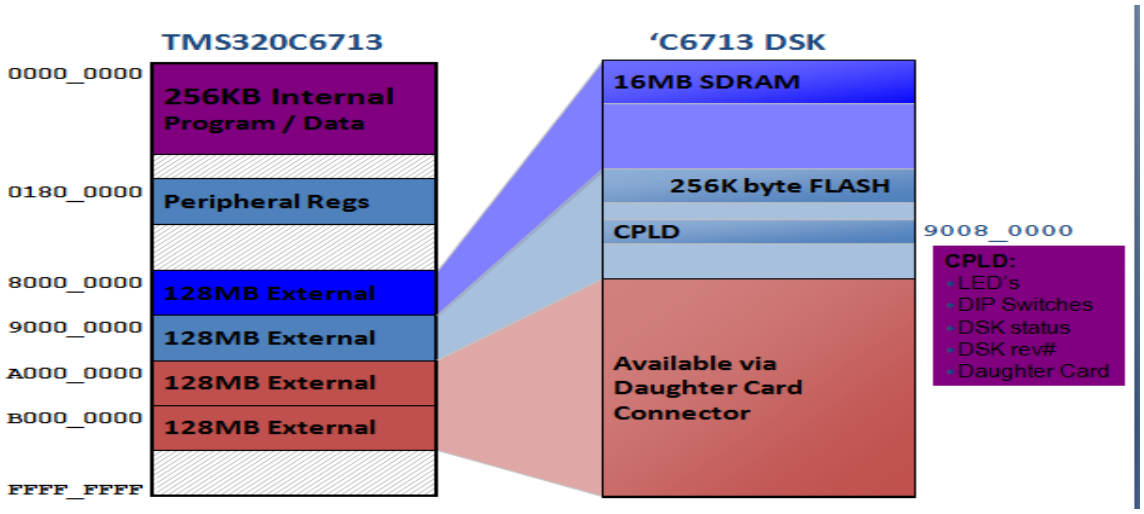

Figure 9.2 Memory map of C6713 DSP

9.3.1 Operation of Nexys 2 Board

The Nexys2 circuit board is a development platform based on a Xilinx Spartan 3E FPGA and it is ready-to-use circuit. The Nexys2 adopts leading technologies to a single platform that can be utilized to gain digital design experience. It can host countless FPGA-based digital systems, and designs can be grown beyond using the different expansion connecters available in the board. Four 12-pin Peripheral Module (Pmod) connectors can accommodate up to eight low-cost Pmods to add features like motor control, A/D and D/A conversion, audio circuits, and a host of sensor and actuator interfaces. All user accessible signals on the Nexys2 board are ESD and short-circuit protected, and it ensures a long operating life in any environment. Figure 9.3 shows the basic building block of the Nexys 2 board with its components [77].

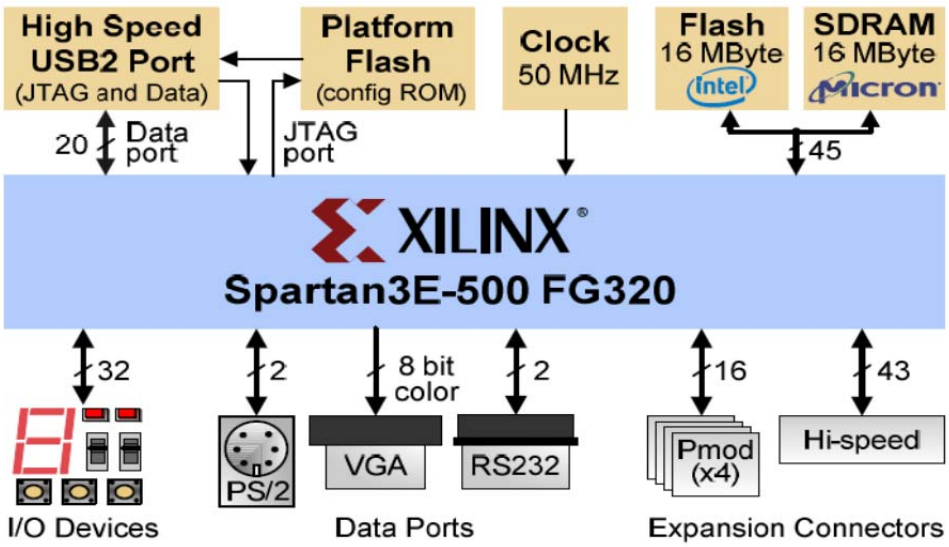

Figure 9.3 Basic building block of Nexys 2 board

9.3.2 EMIF Interfacing Between DSP and FPGA

The interfacing of C6713 DSP with Xilnx Spartan 3E FPGA is performed using the designed interfacing board. In our case, the modulation signal is generated in DSP and interfaced through EMIF connector to FPGA with the help of FX2 hirose connector. The Nexys2 board includes a Hirose FX-2 high density 100-pin connector that is suitable for driving peripheral boards with signal rates in excess of 100 MHz. Many connector signals are routed to the FPGA as differential pairs, and 47 connector pins are tied to ground, resulting in a very low-noise connection system. Figure 9.4 shows the distinctive interfacing circuit of DSP and FPGA using EMIF interfacing to utilize the feedback speed control of the machine using PWM interface. Figure 9.5 shows the connection of DSP and FPGA with the help of designed connector board.

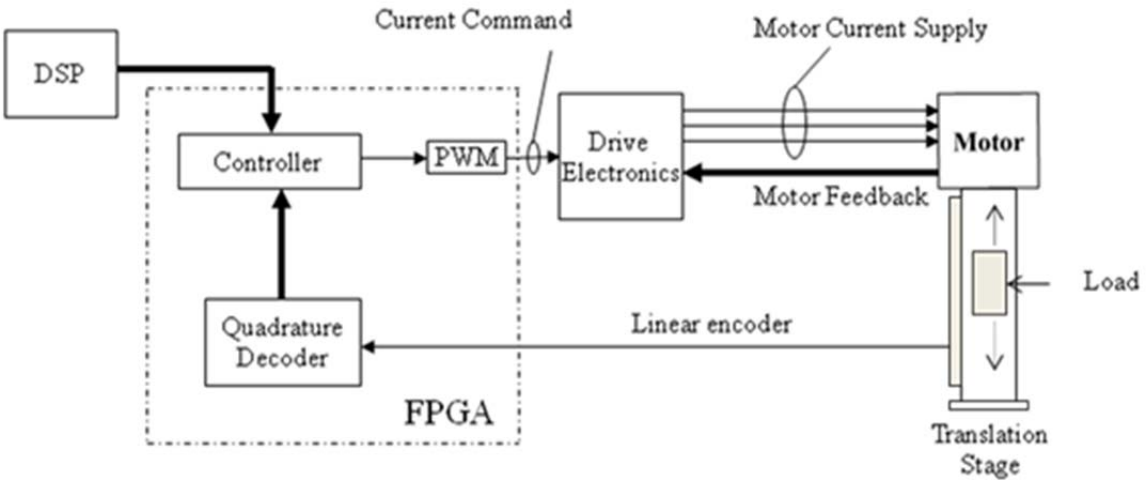

Figure 9.4 DSP-FPGA Control System

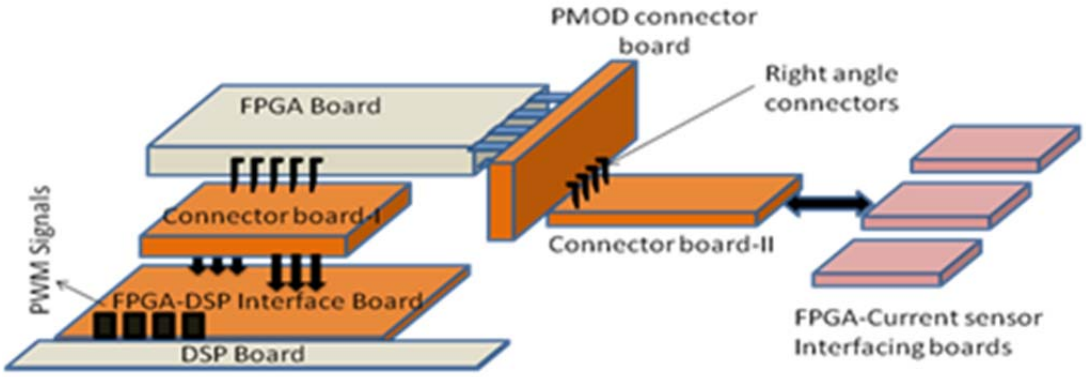

Figure 9.5. Designed architecture of the DSP- FPGA Interfacing

Pins assigned for EMIF connector of DSP:

Eighty pins of the EMIF are used for Voltage, Ground, Address, Data and Control propose out of which 20 pins are address pins, 32 pins are data bus pins, 10 pins are control bus pins, 4 pins are +5 V pins, 12 pins are Ground pins and 3 pins are 3.3V level pins. Out of the 20 address pins, only pin numbers 17, 18, 19, 20, 23, 24, 25 and 26 are used in our design. Similarly, out of 32 data bus pins, pin numbers 53, 54, 55, 56, 57, 58,

59, 60, 63, 64, 65, 66, 67, 68, 69 and 70 are used for data pins. Similarly, pins numbers 27, 28, 29, 30, 73, 74, 75, 76, 77, 78 are used as control pins. The connection between the DSP and FPGA is shown in Figure 9.6 with the connector board interfaced between them.

Pins assigned for FX Hirose connector of FPGA:

To connect the corresponding pins of FPGA to DSP, the connector board is connected to FX Hirose connector of FPGA with the configuration as given in Figure 9.7.

9.4 Switching Signals Generation Using DSP and FPGA

In this section, results from the the switching signals generation using the data, address and control pins of DSP is illustrated. Firstly, the address signals and control signals are shown for one voltage signal. Then, the outputs of PWM pins from FPGA are illustrated.

Figure 9.8 depict the control and address signal obtained from the DSP for the assignment of first voltage of the DSP output.

9.4.1 Output Using 9-Phase Resistor as Load

As the first part of the experiment, nine resistors each of 100 Ohms are connected in star across an inverter driven from the PWM signals obtained from FPGA. Figure 9.9 shows the voltage signal Vab. Similarly, Figures 9.10, 9.11, and 9.12, respectively show the voltage signals V_{ac}, V_{ad} and V_{ae}, respectively compared with signal V_{ab}.

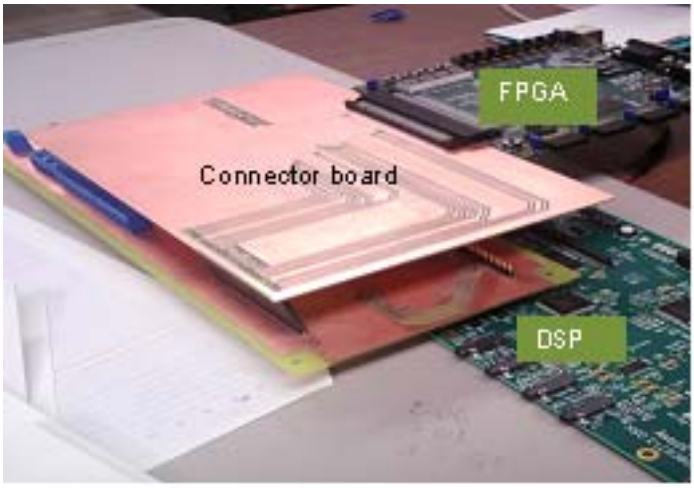

Figure 9.6 Connector board for FPGA and DSP interfacing

FPGA	DSP	FPGA	DSP	FPGA	DSP	FPGA	DSP
27	26	04	51	16	65	15	64
25	24	06	53	18	67	13	60
23	20	08	55	20	69	11	58
22	19	10	57	21	70	09	56
24	23	12	59	19	68	07	54
26	25	14	63	17	66		

Figure 9.7 Hirose FX2 connections with corresponding EMIF pins of DSP

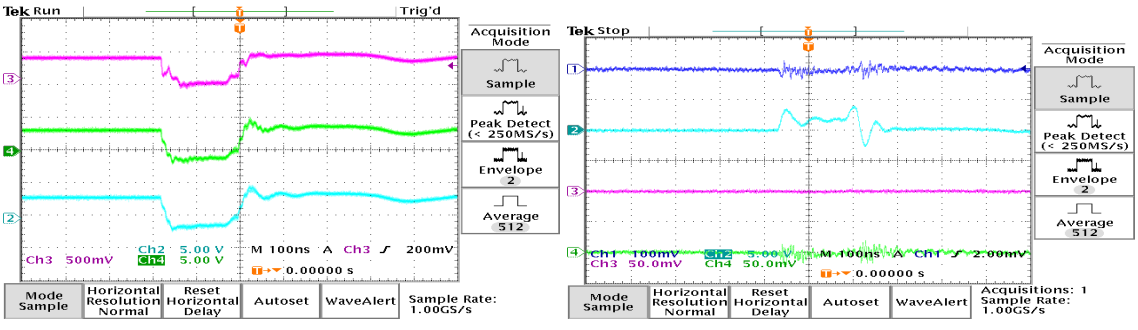

Figure 9.8 Control and address signals from DSP for first voltage output

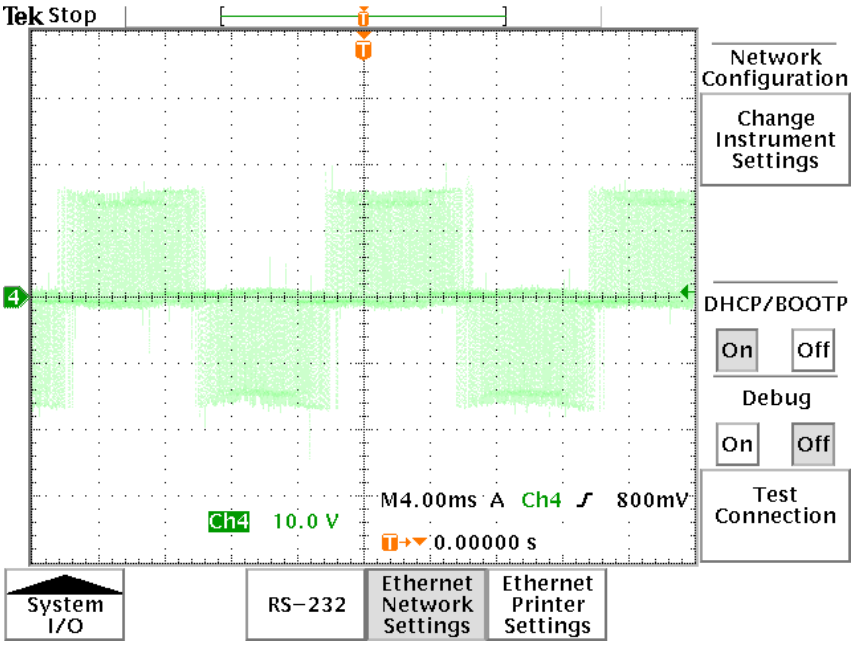

Figure 9.9 Voltage signal V_{ab} across resistor as load

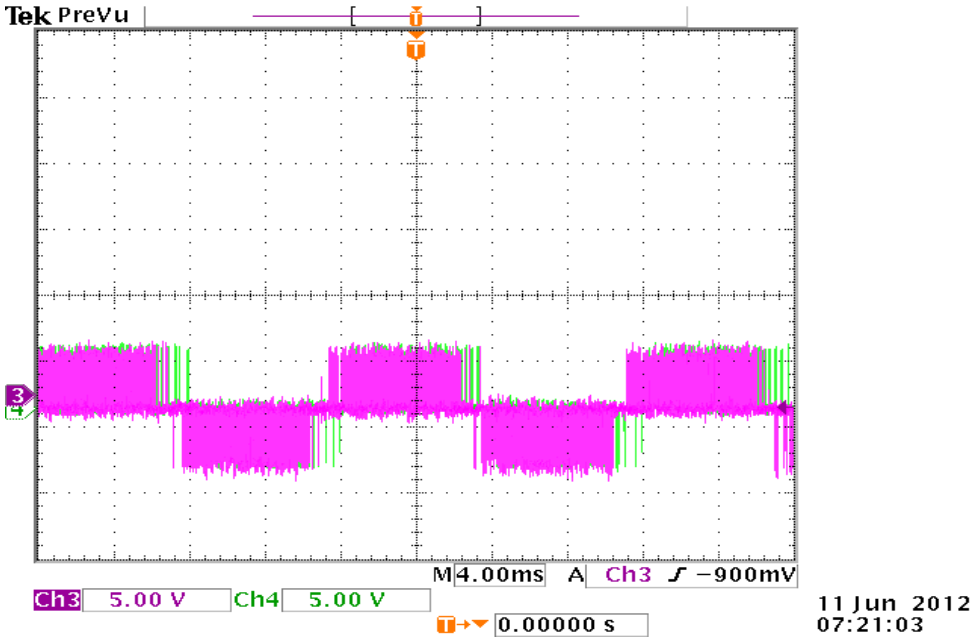

Figure 9.10 Voltage signals V_{ab} and V_{ac}

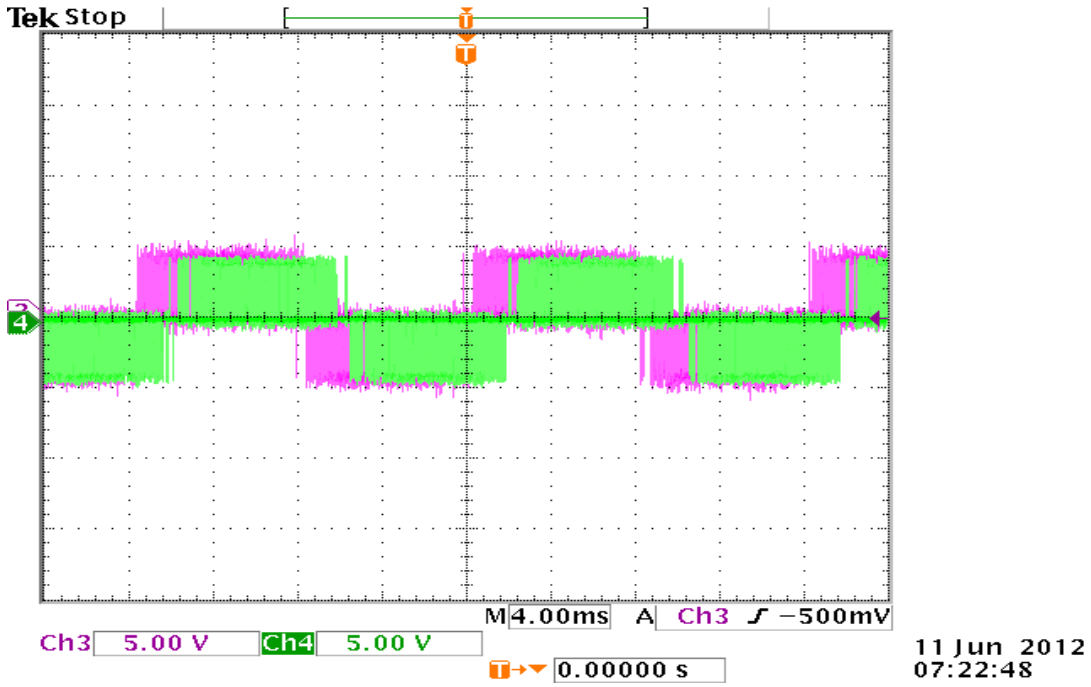

Figure 9.11 Voltage signals V_{ab} and V_{ad}

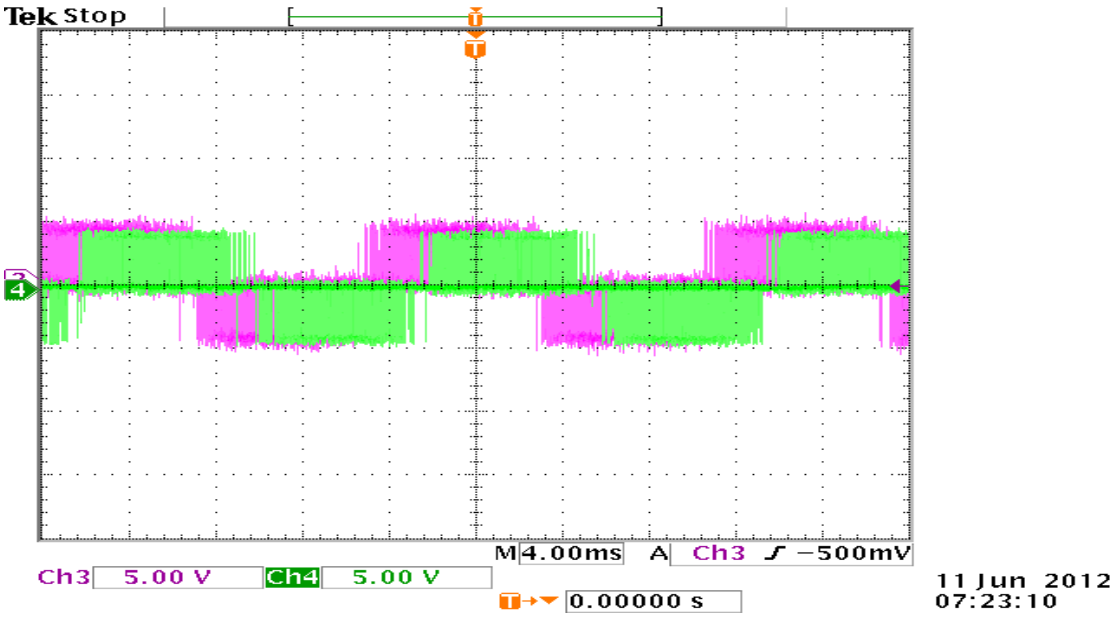

Figure 9.12 Voltage signals V_{ab} and V_{ae}

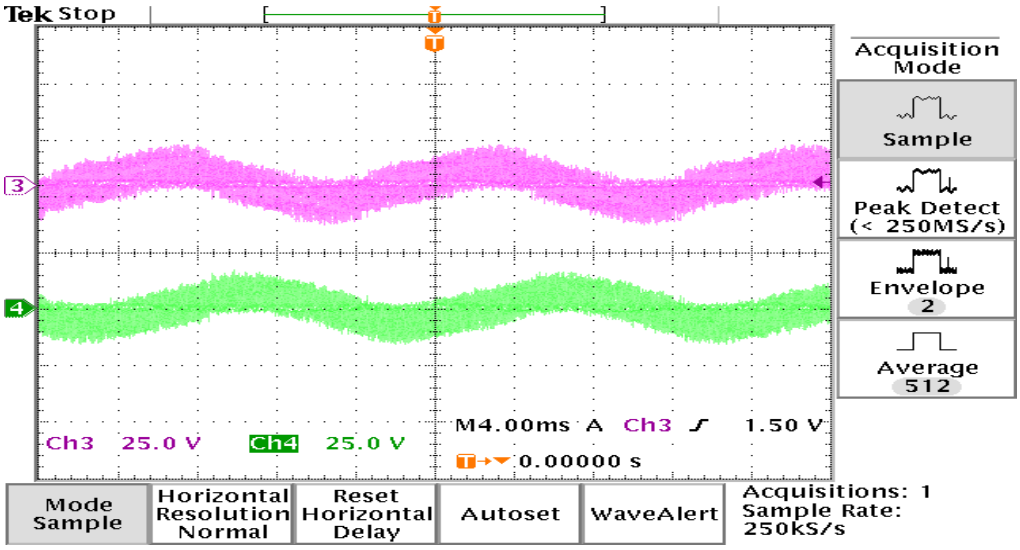

Figure 9.13 Channels 3 and 4, respectively show phase voltages for phase 'a' and phase 'b' for 9-phase resistor load

Figure 9.13 shows the phase to neutral voltage across phase 'a' and phase 'b' of the 9-phase load. Figure 9.14 shows the PSIM simulation of the phase voltage obtained by using the same parameters. The experimental results are in good agreement with the simulation.

9.5 Experimental Results for 9-Phase Induction Motor Driven by PWM Inverter Using DSP-FPGA Interface

In this section, the experimental results using the interfacing of DSP and FPGA are performed driving the 9-phase motor as load from the 9 leg inverter. Figure 9.14 shows the phase 'a' voltage of the inverter connected to load when operated at rated voltage condition.

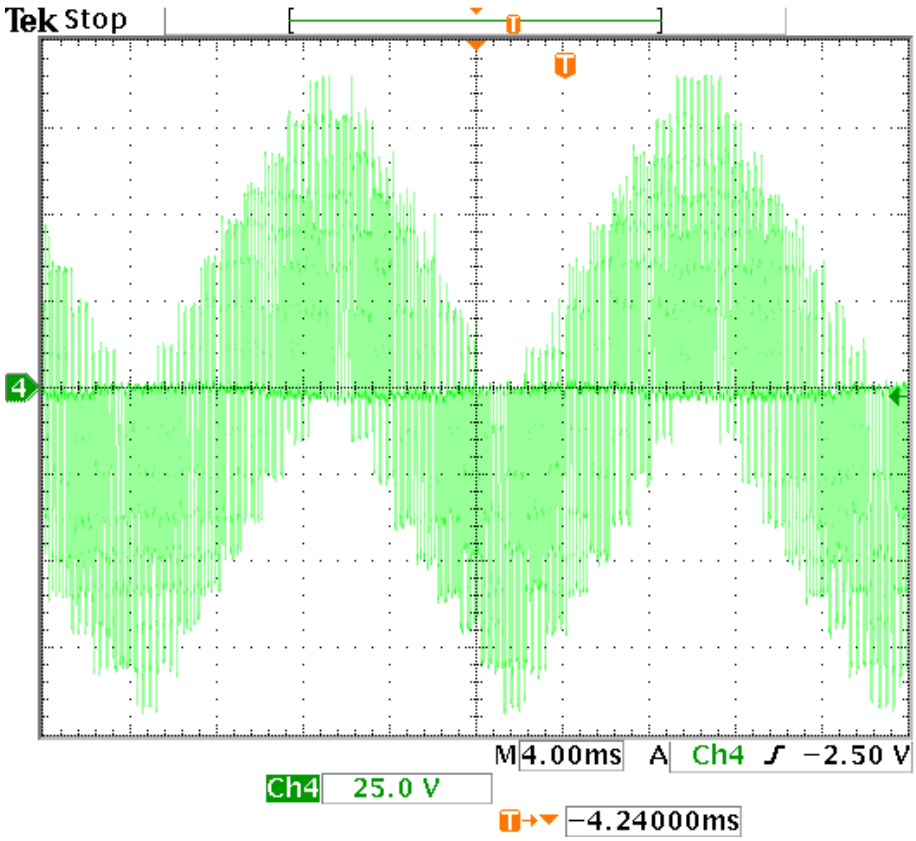

Figure 9.14 Phase ‘a’ voltage for 9-phase induction motor obtained using DSP-FPGA interfacing

Similarly, Figure 9.15 shows the simulation results for 9-phase Inverter phase ‘a’ voltage. Figure 9.16 shows the transient phase ‘a’ current during starting of the 9-phase induction motor and Figure 9.17 depicts the steady state phase ‘a’ current after the machine attains the steady state. The experimental results are in good agreement with the simulation results obtained from MATLAB/Simulink.

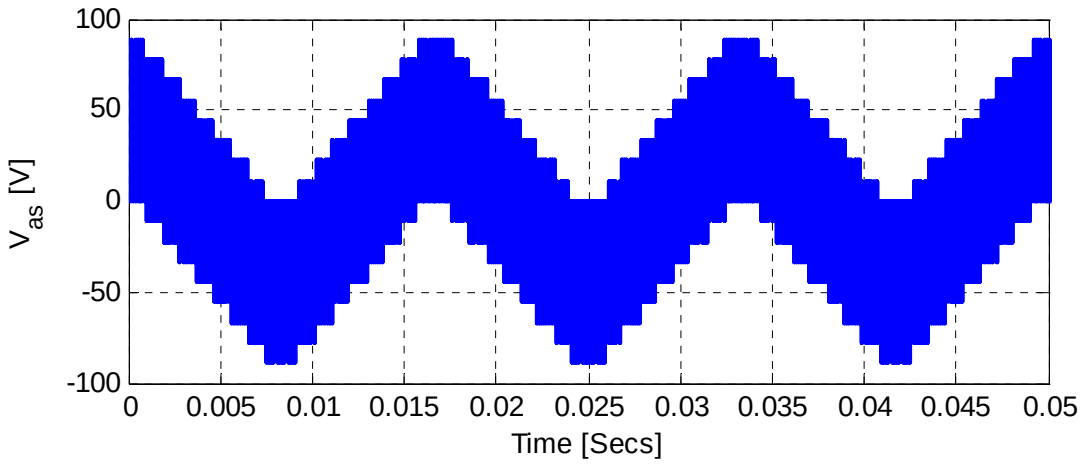

Figure 9.15 Simulation Results for phase '*a*' voltage

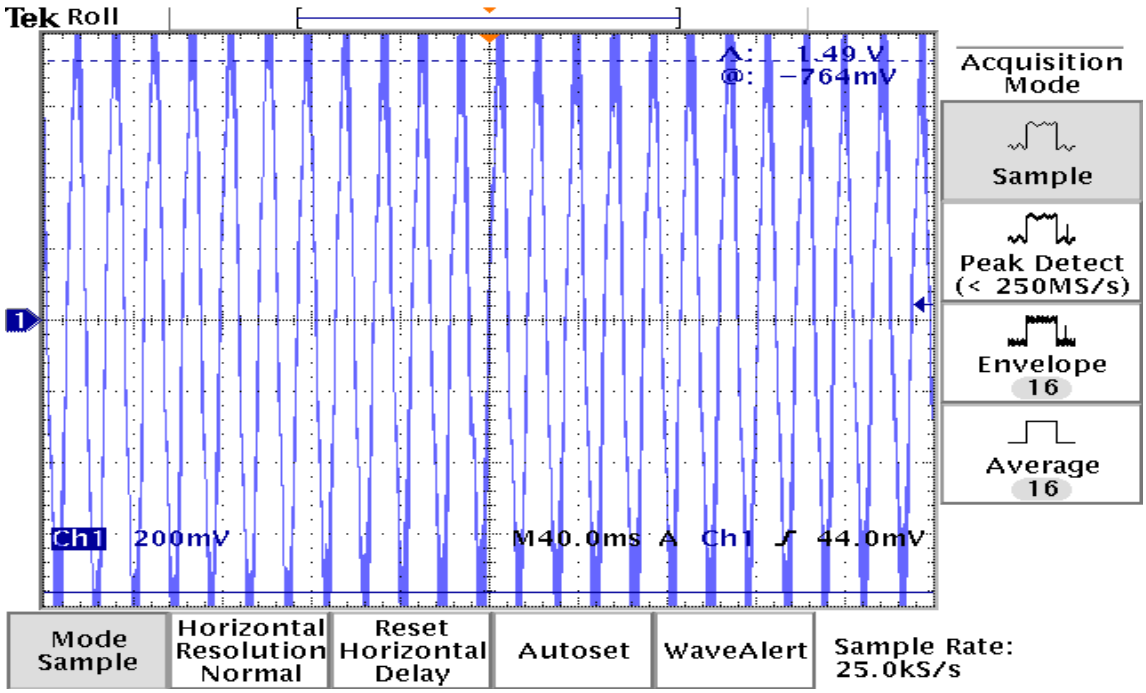

Figure 9.16 Transient phase 'a' current of 9-phase IM using DSP-FPGA interfacing

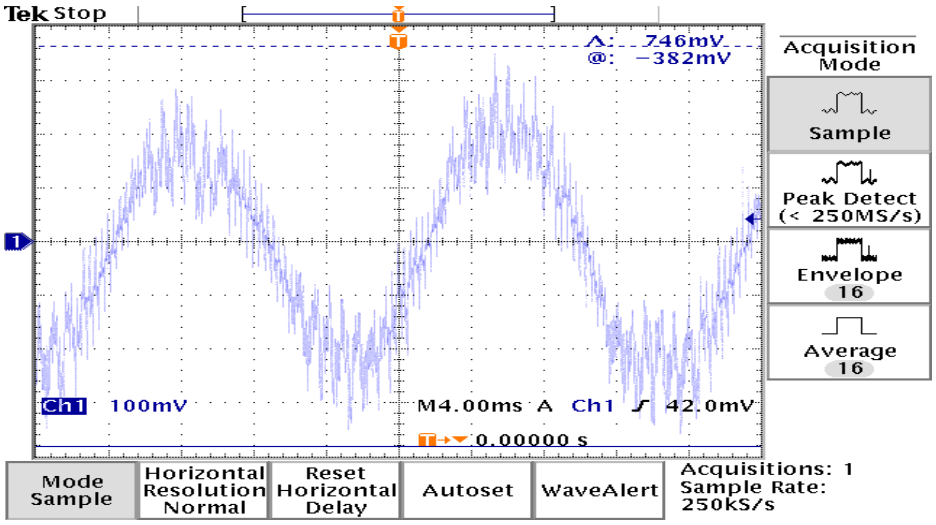

Figure 9.17 Steady state phase 'a' current for 9-phase induction motor using DSP-FPGA interfacing

9.6 Conclusion

In this chapter a hardware interfacing circuit is developed using C6713 DSP and Xilinx Spartan 3E FPGA. Different experimental results are shown in order to validate the operation of the hardware system to generate the PWM signals. The voltage and current output waveforms are traced driving the inverter with 9-phase resistors and 9-phase induction machine. The simulation results are compared with the Experimental waveforms and they are found to be in good agreement.

CHAPTER 10

CONCLUSION AND FUTURE WORKS

In this thesis, multiphase machines are modeled and analyzed in order to realize their advantages for varying speed and torque requirements. Using the Fourier approximation and full order models, the analysis of machine is performed such that the utilization of higher order harmonics is realized. Similarly, high reliability of the 9-phase machine is also realized using three machine configurations of Interior permanent magnet and induction machines. Using the new design technique of turn and winding functions, pole phase modulation of 9-phase induction machine is realized with analytical finite element implementations. Similarly, torque capability of 9-phase induction machine is also studied under different connection schemes using finite elements. This thesis is expected to fill the gap which exists in the modeling and analysis of the 9-phase drives due to the large number of coupled variables. However, many future enhancements can be performed on this research of multiphase systems.

The Fourier series approximation for 9-phase IPM machine described in Chapter 3 can be extended to verify the results experimentally with the help of harmonic injection. Similarly, harmonic control can be performed for each corresponding harmonics order to obtain the better torque requirements. The three machine configurations described in Chapter 5 can be implemented experimentally by connecting the machine as generator. The precise estimation of parameters can be performed using 3-dimesional finite elements for pole phase modulated drive. The pole phase modulation can be implemented using a feedback control loop comprising of DSP and FPGA

interfacing as described in Chapter 9. More enhancements can be performed in reliability analysis of three machine configurations of 9-phase induction machine by operating as motor or generator.

REFERENCES

[1] Emil Levi, “Multiphase Electric Machines for Variable-Speed Applications,” *IEEE Transactions on Industrial Electronics*, vol. 55, no. 5, pp. 1893-1907, May 2008.

[2] P. Krause, O. Wasynczuk and S. D. Sudhoff, Analysis of Electric Machinery and Drive Systems, IEEE Press, Wiley-Interscience, John Wiley & Sons, Inc., 111 River Street, Hoboken, New Jersey, 2002.

[3] J.W. Kelly, E.G.Strangas and J.M.Miller, "Multiphase space vector pulse width modulation," *IEEE Transactions on Energy Conversion*, vol.18, no.2, pp. 259-264, June 2003.

[4] Hyung-Min Ryu, Jang-Hwan Ki and Seung-Ki Sul, "Analysis of multiphase space vector pulse-width modulation based on multiple d-q spaces concept," *IEEE Transactions on Power Electronics*, vol.20, no.6, pp. 1364-1371, Nov. 2005.

[5] A. Lega, M. Mengoni, G. Serra, A.Tani and L.Zarri, "Space Vector Modulation for Multiphase Inverters Based on a Space Partitioning Algorithm," *IEEE Transactions on Industrial Electronics,* vol.56, no.10, pp.4119-4131, Oct. 2009.

[6] A. Iqbal, M. A. Khan, S. M. Ahmed, M. R. Khan and H. Abu-Rub, “A Space Vector PWM Scheme for Multifrequency Output Voltage Generation With Multiphase Voltage-Source Inverters,” *International Journal of Recent Trends in Engineering*, vol. 2, no. 5, November 2009.

[7] D. Dujic, G. Grandi, M. Jones and E.Levi , "A Space Vector PWM Scheme for Multifrequency Output Voltage Generation With Multiphase Voltage-Source Inverters," *IEEE Transactions on Industrial Electronics,* vol.55, no.5, pp.1943-1955, May 2008.

[8] S.M. Ahmed, A. Iqbal, H. Abu-Rub, J. Rodriguez, C.A. Rojas and M. Saleh, "Simple Carrier-Based PWM Technique for a Three-to-9-phase Direct AC–AC Converter," *IEEE Transactions on Industrial Electronics,* vol.55, no.11, pp.5014-5023, Nov. 2011.

[9] O. Lopez, J. Alvarez, J. Doval-Gandoy and F.D. Freijedo, "Multilevel Multiphase Space Vector PWM Algorithm," *IEEE Transactions on Industrial Electronics,* vol.55, no.5, pp.1933-1942, May 2008.

[10] A. Iqbal and S. Moinuddin, "Comprehensive Relationship Between Carrier-Based PWM and Space Vector PWM in a Five-Phase VSI," *IEEE Transactions on Power Electronics*, vol.24, no.10, pp.2379-2390, Oct. 2009.

[11] L.A. Pereira, C.C. Scharlau, L.F. A. Pereira and J.F. Haffner, "General Model of Five-Phase Induction Machine Allowing for Harmonics in the Air Gap Field," *IEEE Transactions on Energy Conversion*, vol.21, no.4, pp.891-899, Dec. 2006.

[12] Huangsheng Xu; H.A. Toliyat and L.J. Petersen, "Five-phase induction motor drives with DSP-based control system," *IEEE Transactions on Power Electronics,* vol.17, no.4, pp.524-533, July 2002.

[13] B. Stumberger, G. Stumberger, A. Hamler, M. Trlep, M. Jesenik and V. Gorican, "Increasing of output power capability in a six-phase flux-weakened permanent magnet synchronous motor with a third harmonic current injection," *IEEE Transactions on Magnetics*, vol.39, no.5, pp. 3343- 3345, Sept. 2003.

[14] L. Parsa and H. A. Toliyat, "Five-phase permanent-magnet motor drives," *IEEE Transactions on Industrial Applications*, vol. 41, no. 1, pp. 30-37, Jan./Feb. 2005.

[15] H. A. Toliyat, S. P. Waikar, and T. A. Lipo, "Analysis and Simulation of 5-phase Synchronous Reluctance Machines including Third Harmonic of Airgap MMF", *IEEE Transactions on Industry Applications*, vol. 34, no .2, March/April 1998.

[16] Hyung-Min Ryu, Ji-Woong Kim and Seung-Ki Sul, "Synchronous-frame current control of multiphase synchronous motor under asymmetric fault condition due to open phases," *IEEE Transactions on Industry Applications*, vol.42, no.4, pp.1062-1070, July-Aug. 2006.

[17] Hyung-Min Ryu, Ji-Woong Kim and Seung-Ki Sul , "Synchronous frame current control of multi-phase synchronous motor. Part I. Modeling and current control based on multiple d-q spaces concept under balanced condition," *Conference Record of the 2004 IEEE Industry Applications Conference, 2004. 39th IAS Annual Meeting*, vol.1, no.1, pp. 3-7, Oct. 2004.

[18] S. Dwari, L. Parsa, "Fault-Tolerant Control of Five-Phase Permanent-Magnet Motors With Trapezoidal Back EMF," *IEEE Transactions on Industrial Electronics*, vol.58, no.2, pp.476-485, Feb. 2011.

[19] E. Levi, M. Jones, A. Iqbal, S.N. Vukosavic and H.A. Toliyat, "Induction Machine/Syn-Rel Two-Motor Five-Phase Series-Connected Drive," *IEEE Transactions on Energy Conversion*, vol.22, no.2, pp.281 -289, June 2007.

[20] E. Levi, M. Jones, A. Iqbal, S.N. Vukosavic and H.A. Toliyat, "Modeling, Control, and Experimental Investigation of a Five-Phase Series-Connected Two-Motor Drive With Single Inverter Supply," *IEEE Transactions on Industrial Electronics* , vol.54, no.3, pp.1504-1516, June 2007.

[21] T. A. Lipo, “A d-q model for 6-phase induction machines,” *Proceedings of the International Conference on Electrical Machines*, Athens, pp. 860-867, Sept 1980.

[22] G. K. Singh, K. Nam and S.K. Lim, "A Simple Indirect Field-Oriented Control Scheme for Multiphase Induction Machine," *IEEE Transactions on Industrial Electronics,* vol.52, no.4, pp. 1177- 1184, Aug. 2005.

[23] R. Bojoi, F. Farina, G. Griva, F. Profumo and A. Tenconi, "Direct torque control for dual 3-phase induction motor drives," *IEEE Transactions on Industry Applications,* vol.41, no.6, pp. 1627- 1636, Nov.-Dec. 2005.

[24] B. Stumberger, G. Stumberger, A. Hamler, M. Trlep, M. Jesenik and V. Gorican, , "Increasing of output power capability in a six-phase flux-weakened permanent magnet synchronous motor with a third harmonic current injection," *IEEE Transactions on Magnetics,* vol.39, no.5, pp. 3343- 3345, Sept. 2003.

[25] K. Hatua and V. T. Ranganathan, "Direct torque control schemes for split-phase induction machine," *IEEE Transactions on Industry Applications,* vol.41, no.5, pp. 1243- 1254, Sept.-Oct. 2005.

[26] Yifan Zhao and T.A. Lipo, "Space vector PWM control of dual 3-phase induction machine using vector space decomposition," *IEEE Transactions on Industry Applications,* vol.31, no.5, pp.1100-1109, Sep/Oct 1995.

[27] M. Jones, S.N. Vukosavic, E. Levi and A. Iqbal, "A six-phase series-connected two-motor drive with decoupled dynamic control," *IEEE Transactions on Industry Applications,* vol.41, no.4, pp. 1056- 1066, July-Aug. 2005.

[28] R.O.C. Lyra and T.A. Lipo, "Torque density improvement in a six-phase induction motor with third harmonic current injection," *IEEE Transactions on Industry Applications*, vol. 38, no. 5, pp. 1351- 1360, Sep/Oct 2002.

[29] A. Tani, M. Mengoni, L. Zarri, G. Serra and D.Casadei, "Control of Multiphase Induction Motors With an Odd Number of Phases Under Open-Circuit Phase Faults," *IEEE Transactions on Power Electronics,* vol.27, no.2, pp.565-577, Feb. 2012.

[30] F. Locment, E. Semail and X. Kestelyn, "Vectorial Approach-Based Control of a Seven-Phase Axial Flux Machine Designed for Fault Operation," *IEEE Transactions on Industrial Electronics,* vol.55, no.10, pp.3682-3691, Oct. 2008.

[31] H.E. Jordan, R.C. Zowarka and S.B. Pratap Jr, "9-phase armature windings design, test, and harmonic analysis," *IEEE Transactions on Magnetics,* vol.41, no.1, pp. 299- 302, Jan. 2005.

[32] Eunsoo Jung, Hyunjae Yoo, Seung-Ki Sul, Hong-Soon Choi and Yun-Young Choi, "A 9-phase Permanent-Magnet Motor Drive System for an Ultrahigh-Speed Elevator," *IEEE Transactions on Industry Applications,* vol.48, no.3, pp.987-995, May-June 2012.

[33] S. Brisset, D. Vizireanu and P. Brochet, "Design and Optimization of a 9-phase Axial-Flux PM Synchronous Generator With Concentrated Winding for Direct-Drive Wind Turbine," *IEEE Transactions on Industry Applications,* vol.44, no.3, pp.707-715, May-june 2008.

[34] A.Rockhill, On the modeling and control of high phase order synchronous Machines, Phd Dissertation, University of Wisconsin, Madison,2012 .

[35] X. Kestelyn and E. Semail, , "A Vectorial Approach for Generation of Optimal Current References for Multiphase Permanent-Magnet Synchronous Machines in Real Time," *IEEE Transactions on Industrial Electronics,* vol.58, no.11, pp.5057-5065, Nov. 2011.

[36] A.S. Abdel-Khalik, M.I. Masoud and B.W. Williams, "Improved Flux Pattern With Third Harmonic Injection for Multiphase Induction Machines," *IEEE Transactions on Power Electronics,* vol.27, no.3, pp.1563-1578, March 2012.

[37] Alexander T. Zaremba and Sergey G. Semenov, Real-time Estimation of Induction Motor parameters using Sinsusoidal Voltage Signals, "United States Patent No. 6661194", February 11, 2002.

[38] A. Boglietti, A. Cavagnino and M. Lazzari, "Computational Algorithms for Induction-Motor Equivalent Circuit Parameter Determination, Part I: Resistances and Leakage Reactances,"*IEEE Transactions on Industrial Electronics*, vol. 58, no. 9, pp. 3723-3733, Sept. 2011.

[39] A. Boglietti, A. Cavagnino and M. Lazzari, "Computational Algorithms for Induction Motor Equivalent Circuit Parameter Determination, Part II: Skin Effect and Magnetizing Characteristics," *, IEEE Transactions on Industrial Electronics*, vol.58, no.9, pp.3734-3740, Sept. 2011.

[40] T.A. Lipo, *Introduction to AC Machine Design*, 3rd ed. Madison, WI: Winsconsin Power Electron. Res. Center, Univ. of Wisconsin, 2007.

[41] N. Bianchi, L. Alberti and S. Bolognani, "*A Modern Approach to the Analysis of Induction Motors"*, Electric Drives Laboratory, Department of Electric Engineering, University of Padova, Italy, January, 2010.

[42] Nicola Bianchi, *Electrical Machine Analysis using Finite Elements*, 1st edition Taylor and Francis Group, New York, 2005.

[43] S.Karugaba, Dynamics and Control of 5-phase Induction Machine, MS Thesis, Tennessee Technological University, Cookeville, 2008.

[44] Z. Wu, An Investigation of Dual Stator Winding Induction Machines, PhD Thesis, Tennessee Tech University, 2006.

[45] Alfredo Munoz and Thomas A. Lipo, "Complex Vector Model of the Squirrel-Cage Induction Machine Including Instantaneous Rotor Bar Currents," *IEEE Transactions on Industry Applications*, vol. 35, No. 6, pp. 1332- 1340, November/December 1999.

[46] L. Alberti, N. Bianchi and S. Bolognani, "Variable-Speed Induction Machine Performance Computed Using Finite-Element, "*IEEE Transactions on Industry Applications*, vol.47, no.2, pp.789-797, March-April 2011.

[47] Jaywant, Induction Machines, McGraw Hill Publishing Company Limited, London, 1968.

[48] M. Osama and Lipo, T.A.; , "A new inverter control scheme for induction motor drives requiring wide speed range," *IEEE Transactions on Industry Applications,* vol.32, no.4, pp.938-944, Jul/Aug 1996.

[49] M. Osama and T.A. Lipo, , "Modeling and analysis of a wide-speed-range induction motor drive based on electronic pole changing," *IEEE Transactions on Industry Applications,* vol.33, no.5, pp.1177-1184, Sep/Oct 1997.

[50] S.Z. Jiang, K.T. Chau and C.C. Chan, "Spectral analysis of a new six-phase pole-changing induction motor drive for electric vehicles," *IEEE Transactions on Industrial Electronics,* vol.50, no.1, pp. 123- 131, Feb 2003.

[51] L.M.Melcescu, M.V. Cistelecan, O. Craiu and H.B. Cosan, "A new 4/6 pole-changing double layer winding for 3-phase electrical machines," *2010 XIX International Conference on Electrical Machines (ICEM),* vol.1, no.1, pp.1-6, 6-8 Sept. 2010.

[52] E.F. Fuchs, J. Schraud and F.S. Fuchs, "Analysis of Critical-Speed Increase of Induction Machines via Winding Reconfiguration With Solid-State Switches," *IEEE Transactions on Energy Conversion,* vol.23, no.3, pp.774-780, Sept. 2008.

[53] J. M Miller, V. Stefanovic, V. Ostovic and J. Kelly, "Design considerations for an automotive integrated starter-generator with pole-phase modulation," *Conference Record of the 2001 IEEE Thirty-Sixth IAS Annual Meeting*, vol.4, pp.2366 – 2373, 30 Sept. - 4 Oct 2001.

[54] Dongsen Sun, Baoming Ge and Daqiang Bi, "Winding design for pole-phase modulation of induction machines," *2010 IEEE Energy Conversion Congress and Exposition (ECCE),* pp. 278 - 283, 12 - 16 Sept. 2010.

[55] John Michael Miller and Vlado Ostovic, "Pole phase modulated torodial winding for an induction machine", U.S. Patent 5977679, Nov 2, 1999.

[56] Stephen B. Kuznetsov, "Electric Machine with continuous pole phase modulation", US Patent 4489265, March 24, 1983.

[57] J.W. Kelly, E.G. Strangas and J.M. Miller, "Control of a continuously operated pole-changing induction machine," *IEEE International , Electric Machines and Drives Conference, 2003. IEMDC'03.* vol.1, no.1, pp. 211- 217 vol.1, 1-4 June 2003.

[58] D. Hadiouche, L. Baghli and A. Rezzoug, "Space-vector PWM techniques for dual 3-phase AC machine: analysis, performance evaluation, and DSP implementation," *IEEE Transactions on Industry Applications*, vol.42, no.4, pp.1112-1122, July-Aug. 2006.

[59] E. J. Bueno, A. Hernandez, F.J. Rodriguez, C. Giron, R. Mateos and S. Cobreces, "A DSP- and FPGA-Based Industrial Control With High-Speed Communication Interfaces for Grid Converters Applied to Distributed Power Generation Systems," *IEEE Transactions on Industrial Electronics,* vol.56, no.3, pp.654-669, March 2009.

[60] M.W. Naouar, E. Monmasson, A.A. Naassani, I. Slama-Belkhodja and N. Patin, "FPGA-Based Current Controllers for AC Machine Drives—A Review," *IEEE Transactions on Industrial Electronics,* vol.54, no.4, pp.1907-1925, Aug. 2007.

[61] Zeliang Shu, Yuhua Guo and Jisan Lian, "Steady-State and Dynamic Study of Active Power Filter With Efficient FPGA-Based Control Algorithm," *IEEE Transactions on Industrial Electronics,* vol.55, no.4, pp.1527-1536, April 2008.

[62] E. Monmasson and M.N. Cirstea, "FPGA Design Methodology for Industrial Control Systems—A Review," *IEEE Transactions on Industrial Electronics,* vol.54, no.4, pp.1824-1842, Aug. 2007.

[63] E.J. Bueno, S. Cobreces, F.J. Rodriguez, A. Hernandez and F. Espinosa, "Design of a Back-to-Back NPC Converter Interface for Wind Turbines With Squirrel-Cage Induction Generator," *IEEE Transactions on Energy Conversion,* vol.23, no.3, pp.932-945, Sept. 2008.

[64] T. Atalik, M. Deniz, E. Koc, C.O. Gercek, B. Gultekin, M. Ermis and I. Cadirci, "Multi-DSP and -FPGA-Based Fully Digital Control System for Cascaded

Multilevel Converters Used in FACTS Applications, " *IEEE Transactions on Industrial Informatics,* vol.8, no.3, pp.511-527, Aug. 2012.

[65] Thomas A. Lipo, Analysis of Synchronous Machines, Wisconsin Power Electronics Research Center, University of Wisconsin-Madison, 2008.

[66] A.S. Abdel-Khalik, S. Mostafa Gadoue, M.I. Masoud and B.W. Wiliams, "Optimum Flux Distribution With Harmonic Injection for a Multiphase Induction Machine Using Genetic Algorithms, "*IEEE Transactions on Energy Conversion*, vol. 26, no. 2, pp. 501-512, June 2011.

[67] A.K Shawney, A Course in Electrical machine Design, Dhanpat Rai and Sons, India, 1984.

[68] Nobert Schimitz and Donald Novotny, Introductory Electromechanics, The Ronald Press Company, New York, 1950.

[69] K. Lee and F. Blaabjerg, "Simple Power Control for Sensorless Induction Motor Drives Fed by a Matrix Converter," *IEEE Transactions on Energy Conversion*, vol. 23, no. 3, pp. 781-788, Sept. 2008.

[70] J. H. H. Alwash, K. S. Ismail and J. F. Eastham, "A novel 16/6-phase modulated winding, "*IEEE Transactions on Energy Conversion,* vol.15, no. 2, pp. 188 - 190, June 2000.

[71] J. E. Slotine and W. Li, *Applied Nonlinear Control,* Prentice Hall, 1998.

[72] M.H. Rashid, *Power Electronics: Circuits, Devices, and Applications,* 2nd Edition, Prentice Hall, 1993.

[73] V.B. Honsinger, "The Fields and Parameters of Interior Type AC Permanent Magnet Machines," *IEEE Transactions on Power Apparatus and Systems,* vol.PAS-101, no.4, pp.867-876, April 1982.

[74] Olufemi A. Osaloni, Performance Analysis and Non-linear Feedback Control of Interior Permanent Magnet Motor, MS thesis, Tennessee Technological University, Cookeville, TN, 2003.

[75] H.A. Toliyat, "Analysis and simulation of five-phase variable-speed induction motor drives under asymmetrical connections," *IEEE Transactions on Power Electronics,* vol.13, no.4, pp.748-756, Jul 1998.

[76] Data sheet for DSK6713 using, C6713 DSP, Texas instruments, Texas, USA.

[77] Data sheet for Xilinx Spartan 3E FPGA using Nexys 2 Board, Xilinx Inc. USA.

APPENDICES

APPENDIX A

Trigonometric Identities

The trigonometric identities used in the derivation of IPM machine are discussed here.

For the variations of $\alpha = \frac{2\pi}{9}$, the sine and cosines are given as

$$\begin{aligned}
&\cos\alpha = 0.766 \\
&\cos 2\alpha = 0.1736 \\
&\cos 3\alpha = -0.5 \\
&\cos 4\alpha = -0.939 \\
&\cos 5\alpha = -0.939 \\
&\cos 6\alpha = -0.5 \\
&\cos 7\alpha = 0.1736 \\
&\cos 8\alpha = 0.766 \\
&\cos 9\alpha = 1
\end{aligned} \tag{A1.1}$$

$$\begin{aligned}
&\sin\alpha = 0.642 \\
&\sin 2\alpha = 0.9848 \\
&\sin 3\alpha = 0.866 \\
&\sin 4\alpha = 0.342 \\
&\sin 5\alpha = -0.342 \\
&\sin 6\alpha = -0.866 \\
&\sin 7\alpha = -0.9848 \\
&\sin 8\alpha = -0.642 \\
&\sin 9\alpha = 0
\end{aligned} \tag{A1.2}$$

Hence the cosine values of

$$\begin{aligned}
&\alpha = 8\alpha \\
&2\alpha = 7\alpha \\
&3\alpha = 6\alpha \\
&4\alpha = 5\alpha
\end{aligned} \tag{A1.3}$$

But for the sine values:

$$\begin{aligned} \alpha &= -8\alpha \\ 2\alpha &= -7\alpha \\ 3\alpha &= -6\alpha \\ 4\alpha &= -5\alpha \end{aligned} \tag{A1.4}$$

The addition of cosine of α from α to 9α gives value of 0.

Similarly, the addition of sine of α from α to 9α also gives value of 0.

Using these simplifications, the equations for inductances can be derived in closed form as many quantities cancel themselves.

Example: Utilization of identities in inductance calculations:

As an example, consider the calculation of first element of the q-d inductance matrix. For this particular element, the fundamental transformation matrix is utilized with the inductance matrix and inverse of the fundamental matrix, i.e.,

$$L_{qdoxs} = T(\theta_1) L_{ss} T(\theta_1)^{-1} \tag{A1.5}$$

where

$$T(\theta_1) = \frac{2}{9}\begin{bmatrix} c(\theta) & c(\theta-\alpha) & c(\theta-2\alpha) & c(\theta-3\alpha) & c(\theta-4\alpha) & c(\theta-5\alpha) & c(\theta-6\alpha) & c(\theta-7\alpha) & c(\theta-8\alpha) \end{bmatrix}$$

$$L_{ss} = \begin{bmatrix} L_{ls}+L_{aa} & L_{ab} & L_{ac} & L_{ad} & L_{ae} & L_{af} & L_{ag} & L_{ah} & L_{ai} \\ L_{ba} & L_{ls}+L_{bb} & L_{bc} & L_{bd} & L_{be} & L_{bf} & L_{bg} & L_{bh} & L_{bi} \\ L_{ca} & L_{cb} & L_{ls}+L_{cc} & L_{cd} & L_{ce} & L_{cf} & L_{cg} & L_{ch} & L_{ci} \\ L_{da} & L_{db} & L_{dc} & L_{ls}+L_{dd} & L_{de} & L_{df} & L_{dg} & L_{dh} & L_{di} \\ L_{ea} & L_{eb} & L_{ec} & L_{ed} & L_{ls}+L_{ee} & L_{ef} & L_{eg} & L_{eh} & L_{ei} \\ L_{fa} & L_{fb} & L_{fc} & L_{fd} & L_{fe} & L_{ls}+L_{ff} & L_{fg} & L_{fh} & L_{fi} \\ L_{ga} & L_{gb} & L_{gc} & L_{gd} & L_{ge} & L_{gf} & L_{ls}+L_{gg} & L_{gh} & L_{gi} \\ L_{ha} & L_{hb} & L_{hc} & L_{hd} & L_{he} & L_{hf} & L_{hg} & L_{ls}+L_{hh} & L_{hi} \\ L_{ia} & L_{ib} & L_{ic} & L_{id} & L_{ie} & L_{if} & L_{ig} & L_{ih} & L_{ls}+L_{ii} \end{bmatrix} \tag{A1.6}$$

$$T(\theta_1)^{-1} = \begin{bmatrix} c(\theta) & c(\theta-\alpha) & c(\theta-2\alpha) & c(\theta-3\alpha) & c(\theta-4\alpha) & c(\theta-5\alpha) & c(\theta-6\alpha) & c(\theta-7\alpha) & c(\theta-8\alpha) \end{bmatrix}^T$$

As leakage inductance L_{ss} are on the diagonals of the stator inductance matrix, it can be skipped and add afterwards. Hence, using Table (3.1) and Equations (A1.5) and (A1.6), the first element of matrix L_{qdoxs} .is calculated.

As an illustration, let's take the coefficient of $\frac{\pi N_3{}^2 a_2}{18}$, and solve for inductances.

$$L_{q11} = \frac{2}{9}[c(\theta)L_{aa} + c(\theta-\alpha)L_{ab} + c(\theta-2\alpha)L_{ac} + c(\theta-3\alpha)L_{ad} + c(\theta-4\alpha)L_{ae} + c(\theta-5\alpha)L_{af} + c(\theta-6\alpha)L_{ag} + c(\theta-7\alpha)L_{ah} + c(\theta-8\alpha)L_{ai}] \quad \text{(A1.7)}$$

$$L_{q12} = \frac{2}{9}[c(\theta)L_{ab} + c(\theta-\alpha)L_{bb} + c(\theta-2\alpha)L_{bc} + c(\theta-3\alpha)L_{bd} + c(\theta-4\alpha)L_{be} + c(\theta-5\alpha)L_{bf} + c(\theta-6\alpha)L_{bg} + c(\theta-7\alpha)L_{bh} + c(\theta-8\alpha)L_{bi}] \quad \text{(A1.8)}$$

$$L_{q13} = \frac{2}{9}[c(\theta)L_{ac} + c(\theta-\alpha)L_{bc} + c(\theta-2\alpha)L_{cc} + c(\theta-3\alpha)L_{cd} + c(\theta-4\alpha)L_{ce} + c(\theta-5\alpha)L_{cf} + c(\theta-6\alpha)L_{cg} + c(\theta-7\alpha)L_{ch} + c(\theta-8\alpha)L_{ci}] \quad \text{(A1.9)}$$

$$L_{q14} = \frac{2}{9}[c(\theta)L_{ad} + c(\theta-\alpha)L_{bd} + c(\theta-2\alpha)L_{cd} + c(\theta-3\alpha)L_{dd} + c(\theta-4\alpha)L_{de} + c(\theta-5\alpha)L_{df} + c(\theta-6\alpha)L_{dg} + c(\theta-7\alpha)L_{dh} + c(\theta-8\alpha)L_{di}] \quad \text{(A1.10)}$$

$$L_{q15} = \frac{2}{9}[c(\theta)L_{ae} + c(\theta-\alpha)L_{be} + c(\theta-2\alpha)L_{ce} + c(\theta-3\alpha)L_{de} + c(\theta-4\alpha)L_{ee} + c(\theta-5\alpha)L_{ef} + c(\theta-6\alpha)L_{eg} + c(\theta-7\alpha)L_{eh} + c(\theta-8\alpha)L_{ei}] \quad \text{(A1.11)}$$

$$L_{q16} = \frac{2}{9}[c(\theta)L_{af} + c(\theta-\alpha)L_{bf} + c(\theta-2\alpha)L_{cf} + c(\theta-3\alpha)L_{df} + c(\theta-4\alpha)L_{ef} + c(\theta-5\alpha)L_{ff} + c(\theta-6\alpha)L_{fg} + c(\theta-7\alpha)L_{fh} + c(\theta-8\alpha)L_{fi}] \quad \text{(A1.12)}$$

$$L_{q17} = \frac{2}{9}[c(\theta)L_{ag} + c(\theta-\alpha)L_{bg} + c(\theta-2\alpha)L_{cg} + c(\theta-3\alpha)L_{dg} + c(\theta-4\alpha)L_{eg} + c(\theta-5\alpha)L_{fg} + c(\theta-6\alpha)L_{gg} + c(\theta-7\alpha)L_{gh} + c(\theta-8\alpha)L_{gi}] \quad \text{(A1.13)}$$

$$L_{q18} = \frac{2}{9}[c(\theta)L_{ah} + c(\theta-\alpha)L_{bh} + c(\theta-2\alpha)L_{ch} + c(\theta-3\alpha)L_{dh} + c(\theta-4\alpha)L_{eh} + c(\theta-5\alpha)L_{fh} + c(\theta-6\alpha)L_{fh} + c(\theta-7\alpha)L_{hh} + c(\theta-8\alpha)L_{hi}] \quad \text{(A1.14)}$$

$$L_{q19} = \frac{2}{9}[c(\theta)L_{ai} + c(\theta-\alpha)L_{bi} + c(\theta-2\alpha)L_{ci} + c(\theta-3\alpha)L_{di} + c(\theta-4\alpha)L_{ei} + c(\theta-5\alpha)L_{fi} + c(\theta-6\alpha)L_{ig} + c(\theta-7\alpha)L_{ih} + c(\theta-8\alpha)L_{ii}] \quad \text{(A1.15)}$$

Now, the equation of including $\frac{\pi N_3{}^2 a_2}{18}$ in the derivation is given as

$$\begin{aligned} L_{qdoxs} &= L_{q1..12349} T(\theta_1)^{-1} \\ &= L_{q11} c(\theta) + L_{q12} c(\theta-\alpha) + L_{q13} c(\theta-2\alpha) + L_{q14} c(\theta-3\alpha) + L_{q15} c(\theta-4\alpha) \\ &\quad + L_{q16} c(\theta-5\alpha) + L_{q17} c(\theta-6\alpha) + L_{q18} c(\theta-7\alpha) + L_{q19} c(\theta-8\alpha) \end{aligned} \tag{A1.16}$$

$$\begin{aligned} L_{q11} = \frac{2}{9}[&c(\theta)c(6\theta_r) + c(\theta-\alpha)c(6\theta_r-3\alpha) + c(\theta-2\alpha)c(6\theta_r-6\alpha) \\ &+ c(\theta-3\alpha)c(6\theta_r-9\alpha) + c(\theta-4\alpha)c(6\theta_r-12\alpha) + c(\theta-5\alpha)c(6\theta_r-15\alpha) \\ &+ c(\theta-6\alpha)c(6\theta_r-18\alpha) + c(\theta-7\alpha)c(6\theta_r-21\alpha) + c(\theta-8\alpha)c(6\theta_r-24\alpha)] \end{aligned} \tag{A1.17}$$

Similarly,

$$\begin{aligned} L_{q12} = \frac{2}{9}[&c(\theta)c(6\theta_r-3\alpha) + c(\theta-\alpha)c(6\theta_r-6\alpha) + c(\theta-2\alpha)c(6\theta_r-9\alpha) \\ &+ c(\theta-3\alpha)c(6\theta_r-12\alpha) + c(\theta-4\alpha)c(6\theta_r-15\alpha) + c(\theta-5\alpha)c(6\theta_r-18\alpha) \\ &+ c(\theta-6\alpha)c(6\theta_r-21\alpha) + c(\theta-7\alpha)c(6\theta_r-24\alpha) + c(\theta-8\alpha)c(6\theta_r-27\alpha)] \end{aligned} \tag{A1.18}$$

Similarly, other terms can be uniquely expressed.

Using rotor reference frame, i.e., $\theta = \theta_r$, and from Equation (A1.16), it is seen that the term L_{q11} needs to be multiplied by $c(\theta_r)$, L_{q12} needs to be multiplied by $c(\theta_r - \alpha)$ and so on.

Utilizing this concept, all the terms will get either of $c(4\theta_r), c(6\theta_r), c(8\theta_r)$ inside them with phase shifts. If all of them are solved and added, the result will come to be zero due to the identities described.

However, to perform the multiplication of the term including $\frac{\pi N_1{}^2 a_1}{2}$, the terms in the table have cosine of $c(2\theta_r)$ inside them. Multiplying this term by $T(\theta_r)_1$, them terms will either be of the form $c(3\theta_r)$ or $c(\theta_r)$. Again, multiplying by $T(\theta_r)_1^{-1}$, the result is either $c(4\theta_r), c(2\theta_r)$ or $c(0)$. The last term is the constant of 1. Hence, all the terms

with the inclusion of rotor angle terms will be cancelled by identities. However, only one of them will remain. Similar is the case for $\pi N_1^2 a_0$ term in Table (3.1).

In this way, all the inductances in q-d frame can be calculated. The calculations can be performed by using softwares such as MATLAB or Mathematica to get the closed solution without any long manual calculations.

APPENDIX B

Parameters of the 9-phase IPM Machine

Stator Data:	
Outer Diameter of Stator	154.432 mm
Inner Diameter of Stator	93.4212 mm
Number of Stator slots	36 mm
Skew Width	1 Slot
Stator Slot Dimensions	
H_{s0}	0.508 mm
H_{s1}	0.762 mm
H_{s2}	11.43 mm
B_{s0}	1.9304 mm
B_{s1}	4.191 mm
B_{s2}	6.39572 mm
Top Tooth Width	4.18319 mm
Bottom Tooth Width	3.97339 mm
Length of Stator Core	95.25 mm
Stacking Factor of Stator Core	0.93
Type of Steel	STATOR_DEF
Slot Insulation Thickness	0.3 mm
End Length Adjustment	0 mm
Number of Parallel Branches	1

Number of Conductors per Slot	24
Rotor Data:	
Air gap	0.635 mm
Inner Diameter of Rotor	31.496 mm
Length of Rotor	95.25 mm
Rotor Stacking Factor	0.93
Magnet Duct Dimensions	
D1	69.073 mm
O1	23.5331 mm
Rib	3.302 mm
Magnet type	Samarium Cobalt
Magnet Thickness	6.35 mm
Total Magnet Width	32.3088 mm
Residual Flux density	0.85 Wb
Coercive Force	629 kA/m
Maximum Energy Density	133.67 kJ/m^3
Relative Recoil Permeability	1.07528
Demagnetized Flux density	0.531245

APPENDIX C

9-phase Induction Machine data and parameters

No. of stator slots = 36

No. of rotor bars = 44

rb= 0.000139 Ω

re= 2.74x10-6 Ω,

le= 5.06x10-7H

lb= 4.11x10-8H

$\alpha r = 2\pi/44$, $\beta = 0.5 \times \alpha r$

r =4.75 inches

l = 0.0704 inches

g = 0.0066 inches

VITA

Amrit Gautam received his Bachelor of Science degree in Electrical Engineering from Tribhuvan University, Nepal in December, 2007. From March 2008 to December 2009, he worked as a Visiting Faculty in the Department of Electrical Engineering, Nepal Engineering College, Nepal. In January 2010, he joined the Master's program at South Dakota State University, and then transferred to Tennessee Tech University in September, 2010. He received his Master's Degree in December 2012. His research interests include Power Electronics, Renewable Energy and Control Systems.

PUBLICATIONS

A. Gautam, S. Karugaba, J. Ojo, "Modeling of 9-phase interior permanent magnet machines (IPM) including harmonic effects," *2011 IEEE International Electric Machines & Drives Conference (IEMDC),* vol.1 , no.1 , pp.681-686, 15-18 May 2011

A. Gautam, J. Ojo, "Computation of Equivalent Circuit Parameters of 9-phase Induction Motor in Different Operating Modes," presented in 2012 Energy Convention and Congress Expo. (ECCE), pp. 142-148, 15-21 Sept. 2012

A. Gautam, J. Ojo, "Variable Speed Multiphase Induction Machine using Pole Phase Modulation Principle," presented in 38th Annual Conference of the IEEE Industrial Electronics Society (IECON-2012), 25-28 Oct. 2012